TIDAL CHANNELS

LISP 89
Littoral Investigation of Sediment Properties

Minas Basin 1989

Final Report

Compiled by
Graham R. Daborn

Acadia Centre for Estuarine Research
Publication No. 17
November 1991

CONTENTS

LIST OF FIGURES

LIST OF TABLES

LITTORAL INVESTIGATION OF SEDIMENT PROPERTIES (LISP)

FINAL REPORT

Part 1. INTRODUCTION

Contract UP A8-001

1.1 Introduction

Estuarine sediments present a particularly challenging problem for anyone attempting to predict the consequences of human modifications to the structure of an estuary. Although much research has been conducted on the dynamics of coarse, non-cohesive sediments, relatively less is known about the dynamic properties of finer sediments, especially where these contain measurable quantities of clay. Coarse, non-cohesive sediments are influenced primarily by physical factors such as current velocity and turbulence, and behave in ways that are determined largely by their predominant grain size. In finer sediments, however, factors such as water and organic matter content, exposure to atmospheric conditions during low tide, and biological phenomena, become increasingly important. The potential importance of biological processes in affecting sediment stability of finer sediments means that results of studies based on samples returned to a laboratory may bear little relationship to the *in situ* properties of the sediment.

During a broad study of a macrotidal flat in Minas Basin, Amos et al. (1988) found significant seasonal changes in the apparent strength of an intertidal sediment, and concluded that exposure at low tide during hot dry conditions resulted in an effective 'armouring' of the surface. It was also recognised, however, that the activities of benthic organisms were extensive, and probably played an important, interactive role. In order to elucidate more clearly the relative roles of physico-chemical, atmospheric, sedimentological and biological processes, a comprehensive, multidisciplinary study was carried out on the Starrs Point tidal flat during July 1989. Entitled LISP (Littoral Investigation of Sediment Properties), an attempt was made to examine all parameters that might have an influence on the stability of the sediment surface, and to monitor atmospheric and oceanographic conditions continuously during a spring-neap cycle.

1.2 Funding

Funding was provided principally through contract UP A8-001 to the Acadia Centre for Estuarine Research, Acadia University, under the Unsolicited Proposals programme of the Department of Supply and Services. The contract funding covered much of the basic logistic costs of the project, enabling a large number of scientists to participate with only a modest cost to their own resources. Additional funding was provided by the Nova Scotia Tidal Power Corporation, and the Natural Sciences and Engineering Research Council (Grant A9679 to G.R. Daborn). Many of the principal and adventitious investigators provided or obtained other funds for equipment or travel that enabled them to participate more completely in the project. These funds came from a variety of sources including : Canada Department of Energy, Mines and Resources, Department of Fisheries and Oceans, Canada Centre for Remote Sensing (Ottawa), The Royal Society (U.K.), U.K. Department of Energy, Lafayette College (U.S.A.), Acadia Centre for Estuarine Research, and Instituto Argentino de Oceanografia (Argentina).

1.3 Background

For centuries, man has freely modified tidal estuaries for purposes of communication, transportation, waste disposal, food and power production. The impacts of such changes have rarely been predicted adequately because of the complexity of natural ecosystems and the lack of understanding of their internal organisation. In eastern Canada, for example, many causeways, bridges and dams constructed in recent decades have had unforeseen and often detrimental effects on local environments. Where turbid, macrotidal estuaries have been involved (such as the Petitcodiac River near Moncton, N.B. and the Avon River at Windsor, N.S.), major changes in sedimentation patterns have been evident (cf. Amos 1977; Amos and Joice 1977; Bray et al. 1982; Daborn and Dadswell 1988). In fact, most engineering activities in turbid estuaries cause long-term changes in siltation that are often dramatic and wide-spread. These changes have fundamental effects on biological and chemical processes. They particularly influence the fate of pollutants, which are commonly closely associated with—and may become highly concentrated upon—fine sediment particles. Consequently, it is extremely important that the behaviour of sediments be sufficiently well known that the consequences of human (and natural) modifications of estuaries can be predicted.

Postma (1961, 1967) proposed that the development of a littoral mudflat was the result of two factors : (1) decreases in flow velocity across the intertidal zone toward the high water mark, which results in deposition of fine sediments; and (2) consolidation of the resulting bed during high water. Because the velocity required for erosion of a settled bed exceeds that which led to its deposition (the so-called 'erosion lag'), Postma argued that less sediment would be eroded than deposited on a given tide, and hence a mudflat would develop. This concept, developed almost three decades ago, is recognised as an oversimplification. Climatic factors such as evaporation have been identified as major influences upon sediment erodibility in the intertidal zone (e.g., van Leussen and van Velzen 1989), especially when there is heavy rain or ice (Anderson 1983). Breaking waves contribute substantial amounts of energy that induce resuspension and transport of deposited sediments, even in sheltered macrotidal estuaries where tidal energy would appear to be dominant. These factors have a combined effect that is greater than the hydraulic controls proposed by Postma. For example, measures of mudflat shear strength made in the Minas Basin intertidal zone showed a 20-fold increase in bed resistance over a six-day period of high evaporation (Amos et al. 1988). This is equivalent to an 80-fold increase in erosion resistance compared with subtidal sediments of similar composition. The significance of this observation is that **it is the properties of continually-wetted or sublittoral sediments that have usually been used to simulate and predict erosion.**

All the above factors (waves, tidal currents, evaporation) play significant roles in determining the stability of fine-grained intertidal sediments. In addition, there is growing evidence that biological processes are extremely important in affecting the strength of deposited sediments, especially through binding of individual particles (e.g., Neumann et al. 1970; Holland et al. 1974; Manzenrieder 1983). Prior to this project, however, their specific and relative contributions were unknown. All these factors also change with time and with distance across the intertidal zone—changes which cannot be adequately represented or recreated in laboratory

experiments. Furthermore, the intertidal zones of an estuary play a complex role in the dynamics of sediments, acting during quiescent times as a 'sink' and under more robust conditions as a 'source' of fine sediments to the water (Anderson 1983).

In general, recent research indicates that the important factors controlling deposition and erosion of fine sediments differ qualitatively and quantitatively from those that have usually been utilised in simulation modelling. The differences are of such an extent that the results of causeway or other construction in estuaries could not be adequately predicted. Simulation models based upon measurements of sediment properties made in laboratory flumes are seriously in error because they have utilised continuously wetted samples, and/or subtidal sediments (Nowell et al. 1981; Luckenbach 1986). They may even have been 'reformed' or homogenised, thus destroying the internal architecture associated with erosion/deposition cycles and biological constructions (e.g., Rhoads et al. 1978; Meadows and Tait 1989). Recognition of these difficulties indicates the need for new and appropriate methods for measurement of sediment properties *in situ*, a principal focus of activity during this project.

1.4 Precepts and Strategy

Recognising the complex interactions taking place between the sediment, the atmosphere, the oceanographic parameters affecting the site, and the biological constituents inhabiting the sediment, LISP 89 was conceived as an integrated, interdisciplinary project aimed at elucidating the relative importance of different factors affecting sediment stability. The principal disciplines involved were identified, and then scientists experienced in each field were invited to participate in the project. An outline of the major elements, their perceived interactions, and the principal investigators responsible for planning and executing the study is shown in Figure 3.1.

Because of the complex nature of the study, and the significant differences between methodology in each discipline, it was considered essential to ensure that all participants accept some basic precepts as a foundation upon which design and conduct of the study would be based. These precepts are outlined below.

(1) Stability of intertidal flats is highly variable in time and space.
(2) Dynamic properties of intertidal sediments differ from subtidal sediments because of exposure during low tide periods.
(3) The potential importance of atmospheric, oceanographic and biological factors on sediment properties requires a coordinated, interdisciplinary approach.
(4) Extensive interaction between variables, and prompt changes on disturbance, demand *in situ* measurement wherever possible.
(5) An integrated, multidisciplinary research project requires measurement of all parameters on compatible (preferably identical) time and space scales and frequency. While this is somewhat idealistic, there is clear potential for much more closely integrated work than is commonly conducted.

(6) Monitoring and correlation between observed variables yield insight, but confidence in interpretation comes from experimental manipulation.

In order to ensure a maximum of interaction between participants, each phase of the project included frequent workshops involving all principal scientists. During the Minas Basin exercise, these workshops were held at two- or three-day intervals. Each meeting provided an opportunity to resolve organisational problems, to discuss the results being obtained, and to design new experiments to clarify the relationships between the major variables being studied.

1.5 Objectives

The objectives of LISP 89 were :

(a) To monitor changes in the important variables that affect sediment stability in an intertidal location;
(b) To determine the relative importance of sedimentary, oceanographic, atmospheric and biological factors influencing sediment properties during the summer months;
(c) To develop techniques for measuring important sediment properties *in situ*;
(d) To obtain accurate *in situ* measurements of sediment erodibility and shear strength necessary for simulation modelling;
(e) To foster interdisciplinary research and communication between scientists working on sedimentary processes.

1.6 Participants

Participants involved in the major study in Minas Basin are listed in Table 3.1. Some of these also contributed to the preliminary exercise in the Annapolis Basin (cf. Section 2.1). Coordination of the project was provided by Dr. Graham Daborn of the Acadia Centre for Estuarine Research, assisted by Ms. Darlene Feener, Ms. Peggy Crawford-Kellock and Mr. Jeff Monchamp (ACER), and Dr. Boris Tsinman (Department of Supply and Services).

LITTORAL INVESTIGATION OF SEDIMENT PROPERTIES (LISP)

FINAL REPORT

Part 2. ANNAPOLIS MINILISP
5-12 April 1989

Contract UP A8-001

2.1 Introduction

The initial exercise of the LISP project was a field study in the Annapolis Basin, conducted at the request of the Department of Fisheries and Oceans. The Annapolis Basin has been the site for significant anthropogenic changes in recent decades by which the estuary has been strongly modified; firstly (in 1960) by the construction of the Annapolis Causeway at Annapolis Royal, and subsequently by construction (1980-84) and operation (since 1985) of the Annapolis Tidal Generating Station in the same causeway. The collapse of soft-shell clam (*Mya arenaria*) stocks on tidal flats below the Annapolis Causeway that took place during the 1980's, has been variously attributed to overfishing, pollution, and sedimentation. Proponents of the last cause have maintained that increased sediment deposition on the clam flats at Thorne Cove, Oak Island Point and Queen Anne Marsh smothered the clams, and was caused by events associated with the building and/or operation of the tidal power station.

The objectives of the Annapolis 'MiniLISP' exercise were :

(1) To obtain basic information on the distribution, composition and abundance of sediments, both in suspension and deposited in intertidal and subtidal areas of the inner Annapolis Basin (seaward of the Annapolis Causeway);
(2) To examine the geotechnical and sedimentary properties of sediments deposited in intertidal areas of the inner Annapolis Basin; and
(3) To test out equipment and techniques designed for the *in situ* measurement of sediment properties.

It was understood that the data gathered during the Annapolis 'MiniLISP' would be passed to consultants who would use it to construct a numerical model of sediment behaviour in the Annapolis Basin for the purpose of evaluating the separate effects of the Annapolis Causeway and the Annapolis Tidal Generating Station. Analysis and interpretation of the data from the viewpoint of the relationship between construction activities and the decline of the soft-shell clam industry were not part of the 'MiniLISP' project.

2.2 Personnel

The following personnel participated in MiniLISP :

Dr. Carl Amos	- AGC/BIO
Mr. Harold Christian	- AGC/BIO
Mr. Anthony Atkinson	- AGC/BIO
Mr. Angus Robertson	- AGC/BIO
Mr. Terry Rowell	- DFO/BIO

Dr. John Grant	- Dalhousie University
Dr. Georges Drapeau	- INRS, Rimouski
Mr. Luc Roseberry	- INRS, Rimouski
Dr. Graham Daborn	- ACER, Acadia University
Dr. Michael Brylinsky	- ACER, Acadia University
Dr. Gary Yeo	- ACER, Acadia University
Ms. Diane Amirault	- ACER, Acadia University
Ms. Diane Baldwin	- ACER, Acadia University
Ms. Gail White	- ACER, Acadia University
Mr. Jeff Monchamp	- ACER, Acadia University
Mr. Michael Shaffelburg	- ACER, Acadia University

2.3 Study Site

The Annapolis MiniLISP exercise consisted of three major components :

(1) Examination of the properties of intertidal sediments along 12 transects in the inner Annapolis Basin, from Thorne Cove to Queen Anne Marsh on the north shore, around Goat Island, and near Upper Clements on the south shore;
(2) Monitoring of the water column at two 25-hour anchor stations in channels north and south of Goat Island; and
(3) Sampling for suspended and bottom sediments along longitudinal transects from Digby to the causeway at Annapolis Royal.

Locations of these study sites are shown in Figure 2.1.

2.4 Methods

A. Intertidal Transects

Twelve transects were laid out from MHWN to MLWN, or approximately from the edge of the saltmarsh (where present) to low water. Stations were marked off at 50 or 25 m distances, depending upon the width of the intertidal zone, and each station was marked with a wooden 5 x 5 cm stake. Sample sites for sediment and biological parameters were taken at varying distances to the right or left of the station stake using a random

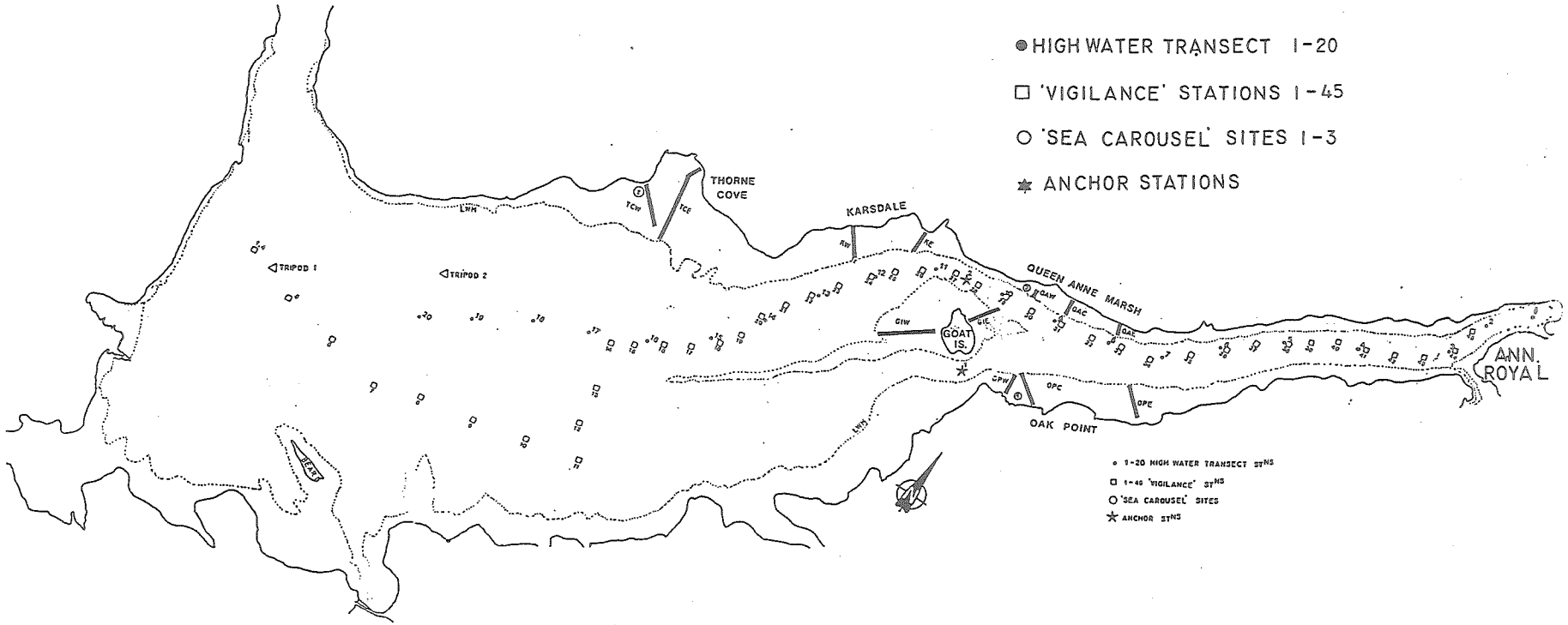

Figure 2.1. Map of Annapolis Basin showing study sites.

numbers procedure. Transects were subsequently surveyed. Locations of transects are given in Figure 2.1, and details of each listed in Table 2.1.

Surface samples were taken for grain size analysis at each sample site. These were returned to the Bedford Institute of Oceanography for analysis using a Sedigraph™. Organic content of replicate pre-dried subsamples was determined following ashing at 550°C in a muffle furnace.

Core samples were taken to a depth of 2 cm into the surface sediment using a 5 ml Neoprene™ syringe. Sediment cores were immediately transferred into a vial containing 10 ml Acetone, wrapped in foil to exclude light, and kept on ice until frozen. Analysis of these cores for chlorophyll *a* and phaeophytins was carried out using a spectrophotometric technique (Strickland and Parsons 1977).

The geotechnical properties of the sediment as a function of depth were investigated at three sites in Thorne Cove near the western transect (TCW). Profiles of undrained strength of the sediment were obtained using a Pilcon Vane and a cone penetrometer. Subsamples of sediment at different depths were taken for laboratory analysis of grain size distribution, Atterberg Limits, water content and specific gravity. Changes in effective stress with the drawdown of the water table were monitored with suction probes inserted at the beginning of the ebb, and recovered on the flood. A discussion of the background to the methodology for geotechnical measurements is included in Appendix 2.1.

Orientation of body and siphons of *Mya arenaria* relative to the prevailent direction of the flood and ebb tidal currents was examined at Thorne Cove.

B. Subtidal Sediments

Bottom sediment samples were taken at 43 stations along a transect from Annapolis Royal to a location south of Digby Gut (Fig. 2.1), using a Van Veen grab deployed from the Fisheries patrol vessel MV *Vigilance*. Surface subsamples were preserved for analysis of grain size using the Sedigraph™, and organic content by ashing pre-dried subsamples at 550°C.

Underwater cameras were leased from Dr. H. Lobsiger and deployed at two stations from a bottom tripod to investigate bottom sediment migration in Annapolis Basin. This study was only partly successful, and no data are presented in this report.

C. Anchor Stations

Two anchor stations were conducted in the channels south (Anchor Station 1) and north (Anchor Station 2) of Goat Island (in what are locally known as Fools Run and Ship Run, respectively). At each hour, depth profiles at one-metre intervals were obtained of temperature and salinity using a Beckman RS 32 salinometer, and current velocity was measured at 1 m depths using a Kahlsico DR current meter. One-litre water samples were taken at surface, mid-depth and near bottom and filtered aboard the vessel through pre-dried 0.4 µm Nuclepore™ filters. Filters were dried and reweighed to provide measurements of suspended particulate matter (SPM).

Table 2.1. Intertidal Transects

Transect Name	Length (m)	No. stations	Distance (m)*
1. Oak Point East (OPE)	350	8	50
2. Oak Point Centre (OPC)	400	9	50
3. Oak Point West (OPW)	400	9	50
4. Goat Island East (GIE)	350	8	50
5. Goat Island West (GIW)	350	8	50
6. Q. Anne Marsh East (QAE)	200	9	25
7. Q. Anne Marsh Centre (QAC)	150	7	25
8. Q. Anne Marsh West (QAW)	150	7	25
9. Karsdale East (KE)	250	6	50
10. Karsdale West (KW)	500	11	50
11. Thorne Cove East (TCE)	900	19	50
12. Thorne Cove West (TCW)	750	16	50

(*Distance between stations on transect)

D. High Water Transit

A survey of suspended sediment concentrations in surface water was conducted along a transect from the outer Annapolis Basin, northeast of Bear Island, to Annapolis Royal, through the channel north of Goat Island (Fig. 2.1). Sampling was carried out from a Zodiac near high water on 10 May in order to obtain as near-synoptic a series as possible (the transit took approximately 1.5 h). One liter samples were filtered through pre-weighed 0.4 μm Nuclepore™ filters before drying and reweighing.

E. Sediment Stability

Direct measurements of *in situ* shear strength of intertidal sediments were obtained at three sites (cf. Fig. 2.1) using 'Sea Carousel', an annular flume designed for field operation. The flume was carried by hand down the intertidal zone during the early stages of the ebb tide, and installed on the sediment in water about 0.5 m depth. This retained water within the annulus, and the flume was operated during the low tide period. Successful deployments were obtained at Thorne Cove, Queen Anne Marsh and Oak Point (Fig. 2.1), but a second attempt at Oak Point failed. Details of operation of the 'Sea Carousel' are provided in Part 3 of this report, relating to the major LISP exercise in Minas Basin.

2.5 Results

A. Intertidal Transects

(a) Grain Size Distribution (Graham R. Daborn)

Results of surface grain size measurements are shown in Figures 2.2 to 2.6. Sediments along the inner transects (Oak Point, Queen Anne Marsh and Goat Island East) were predominantly silty - clays, except for a typical band of coarser sandy deposits at the top of each transect. Clay content tended to increase toward the low water level, although this was far from invariable. The outer transects of Goat Island West, Karsdale and Thorne Cove were predominately sand and silt, and distributions were much more irregular. Each high water to low water transect in Thorne Cove (Fig. 2.6) encountered alternating patches of sand and silt dominated zones, interspersed with occasional gravel areas. Surface characteristics of the Thorne Cove transects were greatly influenced by the presence of boulders and dense beds of blue mussels (*Mytilus edulis*).

(b) Organic Content (Graham R. Daborn)

Percent organic content varied between 0.7% and 3.9% at intertidal transect sample sites (Figs. 2.7 to 2.11). Replicate samples were usually consistent, but occasional wide variations were also found. Distinct patterns were evident in the organic content of some transects : on the innermost lines (e.g., Oak Point East and West,

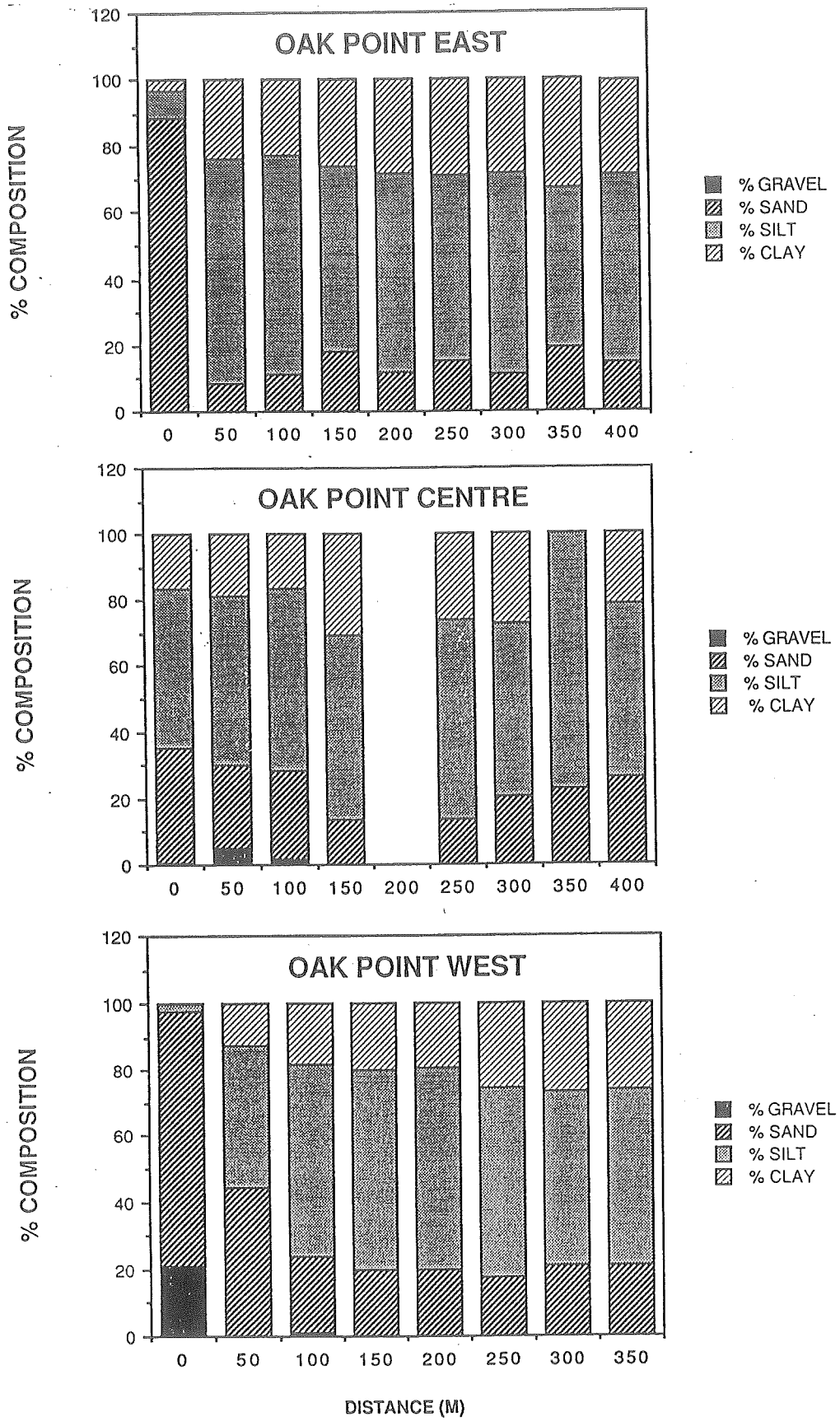

Figure 2.2. Grain size distributions on Oak Point transects.

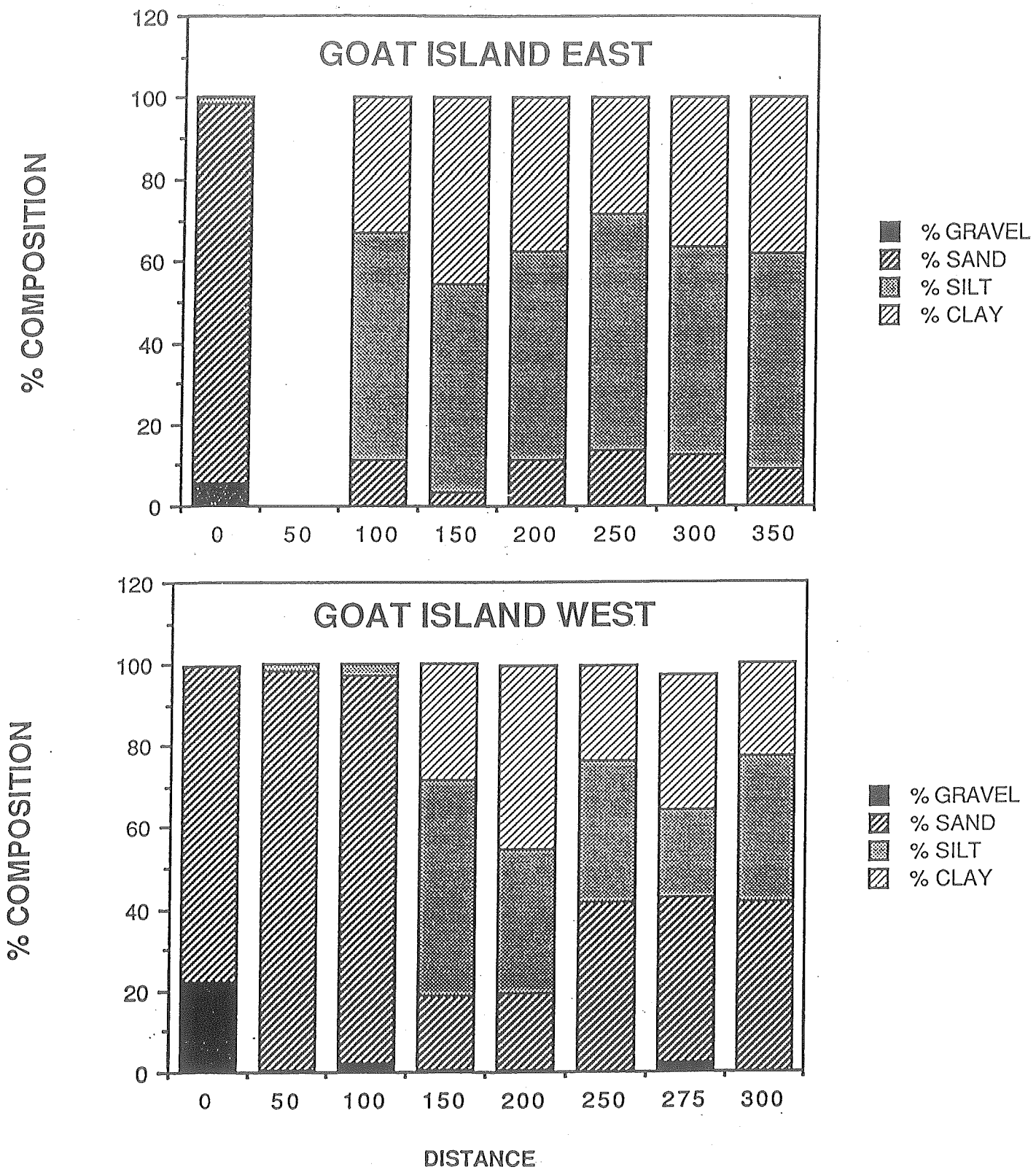

Figure 2.3. Grain size distributions on Goat Island transects.

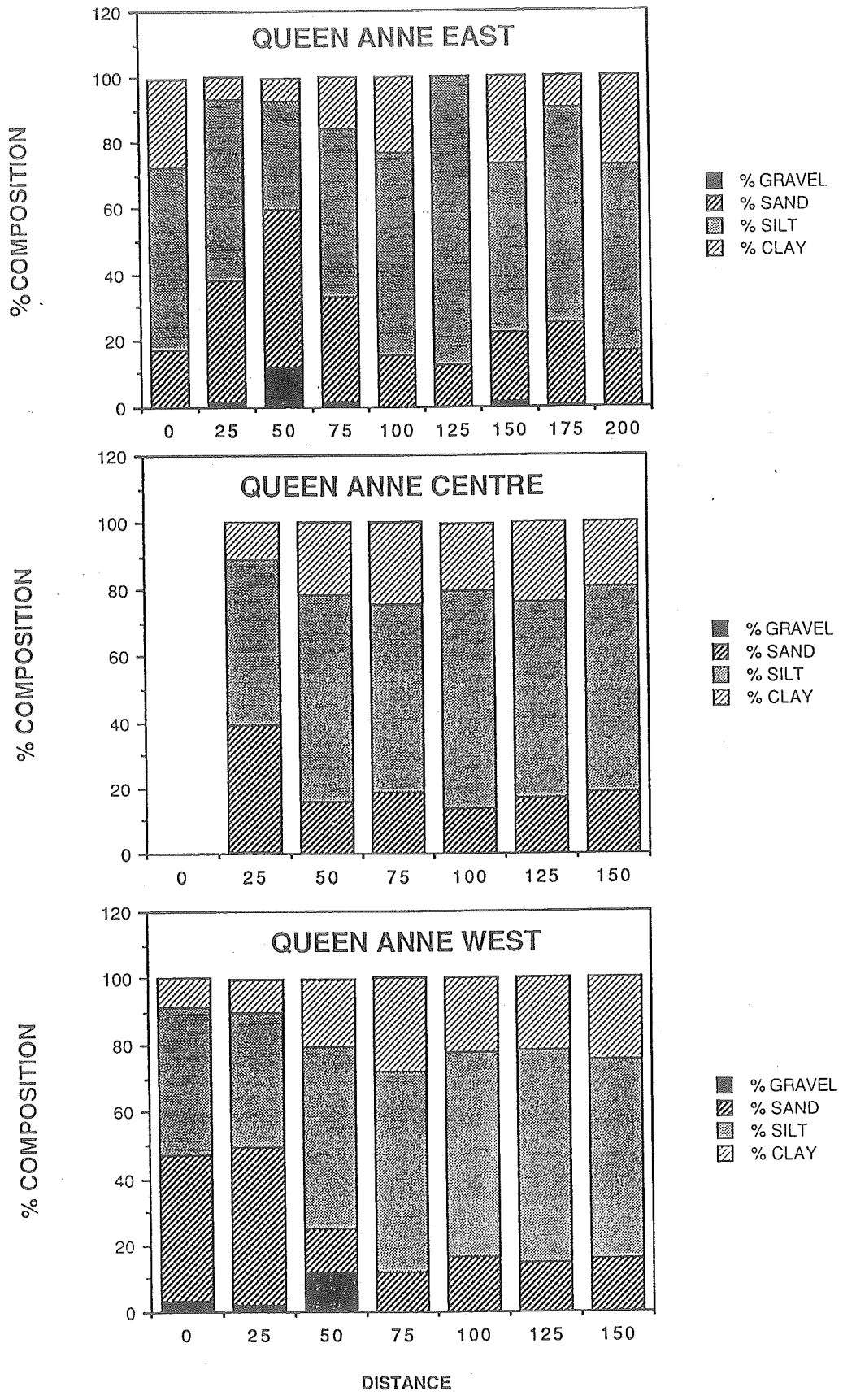

Figure 2.4. Grain size distributions on Queen Anne Marsh transects.

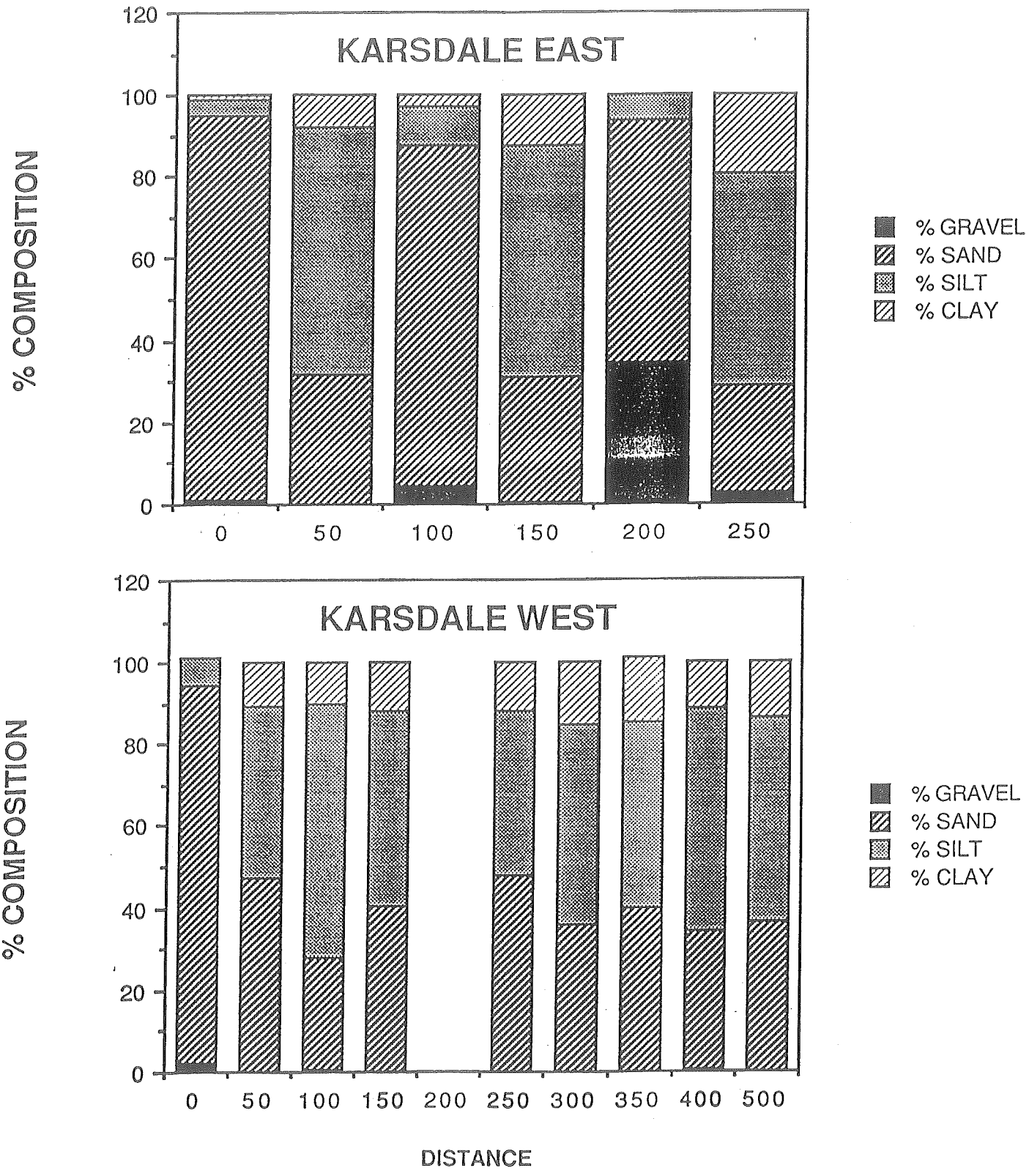

Figure 2.5. Grain size distributions on Karsdale transects.

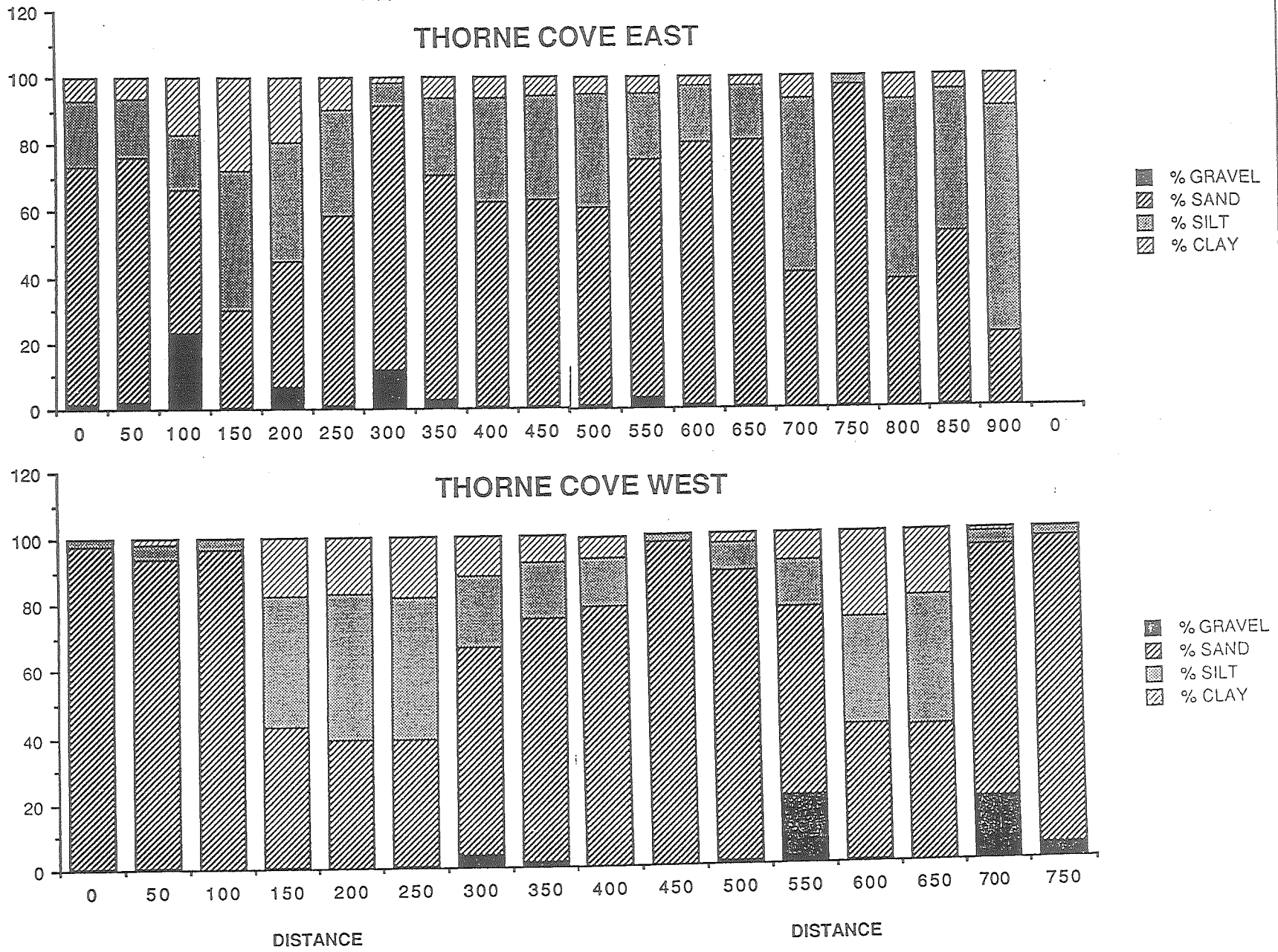

Figure 2.6. Grain size distributions on Thorne Cove transects.

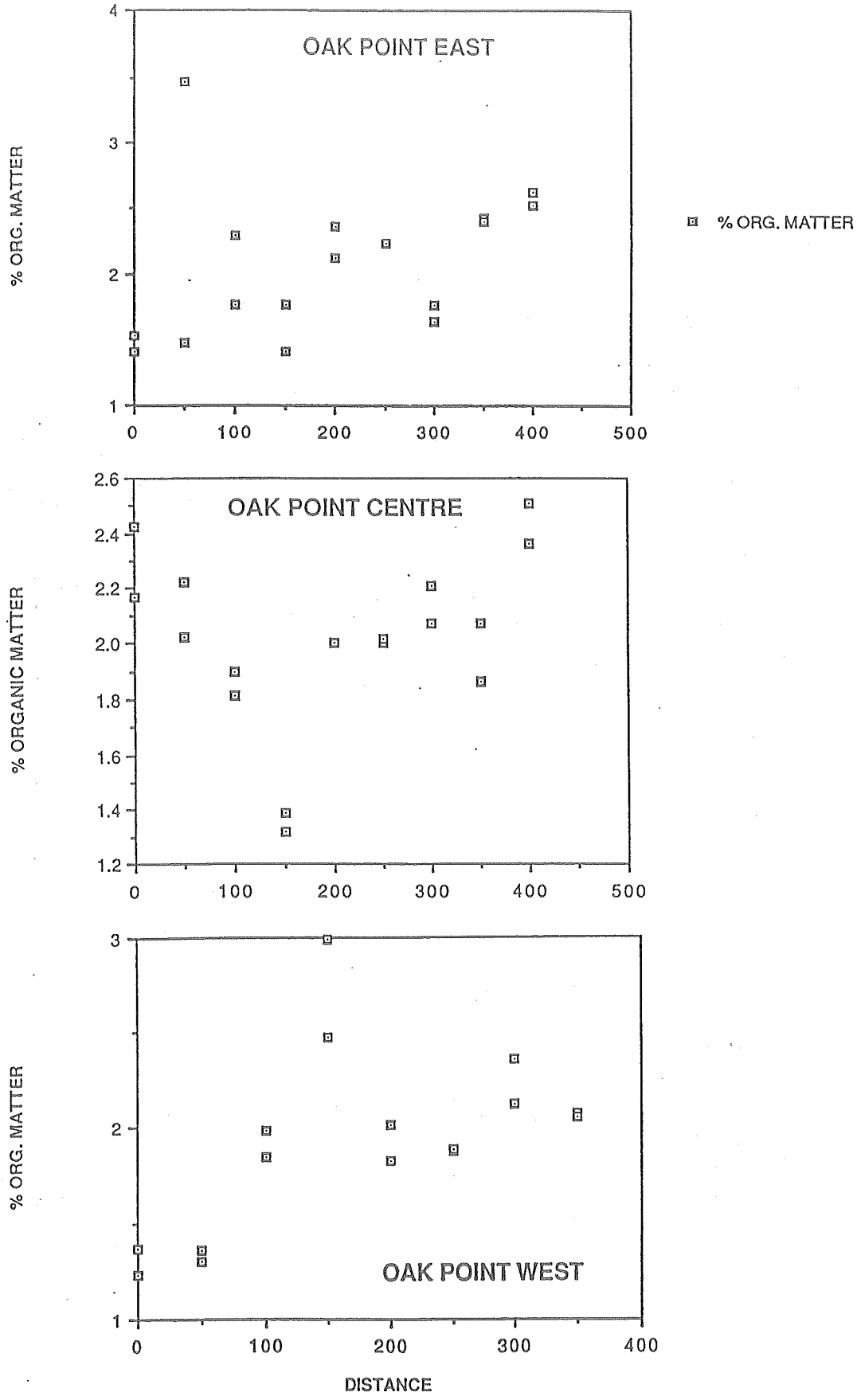

Figure 2.7. Organic content of surface sediments on Oak Point transects.

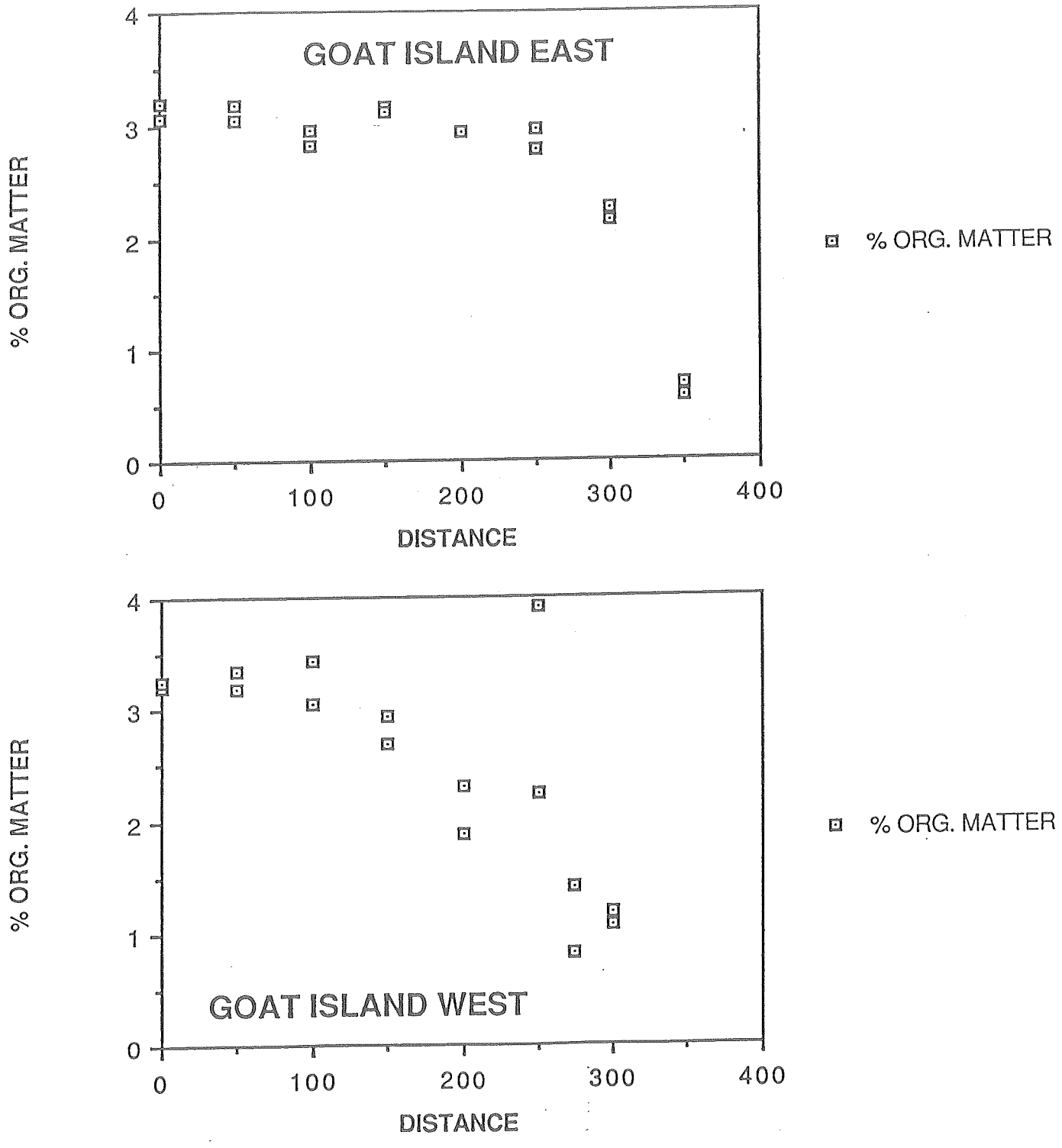

Figure 2.8. Organic content of surface sediments on Goat Island transects.

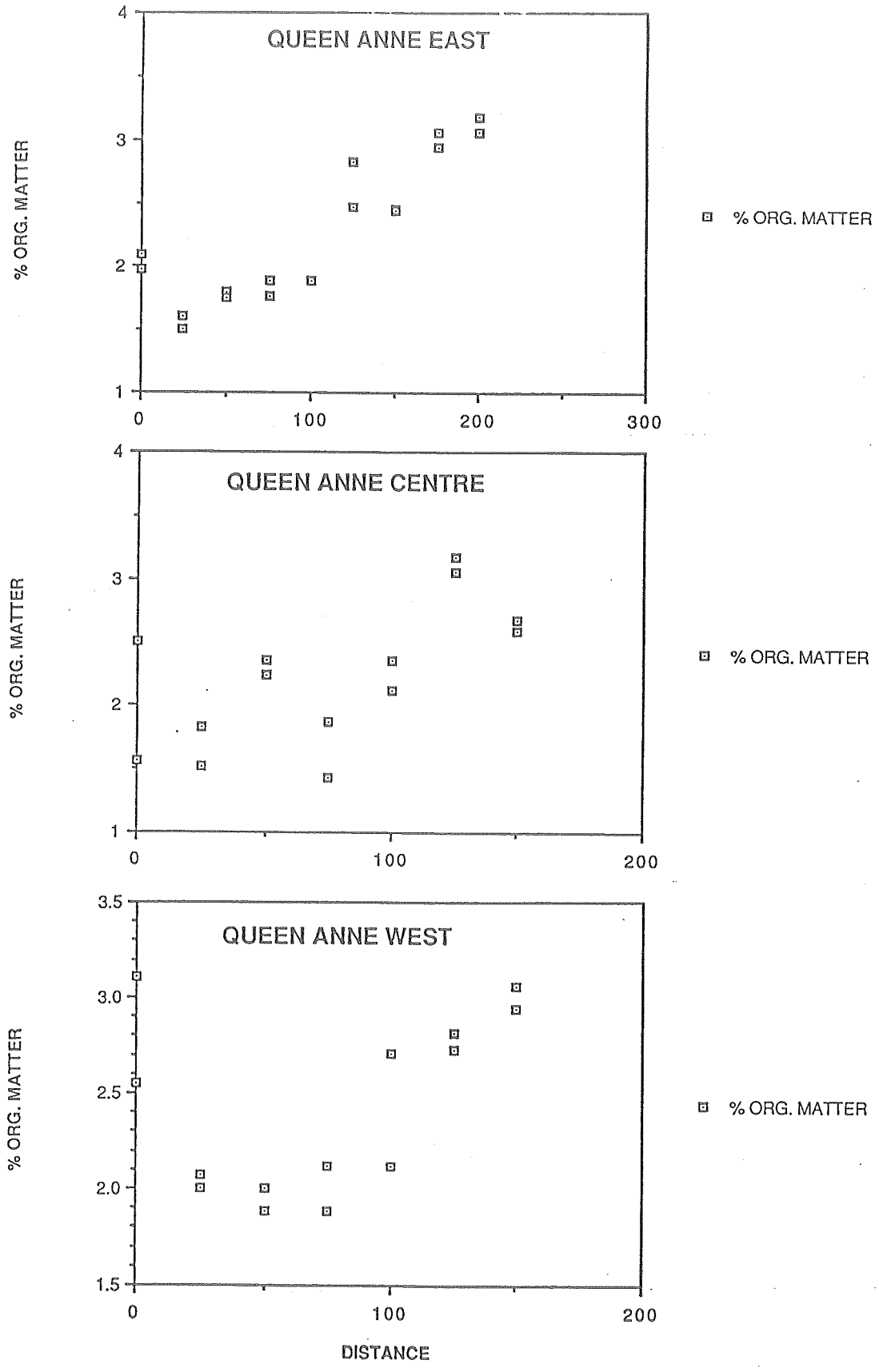

Figure 2.9. Organic content of surface sediments on Queen Anne Marsh transects.

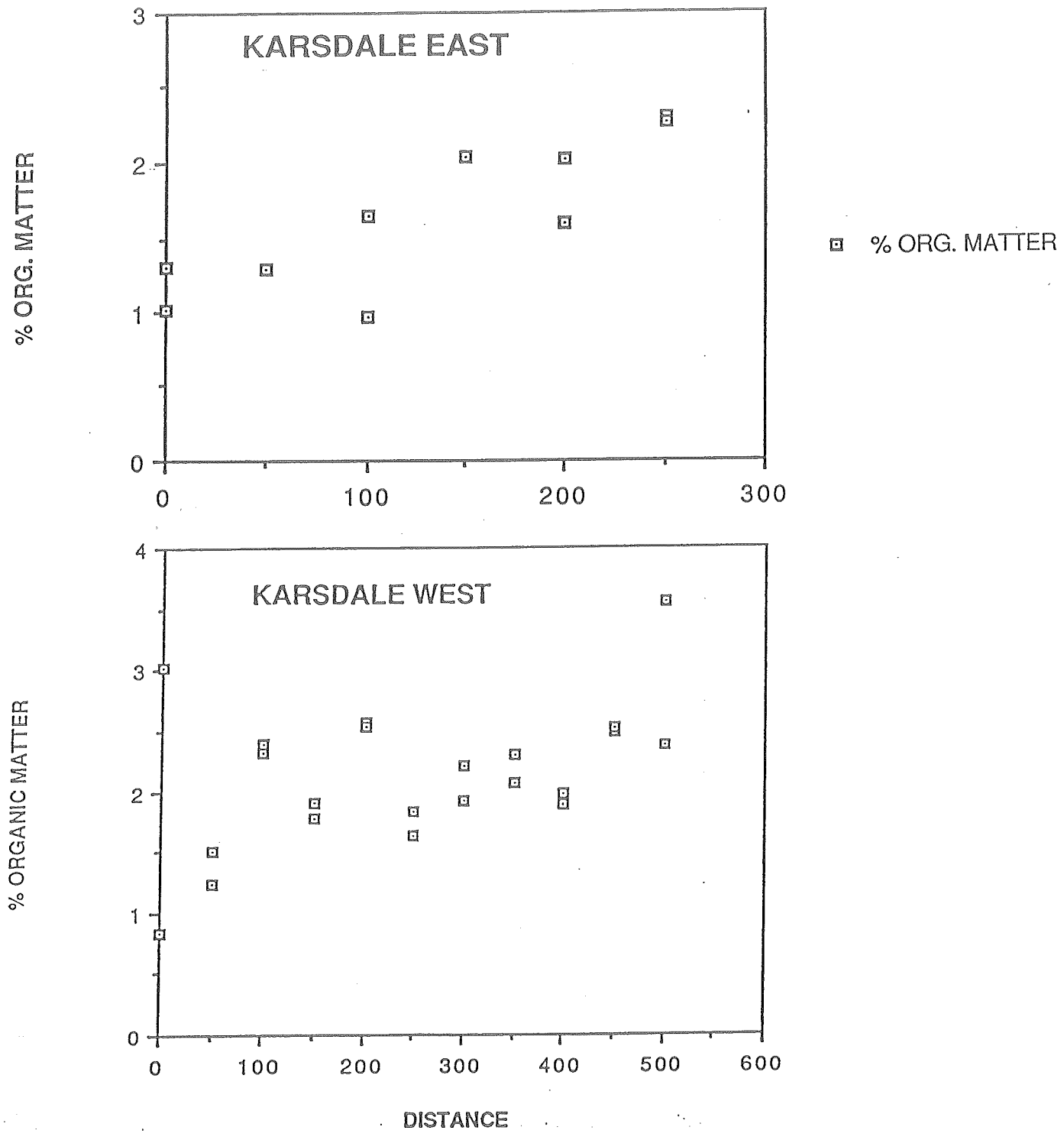

Figure 2.10. Organic content of surface sediments on Karsdale transects.

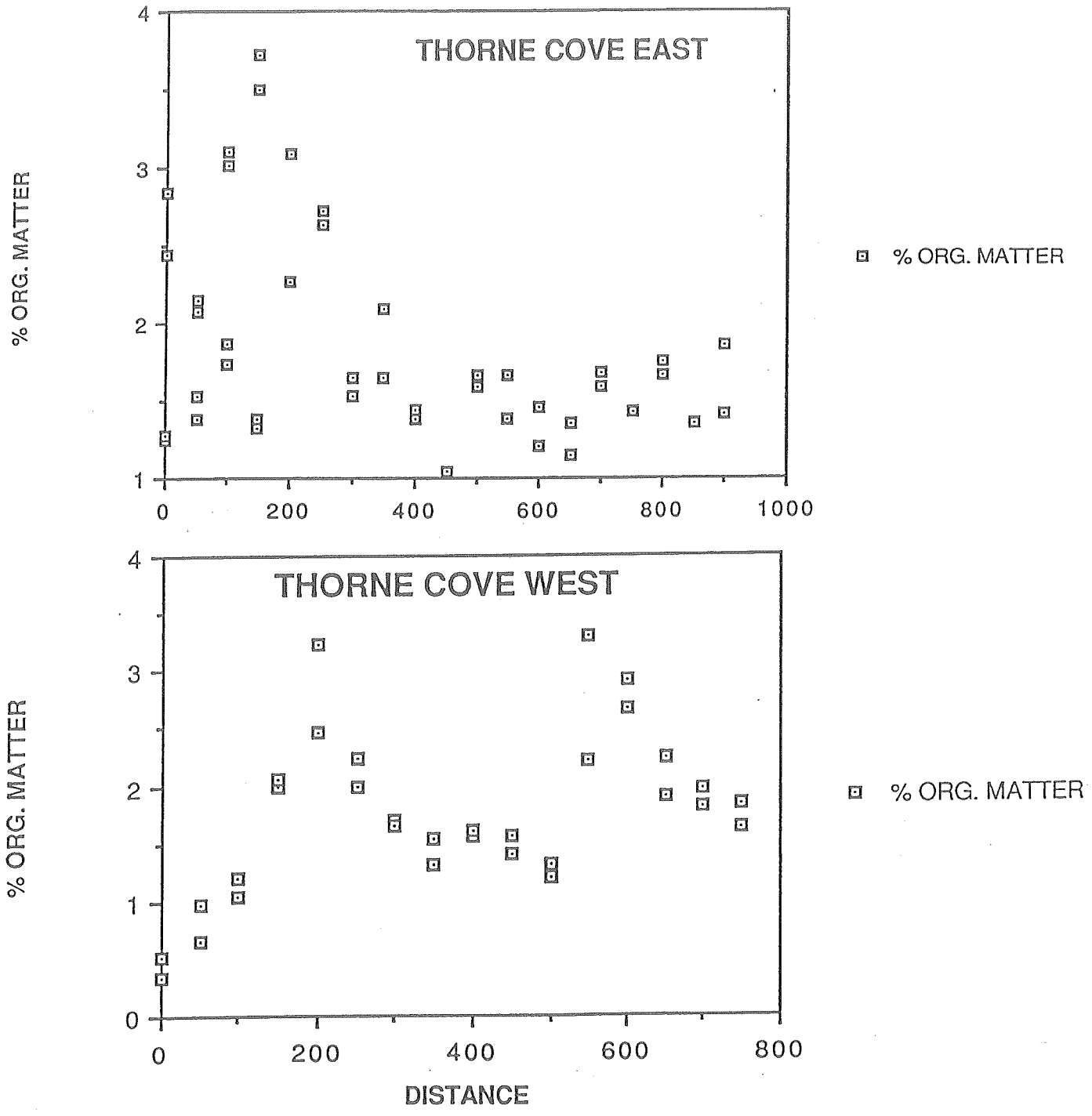

Figure 2.11. Organic content of surface sediments on Thorne Cove transects.

and the three Queen Anne Marsh transects), percent organic matter generally increased from the high water level to the bottom of the transect (Figs. 2.7 and 2.9), in concert with changes in clay content. A similar pattern is evident at Karsdale (Fig. 2.10). In contrast, the two Goat Island transects showed declining organic content with distance down the intertidal zone, despite an increasing clay content. At Thorne Cove a bimodal pattern seemed to be present, with higher organic contents at the landward and seaward ends of the transects, and rather lower, but variable, values in the middle (Fig. 2.11). As indicated before, these transects showed greater variations in topography and roughness in association with gravel deposits and mussel beds.

Average organic content of surface sediments was highest along the Goat Island and Queen Anne Marsh transects, and lowest on the Karsdale and Thorne Cove transects (Table 2.2). These values correspond with the finer sediments that occurred in the inner portions of the study area.

(c) Chlorophyll Content (Graham R. Daborn)

Determinations of total chlorophyll concentration at each station are shown in Figures 2.12 to 2.16. Values were often highly variable from site to site, ranging from 10 to 35 $\mu g/cm^2$. The variability may be attributed to the naturally patchy distribution of benthic diatoms, and the fact that samples were taken at rather wide intervals of time as the transects were established. In addition, fine sediments commonly exhibit high chlorophyll values even though the chlorophyll may be inactive. There was no obvious difference between chlorophyll values at inner and outer transects, but the highest values were found in the more easterly transects.

A more synoptic set of total chlorophyll measurements was obtained from the Queen Anne Marsh intertidal zone during deployment of 'Sea Carousel' on 12 May 1990 (deployment No. 3). A total of 23 samples yielded a mean value of 22.44 ($\pm$ 3.37) $\mu g/cm^2$.

(d) Geotechnical Properties (Harold Christian)

Three sample locations were selected along a transect perpendicular to the shoreline near Thorne Cove (Fig. 2.17), beginning immediately offshore from the zone where sands directly overlie boulders, and ending near the low water mark. The intermediate site (TC-1 and TC-3) was selected near the site of deployment of 'Sea Carousel' (q.v. below). Site TC-1 was tested at 08.00, on 12 May using the Pilcon Vane and the cone penetrometer. Suction probes were installed as the tide ebbed, and registered immediately the state of suction within the sediment; they were removed as the tide covered the site again. Density and fluid content subsamples were obtained by excavating a test pit. On 13 May all three sites (TC-2, TC-3 and TC-4) were tested and subsampled. Table 2.3 lists the site, depth interval below the mudline, and the type of samples taken.

Fluid contents and bulk densities are shown in profile form in Figure 2.18 for all sites. Notice that there is a general reduction in fluid content from a maximum of about 80% in the vicinity of the sediment surface to a minimum of 35% at 20 cm, after which it increases again. The greatest change occurred in the top 5 cm. Without grain size and plasticity data, it is not possible to rule out varying texture as an explanation for the changes in

Table 2.2. Mean Organic Content Along Intertidal Transects

Transect	Mean % Organic Content	N
OPE	2.082	18
OPC	2.019	18
OPW	1.921	16
GIE	2.614	16
GIW	2.492	16
QAE	2.252	18
QAC	2.231	14
QAW	2.427	14
KE	1.645	12
KW	1.992	20
TCE	1.827	46
TCW	1.750	32

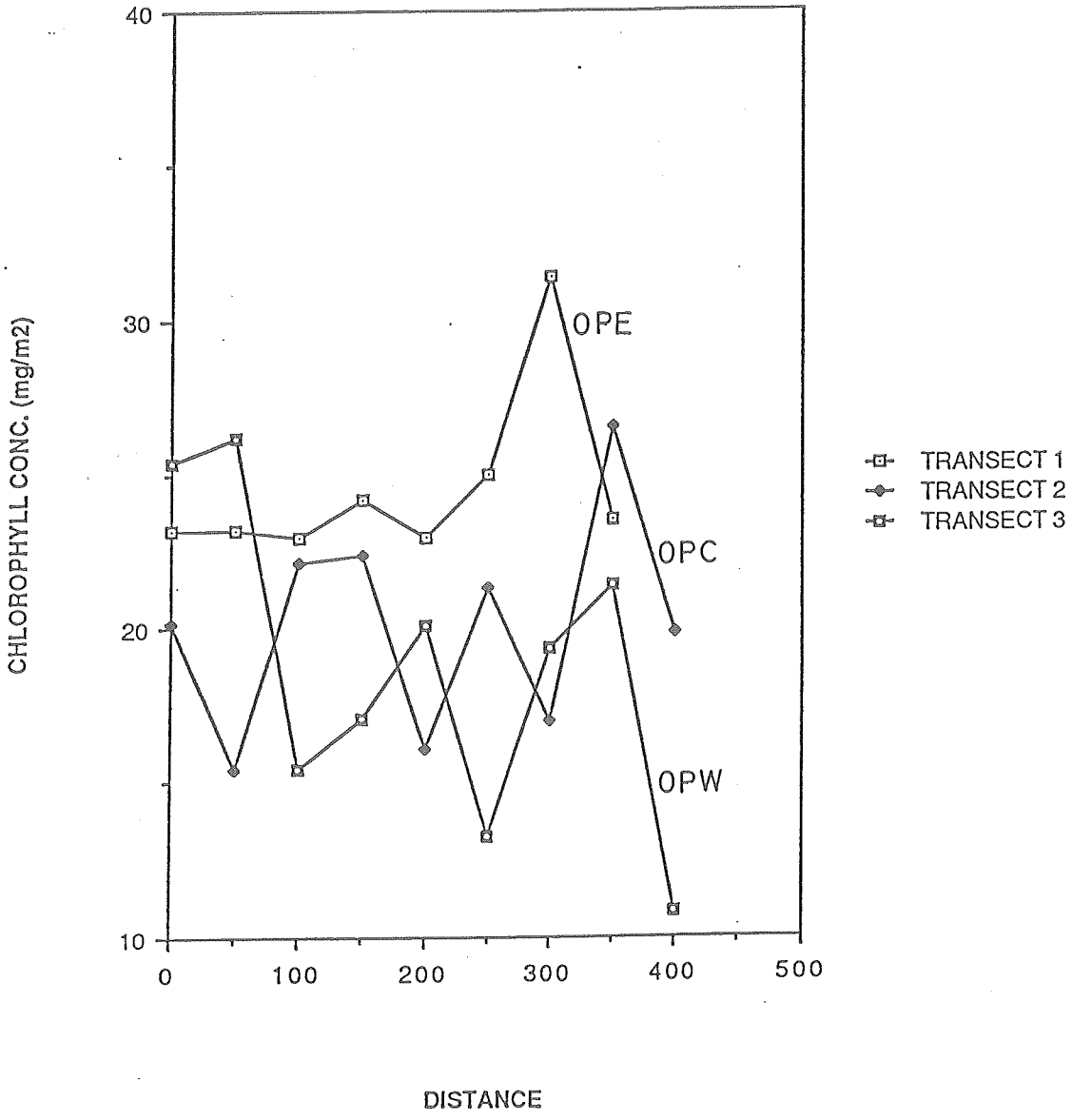

Figure 2.12. Chlorophyll concentrations in surface sediments on Oak Point transects.

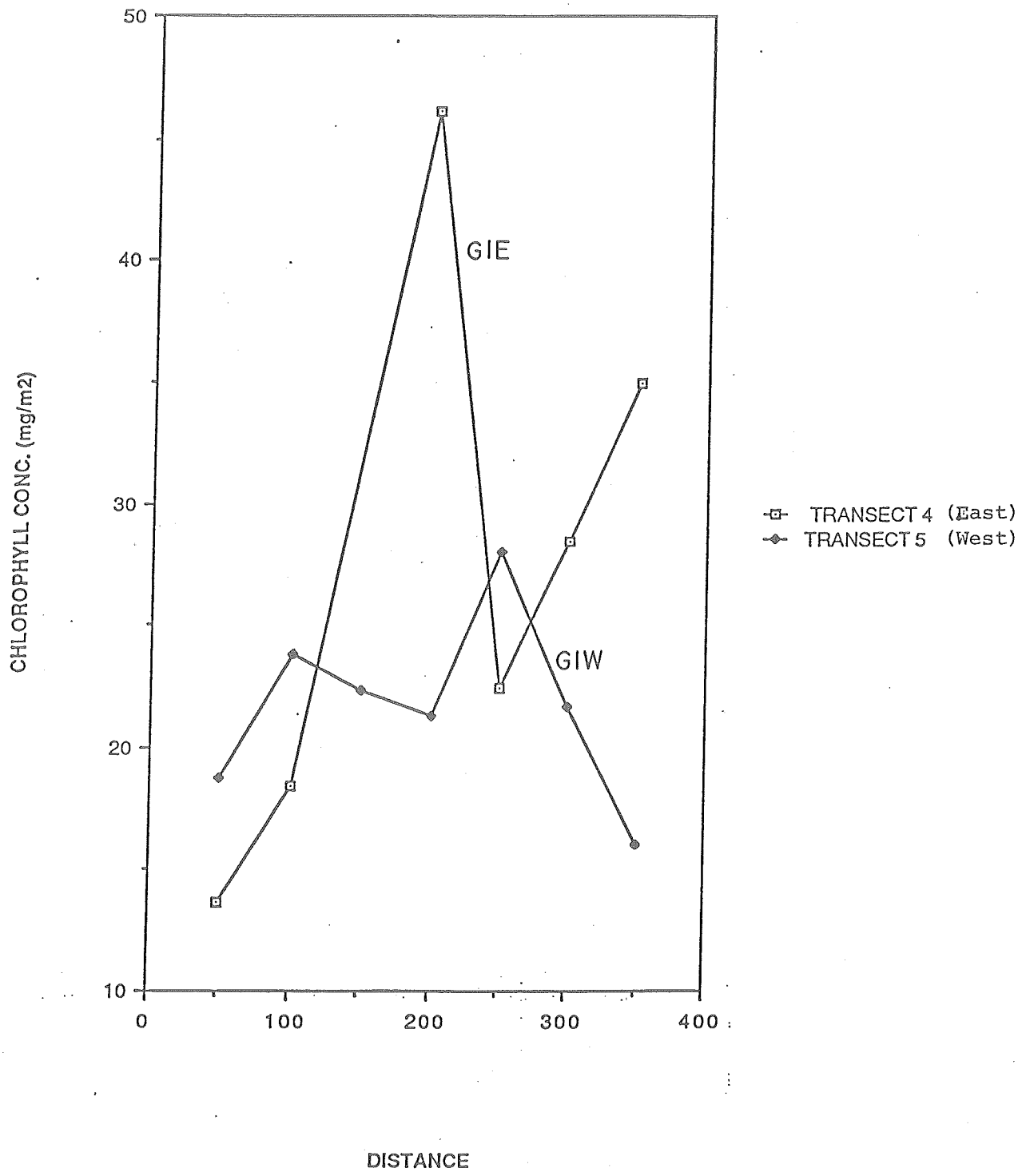

Figure 2.13. Chlorophyll concentrations in surface sediments on Goat Island transects.

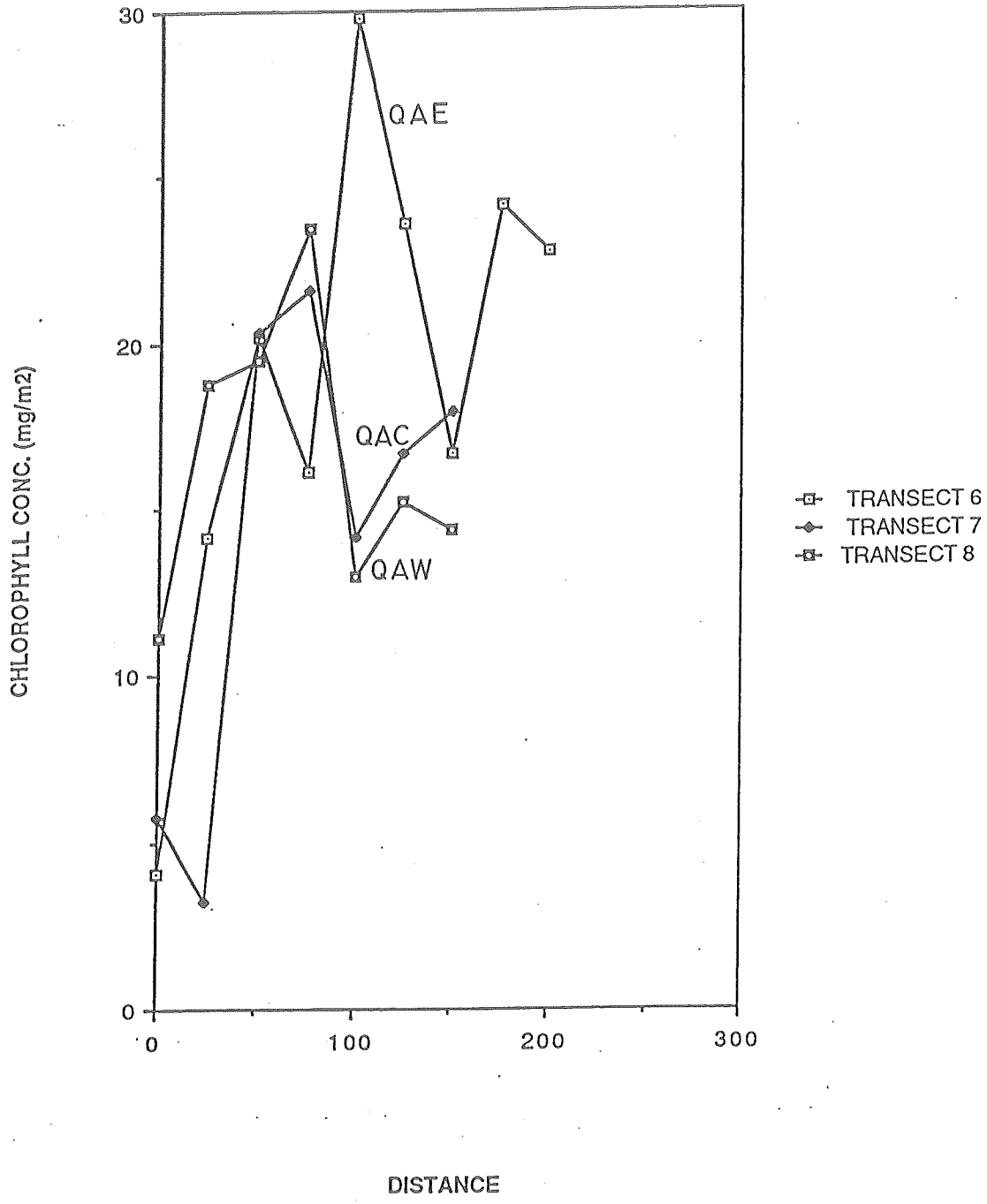

Figure 2.14. Chlorophyll concentrations in surface sediments on Queen Anne Marsh transects.

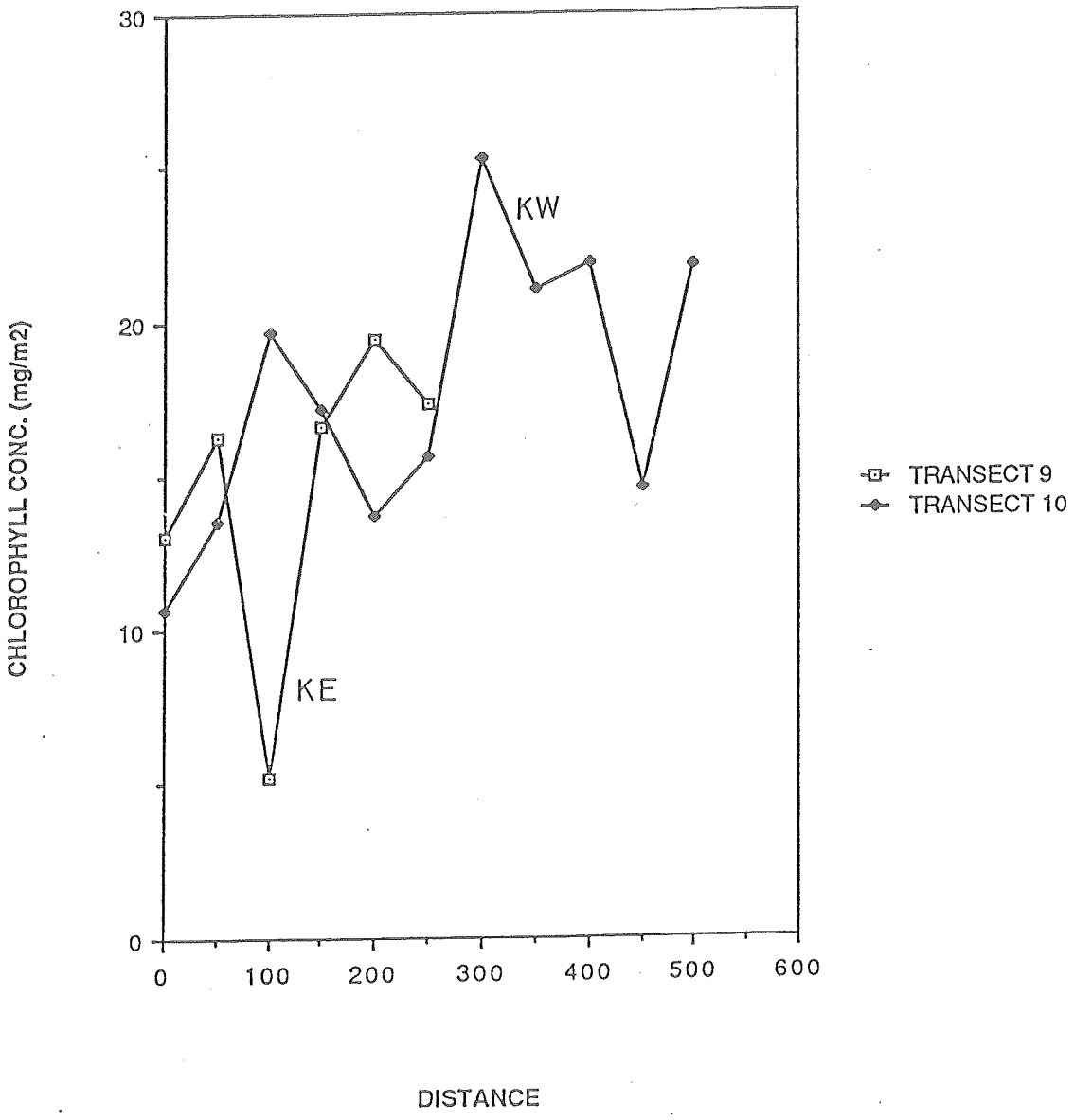

Figure 2.15. Chlorophyll concentrations in surface sediments on Karsdale transects.

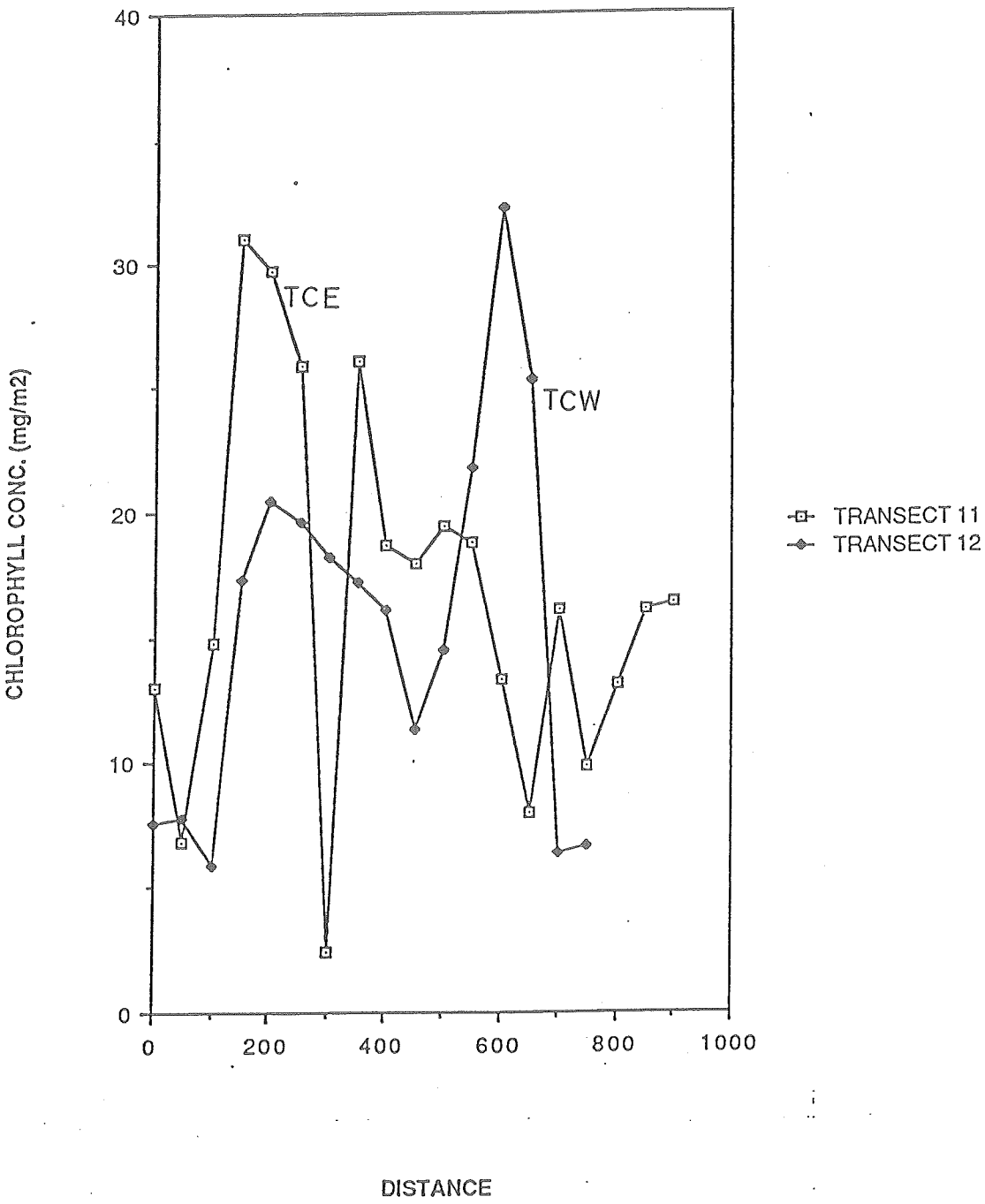

Figure 2.16. Chlorophyll concentrations in surface sediments of Thorne Cove transects.

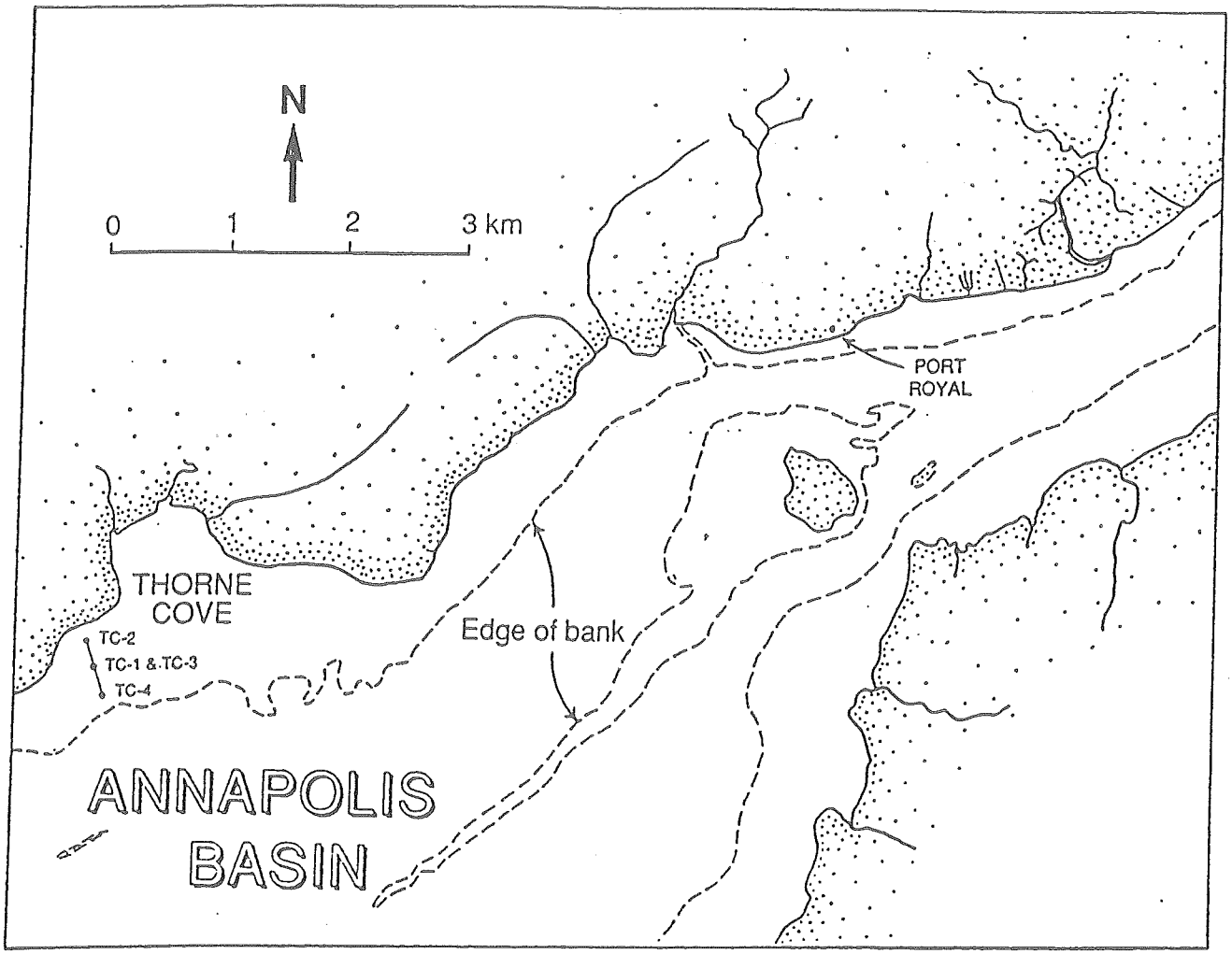

Figure 2.17. Location of sites for geotechnical studies.

Table 2.3. Summary of Geotechnical results from subsamples taken at Thorne Cove

Site	Burial Depth (cm)	Fluid Content (%)	Bulk Density (g/cm^2)	Grain Size	Atterberg Limits	Comments (E=Ebb tide) (F=Flood tide)
TC-1	7	48.3	-	-	-	E
	14	35.3	1.612	-	-	E
TC-2	7	26.0	1.868	-	-	E
	24	35.9	1.841	-	-	E
	35	50.4	1.719	-	-	E
TC-3	0	74.0	1.546	-	-	E
	1	72.5	1.532	-	-	E
	5	41.0	1.528	-	-	E
	10	42.3	1.762	-	-	E
	20	31.2	1.899	-	-	E
	25	36.3 -	-		-	E
TC-4	1	35.1	1.701	-	-	E
TC-2	1	27.4	1.944	-	-	F
TC-3	1	49.2	1.664	-	-	F
TC-4	1	45.2	1.749	-	-	F
TC-1	10	-	-	Y	Y	E
TC-2	0-6	-	-	Y	-	E
	24-30	-	-	Y	Y	E
TC-3	0-1	-	-	Y	Y	E
	0-5	-	-	Y	Y	E
	15-20	-	-	Y	Y	E
	20-25	-	-	Y	Y	E

(N.B. Cone penetrometer tests were only conducted at TC-1; however, this site corresponds to TC-3 which was tested the following day.)

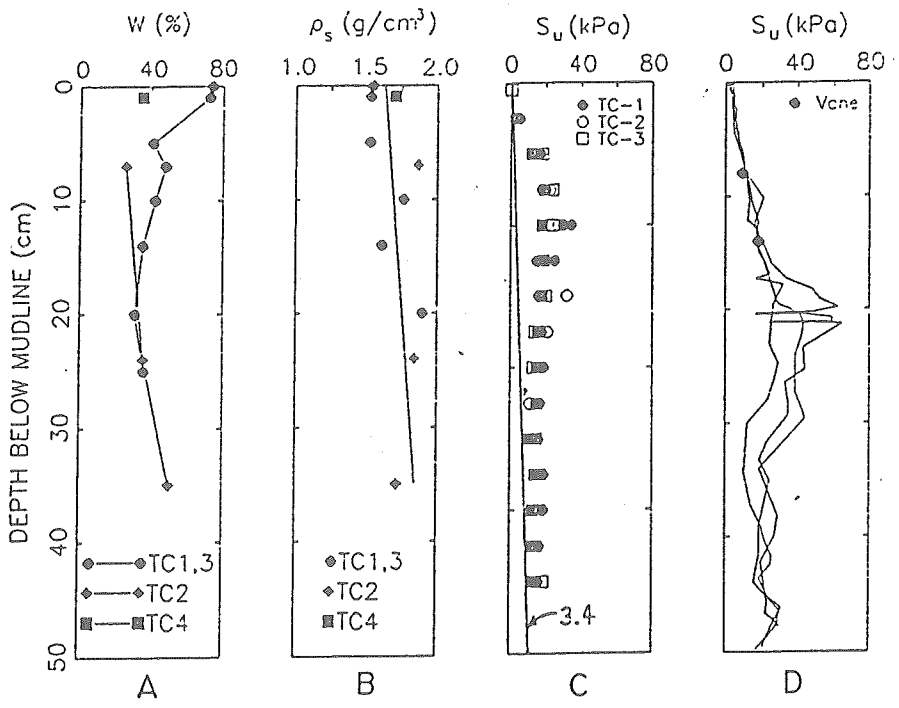

Figure 2.18. Profiles of geotechnical properties from sites in Thorne Cove. A - Water content; B - Bulk density; C - Shear strength from Pilcon Vane at sites TC 1, 2 & 3; D - Shear strength from Pilcon Vane and Cone penetrometer at TC 1 & 3.

moisture content. It may be that variations in fluid content with time and storm activity affect the upper 20 cm only, which is therefore a suspension (and consequently more mobile) rather than a coherent sediment mass that can transmit shear stresses. Presence of old buried shell agglomerations influence the stability of the mudflat, and may directly affect the measured shear strengths. For this reason, some of the strength data (the higher peaks) have been ignored, and a general profile trend has been added to panel c in Figure 2.18 that is believed to represent the best estimate of the intact undrained shear strength. This line corresponds to a ratio of S_u/P'_o equal to 3.4 $kPa.m^{-1}$. A normally consolidated sediment exhibits a S_u/P'_o of 0.25 (Skempton 1970); therefore it may be concluded that this deposit is overconsolidated and is more stable than a freshly deposited sedimentary clay sequence.

Application of SHANSEP in this environment is based on the undrained strength profile produced by the cone penetrometer using a cone factor equal to 15, coupled with an effective stress profile (derived from equation 3, Appendix 2.1), which makes use of the bulk density data collected and given in Table 2.3. Predicted values of OCR (Overconsolidation Ratio) are extremely high (typically >100) and therefore preconsolidation pressures are similarly high (typically 50-100). This supports the previous observation that the sediments below the surface of the mudflat are overconsolidated to a high degree relative to existing stresses. The magnitude of the preconsolidation pressure is unrealistically high and cannot be explained by any physical processes. They are clearly an artifact of limitations of the SHANSEP procedure at very low effective stresses. Generally, S_u/P'_o ratios exceeding 10 have not been widely observed in nature, but they occur frequently in marine settings near the mudline where effective stresses are below 1 kPa. Since the SHANSEP technique is based upon terrestrial clays tested at large stresses, there is a limitation in the technique. Consequently, the stress history cannot be deduced in the absence of proper measurements of preconsolidation pressure in the laboratory. As indicated in Appendix 2.1, it is next to impossible to sample such soft material and maintain it in an undisturbed state.

The assessment of the stability of a mudflat is a complex problem that involves the sediment bulk properties, the stress history, and the environmental loading processes, all of which affect the available shearing resistance. It is not the purpose of this study to investigate the interrelationships between these factors—this is an initial assessment of the present-day profile of bulk properties at one selected site within a much larger estuarine system. The observations made herein reflect the relatively small scale of the investigation; they are therefore preliminary and subject to revision.

Nonetheless, one can draw tentative conclusions about the superficial sediments of Thorne Cove as they presently exist. From the undrained strength observations, the clays are preconsolidated to a high degree compared with most open marine clays. This conclusion is supported by the high ratio of undrained shear strength normalized by vertical effective stress as compared to reported ratios for normally consolidated clays, and indicates that some form of cementation may be present. Other processes that could give rise to such a high level of shearing resistance are winter loading by grounded ice, cyclic wave loading, cyclic desiccation, and biogenic cohesion. The actual cause of the phenomenon at Thorne Cove cannot be ascertained without further detailed study to establish cause-effect relationships between the physical behaviour of the sediments and all local environmental processes.

substantially from that predicted in tide tables. Maximum recorded depth occurred at 0100 and 0600 instead of the predicted high water time of 0310, although predicted times of low water were approximately correct (Fig. 2.25). Very rapid changes of depth occurred around the effective local high water, probably because of movement of the vessel which was anchored only at the bow. It is also probable that the southern channel, which is considerably shallower than the northern channel and shoals towards the eastern end, is influenced by eddies induced by Goat Island itself. No information is available on current direction, however deck notes record that ship direction did not reverse until more than one hour after predicted low water.

Temperature and salinity measurements indicate that the water column varied from being completely mixed during most of the flood tide to being moderately to strongly stratified on the ebb (Fig. 2.24). Salinities ranged from 31-35 ‰ and temperature between 6 and 8°C. Current velocities reached a maximum of 1.1 $m.s^{-1}$, the profiles confirming the existence of at least two-layer flow during both ebb and flood.

Suspended sediment concentrations in surface waters were consistently less than 10 $mg.l^{-1}$, and showed little variation over the tide. Bottom samples, however, ranged up to 25 $mg.l^{-1}$, and were generally higher during the flood period, declining around high water and into the early ebb (Fig. 2.25). Sharp increases in SPM levels on the flood tide indicate that resuspension of deposited sediment was occurring. As noted above, the sediments in this portion of the estuary are fine, non-cohesive silts, and therefore easily resuspended.

Anchor station 2 on the north side of Goat Island was occupied from 1000 h on 10 May to 1100 h on the 11th. As with station 1 depth also varied irregularly over the tidal cycle, from 9 to 16 m (Fig. 2.26). Following low water near the predicted times of 1035 and 2300 h, depth increased during the initial phase of the flood, but then appeared to decrease for 1 to 3 hours before rising again. High water was subsequently delayed by at least an hour beyond that predicted in tide tables. The decline in depth at mid-flood, followed by a steep increase, may be related to drift of the vessel in response to variation in direction of surface outflow.

Unlike station 1, water column profiles demonstrate that the northern channel remains stratified for almost all of the tidal cycle, becoming partially mixed only during the final phase of the flood. Salinity varied between 31 and 35 ‰, and temperature from 6-11°C, reflecting the greater heat contributed by the river outflow (Fig. 2.27). SPM concentrations at this station were always <20 $mg.l^{-1}$; occasionally surface values exceeded those at greater depths, probably reflecting the turbidity of the river water that remained at the surface. Some indication of resuspension may be seen in the bottom samples during the flood, but the pattern was not consistent. Current velocity profiles indicate a complex structure to the water column, with distinct two-layer flow occurring during early flood, and highly variable patterns at other stages. Flow during the ebb reflected the slope between water levels in the estuary and the sea, with maximum velocities of c. 80 $cm.s^{-1}$ near the surface, and declining steadily with depth. Irregularities in the velocity profiles may be related to eddies generated around Goat Island.

D. High Water Transit

Results of the survey of surface suspended sediments conducted around high water on 10 May are shown in Figure 2.28. Values ranged between 10 and 28 $mg.l^{-1}$ on the seaward (westward) side of Goat Island (stations

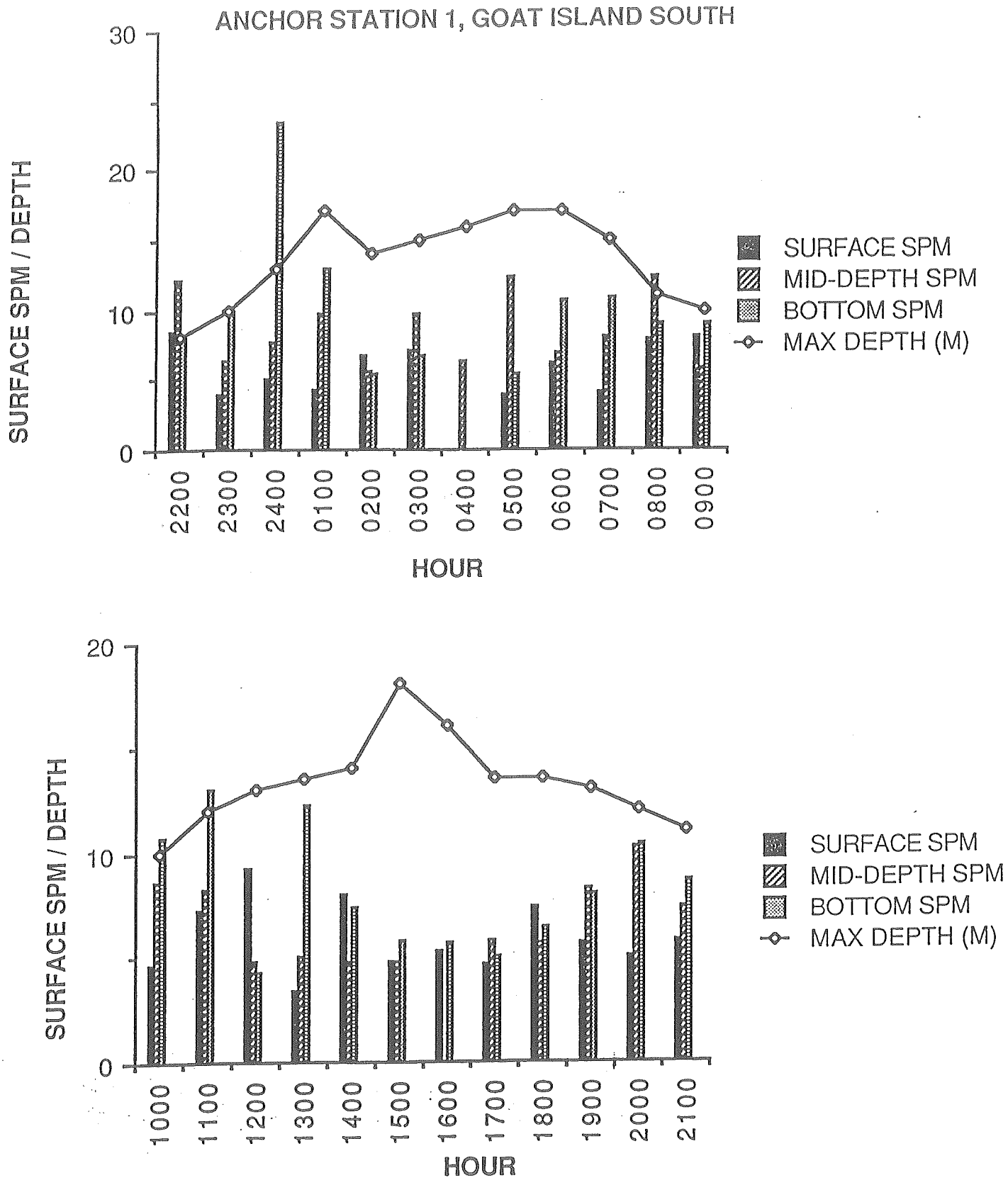

Figure 2.25. Suspended particulate matter during Anchor Station 1, south of Goat Island, 8-9 May 1989.

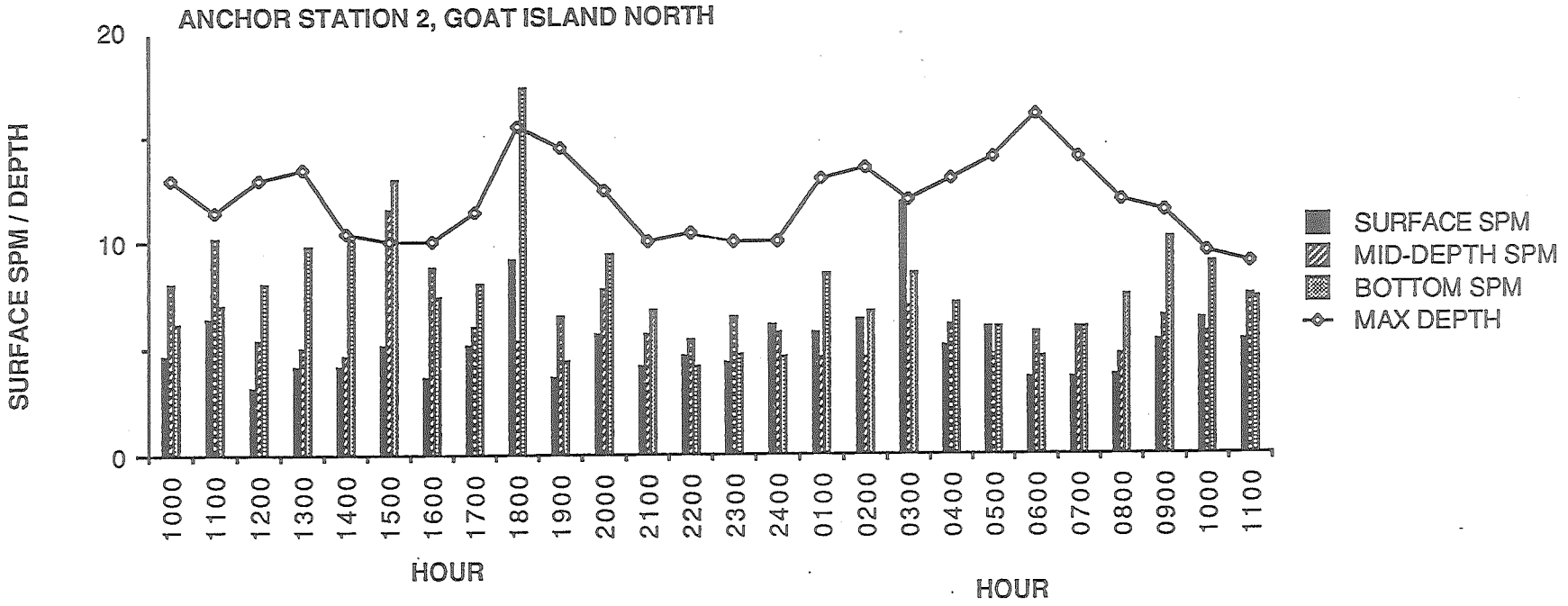

Figure 2.26. Suspended particulate matter during Anchor Station 2, north of Goat Island, 10-11 May 1989.

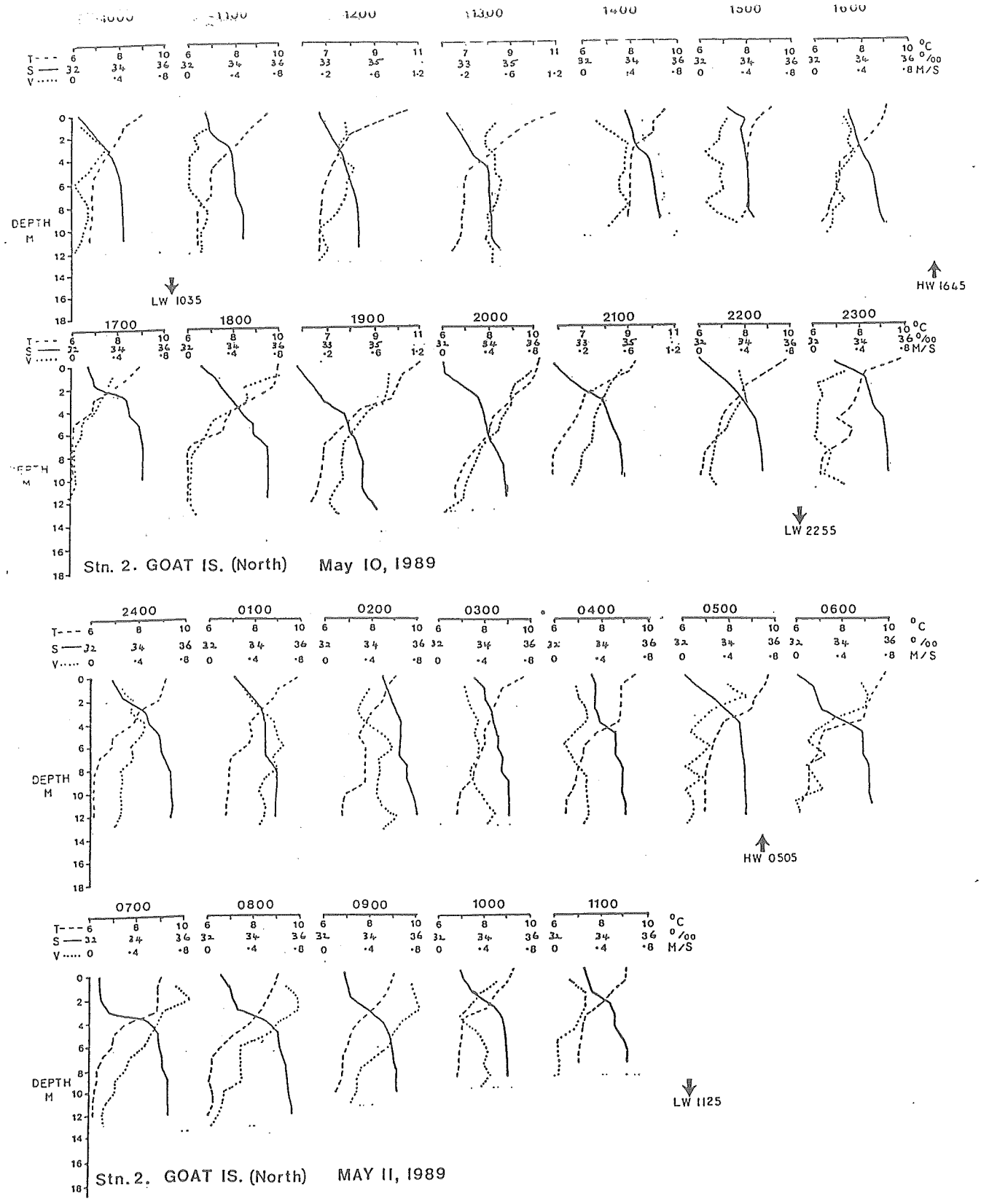

Figure 2.27. Depth profiles of salinity, temperature and current velocity over 2 tidal cycles at Anchor Station 2, north of Goat Island, 10-11 May 1989. T = temp (°C), S - salinity (‰), V - velocity ($m.sec^{-1}$).

11 to 20), and between 15 and 38 mg.l^{-1} at the inner stations. Salinity and temperature data have been abandoned because of a faulty instrument.

E. Sediment Stability

A primary objective of the Annapolis MiniLISP project was examination of the strength of intertidal sediments, and the experimental testing of 'Sea Carousel', a new device for *in situ* measurement of erodibility developed by C.L. Amos. Technical details and description of 'Sea Carousel' are included in Part 2 of this report, which deals with the study in Minas Basin.

Three deployments were obtained during the course of MiniLISP, at Oak Island Marsh, Thorne Cove and Queen Anne Marsh, respectively. Locations are given in Figure 2.1. A fourth attempted deployment on Oak Island Marsh failed. All deployments were intertidal, and conducted during the low water period. The 'Sea Carousel' was carried by hand down the intertidal zone as the tide was falling, and settled into place when water depth was about 50 cm so that the annulus and inner ring were filled with seawater. During the deployment, lid rotation was increased incrementally and maintained at each new speed for several minutes. In all three locations, water level inside the annulus fell during the course of the experiment, partly because of losses around the lid as a result of centrifugal forces, and partly because of leakage beneath the walls, especially where polychaetes or clams were numerous. Attempts to prevent leakage around the annulus through siphon holes by packing mud around 'Sea Carousel' were only partially successful, and the extensive walking around the site while doing so resulted in considerable disturbance of the mudflat. For this reason, it was decided to conduct the measurements underwater during the main LISP exercise in Minas Basin. Calibration of optical backscatter (OBS) sensors was obtained by subsampling the water column in the annulus during the extensive deployment on Queen Anne Marsh, and determining the SPM levels gravimetrically.

Full results of the Annapolis deployments are given in Part 3 of this report, but summary results are shown in Figure 2.29. It is evident from this figure that sediments at Queen Anne Marsh are notably different from those at both Oak Point and Thorne Cove in that the critical shear stress for erosion increases much more rapidly with depth at that location than at the others, indicating that this intertidal location is much more resistant to resuspension. Queen Anne Marsh had a well-developed benthic community, and at the time exhibited an extensive settlement of young clams. Mean organic content at Queen Anne Marsh was higher than at the other two sites (cf. Table 2.2), and mean total chlorophyll of 23 samples taken from undisturbed areas around 'Sea Carousel' was 22.44 μg/cm^2—significantly higher than the average for the three Queen Anne Marsh transects (16.81 ± 6.56 cf. Fig. 2.14). By contrast, Oak Point chlorophyll values collected on 6 May averaged 20.99 μg/cm^2 (± 4.57). Thorne Cove chlorophyll levels averaged 16.43 (± 7.36); as with Queen Anne Marsh, there was a biologically well-developed benthic community at Thorne Cove, although it was dominated mainly by mussels rather than clams.

Results from a study of soft-shell clam behaviour during the 'Sea Carousel' experiment, conducted by T. Rowell and J. Grant, are not currently available.

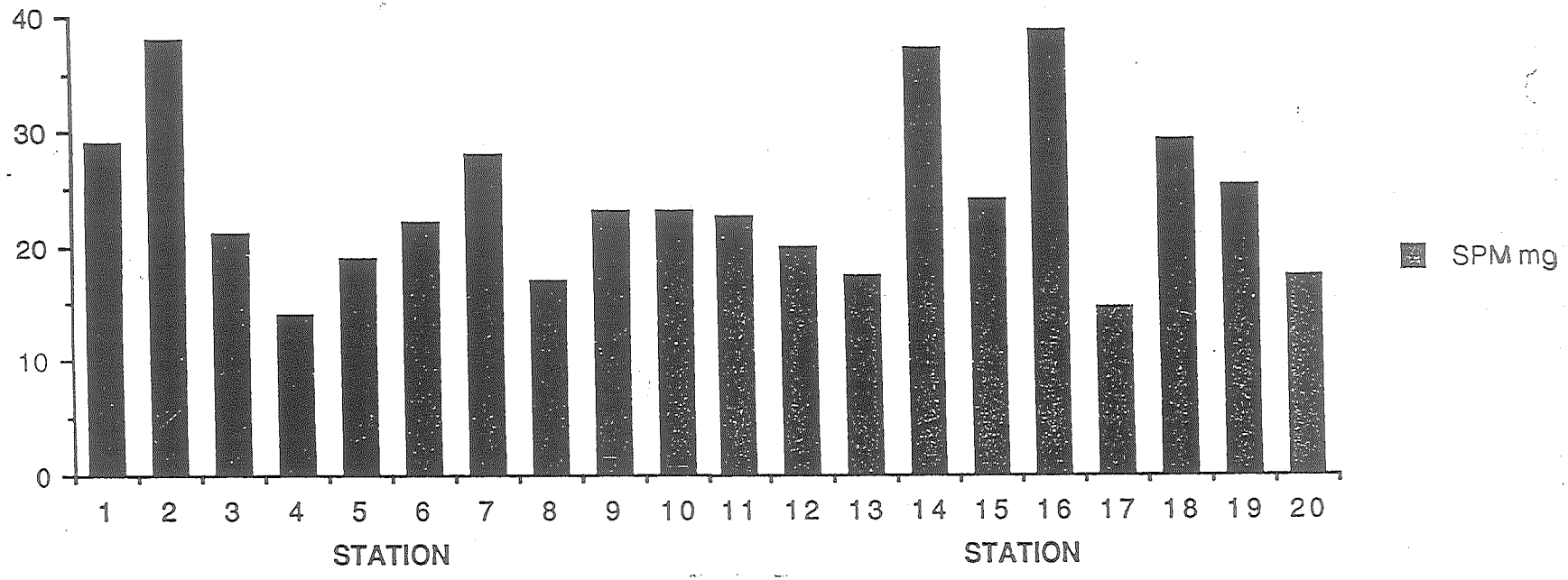

Figure 2.28. Suspended particulate matter in surface waters of the Annapolis Basin, 10 May 1989.

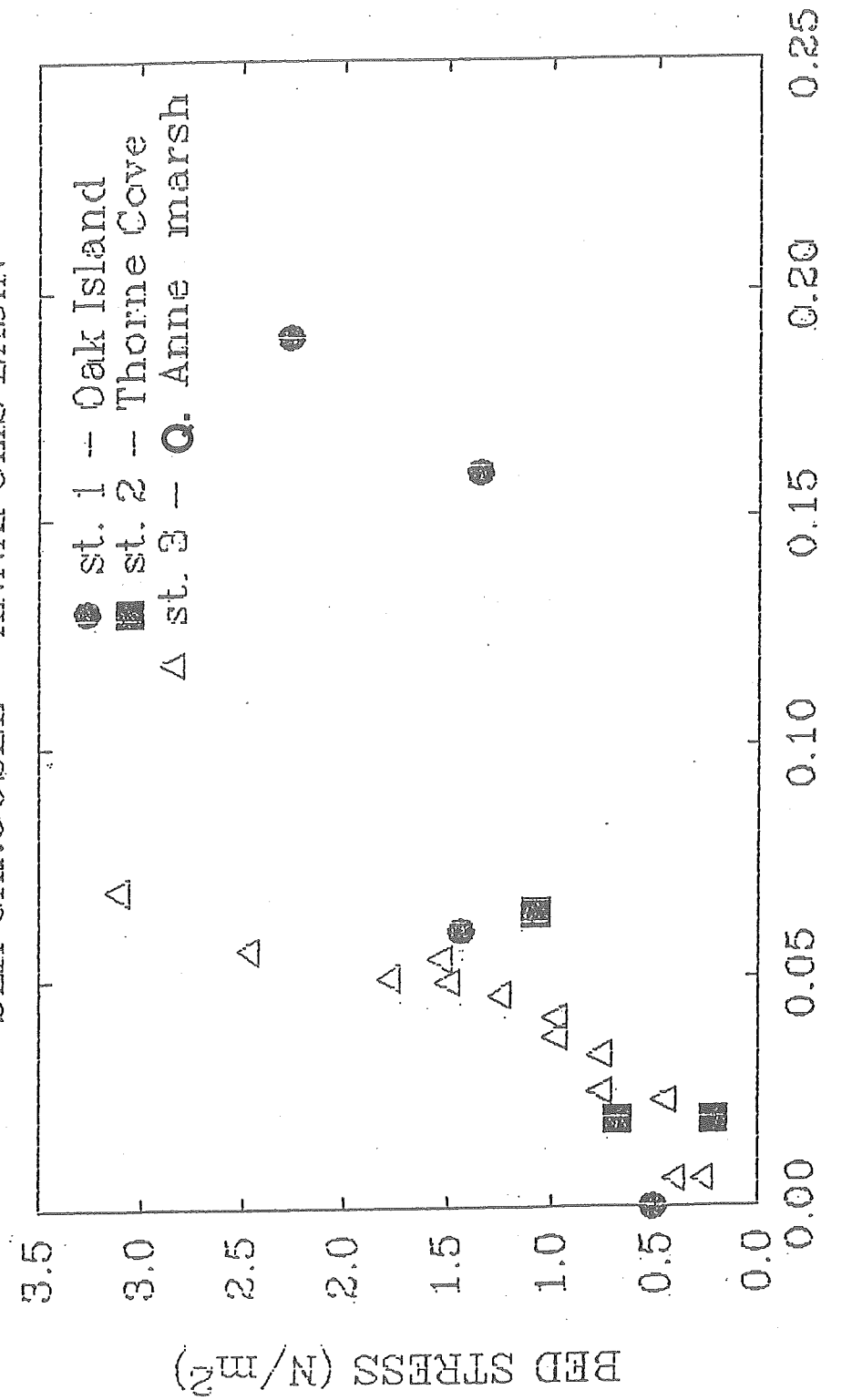

Figure 2.29. Bed stress profiles at three Annapolis Basin intertidal sites.

2.6 Summary

The Annapolis MiniLISP, carried out in early April 1989 provided an excellent opportunity to test and develop some of the new procedures and equipment to be used in the full LISP study during July and August. A great deal of useful information was obtained, particularly in regard to patterns of sediment distribution in the intertidal and subtidal zones of the Annapolis Basin, sufficient to permit development of a good sediment model for the system. Grain size analyses of intertidal and subtidal sediments are archived and available for more extensive examination than was possible for this report. Some intertidal sediment samples have been sent to Dr. K. Oldfield in Liverpool, U.K., for analysis of magnetic properties; at this time results are not fully available, but preliminary indications are that they may throw some light on the environmental effects of activities during construction of the Annapolis Tidal Power Station.

Geotechnical investigations at Thorne Cove indicate that intertidal sediments there possess unusually high shear strengths within the uppermost 50 cm, i.e., are highly overconsolidated compared with present *in situ* shear stress levels. This region, which used to be a major clam-digging site, exhibits great heterogeneity in the intertidal zone, and is extensively colonised by mussels.

Experiments with 'Sea Carousel' have confirmed that sediment erosive properties are quite different at Queen Anne Marsh, where soft-shell clams (*Mya arenaria*) have been maintained successfully, from either Oak Point, where they have been unsuccessful for several years, and at Thorne Cove, where the dominant benthic organism is the blue mussel (*Mytilus edulis*). Experience gained with operating the 'Sea Carousel' intertidally during MiniLISP was extremely valuable, and contributed substantially to the success of the major LISP exercise, described in Part 3 of this report.

Appendix 2.1 Geotechnical Methodology

H. Christian

Introduction

The purpose of this study was to assess the *in situ* physical properties of the uppermost intertidal sediments within Annapolis Basin in a manner that would provide an insight into their possible modification by active intertidal processes. Undrained shear strengths measured were overall much higher than would be expected for a normally consolidated sediment and therefore it is concluded that the sediment profile is overconsolidated to the depth of investigation, possibly due to the loads imposed by the grounding of winter pack ice.

Methodology

To determine the present state of stress within the sediment, two pieces of information must be known. The saturated unit weight (γ_s) of the sediment is required to calculate the total stress, from which the *in situ* pore pressure is subtracted to obtain the effective stress (P'), which corresponds to the pressure transmitted across inter-particle contacts within the sediment mass. It has previously been referred to as the effective overburden pressure (P'_o). The saturated unit weight is directly computed from the saturated or bulk density (ρ_s) simply by multiplying by the gravitational constant. Unit weights are more useful in calculating the effective stress because they are an expression of the gravitational force exerted by a unit volume of material. Stress is simply the force exerted divided by the area over which it acts. For an exposed mudflat the equation to calculate the overburden pressure is as follows:

$$P_o = \gamma_s * Z - u_o \qquad (1)$$

where $\gamma_s = \rho_s * g$, u_o is *in situ* pore water pressure, and Z is the depth below the sediment surface. Then we can say that

$$P'_o = \gamma_s * Z - \gamma_w * Z \qquad (2)$$

If we define the buoyant or effective unit weight as the difference between the saturated unit weight of sediment and the unit weight of water equation (2) reduces to

$$P'_o = \gamma' * Z \qquad (3)$$

This parameter is directly comparable to the preconsolidation pressure, which is a direct measure of the maximum stress applied to the sediment during its previous geological history. The ratio of the preconsolidation

pressure to the overburden pressure is defined as the overconsolidation ratio (OCR). When 0.8 <= OCR <= 1.2 the sediment is said to be normally consolidated and has not been subjected to a load in the past in excess of the present gravitational force exerted by overlying sediments. If OCR > 1.2 we say that the material is preconsolidated or overconsolidated (Lambe and Whitman, 1969). OCR's below 0.8 are unusual and indicate that pore pressures developed within the sediment mass have not fully dissipated to a free-draining boundary and consolidation is hindered. Direct measurement of the preconsolidation pressure is difficult to impossible in such soft sediments and was not attempted. In the absence of direct measurement of preconsolidation pressure, indirect techniques are available that adequately predict OCR based on knowledge of the intact or *in situ* peak undrained shear strength. This approach was developed by Ladd and Foott (1974) and its applicability will be discussed later.

It was felt that a drawdown of the water table might occur while the sediments drained as the flat was exposed, resulting in an increase in effective stress. This increase occurring on a diurnal basis could cause some preconsolidation. Therefore, suction probes capable of detecting a drawdown in pore pressure from 0 to 100 kPa were installed during ebb tide and recovered at flood tide.

A number of techniques are available for determining the *in situ* undrained shear strength profile, many of them requiring that an undisturbed sample be collected and transported to a geotechnical laboratory for analysis. A better alternative in the case of very soft sediments is to perform tests *in situ* by inserting a probe to the appropriate depth and then cause the sediment to undergo failure. This is done with an instrument such as the Pilcon vane which can be conveniently fitted with a long set of rods allowing the engineer to measure the strength at a number of levels in the sediment profile.

Another useful apparatus is the cone penetrometer which fails the sediment as it is pushed into the ground, thereby giving a continuous profile of undrained strength. A miniature cone penetrometer apparatus was developed at the Atlantic Geoscience Centre in association with the University of British Columbia for use in iceberg scours on the Labrador Shelf. The device was operated remotely from a manned ROV and was useful in investigating the strength of the uppermost zone of affected sediments (Parrott et al., 1987). For work on intertidal mudflats, the ROV cone penetrometer was modified for insertion by hand, using the weight of the operator as a reaction force. The electronics package was upgraded to acquire strengths from 0 to 3337 kPa, which is equivalent to a pushing force from 0 to 150 pounds. The tip sensor can resolve shear strength to ±1 kPa. An onboard 8-bit analog to digital converter converts the tip resistance signal from the cone into a form that the Toshiba T1000 computer can understand. Data is transmitted to the computer via an RS-232 (serial) interface and is displayed on the screen versus penetration. Data are also stored in an ascii file for future analysis.

Subsamples were obtained for later analysis in the laboratory to determine the classification parameters of the sediment (Atterberg Limits, specific gravity, and grain size distribution). A small piston subsampler was used to take constant-volume samples from the side of the test hole at each site. Since the volume of the sample was predetermined, it was a simple matter to measure the weight of the saturated sample and calculate the saturated or bulk density. The natural water content was determined by afterwards drying the subsample in an oven at 110°C for 24 hours and dividing the weight of water by the weight of solids as follows :-

$$w_n = W_w / W_s \quad (4)$$

Assuming a salinity of the pore water of 35 ‰ the corrected fluid content can be calculated as suggested by Noorany (1984) whereby

$$w_n = \frac{w_n}{1 - r - r * w_n} \quad (5)$$

where r = salinity in decimal form. For this study the salinity was assumed to be equal to that of sea water (3.5 percent).

LITTORAL INVESTIGATION OF SEDIMENT PROPERTIES (LISP)

FINAL REPORT

Part 3. MINAS BASIN
June-August 1989

Contract UP A8-001

3.1 Summary

An intensive study of sediment distribution, properties, and the environmental factors influencing their behaviour was conducted on the Starrs Point tidal flat in the Southern Bight of Minas Basin, between 15 July and 2 August 1989. More than 30 scientists from 16 institutions and 5 countries participated. The bathymetry and geomorphology of the area was documented using sonar in subtidal areas, and supplemented with surveying techniques over the flat. Continuous records of current velocity and direction, salinity and water temperature were obtained from a moored barge in the centre of the flat, which acted as a base for field work as well as a consistent intertidal monitoring site. Similar oceanographic data were obtained for six tidal cycles from a vessel moored in a channel at the mouth of the Cornwallis Estuary, near the Starrs Point flat. Continuous records of tidal height and water temperature were obtained from a tide gauge, and atmospheric conditions (air temperature, wind speed and direction, relative humidity, solar radiation) monitored from a recording weather station established on the barge. Heat flux between the sediment, tidal water, and the air was measured using a thermistor chain with thermistors arrayed at varying distances above and below the sediment-air/water interface.

Grain size, bulk density, organic and water contents, and viscometric and geotechnical properties of deposited sediments from all parts of the Southern Bight and Cornwallis Estuary system were examined, with particular emphasis upon the tidal flat area. These measurements were repeated at three sites selected along the flat for concentrated study, where, in addition, new *in situ* techniques for measuring the strength of surface sediments ('INSIST' and Paterson's 'Cohesive Strength Meter') and their erodibility ('Sea Carousel') were used. Sediment accumulation and erosion were monitored using a gamma probe buried to known depth at one experimental site. Circulation of water over and around the flat was studied using directional current meters and a surface drifter. Biological parameters investigated in a series of experiments included primary production by benthic microalgae, and abundance of benthic amphipods and polychaetes. The role of biological processes was examined through selective poisoning of test areas.

Surface sediment properties change during low tide exposure. The processes acting upon the surface are complex and sometimes competitive. Results demonstrated that cohesive strength of surface sediments increased during subaerial exposure over the low water period, but reverted to lower strengths upon re-flooding. Atmospheric drying, and the effects of gas ebullition from the sediments were contributory factors, but experiments on biological processes suggested that the mudflat surficial characteristics were also markedly influenced by plant and animal activity, especially photosynthesis of benthic diatoms, and the movements and tube-cleaning activities of the amphipod *Corophium volutator*. Poisoning experiments resulted in winnowing away of the fine sediments, and the subsequent appearance of bedforms (e.g., ripples) that were not evident in biologically active sediments. Measurements of erodibility (from 'Sea Carousel') and of shear strength (from 'INSIST') at the central experimental site (No. 2, near the barge) indicated that during the course of the three-week study, the sediment became somewhat more resistant to erosion, even when measured during the inundation period on each tide. This temporal enhancement of sediment strength was influenced by atmospheric effects, but was also coincident with the arrival of large numbers of shorebirds and the consequent decrease in

surface activities by the dominant benthic animals. This suggests that the enhancement of sediment strength during the mid-summer period may be partly a cascading effect in which the arrival of predators results in a reduction of the activities of benthic organisms, and consequently a release of benthic microalgae from grazing pressure; benthic diatoms are well known agencies of sediment-binding through the extracellular excretion of mucopolysaccharides. Changes in chlorophyll and organic content of sediments support such an interpretation.

The development of new techniques for *in situ* study of sediment properties, and the vast array of information gained regarding all parameters influencing sediment properties in intertidal areas, has led to a substantial enhancement of understanding of the behaviour of fine sediments under natural conditions. Analysis of the data gathered during LISP 89 is still continuing.

3.2 Introduction

GRAHAM R. DABORN

The principal exercise of LISP 89 was a comprehensive, multidisciplinary study of the intertidal flat at Starrs Point, Minas Basin. As indicated in Part 1 of this report, preliminary studies in 1984 (Amos et al. 1988) had indicated that stability of intertidal sediments could undergo substantial changes over periods of weeks during summer months, especially when tidal exposure permitted high evaporation of water from the flat. It was tentatively concluded that atmospheric effects were of special significance in the determination of surface stability of intertidal sediments, but it was also recognised that other oceanographic and biological factors were operative at the same time. Furthermore, elimination of animals and plants from some of the experimental sites resulted in rather different behaviour of deposited sediments. Consequently, it was recognised that an interdisciplinary study was necessary in order to distinguish between the effects of interactive processes.

It was apparent from the earlier study that standard techniques for measuring important sediment properties were either too insensitive, or required removal of sediment samples from the tidal flat to a laboratory. Frequently, the result of the latter is that samples are so disturbed that their measured properties bear little or no relation to those in the field. For this reason, we attempted either to find techniques that were suitable for precise measurement of properties *in situ*, or, where such techniques were not available, to develop them. These techniques were then used in an intensive study of a portion of the Starrs Point tidal flat, conducted between 15 July and 2 August 1989, a period including days when low water coincided with solar noon (25 and 26 July), and hence encompassing the time of maximum subaerial exposure and potential evaporation.

The objectives of the Minas Basin study (formally called LISP 89) were :

(1) To obtain precise measurements of the surface strength, erodibility, water content, bulk properties and grain size from a limited number of locations on the Starrs Point flat at frequent intervals during the study period.
(2) To test and evaluate new techniques for *in situ* measurement of sediment properties.
(3) To measure all atmospheric and oceanographic variables that might influence sediment properties, and attempt to correlate these with observed changes.
(4) To conduct appropriate experiments to investigate the influence of biological factors, especially primary production and animal activities, on the stability of deposited sediments.
(5) To develop a comprehensive conceptual model of the factors determining *in situ* stability of a fine-grained intertidal sediment.

An outline of the principal elements of the LISP 89 project is shown in Figure 3.1, together with some of the major linkages recognised between elements. All attempts were made to ensure that representative information from all elements would be obtained during the course of the field exercise. Because of the comprehensive nature of the study, several subsidiary projects were added to the programme on an opportunity basis. Such studies

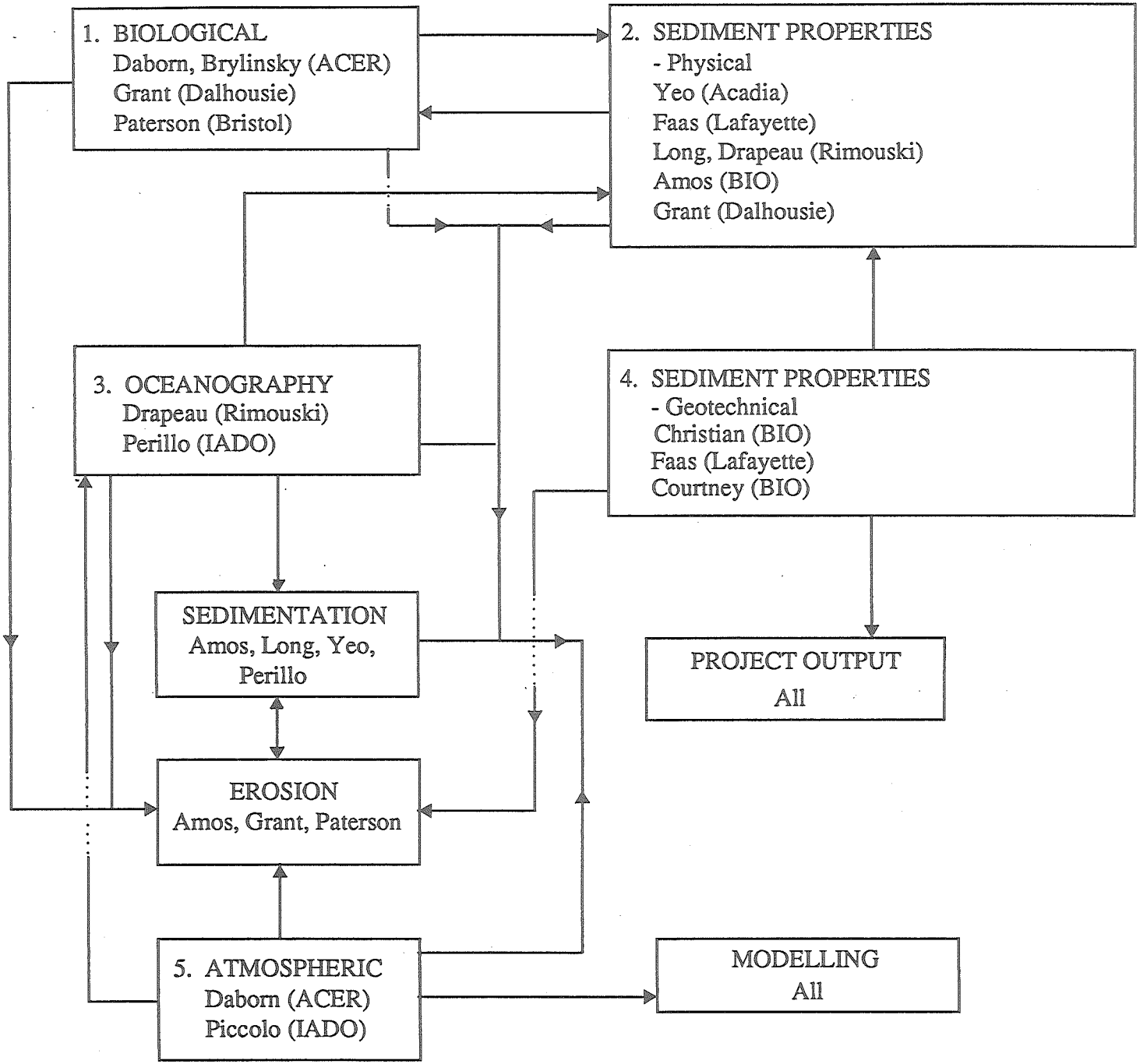

Figure 3.1. LISP Elements and Relationships.

included : use of airborne Synthetic Aperture Radar (SAR) for study of intertidal bedforms and tidal mixing; testing of an acoustic velocimeter for monitoring of water table drawdown; impact of worm-digging on benthic populations of the intertidal flat. These projects are not included in this report.

In order to fulfill the above objectives, a multidisciplinary team was created from scientists representing all of the major disciplines necessary for the study. Most of these were from Canadian laboratories, but selected participants were also included initially from the United States (R.W. Faas) and Argentina (M.C. Piccolo and G.M. Perillo). Subsequently, several other institutions became involved as awareness increased of the approach being taken, and of the technologies being developed. A listing of participants involved is given in Table 3.1.

Coordination of the exercise was provided by G.R. Daborn and the Acadia Centre for Estuarine Research (ACER). At frequent intervals (2-3 days), a planning meeting of all principal participants was held in the ACER Seminar Room to discuss logistic problems, report on current results and their interpretation, and devise new experiments. Following the field programme a workshop was held to summarise the progress of the study and to plan the extensive analytical work still required. Subsequently, further workshops were held at the Bedford Institute of Oceanography (December 1989) and in conjunction with the 13th International Congress on Sedimentology in Nottingham, U.K. (August 1990).

Table 3.1. Participants in LISP 89 (Minas Basin)

1. Acadia Centre for Estuarine Research, Acadia University

   Dr. Michael Brylinsky
   Dr. Graham Daborn
   Ms. Diane Amirault
   Adam Bunin
   Ms. Peggy Crawford-Kellock
   Sean McCormick
   Jeff Monchamp
   Michael Shaffelburg
   Sean Smith

2. Atlantic Geoscience Centre, Bedford Institute of Oceanography

   Dr. Carl Amos
   Dr. Robert Courtney
   Anthony Atkinson
   Harold Christian
   David Froebel
   Fred Joudrey
   Peter MacKenzie
   Robert Murphy
   Angus Robertson

3. Department of Geology, Acadia University

   Dr. Gary Yeo
   Ms. Diane Baldwin
   Ms. Gail Wright

4. Department of Oceanography, Dalhousie University

   Dr. John Grant
   Ms. Andrea Griswold

5. Department of Geology, Lafayette College, Pennsylvania

   Dr. Richard W. Faas

6. Institut National de la Recherche Scientifique, Universite du Quebec

   Dr. Georges Drapeau
   Dr. Bernard Long

7. Department of Botany, University of Bristol, United Kingdom

   Dr. David Paterson

8. Department of Oceanography, University of Wales, Swansea, United Kingdom

   Kevin Black

9. College of Geographic Sciences, Lawrencetown

   Edward Wedler

10. Instituto Argentino de Oceanographia, Bahia Blanca, Argentina

    Dr. Gerardo Perillo
    Dr. M. Cintia Piccolo

11. Guangzhou Marine Geological Survey, People's Republic of China

    Dr. He Chaoxiong

12. Department of Fisheries and Oceans, Bedford Institute of Oceanography

    Dr. Kee Muschenheim
    Dr. Ellen Petticrew

13. Energy Technology Support Unit, Department of Energy, United Kingdom

    Dr. Sandra Muirhead
    Dr. Roger Price

14. Canada Department of Supply and Services, Dartmouth

    Dr. Boris Tsinman

15. Discovery Consultants Inc., Wolfville

    David DeWolfe

16. IKB Technologies Limited, St. John's

    Dr. Peter Simpkin

3.3 Study Area and Methods

GRAHAM R. DABORN

The Minas Basin LISP project was carried out on the Starrs Point tidal flat (45° 09' N; 64° 21' W), in the Southern Bight of Minas Basin. This region has been studied extensively in the past, and described in numerous reports (e.g., Amos and Joice 1977; Amos et al. 1988; Daborn and Pennachetti 1979a, b; Gilmurray and Daborn 1981). The Southern Bight is estuarine, receiving variable amounts of freshwater principally from the Cornwallis River, and salinity varies from 19 to 30 ‰. It is macrotidal and vertically homogeneous, with mixed, semi-diurnal tides averaging 11.5 m. More than 80% of the area is exposed at low water. During winter the intertidal zone is ice-covered, the scouring and compaction effects of ice being potentially important factors in determining the degree of consolidation of the mudflat.

The Starrs Point mudflat, lying between Wolfville and Kingsport, N.S., was chosen for the LISP 89 study because it offered a wide expanse of intertidal zone (up to 4.5 km from high to low water marks) in which there was a gradual change seaward from fine sediments to coarser sands. The flat is largely protected from prevailing westerly winds during the summer months, so that tidal currents are more important in controlling sediment movement than waves. Access on foot was possible at low water from the Starrs Point headland, and at high water the study site could be reached by small boat from the Wolfville Harbour.

Bathymetry of the Starrs Point tidal flat was studied by use of a Raytheon Recording Echosounder deployed from small boats at high water on 21 July and 7-8 August. Position was fixed partly with an electronic range and angle positioning system located on a hill at Evangeline Beach, and partly by using two sextant observers on the boat. The bathymetric survey was completed from the ACER research vessel *Cora Lee II* using Loran C for positioning. This section was run on 10 August, and covered the mouth of the Cornwallis Estuary and Wolfville Harbour.

Sediment changes over the tidal flat were monitored at a series of stations established in one baseline along the length of the flat and in two lines perpendicular to this baseline (Fig. 3.2). All stations were marked with stakes. At selected stations pairs of depth marker stakes were driven to predetermined depths and used as guides to measure depth from a jig suspended from the marker stakes. Interference with some of these stakes by non-participant users of the flat restricted the data obtained in this manner.

Most studies were carried out in the central portion of the flat, approximately at the mid-tide level. At this location a floating barge was moored to act as a platform for water column studies, and as a base of operation for activities on surrounding parts of the flat during periods of exposure. At high water the barge floated on approximately 6 m of water, and was grounded for about 7 hours during each tidal cycle. The barge was monitored 24 hours a day from 1100 h on 16 July to 1400 h on 2 August 1989, crews being changed by boat at every high water. The barge carried two portable generators to provide lighting, power for vacuum pumps and recording equipment, and charging power for 12 v batteries. In the centre of the barge there was a moon pool and gallows for suspension of a sampling cable; deployment of the cable was by portable 12 v winch or by hand.

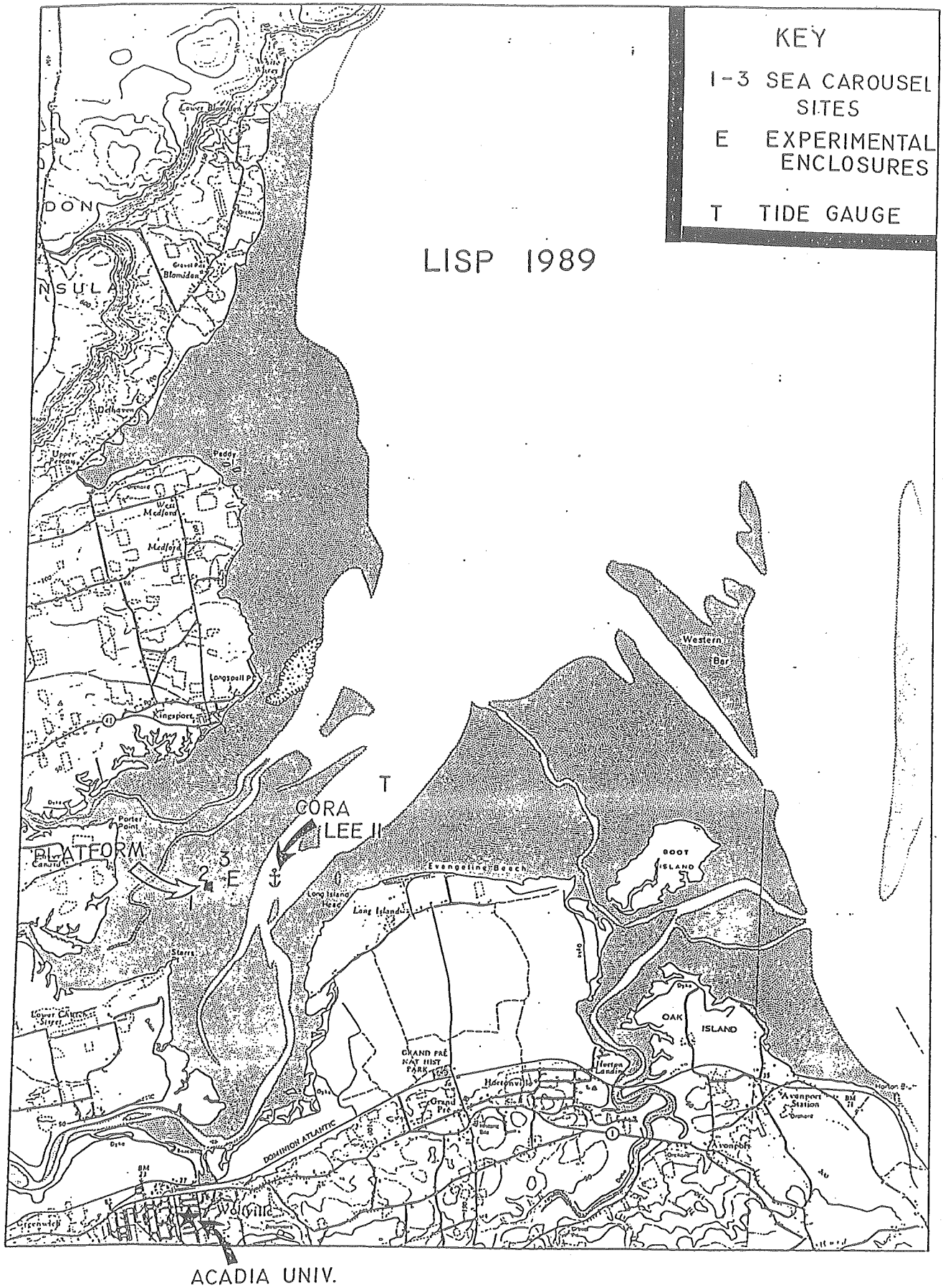

Figure 3.2. Location of LISP 89.

During inundation hourly water column profiles of temperature and salinity were taken with a CTD rented from the Department of Fisheries and Oceans; data were recorded on tape, but owing to lack of funds complete transcription of the data obtained has not been done. Crews maintained records of salinity and temperature at each metre depth using deck sheets; these constitute the data reported herein. Water samples were taken at the surface, mid-depth and about 1 m above the bottom using 1.4 L or 2.1 L oceanographic samplers. One-litre samples were vacuum filtered through pre-weighed 0.4 μm Nuclepore™ filters at the barge, then dried and reweighed in the ACER laboratory to provide estimates of suspended particulate matter (SPM).

Continuous records of pressure, tide height and temperature were obtained from a bottom pressure tide gauge installed subtidally northwest of Evangeline Beach (location T in Fig. 3.2) on 29 June and retrieved on 9 August 1989.

Continuous records of atmospheric parameters were obtained from a Seastar WeatherPak automatic weather station located initially (27 June to 12 July) on a 5 m pole installed on the dyke 2 km south of the eventual barge site, and subsequently (13 July to 2 August) on the barge itself. Elevation of the station was approximately 6 m above the water level when the barge was afloat, and above the tidal flat during exposure. Variables recorded for every minute included : maximum wind speed and direction, atmospheric pressure, air temperature, dew point temperature and relative humidity. When the station was relocated to the barge, a LICOR LI-200S pyranometer was also installed to record total sky radiation; data were stored on a Campbell 21X data logger. A rain gauge was established on the barge and checked daily between 17 July and 2 August.

Near to the barge a thermistor chain was used to record soil, water and air temperatures at levels below and above the sediment surface, from 21 July to 8 August. Thermistors were located at four levels below the sediment surface (-0.5, -0.25, -0.1 and -0.05 m) and at three levels above (+0.05, + 0.3 and + 1.3 m), and data were recorded at 10-minute intervals on an Aanderaa TR-1 recorder installed on the barge.

Water column studies were carried out from the ACER research vessel, the *Cora Lee II*, which was moored continuously at one subtidal location (45° 08.90' N, 64° 18.87' W - cf. Fig. 3.2) from 16 July to 2 August. Three 24-hour series were conducted, providing hourly records of salinity and temperature with depth using a Beckman RS 32 salinometer, and water samples were taken for SPM analysis at surface, mid-depth and near bottom. Water samples were filtered on board and processed at the ACER laboratory. Vertical profiles of current velocity were obtained using a direct-reading Kahlsico Current Meter at each hourly deployment. The vessel was also used to establish a transmissometer and an Optical Backscatter Sensor (OBS) for continuous recordings of turbidity at depths of either 0.5 or 1 m below the surface. Data were stored on a Campbell 21X data logger.

Three sites were selected in the central portion of the flat for detailed studies of sediment erodibility and bulk properties using 'Sea Carousel' and 'INSIST'. These sites, referred to as 'Sea Carousel' Sites 1-3 (cf. Fig. 3.3), were marked out with stakes and ropes on 11 July in order to prevent disturbance by people walking over the flat during exposure. Site 1 was most landward, approximately 580 m from Starrs Point; Site 2 was seaward of the barge at 830 m from Starrs Point, and Site 3 was approximately 1100 m from Starrs Point. All were located in the predominantly fine sediment portion of the flat (Site 3 was slightly coarser in texture); Site 3 had to be abandoned part way through the study because of interference by local worm-harvesters. These three sites were

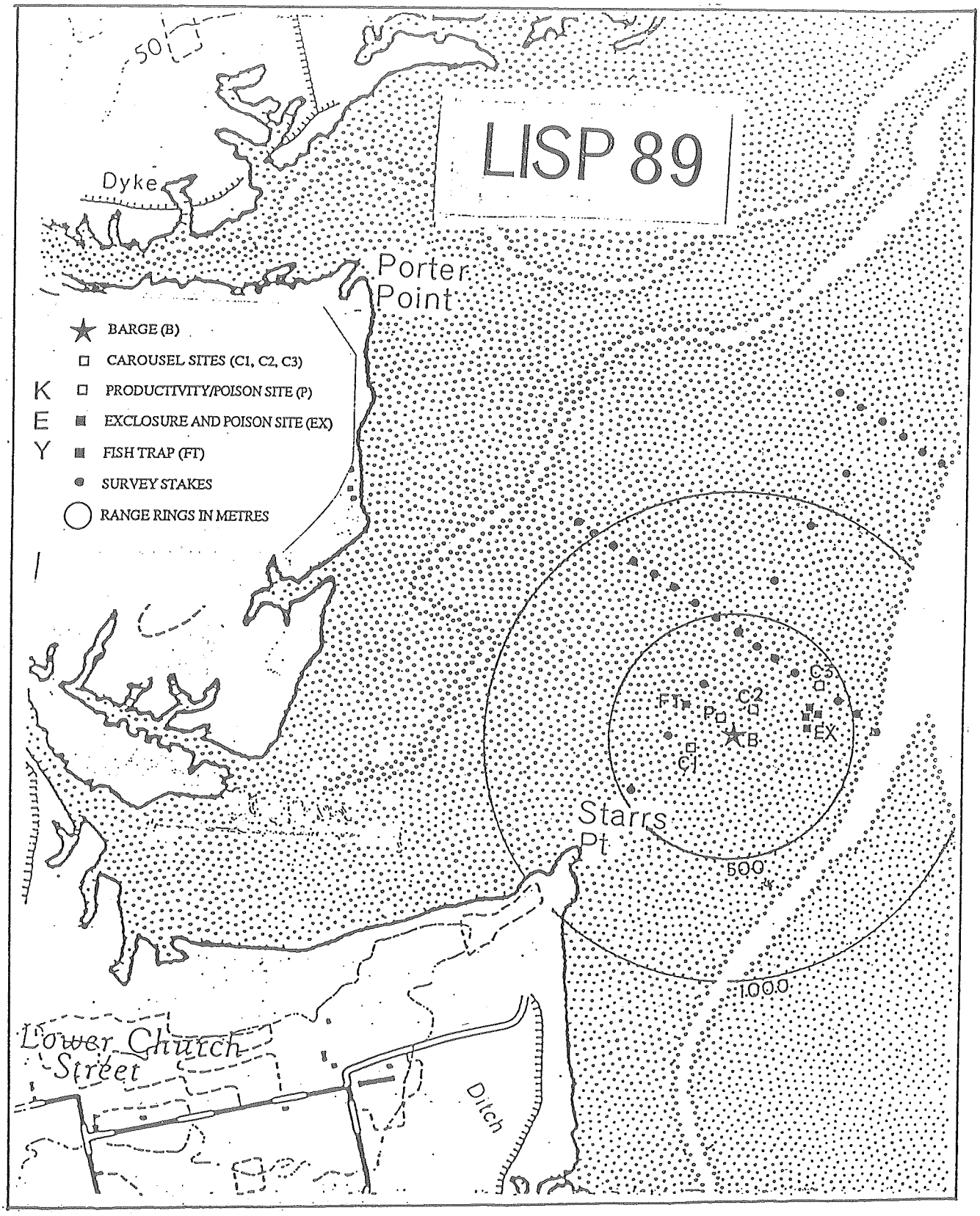

Figure 3.3. Locations of LISP experimental sites.

visited daily in rotation during the experimental period from 17 July to 2 August. Sediment erodibility was examined using 'Sea Carousel' during inundation, and shear strength (etc.) examined at the same site using 'INSIST' during the next exposure period. Current velocity and direction were recorded at each of the three sites for varying lengths of time (several tides) using InterOcean S4 Recording Current Meters set at a height of 0.5 m above the sediment surface. Variations in sediment depth and density were recorded at Sites 1 and 2 using a gamma probe in which the emitter was buried at a depth of 0.25 m.

Following demonstration of the effects of poisoning on sediment surface features (cf. section 3.10 below), an additional experimental area was established north of the barge for investigation of the changes in productivity and sediment properties following poisoning with formalin (Site P, Fig. 3.3).

Experimental plots to examine the biological factors affecting sediment behaviour were established in an area 300-350 m seaward of the barge, near 'Sea Carousel' Site 3 (Fig. 3.3). These sites included a 3 x 3 m Sedimentation Enclosure (SEDEX) with 2.5 m high walls on three sides, consisting of tarpaulin stretched over metal frames made from 1 cm reinforcing bar ('rebar'); a 3 x 3 m Poison Site, together with a similar Control Site, both marked out with corner stakes and rope; and a 2 x 4 m Predator Exclosure (FISH EXCL) consisting of 'rebar' frames covered by 1 cm mesh screening on all sides, including the top. Another control enclosure (FISH CONTROL) of the same dimensions and construction as the Predator Exclosure, but without the screening, was established adjacent to the Predator Exclosure. These sites were set up on 11 July in order to allow time for disturbed sediment to settle prior to the experimental period. The Poison Site was sprayed with 4 L of 100% formalin on 19 July (Julian day 199).

All sites were provided with paired marker stakes (of 1 cm 'rebar') inserted to a predetermined depth for monitoring relative height of sediment. At each visit, depth of the sediment surface below a metal jig suspended between the marker stakes and fitted with liquid levels was measured with a steel tape. Sediment cores (2 cm^3, with surface area of 1 cm^2) were taken with a syringe from each experimental enclosure and analysed for chlorophyll concentration. Samples for macrofauna were taken using a bulb corer having a surface area of 40.7 cm^2, washed through a sieve having a 400 μm mesh, and all organisms were stored in formalin for subsequent analysis. All samples were normally taken in triplicate and analysed separately.

In order to monitor fish movements in relation to the tidal flat being studied, a fish trap was established in a tidal channel north of the barge. The trap was constructed of 'rebar', 1.0 x 1.3 x 1.3 m in dimensions, covered with 1 cm mesh netting. The rear panel consisted solely of netting that could be removed when sampling was not desired. Wing nets of 1 cm mesh were constructed on either side of the trap to funnel fish into the trap during the falling tide. Sampling was carried out on 9 occasions between 7 July and 4 August.

All sample locations were accurately surveyed in by reference to a pin on the Starrs Point headland. Subsequently the height of this pin was determined relative to the high water level of a spring tide on 15 November 1989, and the elevation of all important experimental and observation sites was determined relative to this pin. Location of the major experimental sites is given in Figure 3.3. Table 3.2 lists the elevations of the major sites, and their distances relative to the barge.

Table 3.2. Locations and Elevations of Experimental Sites

Location	Elevation* (m)	Distance from Barge (m)
Starrs Point Pin	+ 4.73	749
Barge	- 7.26	0
Carousel Site 1	- 6.92	199
Carousel Site 2	- 7.69	123
Carousel Site 3	- 8.53	410
Gamma Probe 1	- 6.93	209
Thermistor Chain	- 7.27	22
Predator Exclosure	- 8.07	298
Sedimentation Enclosure	- 8.17	318
Poison Enclosure	- 8.24	338
Control Enclosure	- 8.25	338
Fish Trap	- 8.50	217
Productivity/Poison Site	- 7.38	66

*Elevation Relative to High Water Level Spring Tide, 15 November 1989.

3.4 Bathymetry of the Starrs Point Tidal Flat

GRAHAM R. DABORN and GARY YEO

Participants :

G.M.E. Perillo, G. Yeo, D. DeWolfe, G.R. Daborn, J. Monchamp and S. Smith.

Bathymetric studies of the lower tidal flats and subtidal areas of the Southern Bight were carried out by echosounding during periods when the flats were covered by water, using a Raytheon Recording Echosounder.

3.4.1 Bathymetry of the outer Cornwallis estuary

A bathymetry map of the outer Cornwallis River estuary has been produced from echo-sounder profiles measured in August 1989 (Fig. 3.4A). The location of the profiles was controlled by simultaneous, three-point sextant readings except for a small area within 2 km of Wolfville harbour, where Loran C was used. Spot data from the echo-sounder strip charts were corrected using tide gauge data provided by Dave DeWolfe, plotted on a 1:10,000 base map and contoured at 1 m intervals. The accuracy of measurements over the Starrs Point bar is confirmed by grid surveys on the exposed bar. The morphology of the outer estuary has remained essentially as shown on the 1:37,500 hydrographic chart of Avon River and Approaches surveyed in 1969 (C.H.S. No. 4140), but is shown in much greater detail.

3.4.2 Sedimentology of the Starrs Point bar and outer Cornwallis estuary

Samples were collected from 64 stations on a grid 3.2 km long on the Starrs Point bar and from scattered points along the main Cornwallis channel in August 1989. Grain size distributions were determined by the hydrometer method. This gives results comparable to sedigraph and pipette analyses. On the Starrs Point bar grain size (calculated graphic mean) increases seaward and toward the bounding channels from >5 phi (0.44 mm) to between 3 and 2 phi (0.125 - 0.25 mm). The coarsest sediment observed in the outer estuary was 0.39 phi (1.3 mm) in 2D megaripples near Long Island Head. Sorting (calculated graphic standard deviation) improves seaward and towards channels from the central part of the bar crest (between 2 and 2.2 km from the point). The sorting pattern is asymmetric about the bar crest, improving more rapidly westward towards the Canard channel. C-M plots (coarsest percentile vs median size) of the grain size data suggest that the sediment on the Starrs Point bar results from a mixture of graded and uniform suspension deposition, while sediment on the outermost bar and Cornwallis channel results mainly from bedload deposition.

The geomorphology of the flat is also being depicted from analysis of the positions and elevations of the base line and two cross transects established along the Starrs Point intertidal zone. Positions of sites on these transect lines are shown in Figure 3.3. Elevations of the stations on these transects are shown in Figure 3.4B, together with specific tidal elevations obtained from pressure readings on an S4 current meter and the tide gauge.

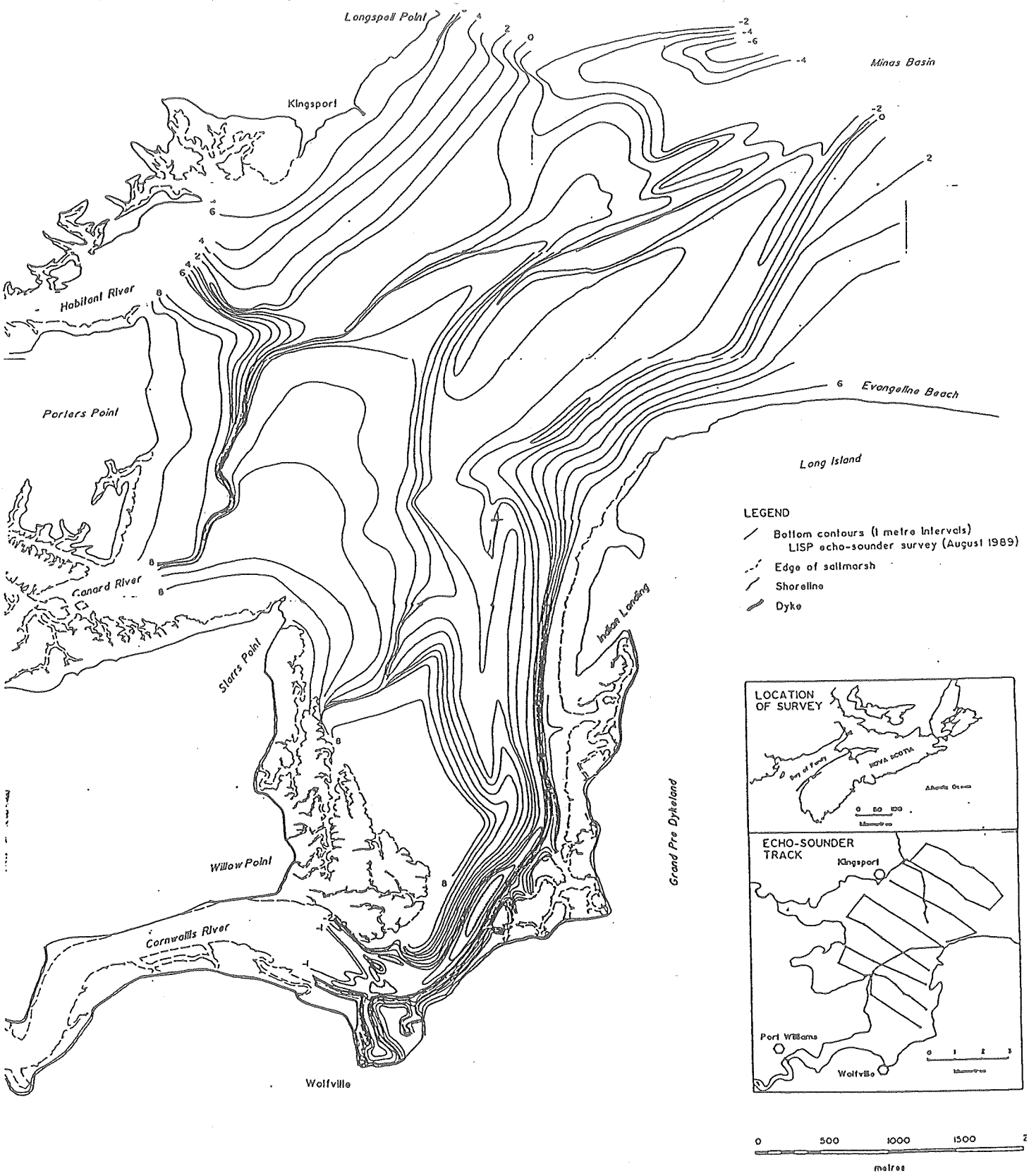

Figure 3.4A. Bathymetry of the outer Cornwallis Estuary.

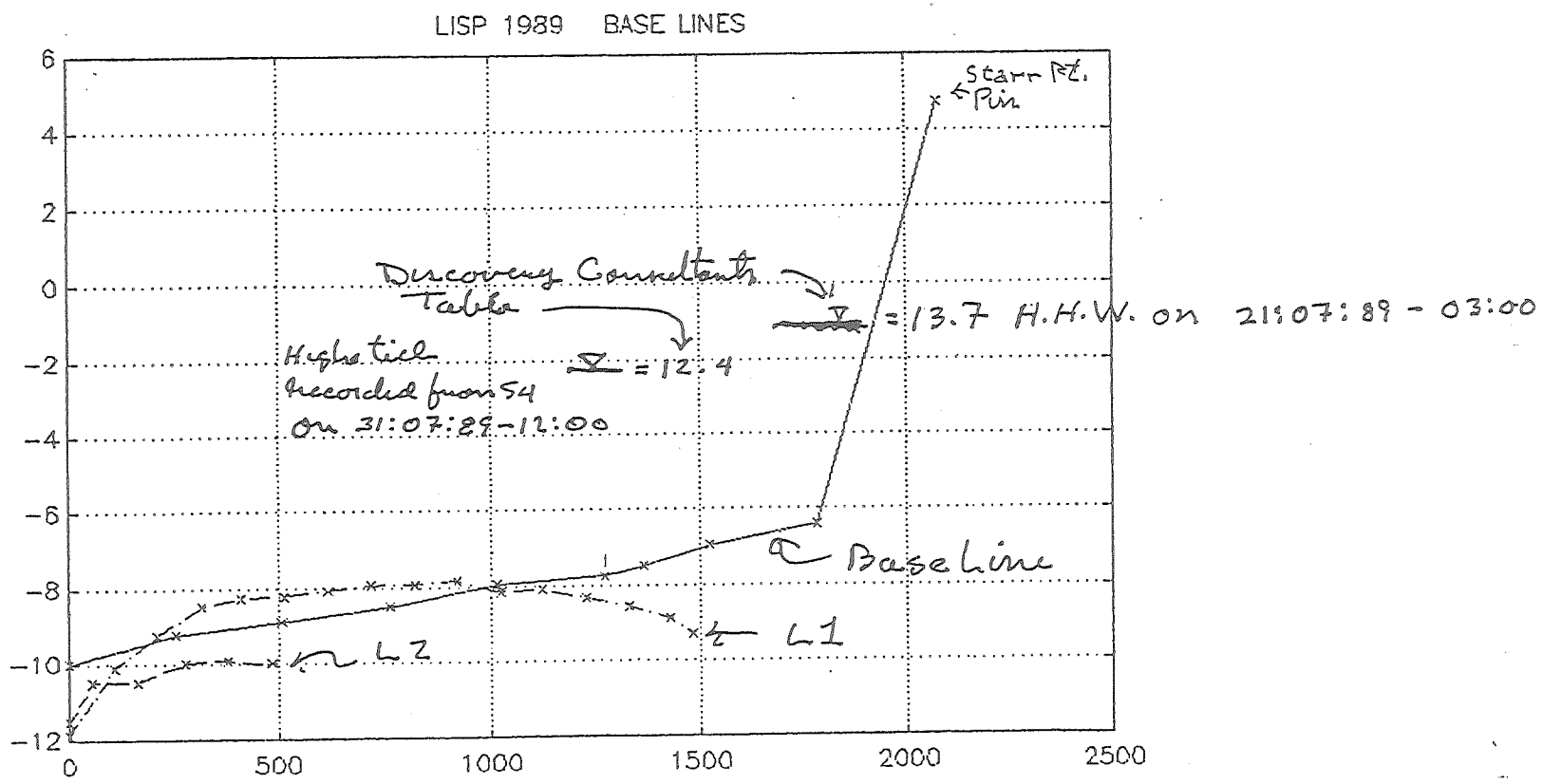

Figure 3.4B. Elevations of baseline and transect lines relative to Geodetic Datum.

3.5 Oceanography

GRAHAM R. DABORN

Participants :

G.R. Daborn, D. DeWolfe, G. Drapeau, G.M.E. Perillo, M.C. Piccolo.

3.5.1 Tides (DeWolfe)

A preliminary plot of tidal data is shown in Figure 3.5, together with water temperature and atmospheric pressure. Tidal range at this point in the Southern Bight varied from 10.5 m on neaps (e.g., 14 and 29 July) to 13 m on springs (e.g., 4 and 23 July). During the study period mean water temperature steadily rose from c. 14.5°C to nearly 17°C following the period of maximum warming associated with the noon-time low water on 25-26 July. Daily temperature range is strongly influenced by the spring-neap tidal rhythm, with the highest maximum daily temperatures occurring following the springs. Further analysis of tide gauge data, including computation of spectra of tides, temperatures and barometric pressure, and cross-spectra, will depend upon need for such information and the opportunity to process it.

3.5.2 Circulation Patterns (Drapeau, Perillo, Piccolo)

Circulation patterns of water around and over the Starrs Point tidal flat are being determined from current velocity and direction data recorded with remotely-deployed S4 current meters, and also from drifter experiments. A surface drifter was released on three separate occasions near the low water mark of the Starrs Point flat, and its position determined at five-minute intervals by sextant angles obtained by an observer on the roof of the barge over a tidal cycle. An example of the drifter track during the experiment of 31 July is shown in Figure 3.6. During this experiment, the drifter passed approximately 150 m to the north of the barge during the flood, drifted further northwest at the end of the flood, and then moved progressively to the north (i.e., down the slope of the flat) on the ebb. During another experiment, the drifter was released at a more southerly point during the early flood, passed to the south of the barge and left the flat in a southerly direction during the ebb. These patterns reflect the flow separation occurring as water ebbs in response to topography on either side of the baseline of the flat.

Records of current velocity and direction were obtained from S4 meters deployed at each of the 'Sea Carousel' sites during the study. Examples of results for Sites 1 to 3 are shown in Figure 3.7. At station 1, the highest and most landward site, maximum flood velocities were only 15-20 $cm.s^{-1}$, because this site was only inundated toward the end of the flood; ebb velocities, however, commonly exceeded 20 $cm.s^{-1}$. At station 2, just seaward of the barge, flood and ebb velocities reached 30 $cm.s^{-1}$, and at station 3 were up to 35 $cm.s^{-1}$ during the flood. At all three sites, currents were reversible, but separated by an angle of 200° rather than being directly opposite (e.g., flood = 45°, ebb = 245°). A minor rotation around the northern side was observed at high tide.

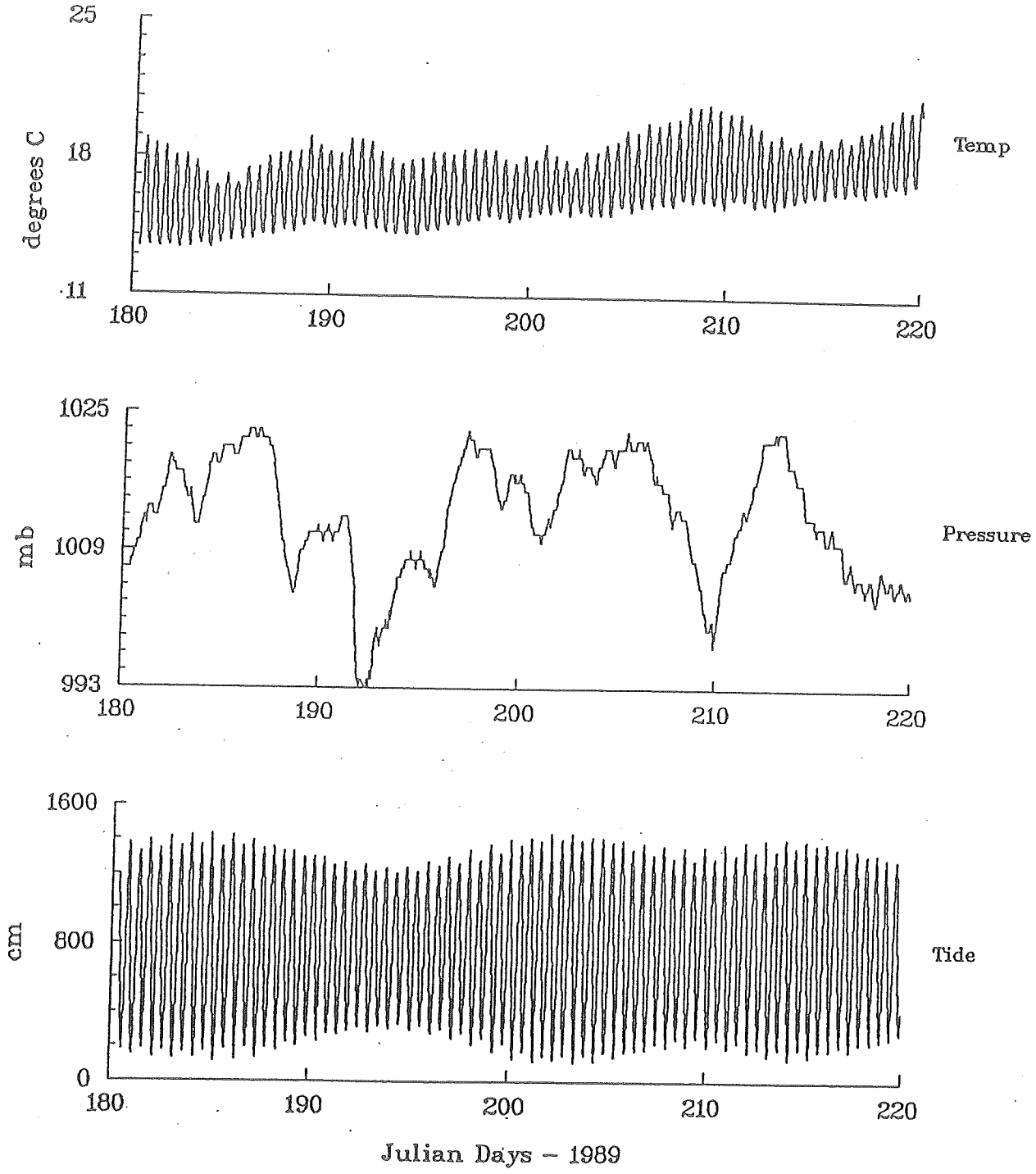

Figure 3.5. Tide, air pressure and bottom temperature at Starrs Point, June 29 - August 9, 1989.

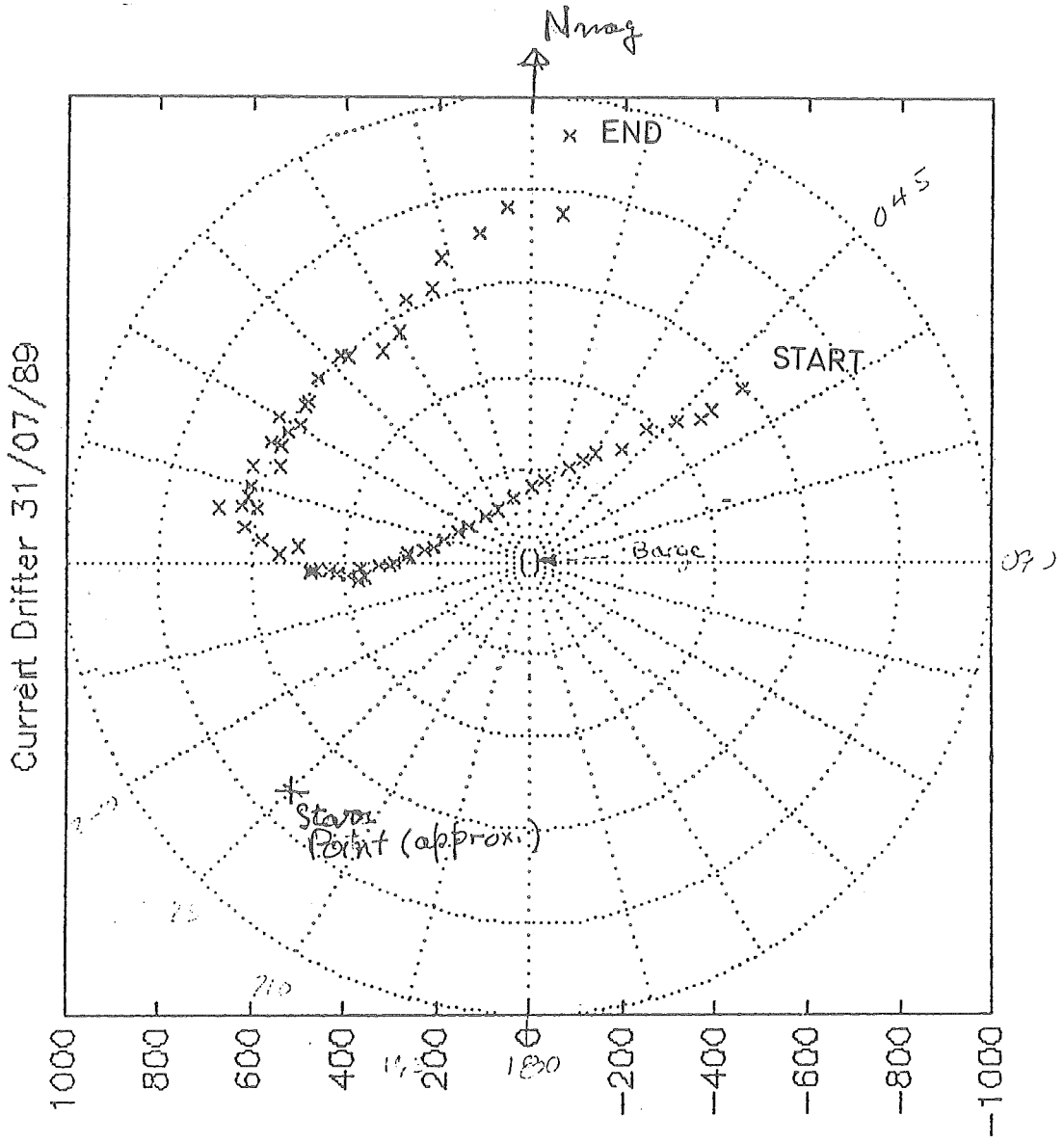

Figure 3.6. Drifter study 31 July 1989.

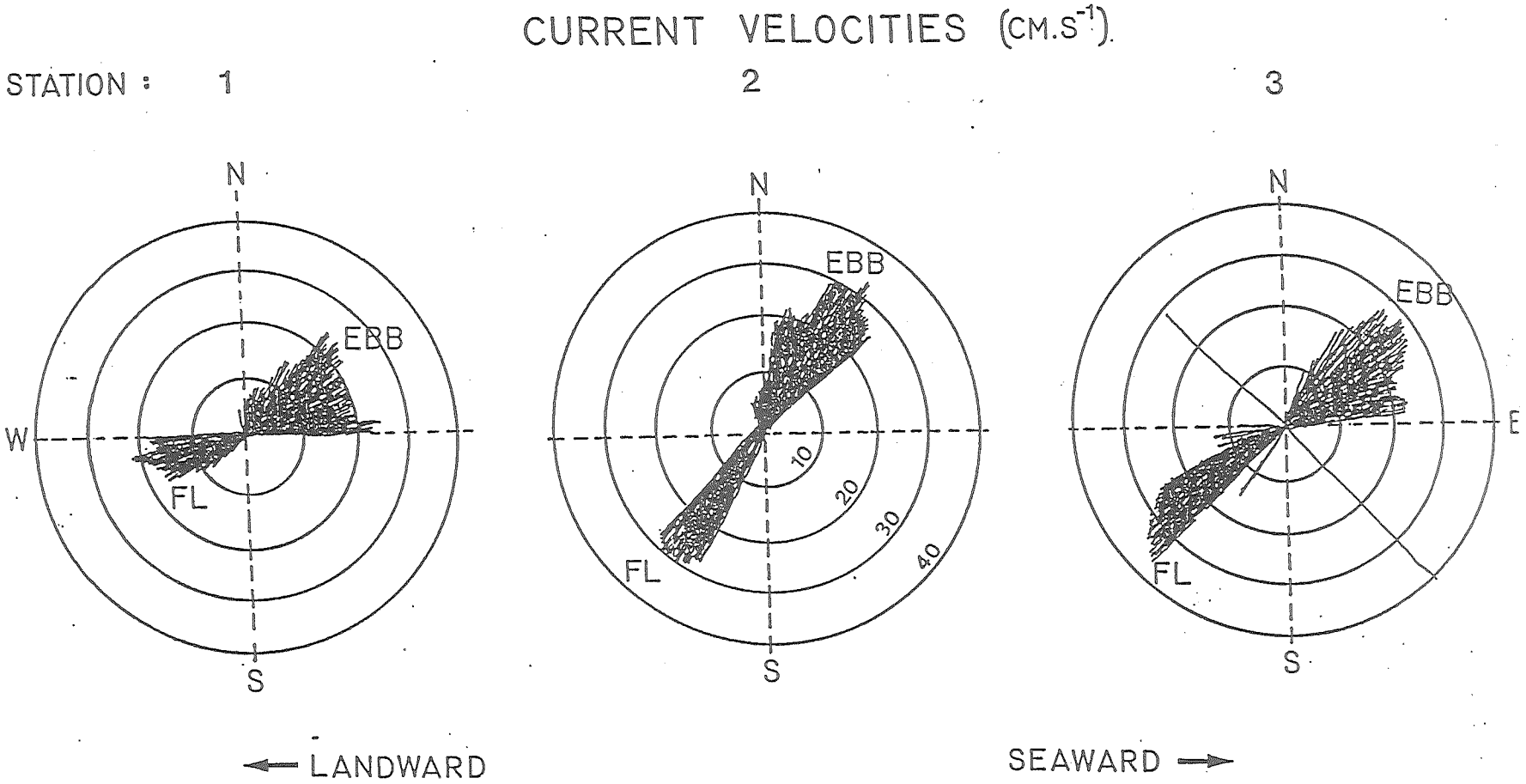

Figure 3.7. Current velocity (cm.sec^{-1}) and direction at Stations 1-3, Starrs Point, Minas Basin. FL - Flood.

Ebb currents tended to fluctuate more than flood currents, although both were contained within 40° of the average direction. During the 34 tidal cycles monitored at the three sites, average currents were 17 $cm.s^{-1}$ in both ebb and flood directions; peak velocities were always less than 45 $cm.s^{-1}$.

Current velocity at station 2 over the daytime tidal cycle of 31 July, when the drifter experiment described above was conducted, is shown in Figure 3.8A. High water occurred shortly after noon, at which time velocity fell to 2-3 $cm.s^{-1}$, but current direction did not reverse until about 1300 h (Fig. 3.8B). Current progressive vectors from this data set are shown in Figure 3.8C. The fact that these vectors show a similar pattern to that of the drifter track indicates that the tidal circulation over the study area is uniform, and therefore the current meter data can be used to describe the circulation over the whole of the tidal flat.

Four tidal cycles representing calm (run 58) and windy (runs 46, 52 and 54) conditions were selected to examine the effects of wind strength and direction on current velocity and direction. For every run at each of the sites, both series (current and wind) were divided into ebb and flood subcycles, and the vectors decomposed into v and u components. The currents were corrected with an angle of 55° (from the average of the mean ebb and flood directions) such that u was positive in the ebb direction and v positive to its right. The wind vectors were corrected with an angle of 235°, resulting in a commensurate series having the same coordinate system. The resulting time series were analysed using a FFT technique, with 14 degrees of freedom and effective spectral band of 0.016 cpm.

The spectra of both current components measured during calms in all sites and during ebb and flood have representative peaks at 16 and 2.78 min. These two peaks are also significant on the spectra of wind-influenced records, but the latter show additional peaks at other frequencies. Further analysis of the wind-influenced spectra indicates distinct differences between ebb and flood records depending on the general direction of the wind. In general, when the current is approximately co-directional with the wind, the spectra have extra peaks at 64 and 2.3 min, while the coherence is relatively important only at low frequencies (periods >8 minutes). On the other hand, when wind and current directions are opposite, the records are highly coherent (>0.75) at periods >4 minutes, and peaks are more common in the high frequency portions of the spectra.

The relatively high energy observed near the 2 minute period indicates the marked influence of the wind at very high frequencies (periods <2 minutes), which were not sampled in this study and introduced into the spectra due to aliasing processes. Further analysis of the records is required in combination with the morphology data to establish the physical meaning of the spectral peaks, particularly those found at 16 and 2.78 min.

3.5.3 Salinity and Temperature (Daborn, Perillo)

Salinity was recorded for each metre of depth using a CTD at hourly intervals whenever there was water of sufficient depth beneath the barge. The data set covers 33 consecutive tides. Salinity varied little at the barge either during a tidal cycle or throughout the experiment, being usually between 29.6 and 30.4 ‰. Selected data for the afternoon tides of 23 July (a spring tide) and 29 July (a neap tide) are shown in Figure 3.9A and B.

At all times during the flood and most of the ebb the water column at the barge site was well mixed, so that

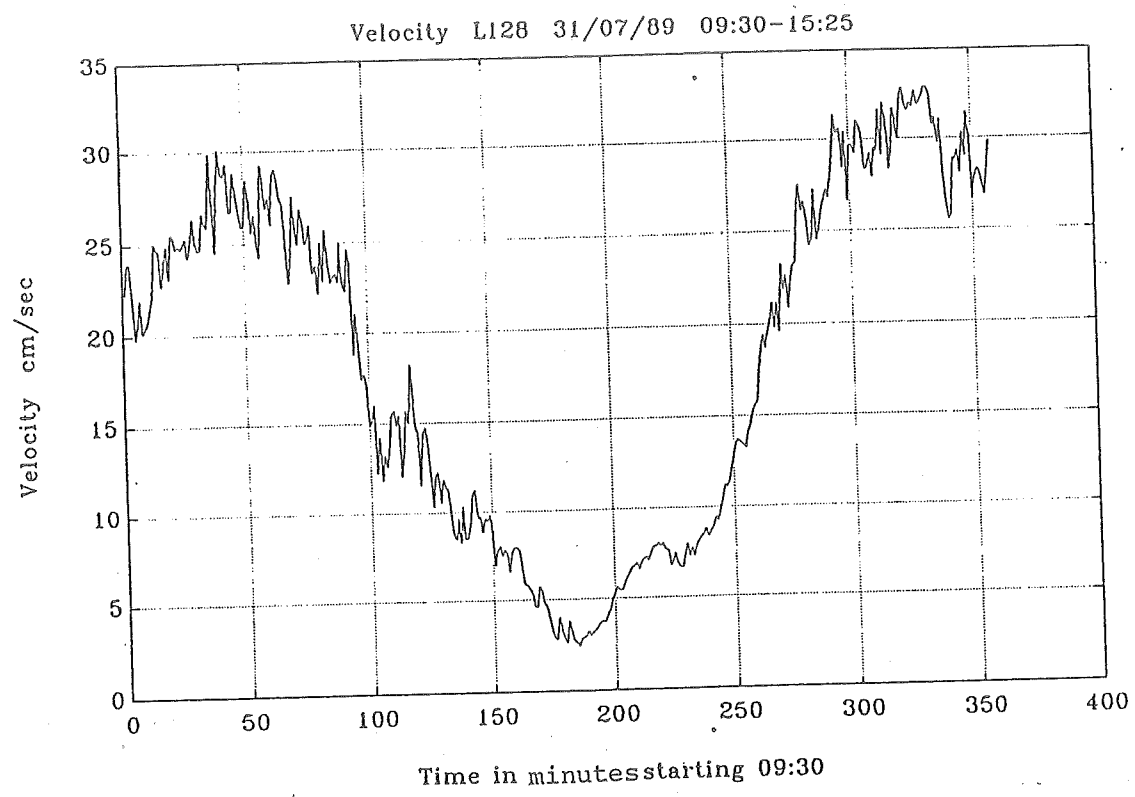

Figure 3.8A. Current velocity at Site 2 during drifter study.

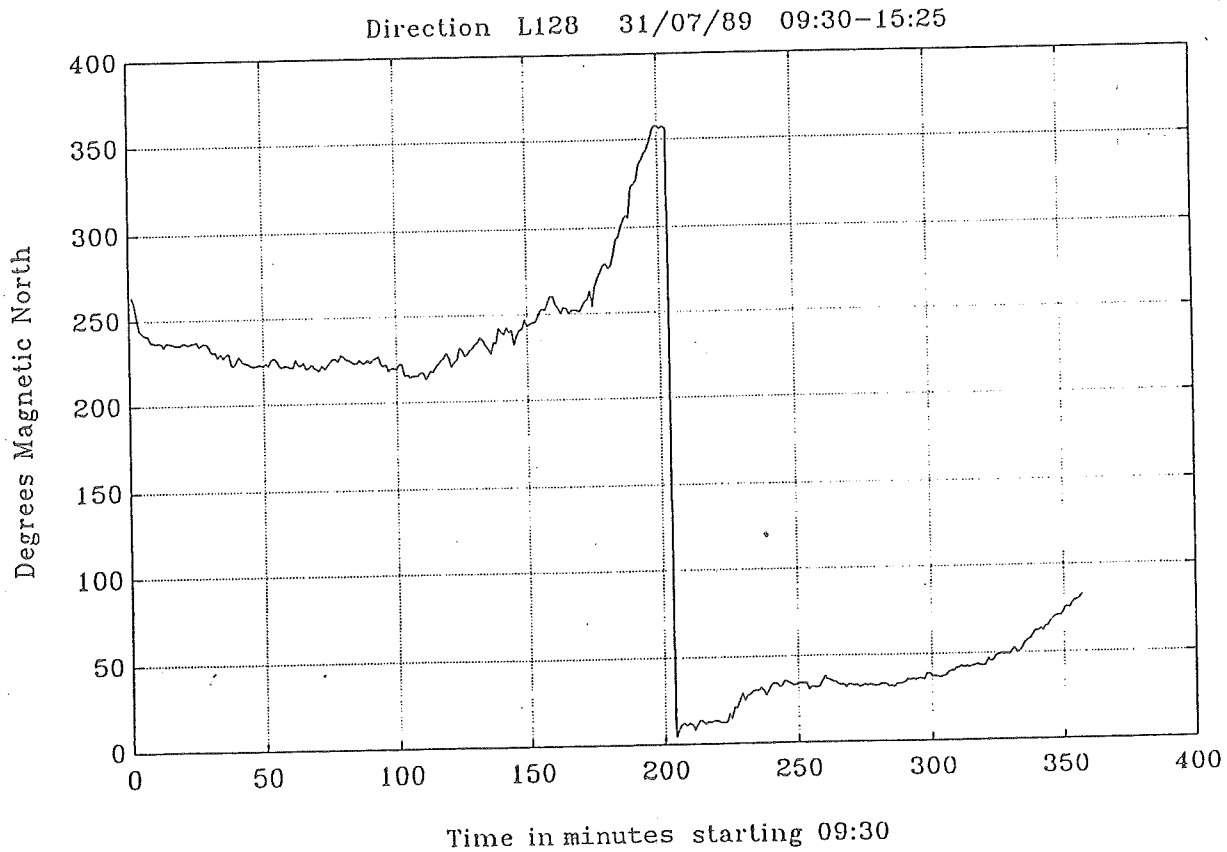

Figure 3.8B. Current direction at Site 2.

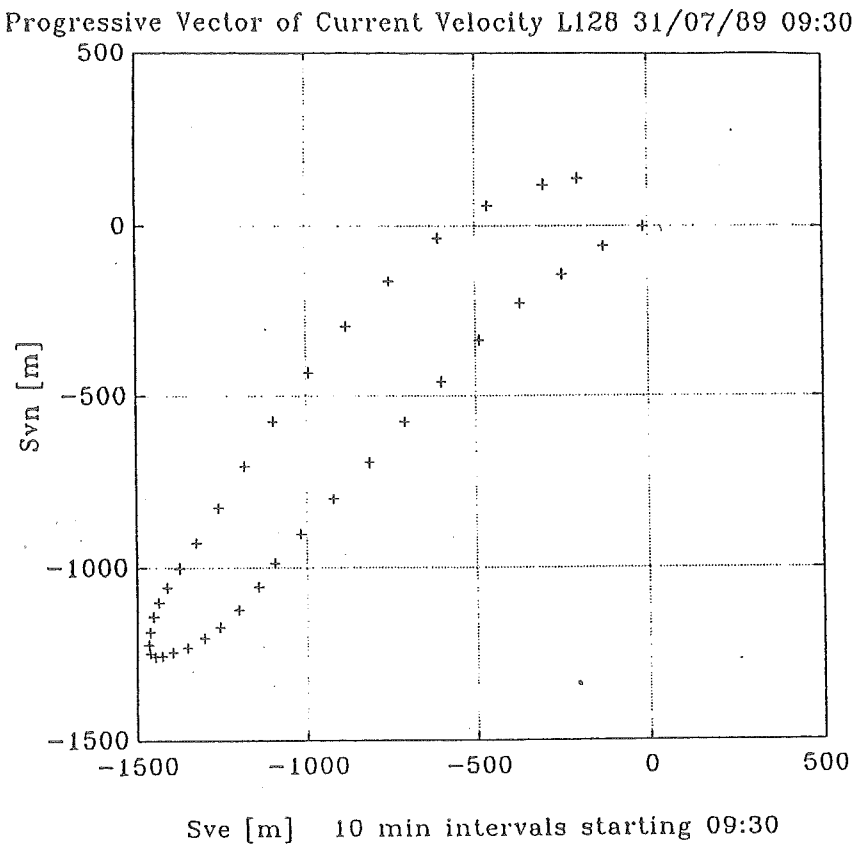

Figure 3.8C. Progressive vectors during drifter study.

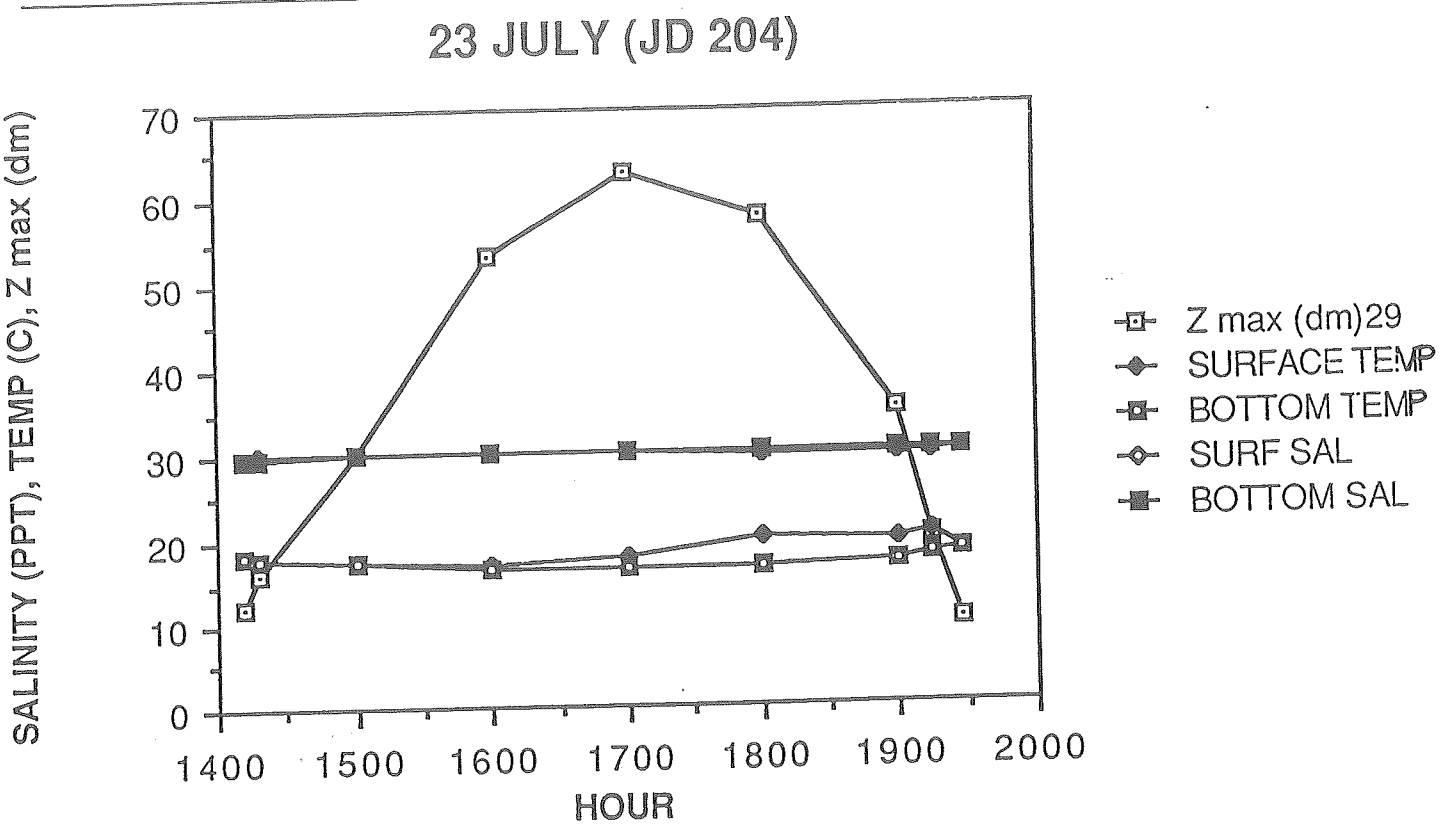

Figure 3.9A. Salinity, temperature and depth over a tidal cycle at the barge.

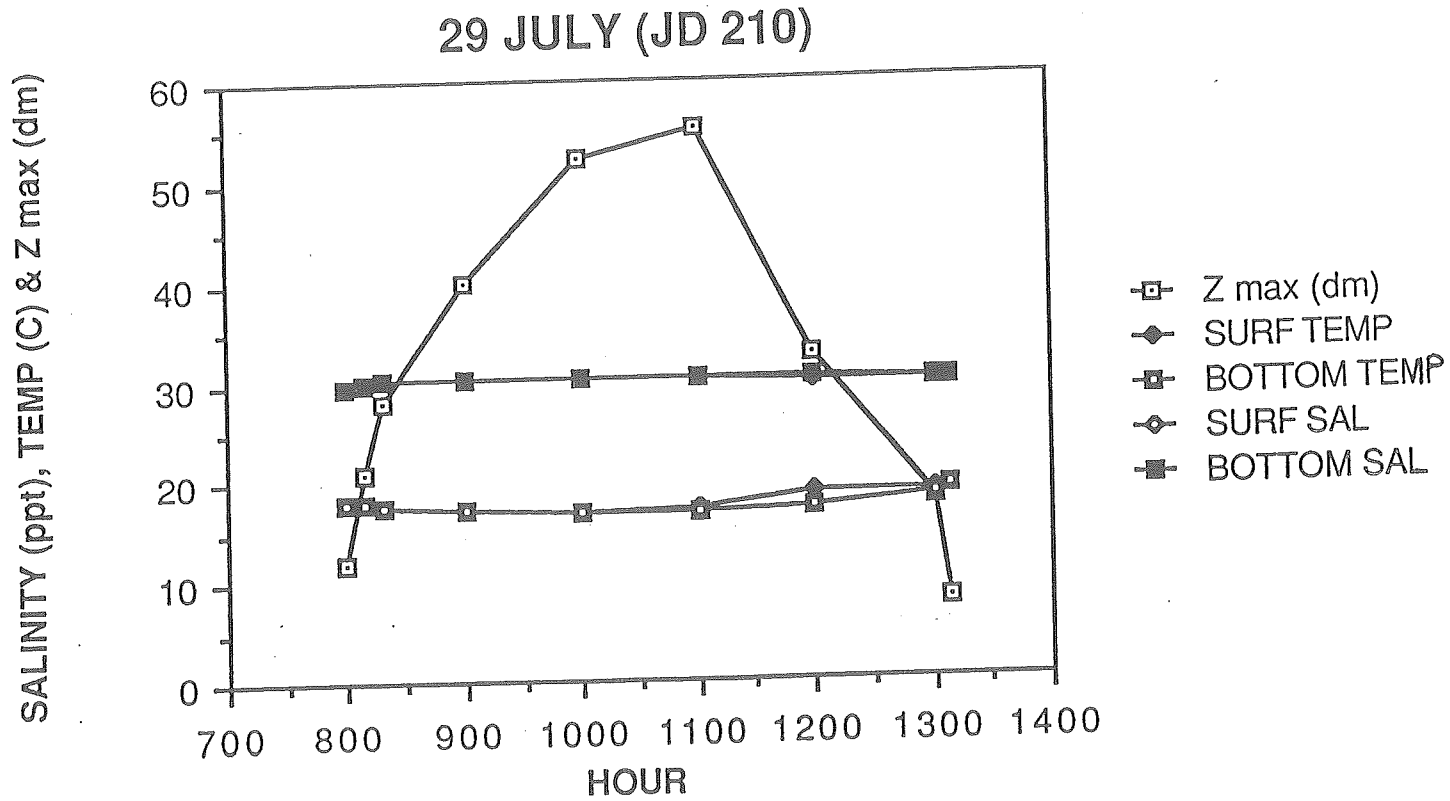

Figure 3.9B. Salinity, temperature and depth over a neap tidal cycle at the barge.

surface and bottom waters differed usually by less than 0.5 ‰ in salinity, and less than 1°C in temperature. Frequently during the early part of the ebb the upper 1 m of water would exhibit a higher temperature and slightly lower salinity than deeper water, presumably because of the movement of fresher surface water from higher up the slope.

Vertical profiles of salinity, temperature and current velocity were taken at hourly intervals over two successive tidal cycles on each of three occasions from the *Cora Lee II* anchor station (location indicated in Fig. 3.2). Results are shown in Figures 3.10A, B and C, and 3.11A, B and C. Tidal range at this site was measured at 11.5 to 13 m, whereas depth was 14 m at high water so that the vessel grounded at low water. Salinity varied little around 30-31 ‰, with slightly lower values in the top 1 m around high water. At all other stages of the tide, the water column was well mixed as a result of strong tidal movements on both ebb and flood. Some thermal stratification was also evident around high water, the somewhat cooler tidal water underlying warmer river water. Current velocity profiles occasionally indicated a complex flow pattern, with surface velocities being less than deeper water during the flood, and considerably greater during the ebb.

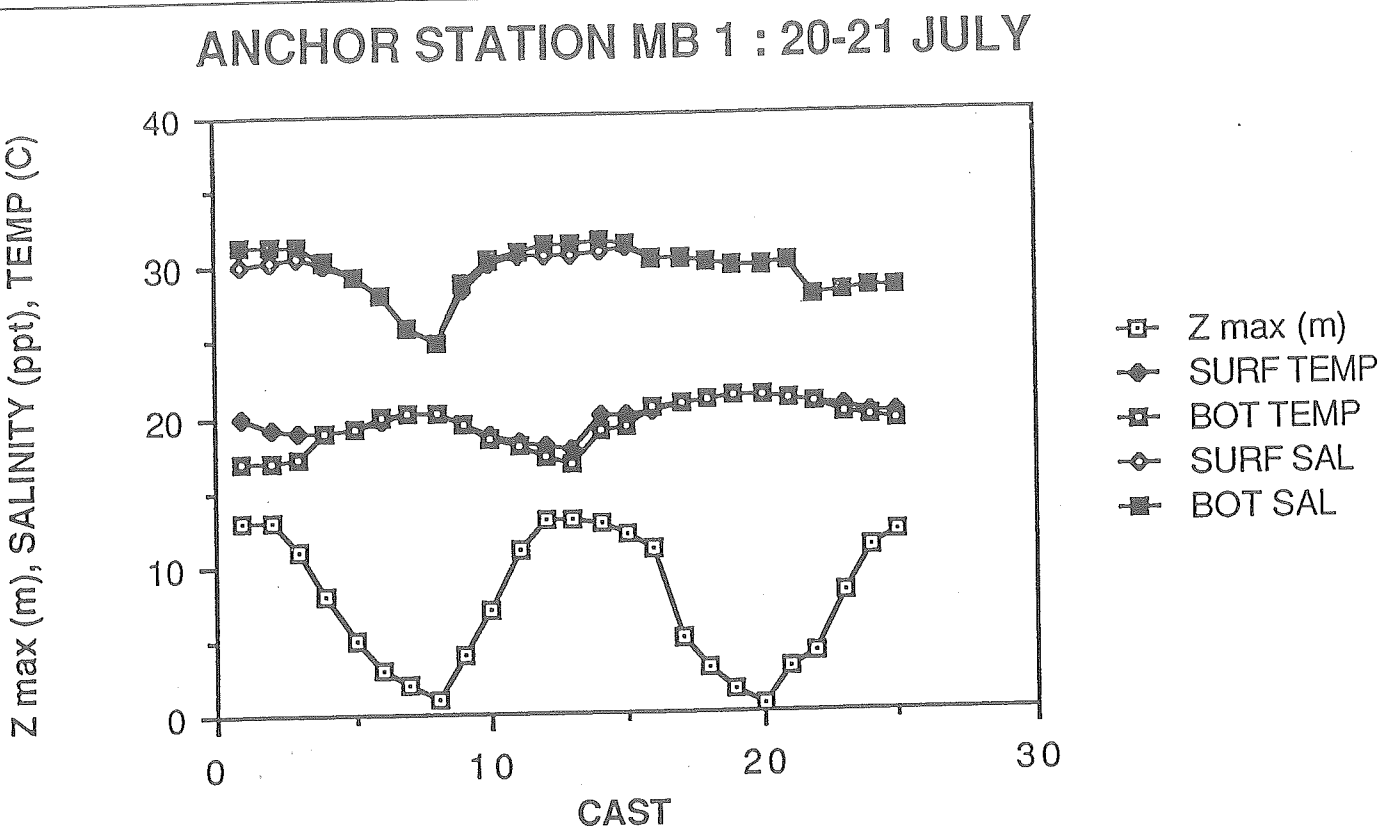

Figure 3.10A. Salinity, depth and temperature during anchor station 1.

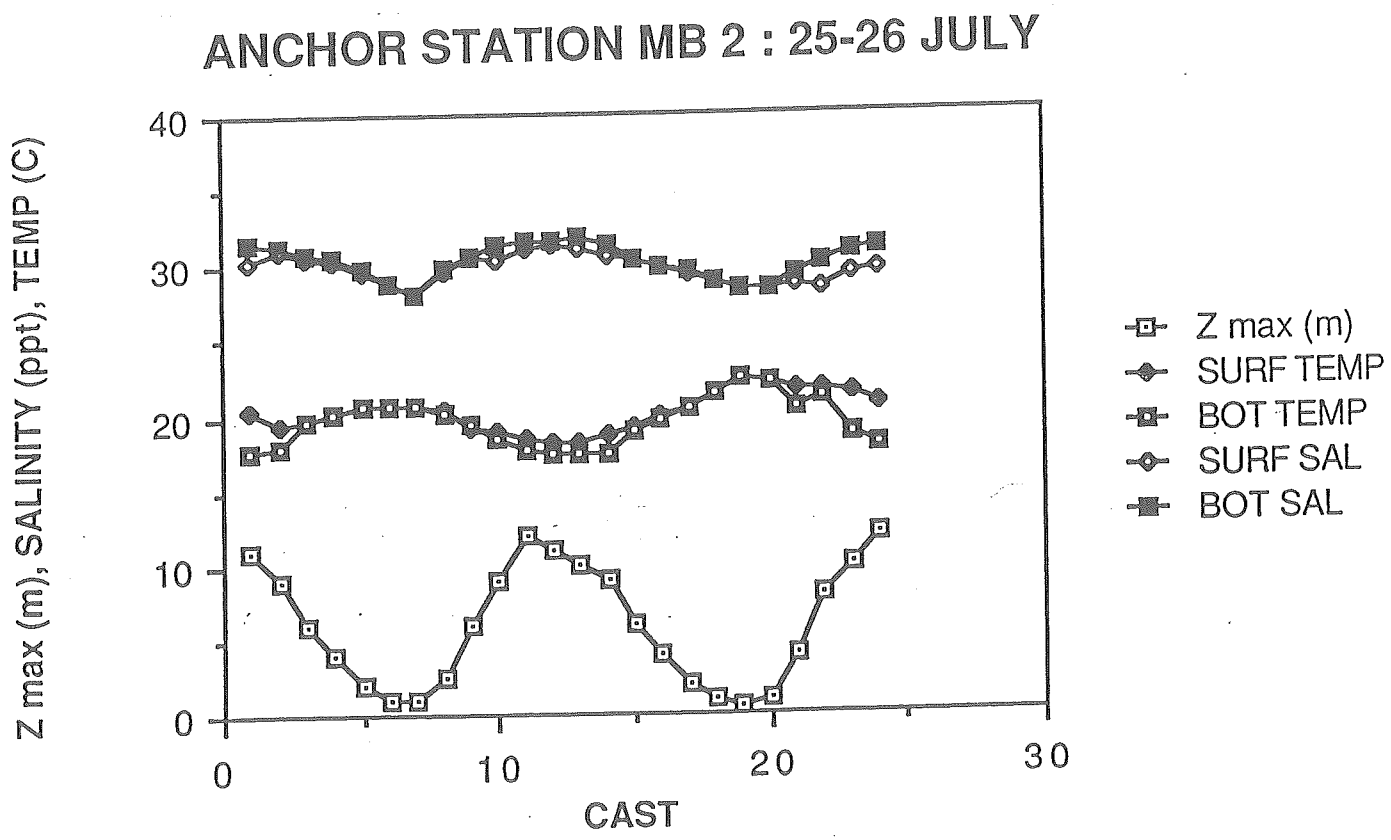

Figure 3.10B. Salinity, depth and temperature during anchor station 2.

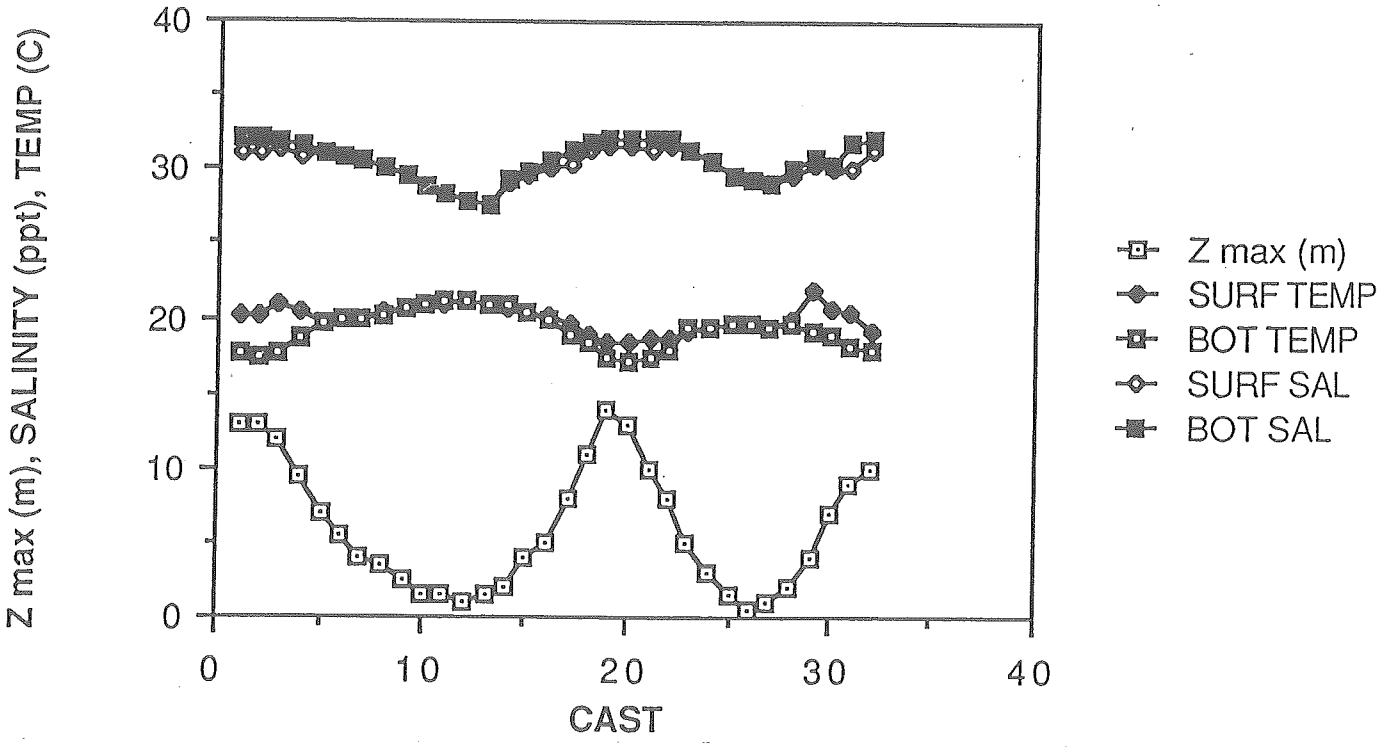

Figure 3.10C. Salinity, temperature and depth during anchor station 3.

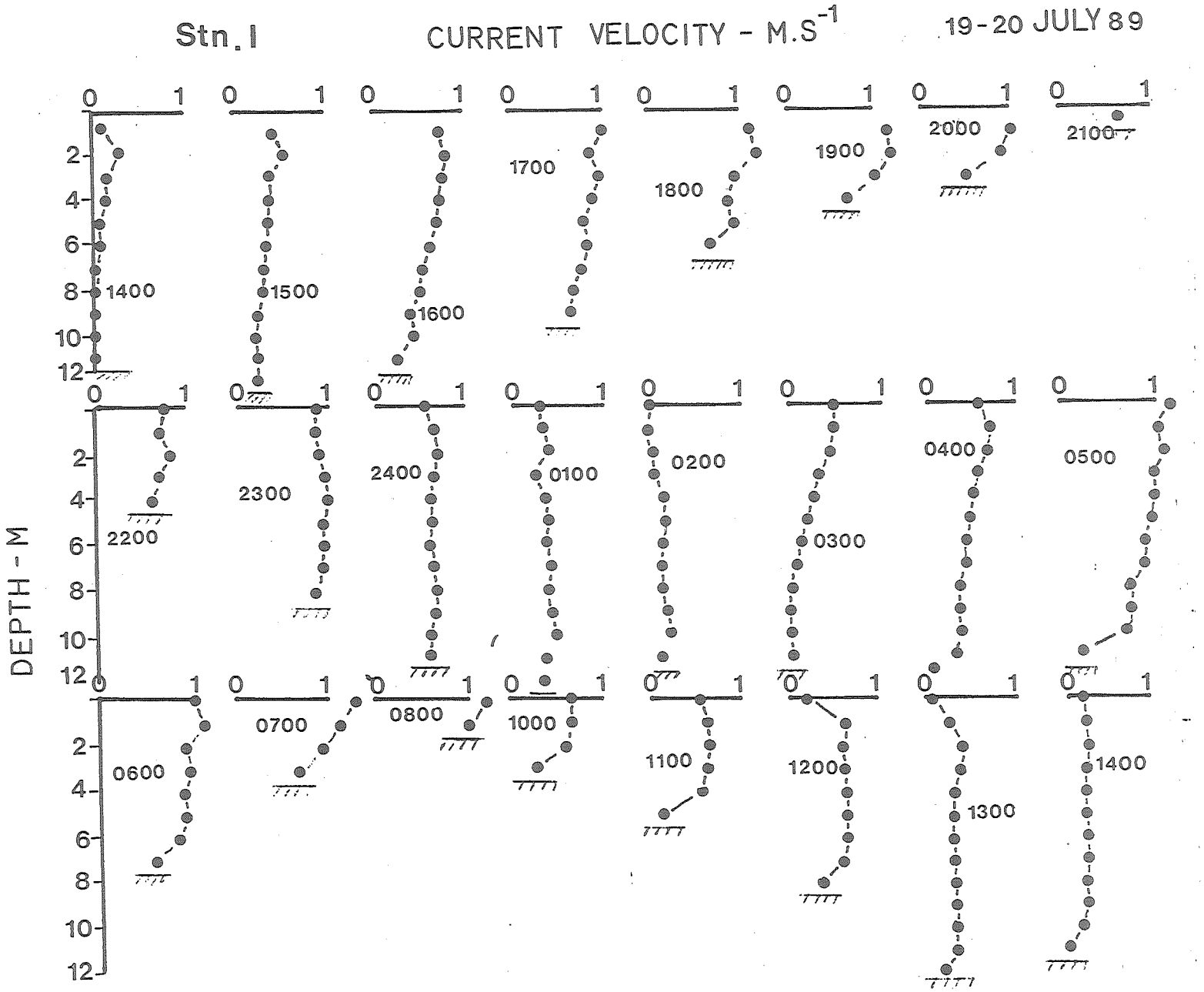

Figure 3.11A. Hourly profiles of current velocity during Anchor Station 1, 19-20 July 1989. Maximum depth indicated by hatched line.

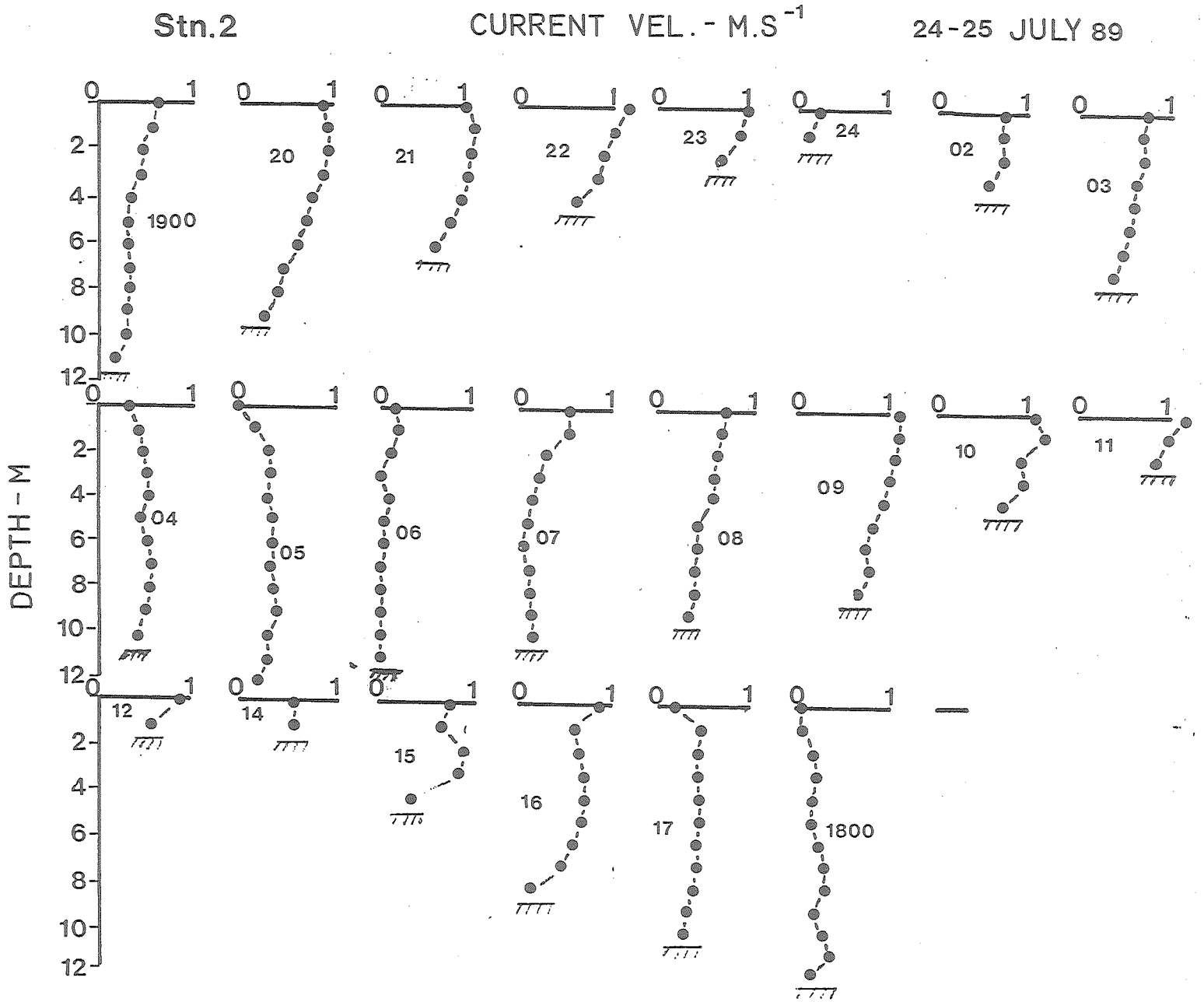

Figure 3.11B. Hourly profiles of current velocity during Anchor Station 2, 24-25 July 1989. Maximum depth indicated by hatched line.

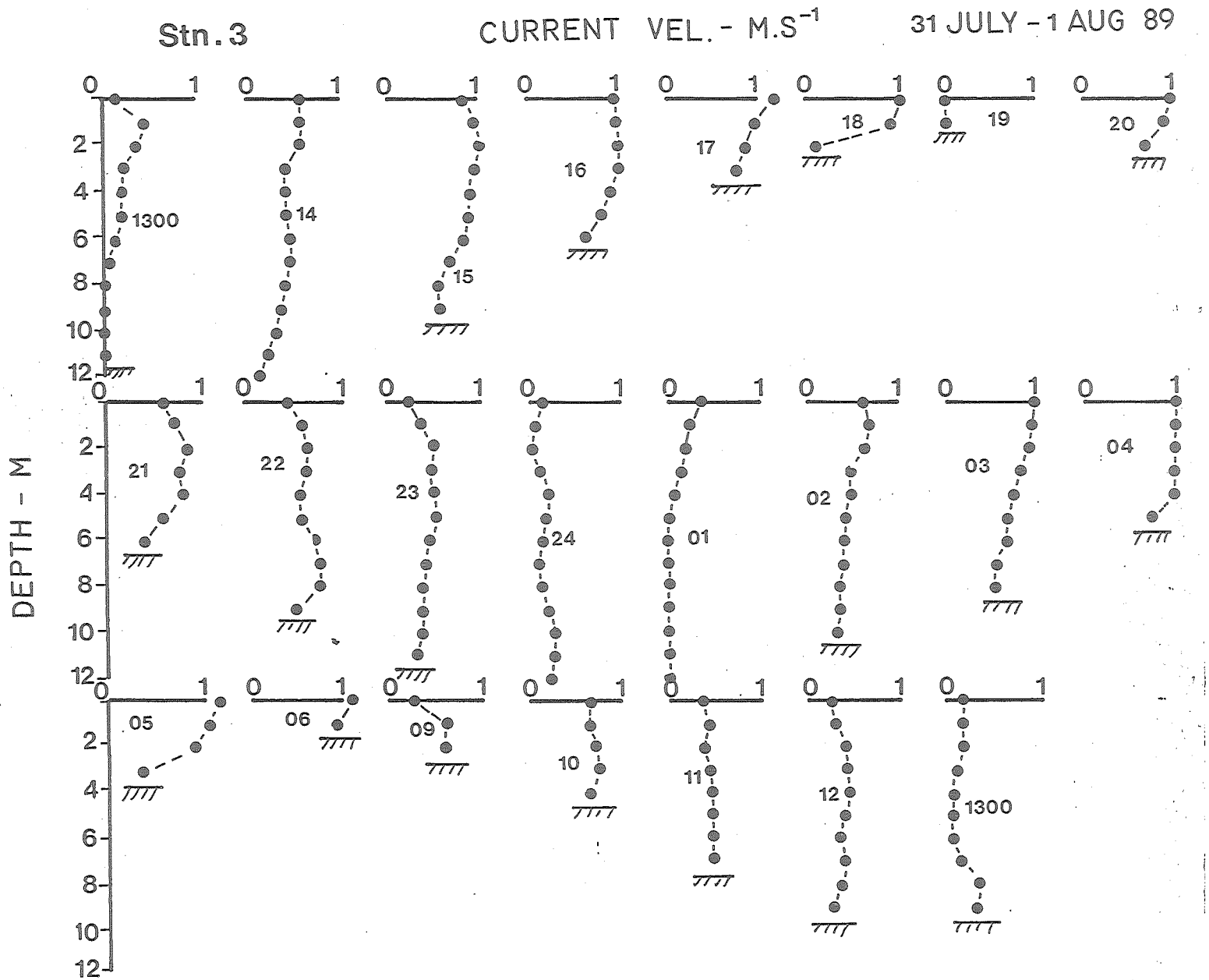

Figure 3.11C. Hourly profiles of current velocity during Anchor Station 3, 31 July - 1 August 1989. Maximum depth indicated by hatched line.

3.6 Sedimentological Studies

GRAHAM R. DABORN

Participants :
R.W. Faas, H. Christian, G.R. Daborn, J. Grant

3.6.1 Grain Size and Viscometry (Faas, Daborn)

Surface samples of sediment were taken by several participants in the course of their studies and analysed by Dr. R.W. Faas. The <63 μm portion of each sediment sample was analysed with a Bouyoucos 152 H hydrometer (Bowles 1970). Following the hydrometer analysis, the sample was washed through the 63 μm sieve; the fraction >63 μm was oven-dried at 105°C, weighed, and passed through a nest of sieves of 0.5 phi intervals, with 15 minutes shaking on a mechanical shaker. Data from both analyses were combined to form cumulative curves from which relevant parameters could be extracted. Selected samples of fine-grained material (<63 μm) were analysed using the ACER Coulter Counter.

Organic matter was determined by the loss on ignition method (Davies 1974). Bulk samples were oven-dried at 105°C, ground in a mortar, and passed through a 63 μm sieve; thus, only silt and clay-sized material was ultimately placed in a ceramic crucible and combusted at 450°C for eight hours in a muffle furnace. Organic content was calculated as :

$$OM = \frac{(\text{Dry wt. at } 105^{\circ}C - \text{Dry wt. at } 450^{\circ}C) \times 100}{(\text{Dry wt. at } 450^{\circ}C)}$$

Hindered settling of selected samples was performed at four sediment concentrations (5, 10, 25 and 50 $g.L^{-1}$) and at four salinities (5, 7.5, 15 and 30 ‰). The sediment was mixed in a blender for 15 minutes and placed in 1 L sedimentation tubes to which scales marked in centimetres had been attached. The change in height of the lutocline which formed after the sample was thoroughly stirred with a plunger was plotted against time to show the hindered settling behaviour. No attempt was made to duplicate the similar work using similar apparatus (Owen 1970), or to develop comparative data, due to multiple forms of settling (Kranck 1985) and uncertainties in interpretation (Burt 1985).

Rheological measurements were made with a Brookfield RVT 8-speed rotational viscometer (Faas 1990). The instrument, equipped with the UL adaptor, rotates a cylindrical bob within a cylindrical cup, having a narrow gap (2.47 mm) and a cup-to-bob ratio of 1.098. This configuration allows for the determination of 'apparent' viscosity for non-Newtonian fluids from absolute values of shear rate and shear stress up to shear stresses of 7200 $dynes.cm^{-2}$ (720 Pa) and controlled shear rates of up to 122.36 $.s^{-1}$ (Van Wazer et al. 1963). Parameters used to characterise the non-Newtonian rheological behaviour of sediment/water systems (slurries) include 'apparent'

yield stress and 'apparent' viscosity (reported as measured at a specific shear rate). A qualitative description of flow behaviour (e.g., pseudoplastic/shear-thinning, Newtonian, or dilatant/shear-thickening) can be made, as well as an estimate of the thixotropic behaviour of the slurry.

Atterberg limits were determined (Lambe 1951) for selected samples from the Cornwallis Estuary and compared with others obtained previously (Amos et al. 1988) for the Starrs Point tidal flat. Liquid limits and plasticity indices were plotted on the Casagrande Plasticity Chart to classify the sediments (Fig. 3.12).

Sites 1 and 2 appeared to be texturally similar, if not identical, and were classified as 'sandy silt' (Shepard 1954); results are shown in Figure 3.13. Site 3 exhibited a distinctly different texture, and was classified as a 'silty-sand'. Surficial sediment samples were taken frequently at each site during the study, and their relative grain size distributions are given in Table 3.3.

Vertical sampling at 5 cm intervals was done by H. Christian in a pit at each site during the early phase of the study; results are shown in Figure 3.14. The granulometric character of the tidal flat was noted in an earlier study (Black 1985), but these granulometric profiles show that the sediment coarsens upwards, beginning at depths of about 10 cm at each site. This phenomenon has been reported frequently before, and is generally attributed to bioturbation and winnowing of the finer particles from the substrate and relative enrichment of the coarser grains (e.g., Faas and Nittrouer 1976; Rhoades and Stanley 1966). However, Featherstone and Risk (1977) detected no evidence of 'biogenic grading' in the Minas Basin, despite animal densities (principally the polychaete *Clymenella torquata*) of 400-500 $.m^{-2}$. Therefore, two hypotheses must be considered :

(1) winnowing of the upper 10-15 cm by bioturbation leaves an upper coarser lag deposit;

(2) downward emplacement of fine-grained material, perhaps by the animals to strengthen their burrows, and by flocculation and settling of aggregates within the animal tubes. In the first place, there is the problem of explaining the silty condition of the substrate below 10 cm. If bioturbational winnowing is an appropriate mechanism, then it should have been operating within the upper 10 cm of the depositional interface as it accreted upward through time, creating a completely winnowed sediment column. On the other hand, it is possible that this distribution could result from addition of fine-grained sediment to the coarser-grained substrate. X-ray photographs of *Corophium* (the most abundant and important benthic invertebrate present on the Starrs Point flat) burrows from tidal flat deposits in the Scheldt Estuary, a macrotidal estuary in Belgium, indicates a concentration of clay particles at the base of *Corophium* burrows (Faas - unpublished data). Due to the rapid settling of single grains or small flocs observed in the present study at concentrations less than 10 $g.L^{-1}$, it is not inconceivable that vacant, water-filled burrows could serve as still-water settling tubes, easily accommodating a new layer of clay-size particles at their bases during an intertidal exposure. This would be enhanced if the animals die or are eliminated from the sediment, and hence unable to keep these tubes clear of settled material. Observations of biologically active sediment cores taken from Starrs Point by Dr. J. Grant and inserted into a laboratory flume indicate that tube clearance activities are important factors contributing to mobilisation of fine sediments under such conditions (Grant - personal communication). Other hypotheses (Azmon 1990; Matlock et al. 1989) may be applicable, but may be unable to explain the abrupt textural change at approximately 10 cm depth. Whichever hypothesis is accepted, the end result is that the shear strength and potential resistance to erosion will increase with depth as the sediment changes character from less cohesive to more cohesive.

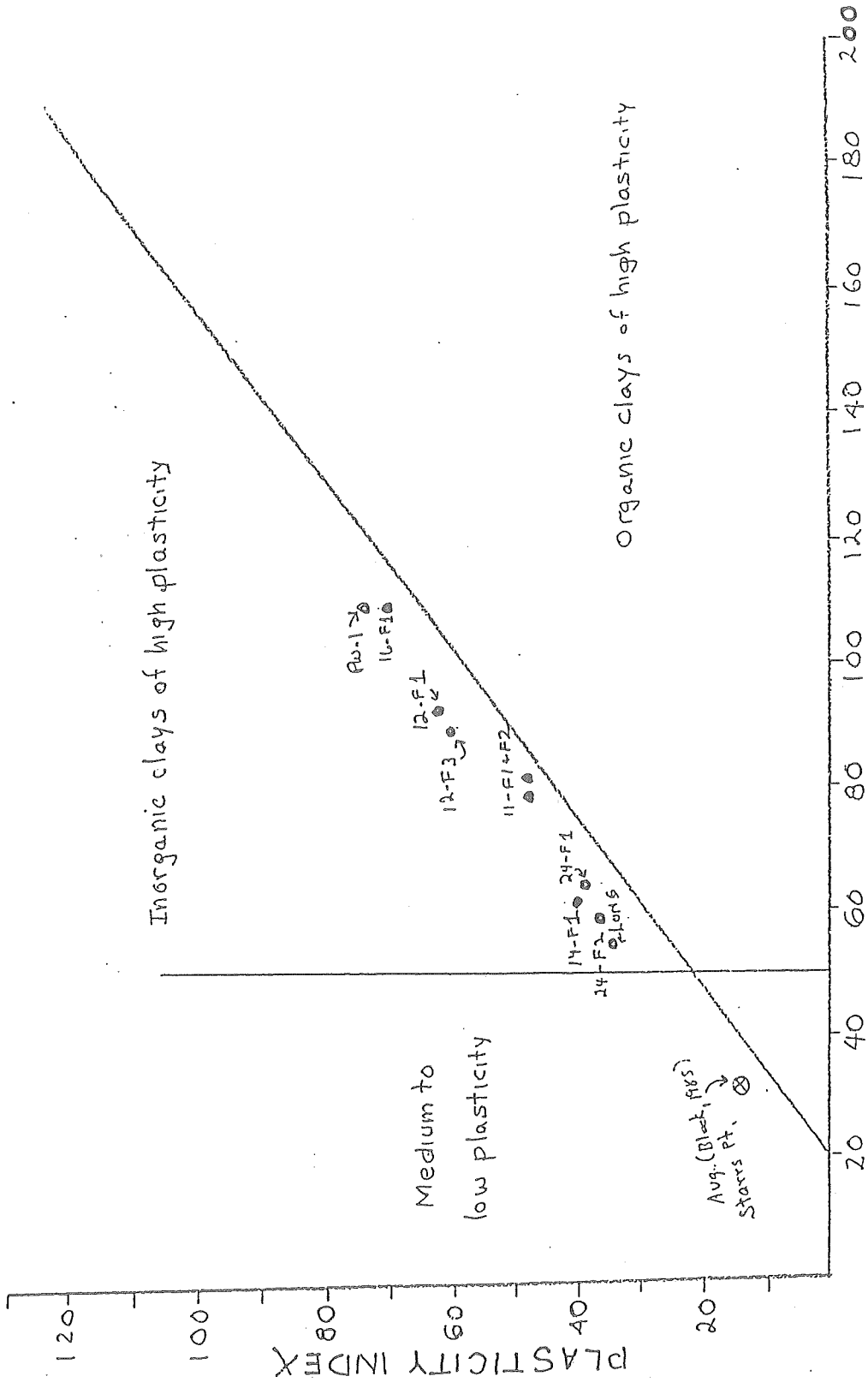

Figure 3.12. Plasticity of Sediments from the Southern Bight and Cornwallis Estuary.

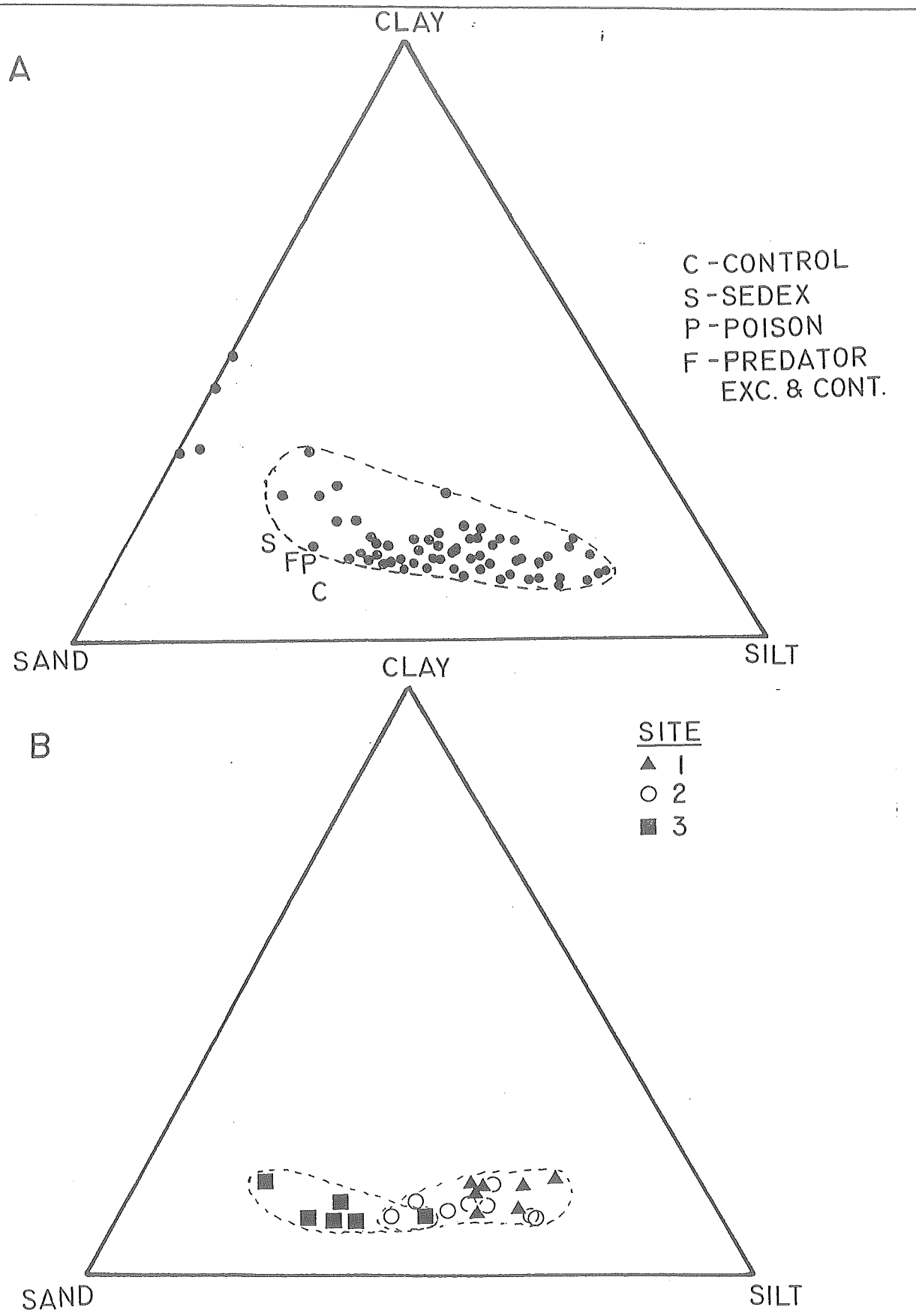

Figure 13 (A). Grain sizes (Shepard Classification) of sediments from Experimental Plots on Starrs Point Tidal Flat. (B). Grain sizes (Shepard Classification) of sediments at sites 1-3.

Table 3.3. Grain size distributions

Label	Sand	Silt	Clay	S/C	Md (mm)	OM
			Station One			
9-1A	33.9	49.6	16.5	3.00	0.035	2.75
14-1A	32.9	51.1	16.0	3.19	0.046	1.34
15-1A	37.1	51.1	14.0	3.65	0.050	0.77
15-G1	29.5	58.5	12.0	4.87	0.046	2.50
18-1A	35.0	52.0	13.0	4.00	0.050	1.45
22-1A	26.7	57.3	16.0	3.58	0.040	2.16
26-1A	42.0	61.0	17.0	3.59	0.061	1.34
30-1A	33.3	51.2	15.5	3.30	0.044	1.42
x	33.8	54.0	15.0	3.65	0.046	1.72
s	4.6	4.3	1.8	0.58	0.003	0.68
s/x (%)	13.7	7.9	11.9	16.0	16.7	39.4
			Station Two			
9-2A	28.7	61.3	10.0	6.13	0.054	2.29
14-2A	35.5	51.0	13.5	3.78	0.056	1.31
15-2A	43.5	41.0	10.5	3.90	0.073	2.12
17-2A	33.8	53.2	13.0	4.09	0.054	2.46
19-2A	38.2	43.3	13.5	3.53	0.058	2.09
19-G2	28.9	60.1	11.0	5.46	0.050	--
21-G2	39.8	48.2	12.0	4.01	0.054	2.30
24-G2	32.2	51.8	16.0	3.24	0.058	3.24
x	35.7	51.9	12.4	4.27	0.057	2.24
s	6.5	6.6	2.0	0.99	0.007	0.57
s/x (%)	13.3	12.7	15.9	23.2	12.3	25.4
			Station Three			
9-3A	55.4	35.1	9.5	3.69	0.060	1.82
10-3A	44.4	44.6	11.0	4.05	0.056	2.72
15-3A	60.7	29.3	10.0	2.93	0.078	1.19
15-G3	55.3	34.7	10.0	3.47	0.068	2.03
20-G3	61.9	28.1	10.0	2.81	0.070	1.04
24-3A	54.1	32.4	13.5	2.40	0.070	1.04
28-3A	63.5	19.5	17.0	1.15	0.073	1.54
x	57.6	30.9	11.4	2.84	0.069	1.74
s	6.8	7.7	2.6	0.93	0.008	0.52
s/x (%)	11.9	24.9	22.5	32.6	1.4	30.0

s/x (standard deviation divided by the mean x 100) is defined as the coefficient of variation reported in percent.

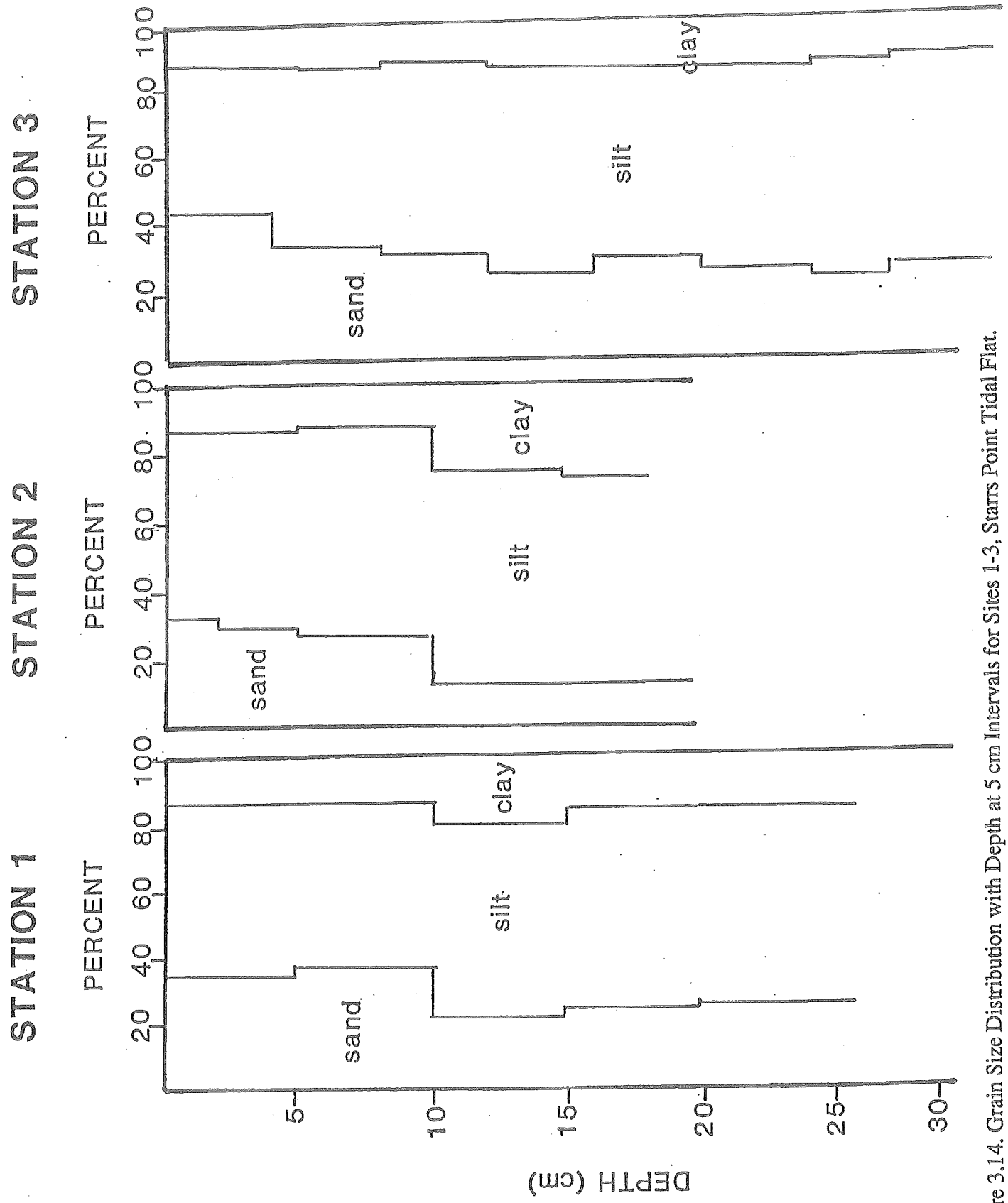

Figure 3.14. Grain Size Distribution with Depth at 5 cm Intervals for Sites 1-3, Starrs Point Tidal Flat.

Pseudoplastic (shear-thinning) flow behaviour was exhibited throughout the entire range of shear stresses and shear rates with low-density slurries (<1.2 $Mg.m^{-3}$). As density increased, progressively greater shear stresses were required to cause flow and the flow behaviour at shear rates to 6.12 $.s^{-1}$ approached those of a Newtonian fluid. Flow behaviour once again became pseudoplastic (shear-thinning) at greater shear stresses and shear rates. Dilatant (shear-thickening) flow behaviour, usually observed to occur with the more concentrated suspensions, was conspicuously missing. While no specific study of the mineralogy of the <63 μm fraction has yet been done, the mineralogy most likely approaches that of Evangeline Beach (located east of Starrs Point tidal flat - cf. Fig. 3.2.). The fine fraction is dominated by quartz (24%) and feldspar (18%), with illite (18%) and chlorite (12%) dominating the clay mineral assemblage (Amos and Mosher 1985). Smectite was non-existent and kaolinite and vermiculite existed only in trace quantities. A similar mineralogy can be assumed for the Cornwallis Estuary and Starrs Point samples, as indicated by their low plasticity and non-cohesive character.

The Cornwallis River is the major source of freshwater to the Southern Bight of Minas Basin; the estuarine portion between Kentville and Wolfville is approximately 25 km in length, is well mixed and turbid. Previous work in the Cornwallis Estuary showed that a pronounced turbidity maximum occurs near the upper limit of tidal influence, with surface SPM values approaching 5 $g.L^{-1}$, and underlying water having <15 $g.L^{-1}$ (Daborn and Pennachetti 1979a). Concentrations decrease regularly towards the mouth (north of Wolfville) to values in the range of 50-70 $mg.L^{-1}$, and thus are somewhat higher than waters overlying Starrs Point flat. Sediment distribution within the Cornwallis Estuary is similar to that described for the nearby Avon Estuary, i.e., there is an inverse relationship between particle size and current velocity, with the latter increasing up-estuary from an average of 80 $cm.s^{-1}$ at the mouth to 130 $cm.s^{-1}$ near the Windsor Causeway (Lambiase 1980). Comparable current measurements are not yet available for the Cornwallis Estuary. The mechanism invoked by Lambiase (1980) to explain this distribution is 'hydraulic sorting'. The hypothesis is that coarser grains remain in a bottom traction mode at the estuary mouth where current velocities are lower; finer-grained sediments become intermittently suspended from the traction blanket, joining the fine-grained suspended load as current velocity increases up-estuary; each smaller particle size will bypass its nearest larger neighbour as longitudinal sorting takes place in an increasing velocity field. At some (null) point, the velocity must decrease to zero, and sedimentation takes place. This form of sedimentation was not addressed by Lambiase (1980), nor was any consideration given to the source of the fine-grained material which was accumulating at the head of the estuary (Allen et al. 1980).

Sampling in the bed of the estuary during ebb tide indicates that significant bedload transport occurs, resulting in ebb-oriented bedforms (sandwaves and dunes), particularly around the inside bank of meanders. Numerous well-rounded and generally unarmoured mud pebbles, ranging in length from 29 to 75 mm (A axis), between 35 and 40 mm wide (B axis), and from 22 to 38 mm in height (C axis), were found in the troughs between the bedforms. Surprisingly, a considerable amount of fine-grained material (existing as 'fluid mud') was found draped over the sand bars and accumulating in pits, inside cusps, and in depressions on the sand bar surface, and in quiet water embayments between the bar and the shore into which runoff from the bar surface was directed. In some places these depressions extended for several decameters in length, and were a few metres in width.

They lay parallel to the bar axis, providing a depositional trough emptying downstream into which the fine-grained sediments (fluid mud) were flowing. Flocculation and hindered settling occurred within this quiescent environment, as demonstrated by the formation of a distinct lutocline (Kirby and Parker 1977) with several centimetres of clear water above (Wells and Coleman 1981; Wolanski et al. 1988). The bar surface showed a dramatic example of expansion due to excess pore pressure release following removal of the hydrostatic load superimposed during the flood tide. The expansion of the bar surface created a series of parallel-oriented normal faults (horst-graben topography), into which 'fluid mud' was injected from a buried, thixotropic, underconsolidated mud layer which fluidized upon release of excess pore pressures. This material filling the graben exhibited a totally different particle size distribution than that of the horst, the latter being a mixed "sand-silt-clay", possessing a median diameter of 0.068 mm (Fig. 3.15 B), the former a "silty-clay" with a median diameter of 0.022 mm (Fig. 3.15 A). Once the depression (graben) was filled, the mud flowed over the surface and down the slope of the bar toward the depressions. Several short cores (20 cm) were taken from the bar surface to examine the fine stratigraphy of the deposit. One core, taken just above the water level, showed an alternating series of clay-sized/sand-sized materials with sharp contacts above and below the clay-sized material, indicating no mixing.

'Fluid mud' deposits appeared to occur with greater frequency upstream from the estuary mouth near Wolfville. This was particularly noticeable when descending the channel sides to approach the channel bottom during low tide : often thicknesses of 0.5 m and more of soft mud had to be crossed before reaching a stable substrate. Much of this material resulted from mass downslope movement due to undercutting and slumping of the channel sides. However, it is likely that some of this mud represented material recently deposited, perhaps during the preceding high tide. Many instances of "perched" depressions containing settled mud were observed at various elevations between the channel bottom and the top, with most occurring at mid-slope. These depressions trapped water with suspended sediment as the water level dropped during ebb tide. Flocculation and hindered settling of the suspended sediment occurred rapidly under still-water conditions, resulting in a coating of newly-deposited mud (average density of 1.319 $Mg.m^{-3}$ and depositional water content of 177% dry weight) of variable thickness, depending on the concentration of suspended sediment in the water trapped in the "perched" depressions. This concentration will increase up-estuary due to the greater suspended sediment concentrations in the turbidity maximum. The suspensions, as they settle, have been shown to develop a significant time-dependent yield stress, particularly between suspension densities of 1.10 to 1.30 $Mg.m^{-3}$ (Fig. 3.16). For settled muds accumulating in the "perched" depressions between the channel base and halfway up the channel sides, the time available for yield stress development increases upslope and these deposits are more likely to require greater shear stresses to be eroded and resuspended than the muds accumulating in depressions on the channel bottom. The general flow behaviour of the Cornwallis Estuary sedimentary suspensions, characterized as dominantly pseudoplastic (shear-thinning), at least to a density of 1.30 $Mg.m^{-3}$, facilitates easy resuspension and maintains a high level concentration of suspended sediment throughout the entire water column, particularly on the flood.

Hindered settling experiments performed with different salinities and sediment concentrations shows that

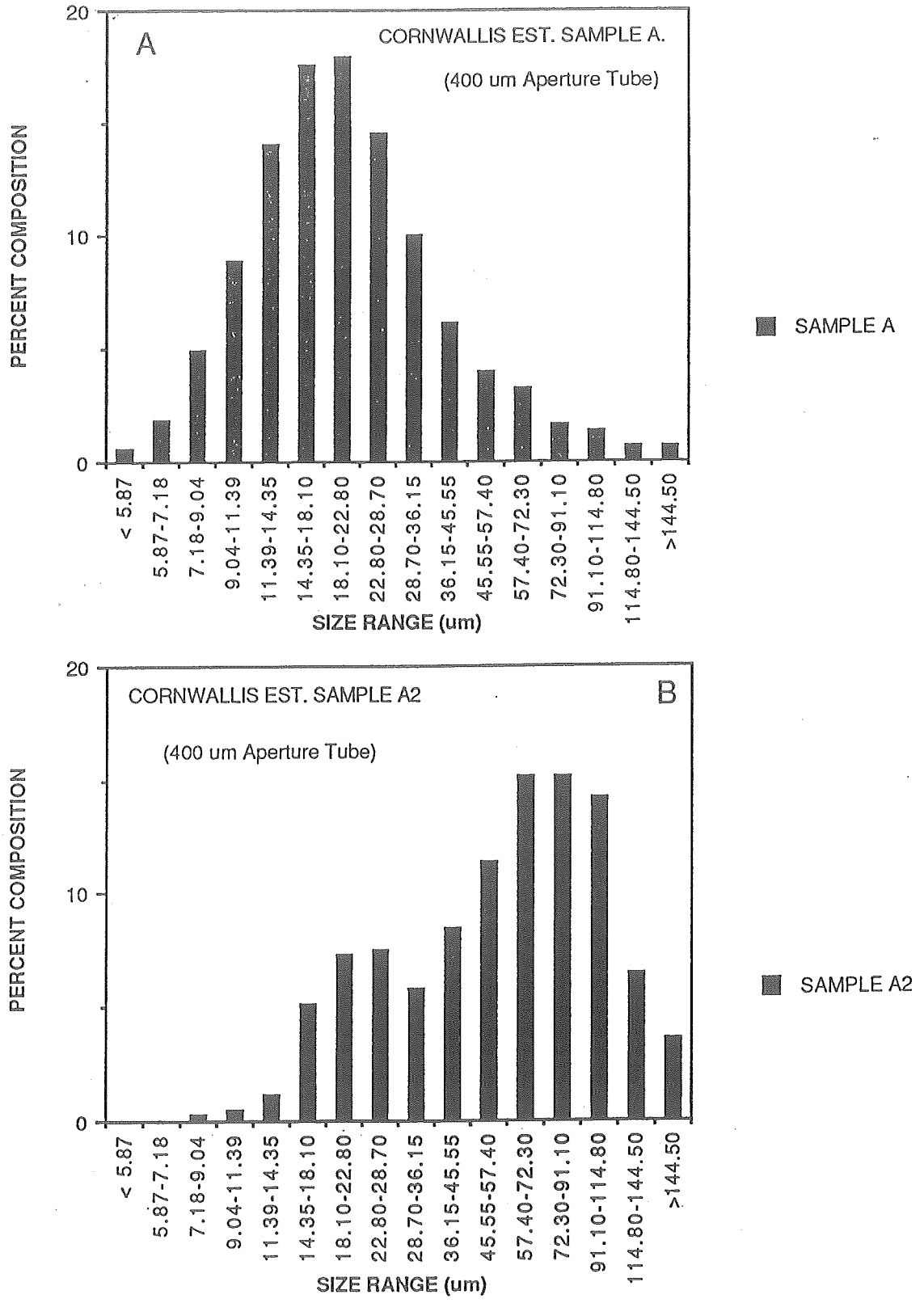

Figure 3.15. Grain Size Distributions for Cornwallis Estuary samples obtained with a Coulter Counter 400 µm Aperture Tube.

A - Fine "silty-clay" from filling material in a depression.

B - "Sand-silt-clay" from surrounding deposit.

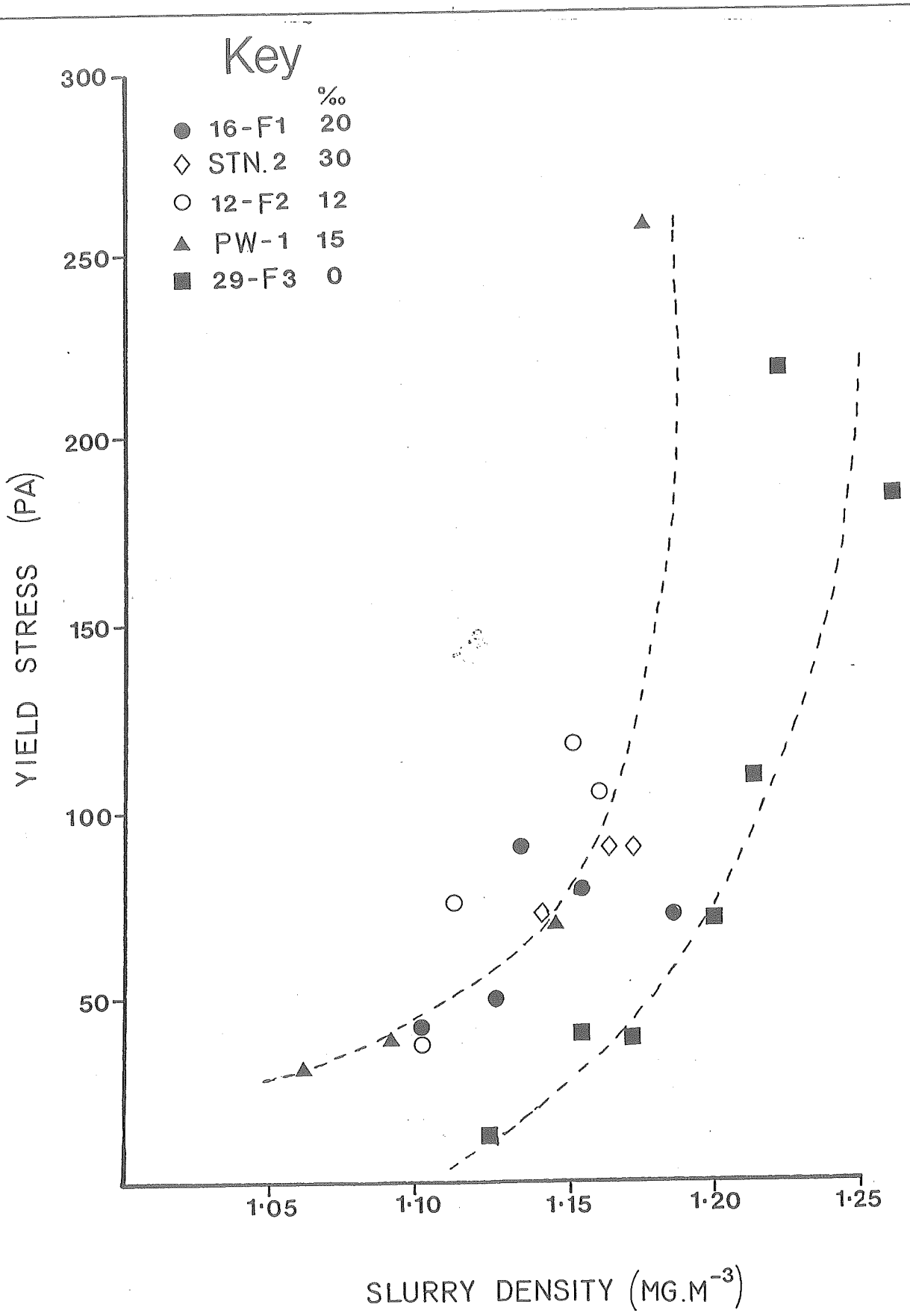

Figure 3.16. Relationship between Yield Stress and Slurry Density for Cornwallis Estuary Muds.

still-water settling of non-flocculated particles (or very small flocs) occurs rapidly in concentrations between 10 and 25 $g.L^{-1}$ (2.5 to 5.2 x 10^{-2} $cm.s^{-1}$), decreasing to 6.8 to 8.6 x 10^{-3} $cm.s^{-1}$ at concentrations to 50 $mg.L^{-1}$ (Fig. 3.17). These data compare favourably with Amos and Mosher (1985) who measured settling velocities of 2.1 x 10^{-2} $cm.s^{-1}$ in the field, and 3.0 x 10^{-3} $cm.s^{-1}$ from settling tubes using Avon River muds. There appears to be some dependency upon salinity, with slower hindered settling occurring at salinities up to 5 ‰ (Fig. 3.18). This seems particularly effective at high concentrations (e.g., 50 $g.L^{-1}$), but more work needs to be done to clarify this relationship. However, it is certain that this phenomenon is occurring in all of the residual pools of standing water and sediment that occur during each ebb tide.

The data presented allow a few interpretations to be made regarding the interactions which seem to exist between the sediment-laden Cornwallis Estuary and the Starrs Point tidal flat. Fine-grained sediment is more prevalent at greater depths in the sediment, changing its texture and making it more cohesive. Suspended sediment concentrations (see below) in the water column of the Southern Bight are quite low, from 19-34 $mg.L^{-1}$ nearshore, to 6-10 $mg.L^{-1}$ offshore, and to <6 $mg.L^{-1}$ in the centre of the Minas Basin (Greenberg and Amos 1983). These concentrations are unlikely to provide a sufficient source of fine-grained sediment to the tidal flat.

It seems very likely that the Cornwallis Estuary serves as an effective sedimentary filter (cf. Schubel and Hirschberg 1980). However, type C (completely mixed) estuaries are considered to be major exporters of sediment, with little trapping efficiency—yet it appears that the Cornwallis Estuary exports very little sediment. Instead, the data suggest that the opposite is true : sediment is imported and retained within the estuary during the summer months, accounting for the low ambient turbidity and suspended sediment concentrations of Minas Basin. It needs to be emphasised that the studies here were conducted during summer months. During winter, the tidal flats are covered for long periods of time by ice formed *in situ*, but which is broken up and moved around by tidal action. This is undoubtedly a major annual signal that influences the degree of compaction or consolidation of sediment, and also may result in substantial export of surficial sediment during the spring.

It is also apparent that the vertical pattern of grain size distribution is anomalous, but may well be related to the activities and abundance of benthic organisms such as the amphipod *Corophium* or the several species of polychaetes. The deficiency of fine-grained cohesive sediments in the upper 10-15 cm at each site, combined with intense ebullition of gases during exposure to the atmosphere (a phenomenon that is strikingly audible during a low tide walk on the flats), results in an upper layer of low intrinsic cohesion. Changes in the degree of cohesion were the subject of studies reported here in sections 3.7 to 3.10.

3.6.2 Organic Content of Deposited Sediments (Faas, Daborn, Paterson)

Organic matter content, determined by loss on combustion at 450°C varied quite widely both with location and time during the study, but within the limits of 0.6 to 3.5%. Station 2, near the Barge, exhibited a higher average organic content (2.24 % ± 0.57) than either Stations 1 (1.72 % ± 0.68) or 3 (1.74 % ± 0.52). Selected results are given in Table 3.3; the temporal change in organic content is discussed in Section 3.10.

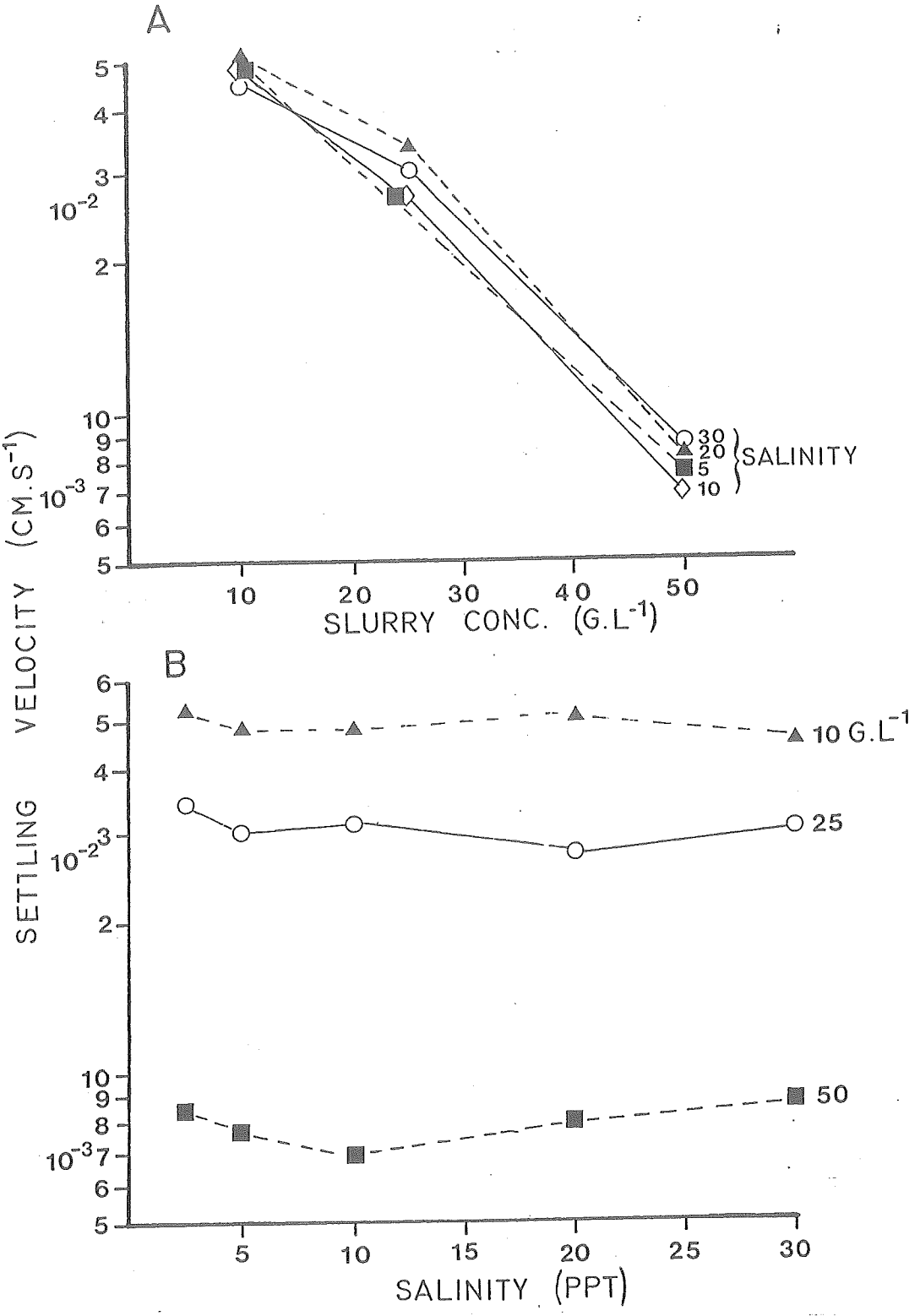

Figure 3.17 (A). Plot of the velocity of the Hindered Settling Interface of Cornwallis Estuary muds at different concentrations and salinities. Settling is more rapid at sediment concentrations between 10 and 25 g.L^{-1}, and more hindered at greater concentrations. (B). Plot of the velocity of the Hindered Settling Interface of Cornwallis Estuary muds at different concentrations and salinities. Faster settling occurs at lowest salinity at concentrations to 5 g.L^{-1}; the effect is reduced or non-existent at S > 5 g.L^{-1}.

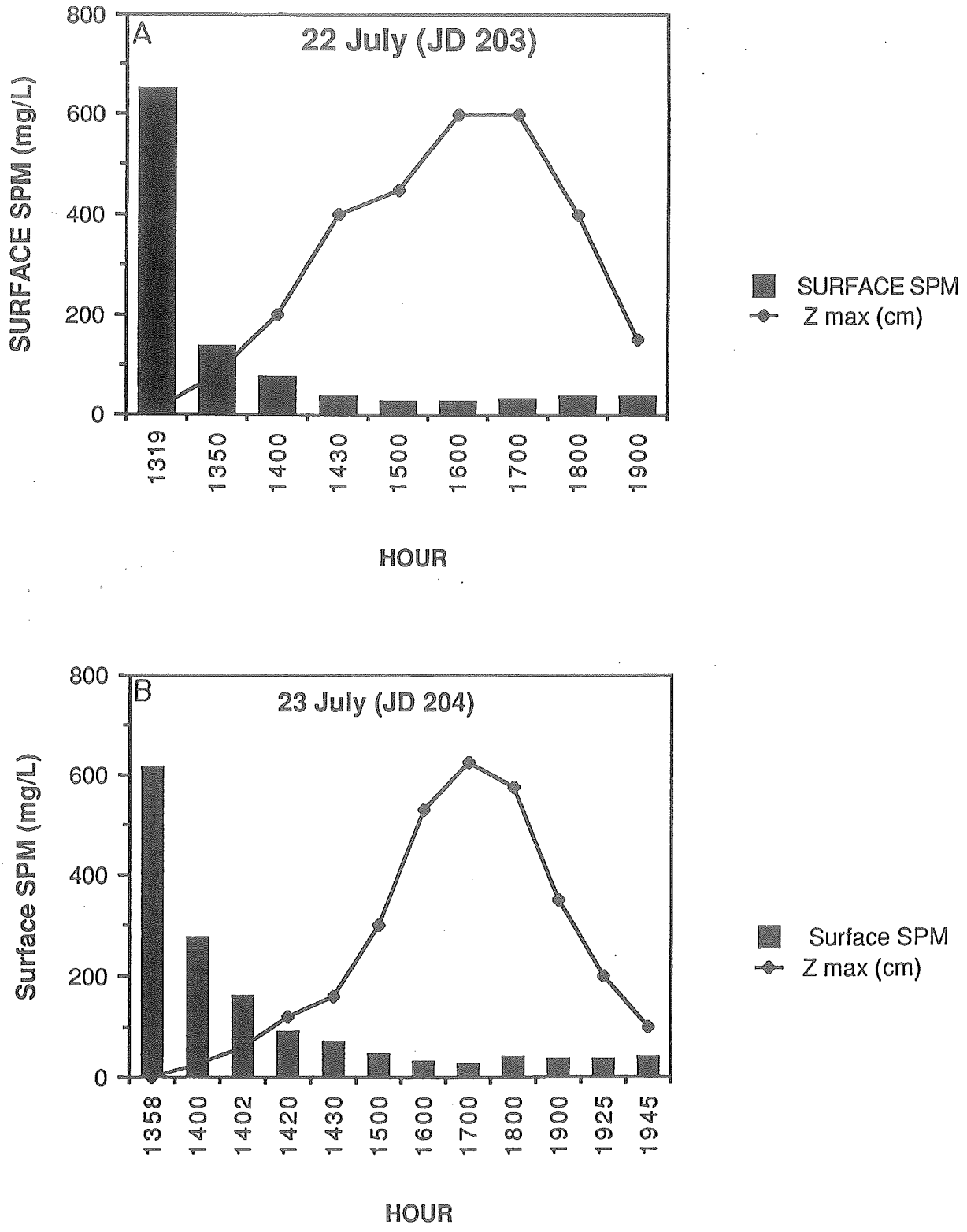

Figure 3.18. Surface SPM concentrations over three tidal cycles.

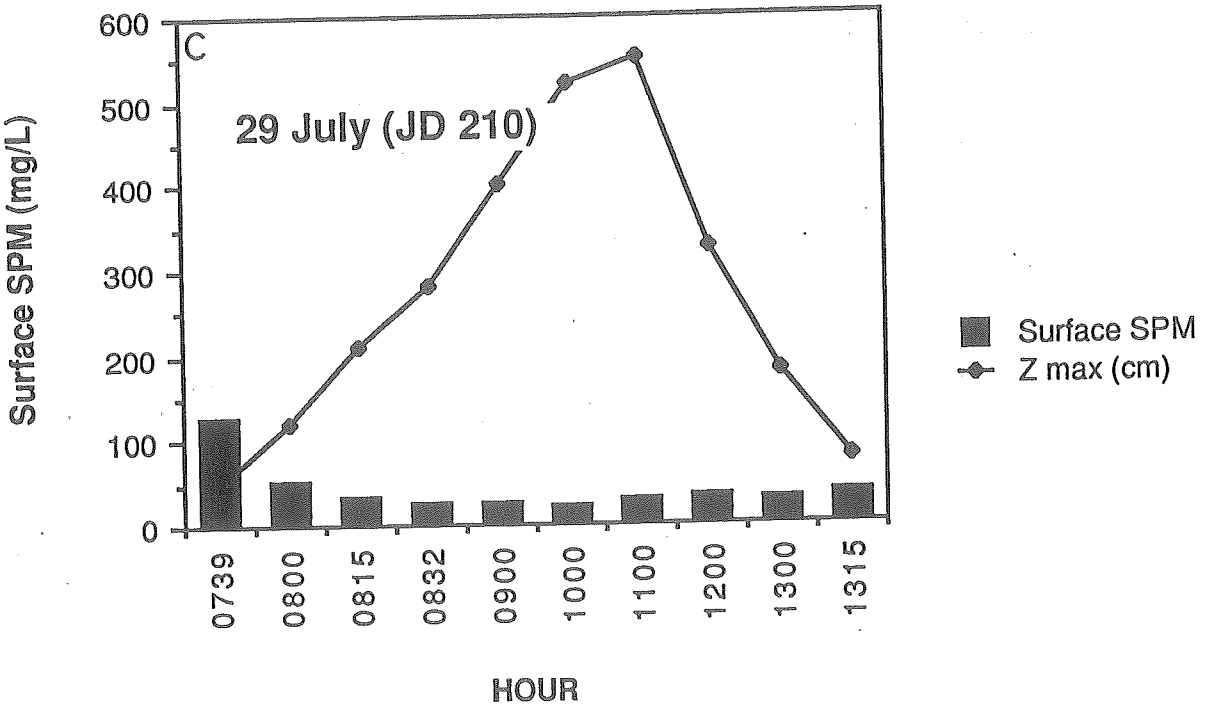

Figure 3.18. Cont.

3.6.3 Suspended Particulate Matter (Daborn)

Suspended sediment concentration (SPM) was determined gravimetrically from 1 L water samples taken on every hydro cast at the barge and the *Cora Lee II* anchor stations. Samples were taken at the surface, mid-depth, and near the bottom (usually c. 1 m above the substrate because of instrumentation on the hydro wire). At the barge site, because it was obvious that SPM concentrations were greater during the first few minutes of the flood and the last few minutes as the tide ebbed from the site, additional water samples were taken by hand at these times even though water depth was insufficient for deployment of the CTD.

For most of the time when the Barge site was inundated, SPM values were similar throughout the water column, and generally less than 50 $mg.L^{-1}$. Cursory examination of wind and SPM data indicates that winds >6 $m.s^{-1}$ can increase the turbidity substantially, even when the water is several metres deep. Examples of SPM values for three selected tides are shown in Figure 3.18 A-C. These data were chosen to represent both spring (22, 23 July) and neap (29 July) tides, and also windy (22 July) vs. calm (23 July) conditions. It is apparent that once water depth exceeded 1 m, SPM concentrations did not vary greatly during the tidal cycle. These data reinforce the previous observation that despite the high tidal range, the water over the Starrs Point tidal flat is not very turbid.

However, as water first advanced on the flood to the Barge position, the leading edge of the tide (conveniently referred to as a 'microbore') exhibited much higher SPM concentrations. Samples taken when water depth was less than 50 cm generally exceeded 100 $mg.L^{-1}$, and reached values in excess of 600 $mg.L^{-1}$ when depth was less than 10 cm. This relationship is shown in Figure 3.19, based upon a series of samples taken within 30 minutes of water arriving at the Barge site. As the tide receded and water depth fell below 50 cm, SPM values rose again, but were generally somewhat lower than those at comparable depth on the flood. Previous studies have shown that the 'microbore' is an extremely dynamic microenvironment, often being densely populated by microzooplankton, especially larvae of polychaetes and molluscs (Daborn and Pennachetti 1979b; Daborn - unpublished data).

The apparently rapid clearing of the water as depth increased to more than 1 m on the flood might have been partly an artifact of our inability to sample at depths of only a few centimetres above the bottom when water depth is much greater; it is possible that comparably high SPM values might be found in a near-bottom slurry that is missed by our regular sampling techniques. In order to examine this possibility, syringe samples were taken using BOSS, a remotely-triggered array for sampling water in narrowly-defined strata near the bottom during submergence. A full account of the data from this deployment is not available, however, preliminary examination of the lowermost syringes (situated approximately 25 cm above the bottom) showed no evidence of high SPM concentrations near to the bed (K. Muschenheim - personal communication). The cumulative evidence suggests that any material resuspended from the bottom by the 'microbore' settles very rapidly or is borne away from the site. This is compatible with the grain size results, which show very low quantities of clay-size particles in the upper sediments.

Examination of grain size distributions of suspended sediments was carried out using a Coulter Counter, with

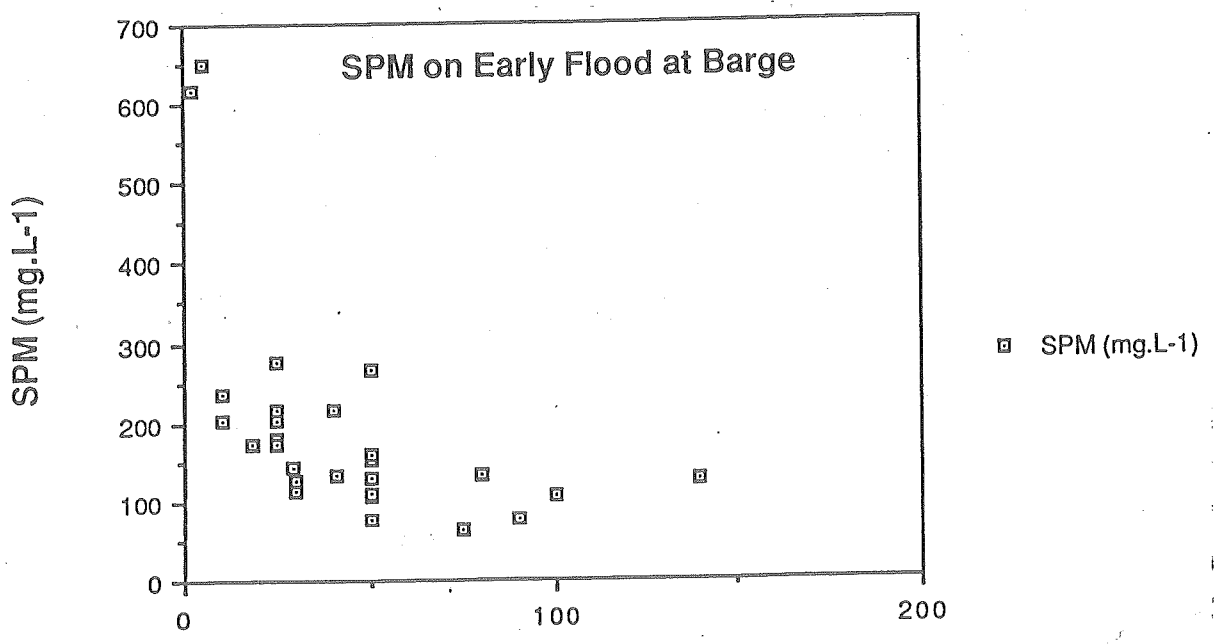

Figure 3.19. Surface SPM as a function of depth during early flood (i.e., the "microbore").

aperture tubes of 100 μm and 280 μm. Examples are shown in Figure 3.20 A-C, based upon water samples taken at the barge just after high water on a spring tide (23 July) at the surface, 2 m and 5 m depth and passed through the 280 μm aperture. At this time, SPM concentrations were essentially the same at all three sample depths (26.9, 26.8 and 26.6 mg.L^{-1}). The distributions are not notably dissimilar, being more or less unimodal around 36-45 μm, except that the uppermost channel (accumulating all particles >144.5 μm) of the near-bottom sample indicates a preponderance of larger particles in this sample. This distribution is common to near bottom samples taken during the study, and may be attributed either to settling of larger or flocculated particles, or to resuspension of flocs from the bottom. At this particular time (early ebb), it is possibly more likely a reflection of differential settlement during the high water still stand.

Comparison of SPM concentrations during flood and ebb tides at the Barge site shows no consistent differences, except for the events associated with the 'microbore' described above. This reinforces the conclusions related to the relative lack of fine-grained material in surface deposited sediments, since it is apparent that little material is resuspended despite the vigorous mixing associated with flood and ebb currents. Preliminary examination of the wind and sediment data suggest that only very strong winds (e.g., >7 m.s^{-1}) could produce a notably greater suspended sediment load over the flat with water depths greater than 1-2 m.

SPM concentrations in water samples taken at each hourly cast during the three anchor stations and analysed gravimetrically are shown in Figure 3.21 A-C. At this location, minimum SPM values of 25-30 mg.L^{-1} were found at high water times; concentrations rose rapidly during the ebb tide to 300-1,000 mg.L^{-1} at low water. Despite strong currents throughout much of the tidal cycle, and evidence of vigorous vertical mixing in areas near the vessel, there were occasionally greater concentrations at depth than near the surface. An attenuance meter suspended in the upper 0.5-1 m of the water column provided continuous readings of turbidity during the study period. Results have not been fully examined to date, however representative data from the anchor station of 19-20 July are shown in Figure 3.22. As turbidity increased during the ebb tide, transmittance decreased to almost zero at low water. However, over a half-hour period of relatively calm water around low tide, before the tide turned, transmittance increased quite sharply. This may be attributed either to gravity settling and/or flocculation of suspended particles, but the possibility of it being caused by local circulation of less turbid water around the site cannot be entirely discounted. With the turning tide, transmittance decreased for a while, presumably as a result of remixing of the water column, before the clearer water of the flooding tide resulted in higher transmittance.

Grain size analysis using the Coulter Counter gave some indication that the water column was not homogeneous, despite the strong tidal flows. Suspended sediments covering a wide range of particle sizes were present throughout the water column, but deeper samples often showed a shift in mode towards greater sizes than at the surface. A representative series is shown in Figure 3.23, taken near high water on 25 July.

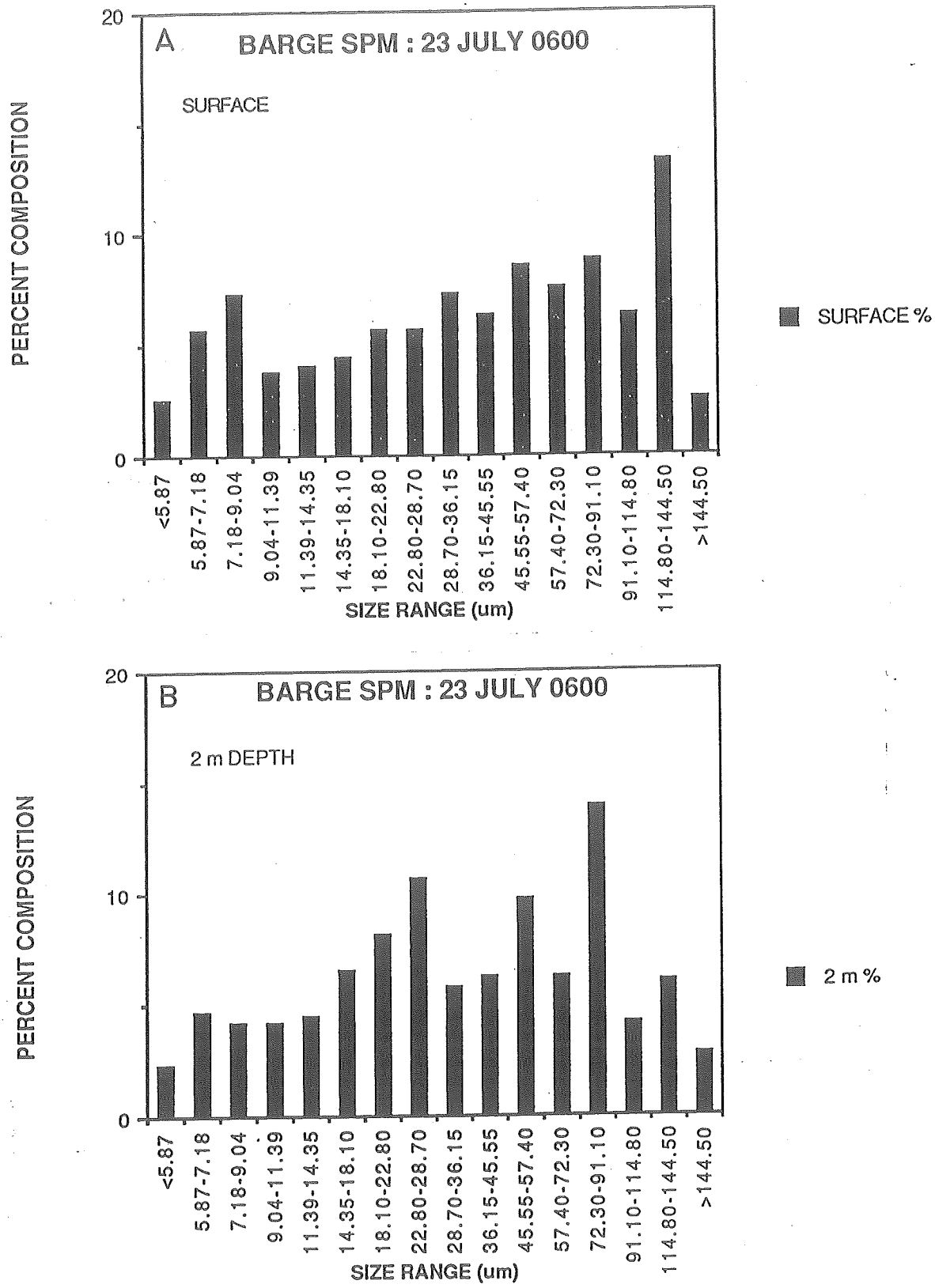

Figure 3.20. Grain size distributions near high water at the barge.

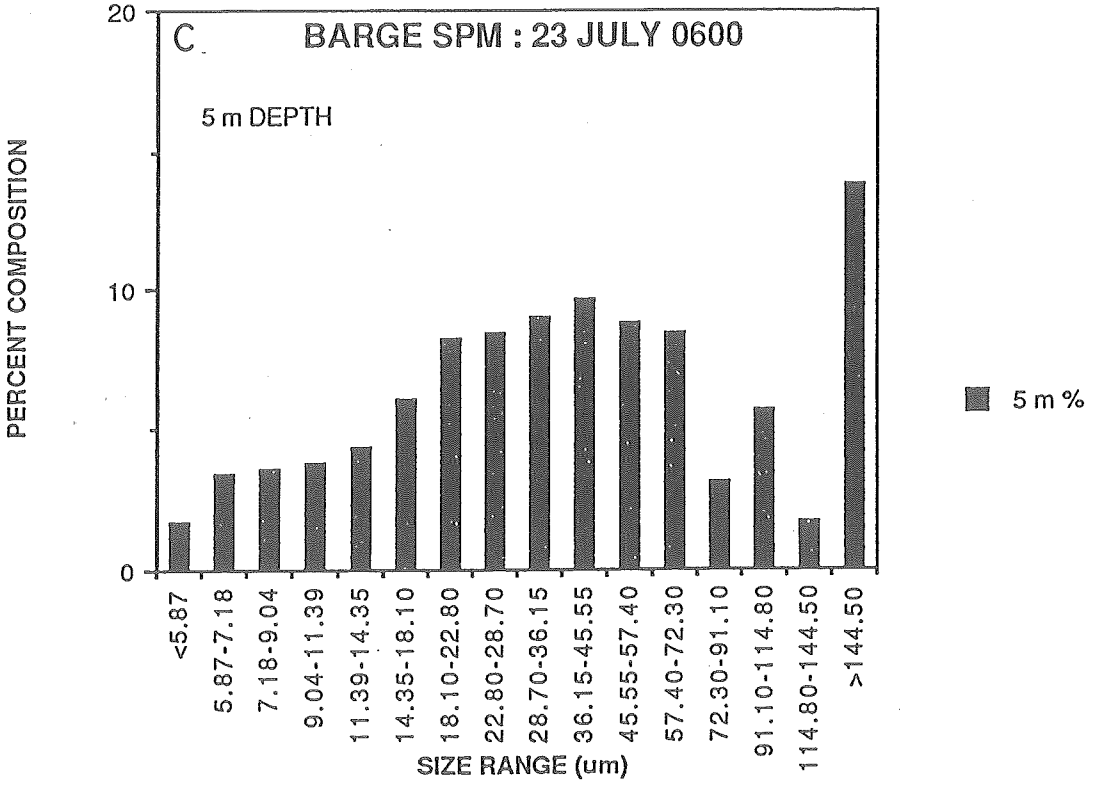

Figure 3.20. Cont.

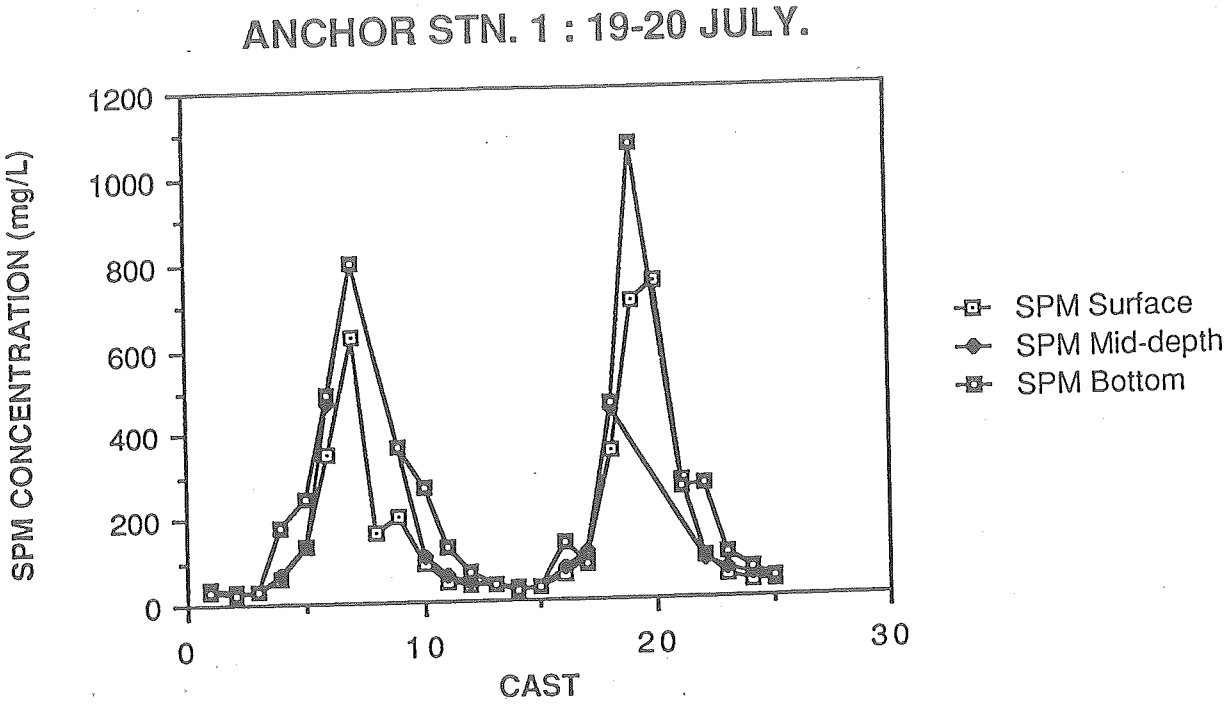

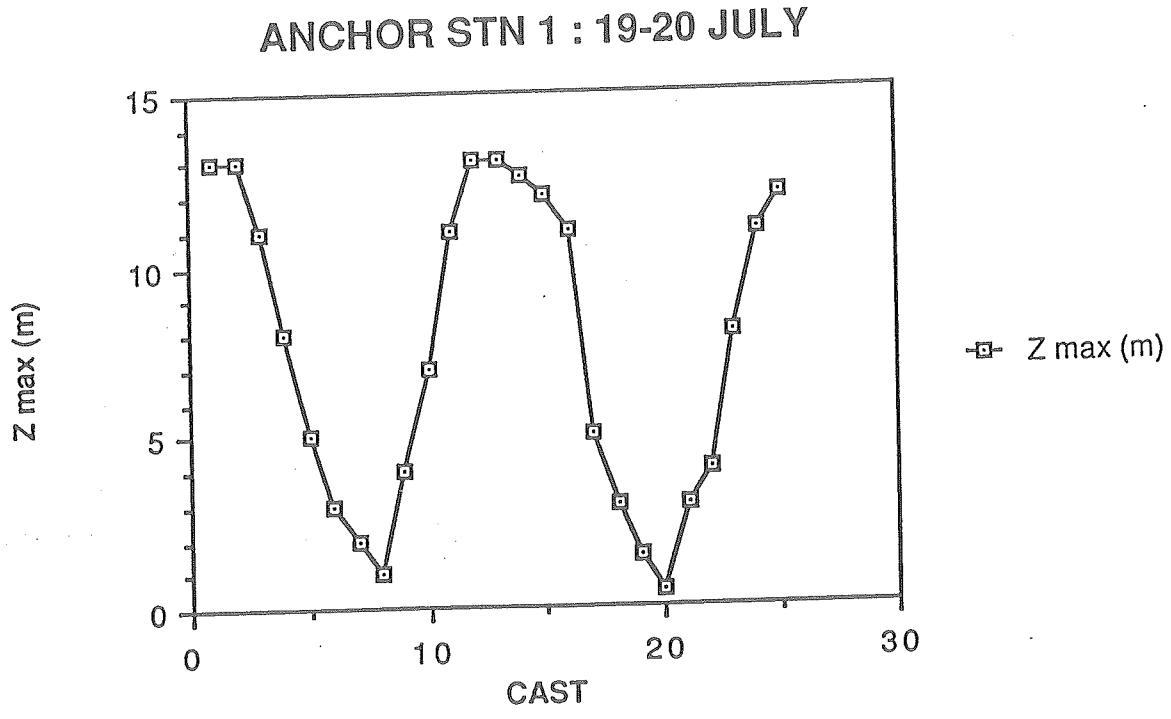

Figure 3.21A. SPM concentrations at anchor station 1.

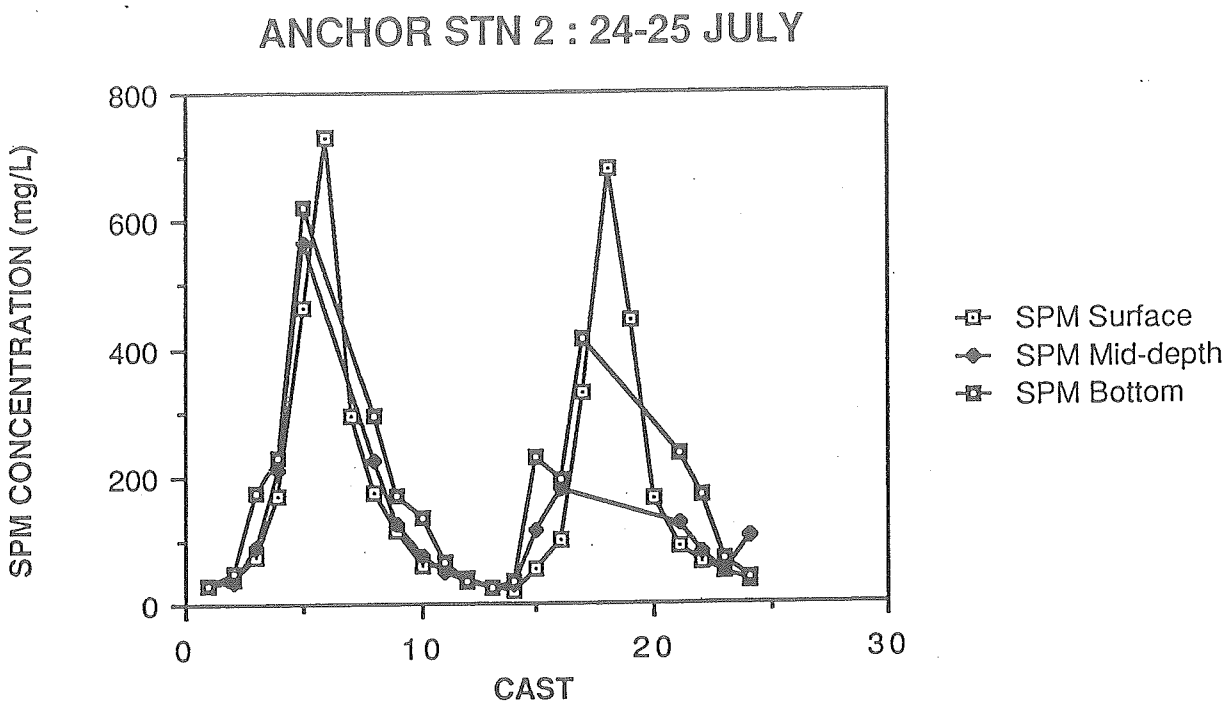

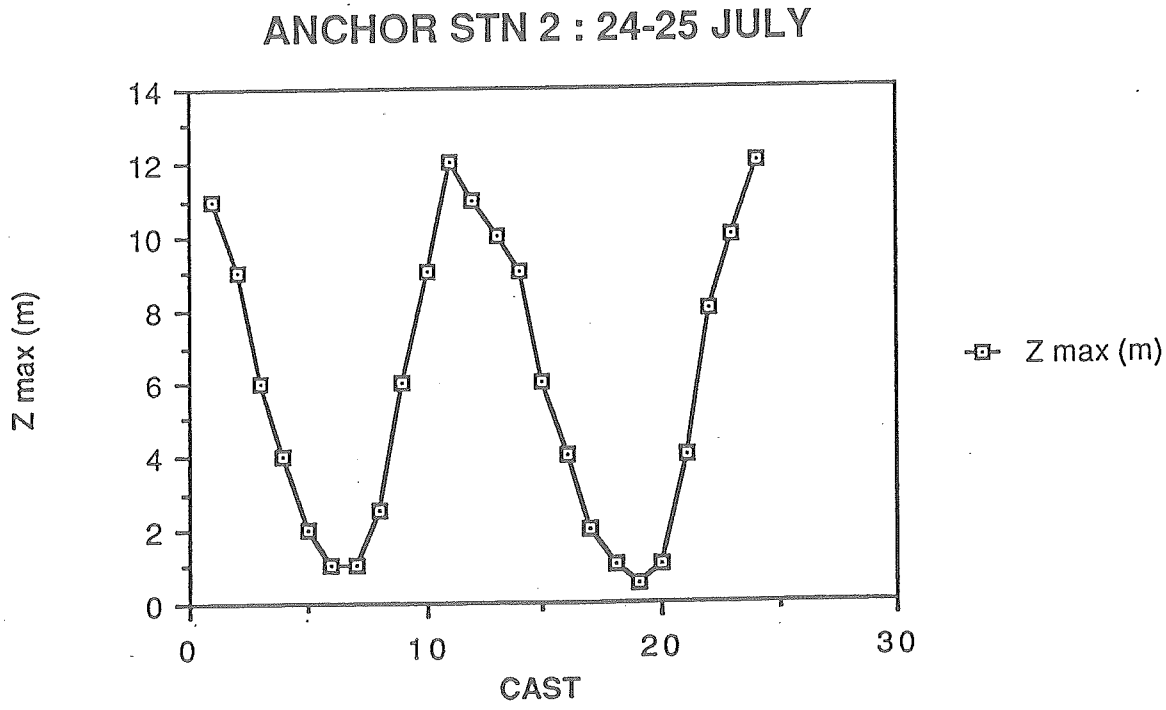

Figure 3.21B. SPM concentrations during anchor station 2.

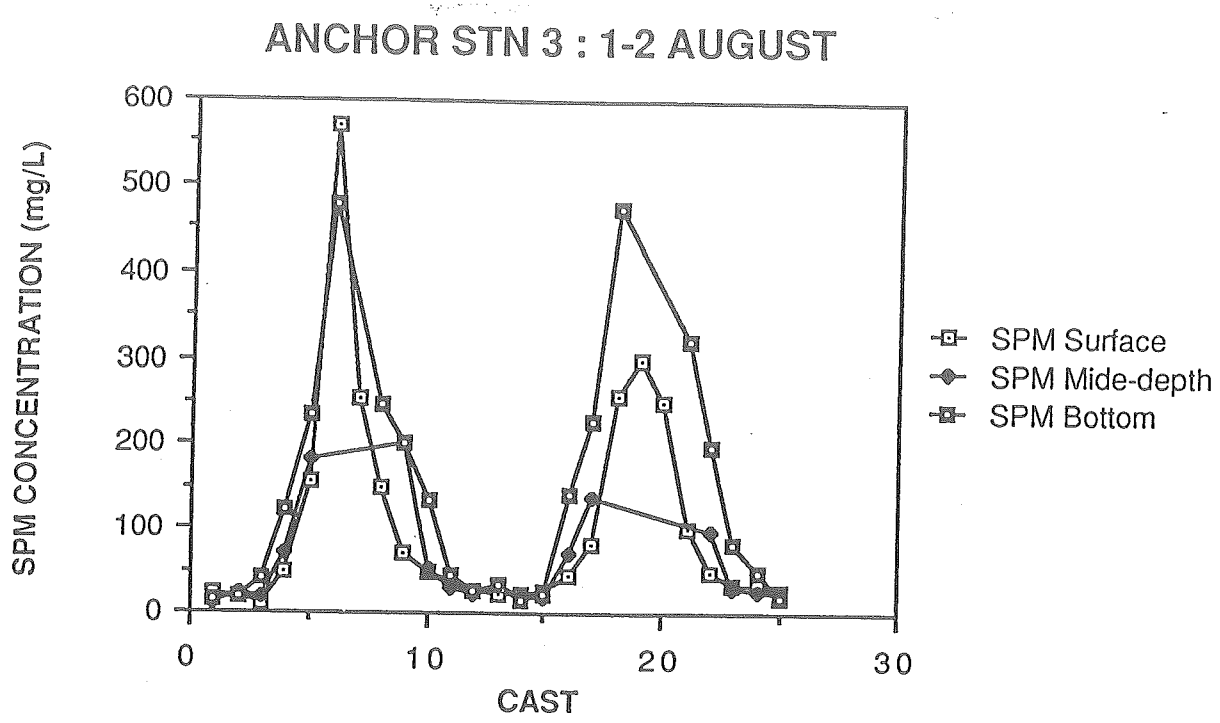

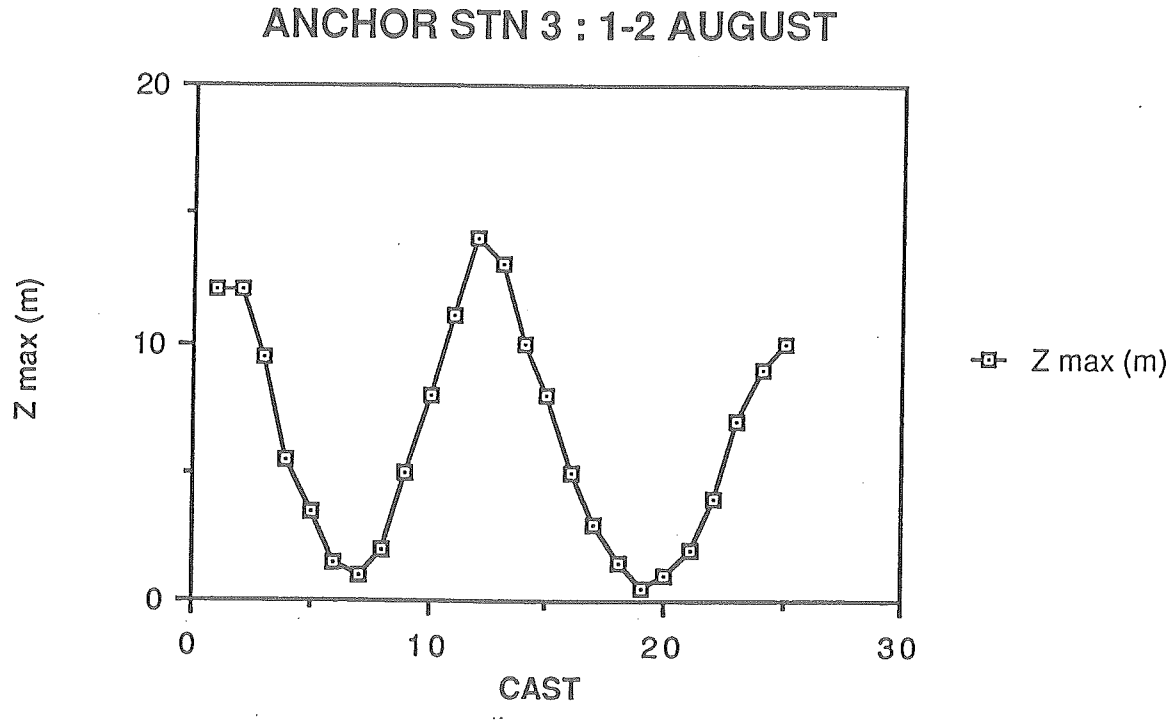

Figure 3.21C. SPM concentrations during anchor station 3.

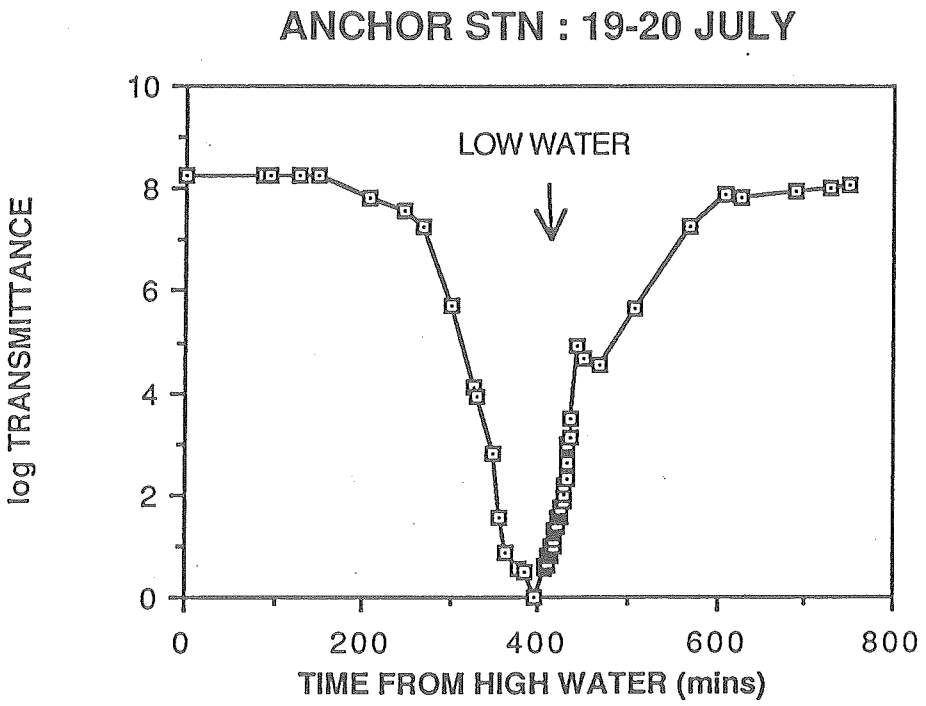

Figure 3.22. Attenuance meter record during anchor station 1.

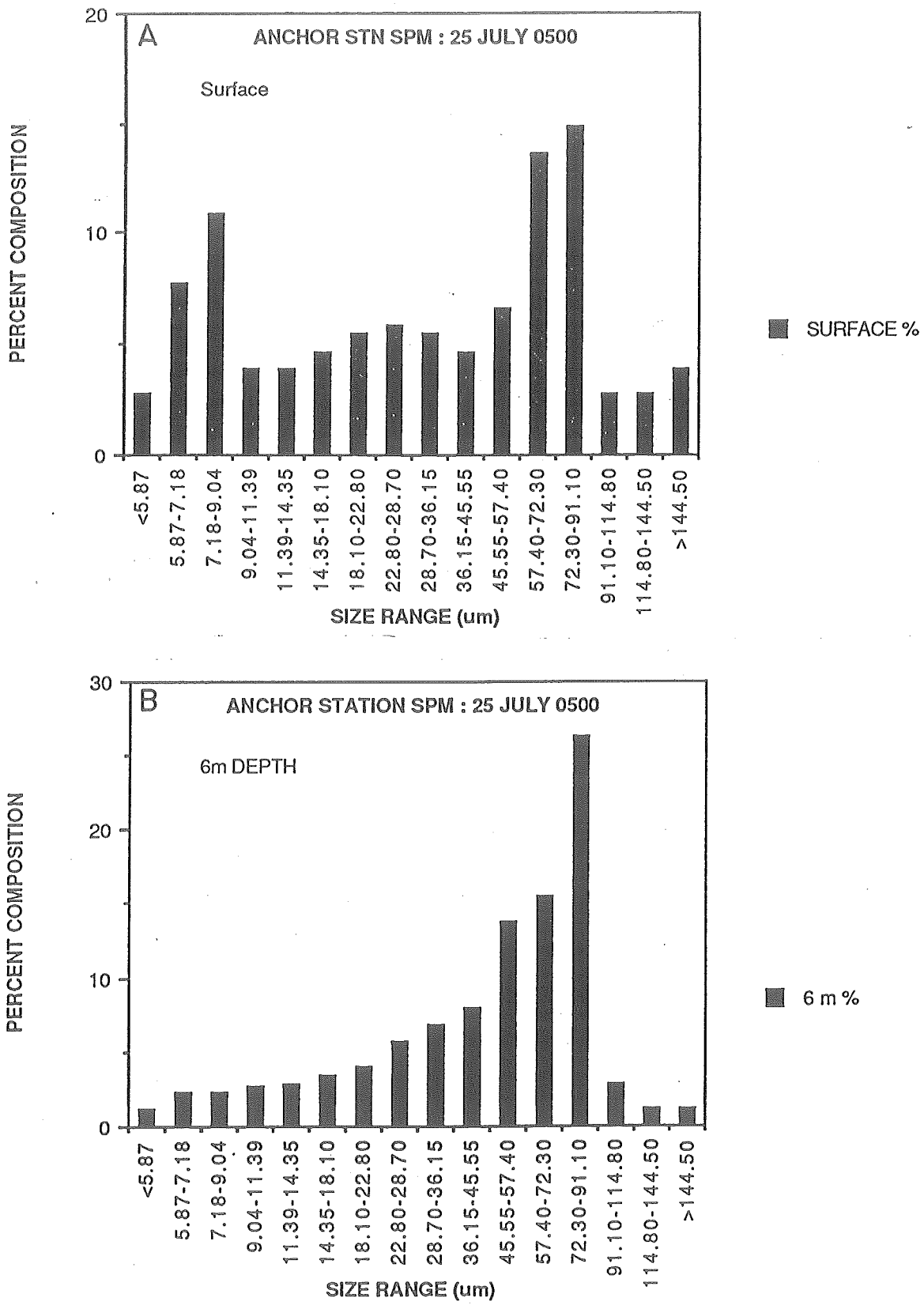

Figure 3.23. Grain size of suspended sediments during anchor station 2.

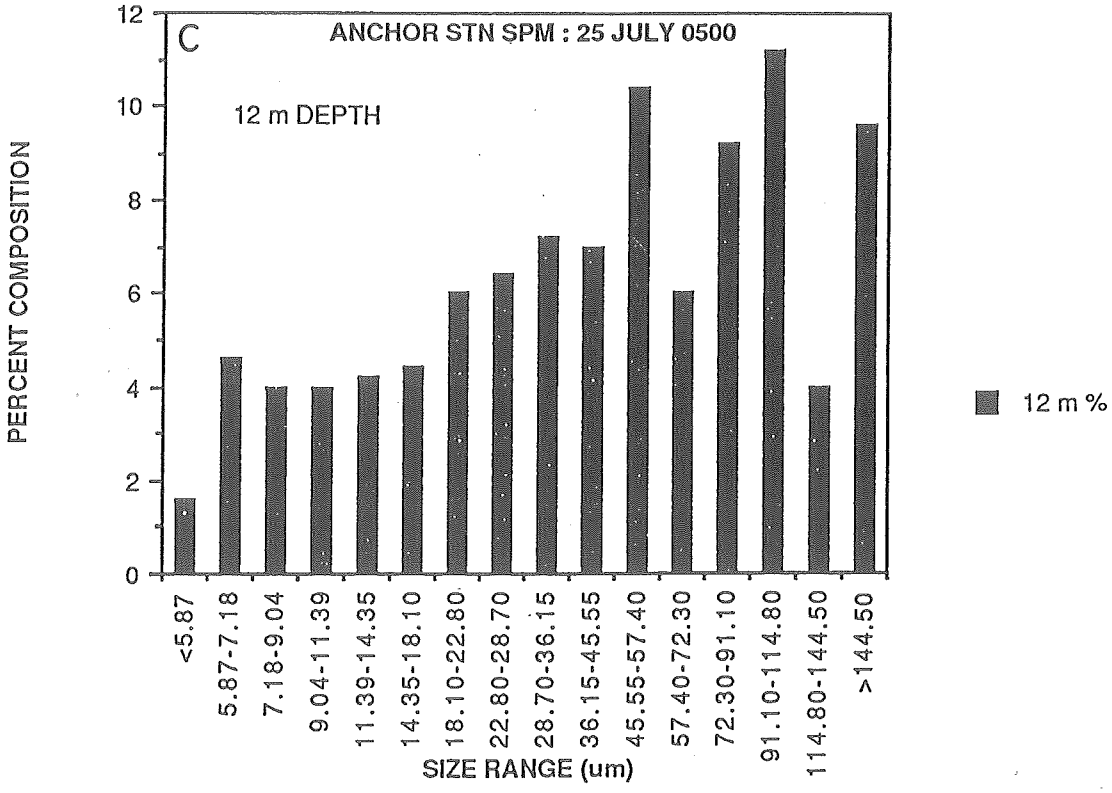

Figure 3.23. Cont.

3.7 Geomechanics of the Starrs Point Tidal Flat

HAROLD A. CHRISTIAN

3.7.1 Introduction

This report summarizes the geotechnical field data and laboratory analyses resulting from the 1989 LISP project at Starrs Point in Minas Basin, Bay of Fundy. New and innovative methods were used to obtain *in situ* shear strength data for both the surficial veneer of unconsolidated sediment using the INSIST apparatus as well as the underlying, compacted material as deduced from cone penetration testing. Previous studies (Amos et al. 1988) have found that dramatic shear strength increases within the upper few centimetres of sediment occurred at this site over a similar time frame, which was at that time attributed solely to the drying effects of solar radiation and wind. The present study found that long-term shear strength gains did indeed occur, although they were partly or completely reversible under storm wave conditions; furthermore it has shown that biological cementation is also a significant factor affecting surface shear strength (Christian and Daborn 1990).

The effect of biological processes cannot be easily discounted. Observations were made in this study showing that a significant portion of the strength increase occurring during each daytime exposure was inversely related to the numbers of tubicolous (i.e., tube-dwelling) amphipods (*Corophium volutator*) present. Strength was also directly related to carbohydrate concentration : a mucopolysaccharide mucilage secreted by diatoms (algae) that binds sediment particles together producing a framework that is more resistant to erosion by waves and currents (Paterson 1989). *Corophium* feed on the carbohydrates as well as the diatoms themselves, and therefore play an integral role in inhibiting the buildup of strength through each tidal cycle by controlling the diatom population.

This process was studied in some detail after it was recognized at the beginning of the LISP experiment that *Corophium* were present in very high concentrations (up to 40,000 per square metre) and that they appeared to be completely altering the surface appearance, smoothing out irregularities and leaving numerous undulating trails in their wake. Accordingly, several poisoning experiments were conducted to selectively eliminate biota from a 2 by 10 m portion of the mudflat at site 2 which would permit direct comparisons to be made with the adjacent control area in terms of the physical sediment characteristics and how they changed with time.

An observation was made late in LISP that the population of *Corophium* on the surface of the mudflat was overall markedly decreased outside the areas that had been poisoned (cf. Section 3.11). This event coincided with the arrival of large flocks of migratory shorebirds (semi-palmated sandpipers) travelling south in anticipation of winter. The primary source of food for these birds is *Corophium* (Hicklin and Smith 1979) and by the end of LISP they had either consumed most of the *Corophium* on the surface or had induced a change in the behaviour of *Corophium* so that they remained hidden inside their burrows (Boates and Smith 1988). This unexpected finding gave extra weight to the argument that biological processes are important, since the largest strength gains were made through this period. The poisoning experiments have little relative value for this period since the control area began to behave in a similar manner to the poisoned sites, but it does show that the absence of

Corophium achieved in different ways has the same net effect on physical properties.

It is concluded that strength increases do occur over time coupled with reductions in water content and increases in density of sediment. These changes are due in part to drying through evaporation but also to bonding created by interdependent biological processes. The relative contribution of these factors is unknown and represents an area for continued study since any physical model attempting to relate sediment erodibility to environmental processes would be inaccurate without consideration of all processes contributing to significant shear strength changes of the bed.

3.7.2 Methodology

Measurements of index properties were made at three sites designated 1, 2 and 3, with the latter located on the distal portion of the flat (cf. Fig. 3.2). The three sites fall along a transect surveyed across the mudflat from high to low water. Data were recorded during each daytime exposure both immediately after ebb tide and preceding flood tide. This resulted in a set of high-low data that is specific for the same location, with repeat visits made to each site in turn in a regular rotation. Some parameters were only measured once during each exposure (e.g., grain size, plasticity). INSIST tests were run both on the ebb and flood tide and subsamples were collected for water content, bulk density, and salinity. Index property testing followed accepted ASTM geotechnical procedures wherever published standards were applicable (ASTM 1990).

Subsurface profiles of index properties were similarly obtained by subsampling the wall of a test pit dug down to dense strata occurring at a depth of 20 to 30 cm. This zone prevented penetration beyond 70 cm by any handheld instrument, including the miniature cone penetrometer (2 MPa maximum strength) developed for this project (Christian 1989). The cone gave a continuous record of tip resistance with a maximum value at 2 MPa. The device was inserted at a nominal rate of approximately 2 cm per second. Data were recorded at 2-cm intervals on diskette using a Toshiba T1000 computer. Hand-held Pilcon vane measurements to 70 cm were made nearby each cone push to provide a comparison of undrained shear strength, however strength obtained with this instrument is not reliable in such a coarse-grained sediment, and is therefore not reported.

INSIST is an acronym for the in situ simple shear test, which provides reproducible measures of very low drained shear strength at the surface of a mudflat and fills a gap in equipment for *in situ* testing (Christian et al. 1990). The device consists of a pad which rests on the sediment surface, and is attached to a yoke passing through a gallows. A force in shear is applied to the pad until it begins to move by hanging weight on the gallows in the form of an increasing volume of water. The point at which the bed fails is defined as the shear stress beyond which unlimited deformations occur at a given vertical consolidation stress.

The procedure is repeated at different vertical stresses until sufficient data exist to define a complete failure envelope. Standard geotechnical devices such as shear vanes and cone penetrometers produce shear strength data which are too high by at least three orders of magnitude, due to their poor low-end sensitivity. INSIST applies a stress to the top 1 mm of sediment in the horizontal plane, closely modelling hydrodynamic shear stresses, a feature not available with a shear vane or a cone penetrometer. The INSIST device is ideally suited for obtaining

in situ drained shear strengths at very low consolidation stress levels on intertidal mudflats and gives results that compare favorably to other *in situ* techniques (Amos - personal communication).

Results of applied consolidation stress plotted against shear strength at failure for intertidal mudflats at Starrs Point gave reliable and repeatable failure envelopes with finite cohesion intercepts derived by extrapolating back to the y-axis. Lambe and Whitman (1969) define the **friction angle** as the slope of the failure envelope and **cohesion** as the intercept on the shear strength axis.

3.7.3 Surface Index Properties

Figures 3.24, 3.25 and 3.26 show the grain size distribution for sites 1, 2 and 3, plotted as a function of time. Actual data are listed in Table 3.4. Note that site 3 was very sandy, having over 60% sand by weight, while sites 1 and 2 had similar sand contents of 35 to 40%. Site 1 had a silt content approaching 60% whereas site 3 had a value of 30%. All sites had clay contents of 15 to 18%. The data indicate that finer sediment is evenly distributed over the mudflat while silt is carried inshore where it settles out; the distal portions of the flat are composed mainly of sand. Table 3.5 lists the two Atterberg Limits results that were obtained, indicating that the surficial sediment is an inorganic silt of very low plasticity according to the Unified Soil Classification system (Holtz and Kovacs 1981).

The next series of graphs show changes in salinity, water content and bulk density occurring for each daytime exposure. Figure 3.27 shows the length of time between the ebb and the flood tide measurements; note that on July 21, the time of initial exposure had changed sufficiently to require a modified sampling programme.

Ebb tide salinities were close to those in the water column (29 ‰) with salinity increasing each day as the mudflat dried out (Fig. 3.28). The surface water content is plotted in Figure 3.29, showing that the upper 1 cm of sediment does indeed dry to some degree during each exposure. It would appear that the standard deviation in water content is of the order of $\pm 2\%$ by weight. Water content remains fairly stable over the long-term except for an increase after July 28 which closely mimics the trend observed by Amos and Mosher (1985) and occurred roughly in the same time period. An increase in water content usually corresponds to a reduction in cohesion unless there is a textural change occurring where more clay is coming into the system. The increase in water content toward the end of July coincides with a reduction in bulk density (Fig. 3.30), suggesting that the trend is real.

3.7.4 INSIST Measurements

Figure 3.31 shows a diagram of the INSIST apparatus in use with a small inset showing the application of stress. The test is carried to failure and then the pad is moved to a fresh area nearby for a test at a higher vertical stress. Figure 3.32 shows the results of a calibration study using a cohesionless sand to check the sensitivity and repeatability of the apparatus.

Table 3.6 gives some key information for each of test sites 1 to 3. Figures 3.33 through 3.35 show all of the

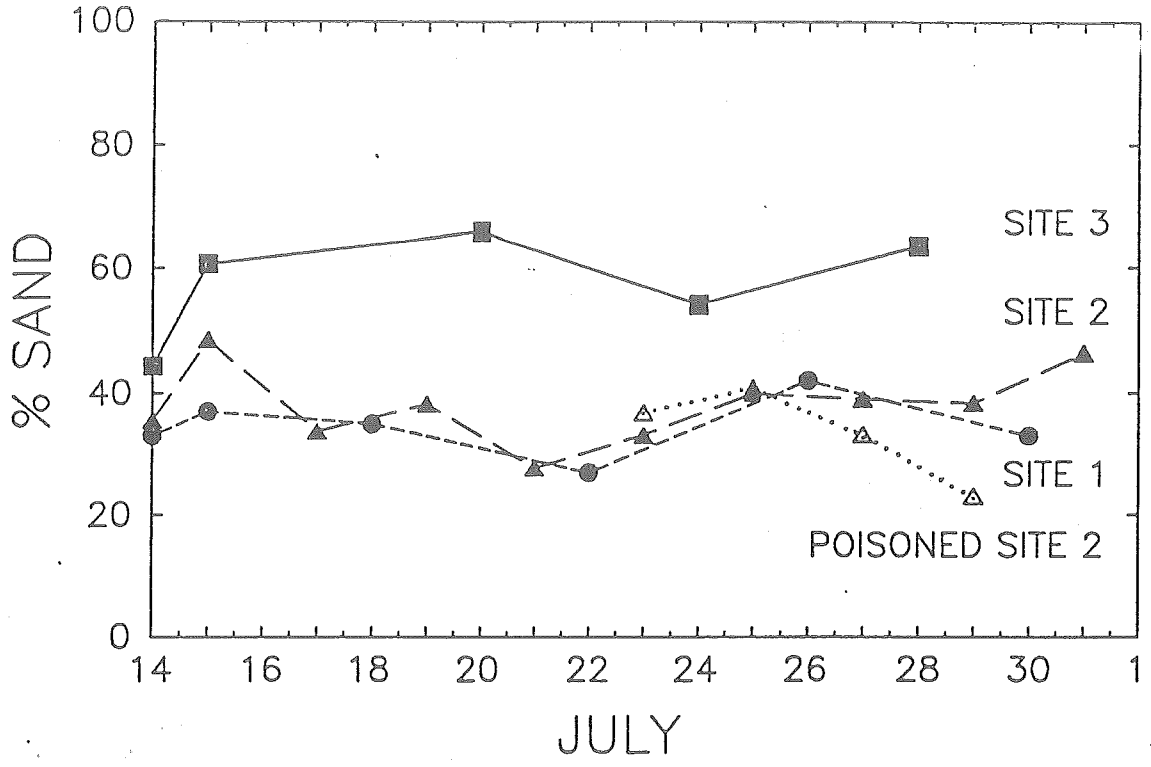

Figure 3.24. Percent sand content (upper 1 cm) versus date of sampling for all sites.

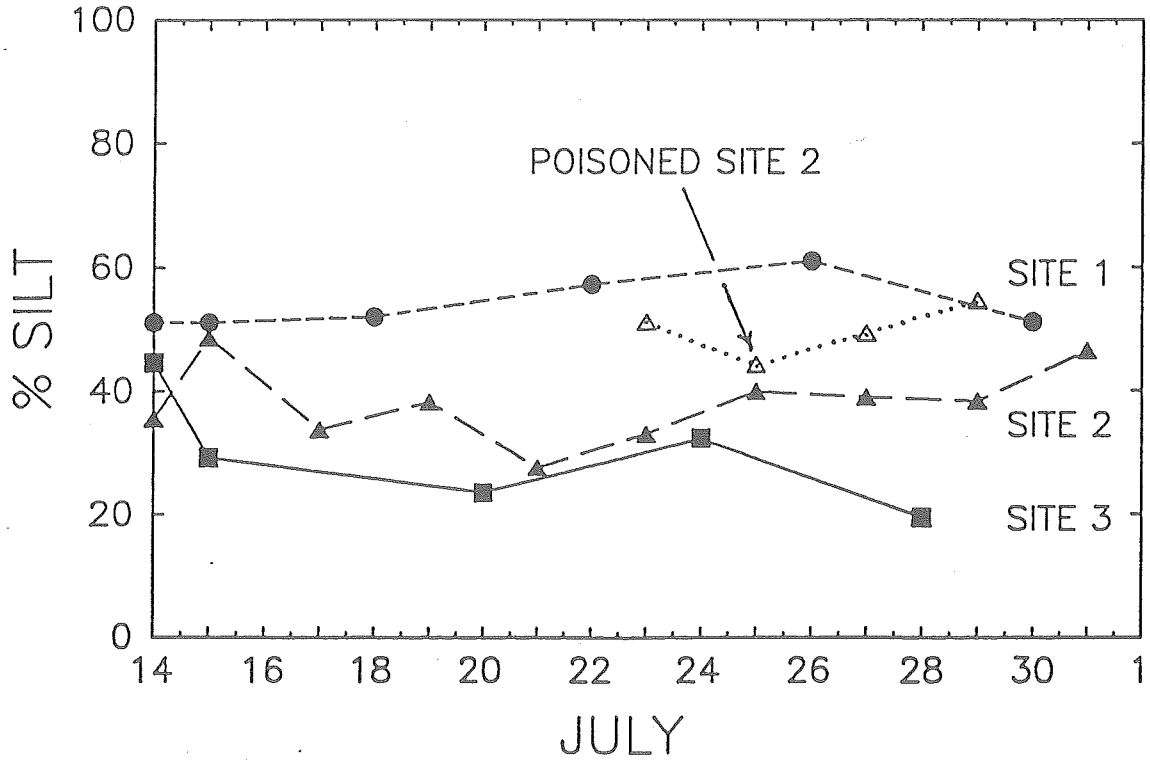

Figure 3.25. Percent silt content (upper 1 cm) versus date of sampling for all sites.

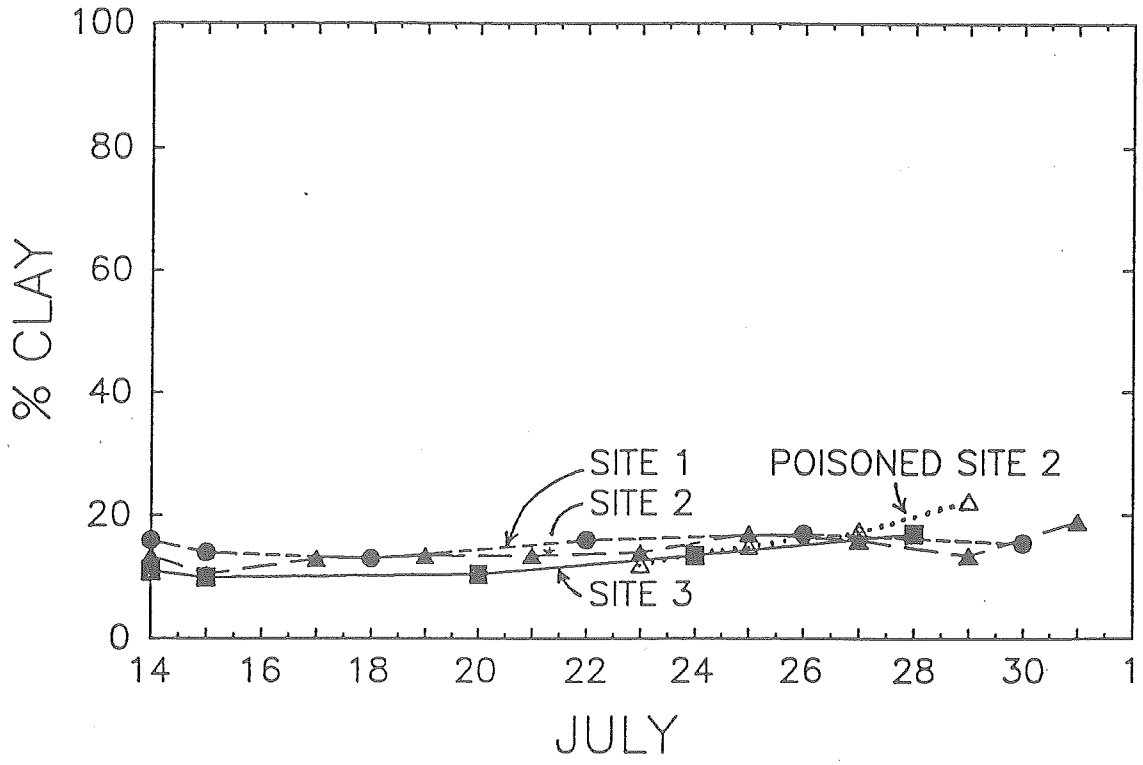

Figure 3.26. Percent clay content (upper 1 cm) versus date of sampling for all sites.

Table 3.4. Summary of surface grain size data for geotechnical sites

Control Sites

Sample	Date	Site	Depth (cm)	Sand (%)	Silt (%)	Clay (%)
14-1A	14	1	0-2	32.9	51.1	16.0
15-1A	15	1	0-1	37.1	51.1	14.0
18-1A	18	1	0-1	35.0	52.0	13.0
22-1A	22	1	0-1	26.7	57.3	16.0
26-1A	26	1	0-1	42.0	61.0	17.0
30-1A	30	1	0-1	33.3	51.2	15.5
14-2A	14	2	0-5	35.5	51.0	13.5
15-2A	15	2	0-1	48.6	41.0	10.5
17-2A	17	2	0-1	33.8	53.2	13.0
19-2A	19	2	0-1	38.2	48.3	13.5
21P2A	21	2	0-1	27.7	58.8	13.5
23NPA	23	2	0-1	33.1	52.9	14.0
25OPA	25	2	0-1	39.9	56.9	17.0
27-OP	27	2	0-1	39.0	45.0	16.0
29CON	29	2	0-1	38.3	48.2	13.5
31-2E	31	2	0-1	46.4	34.6	19.0
14-3A	14	3	0-4	44.4	44.6	11.0
15-3A	15	3	0-1	60.7	29.3	10.0
20-3A	20	3	0-1	65.9	23.6	10.5
24-3A	24	3	0-1	54.1	32.4	13.5
28-3A	28	3	0-1	63.5	19.5	17.0

Poisoned sites

Sample	Date	Site	Depth (cm)	Sand (%)	Silt (%)	Clay (%)
23-P	23	2FORM	0-1	36.8	51.2	12.0
25-PA	25	2FORM	0-1	40.8	44.2	15.0
25-PS	25	2FORM	0-1(CLAY)	24.9	54.7	20.4
27-PA	27	2FORM	0-1	33.2	49.3	17.5
29-DCM	29	2DCMU	0-1	18.8	57.2	24.0
29-BP	29	2BOTH	0-1	19.3	54.7	26.0
29-CY	29	2CYAN	0-1	31.2	51.9	16.9

Note: Sample 25-PS was taken within clayey flat spots between bedforms that had appeared within the poisoned area at site 2; sample 25-PA was taken from the bedforms themselves. Note that these data indicate that a separation of the fines from the coarse matrix had occurred following poisoning.

Table 3.5. Summary of Atterberg Limits data for the control sites

Sample	Date	Site	Depth (cm)	Specific Gravity	Plastic Limit (%)	Liquid Limit (%)
14-1	14	1	0-2	2.70	22.4	27.0
14-2	14	2	0-2	2.75	21.5	26.1

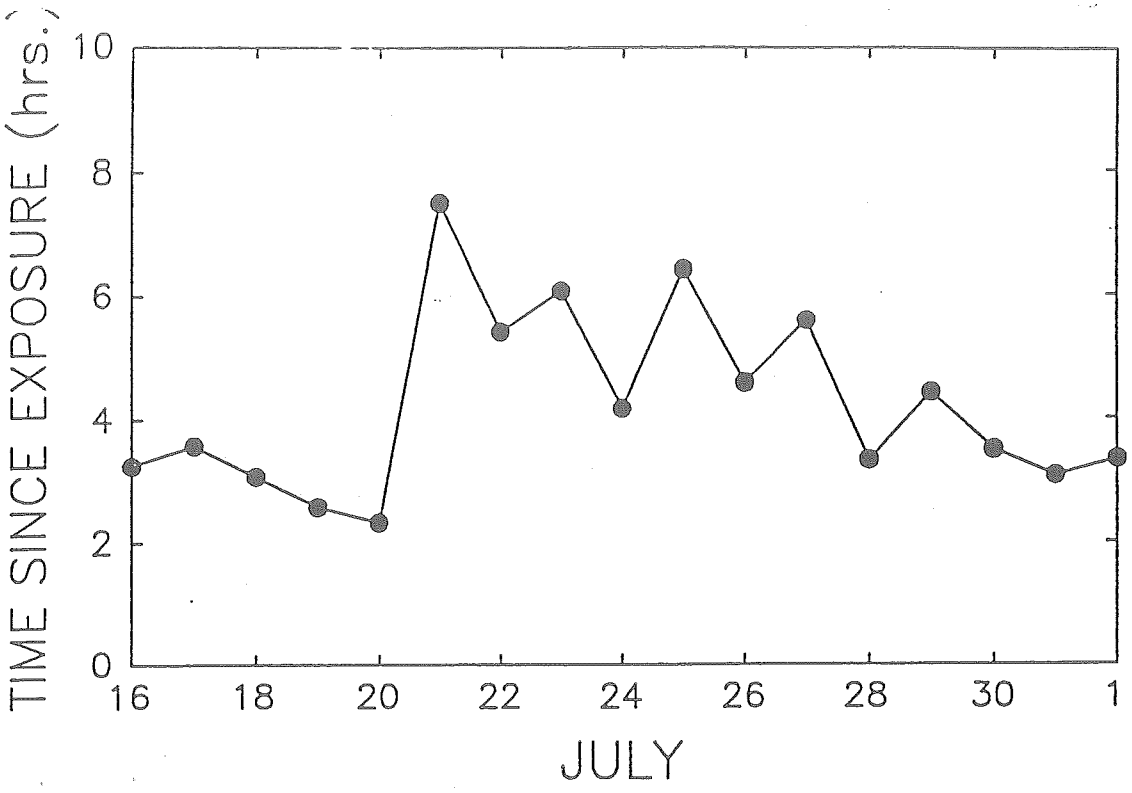

Figure 3.27. Elapsed time between ebb tide and final measurement before flood tide for each day of field work.

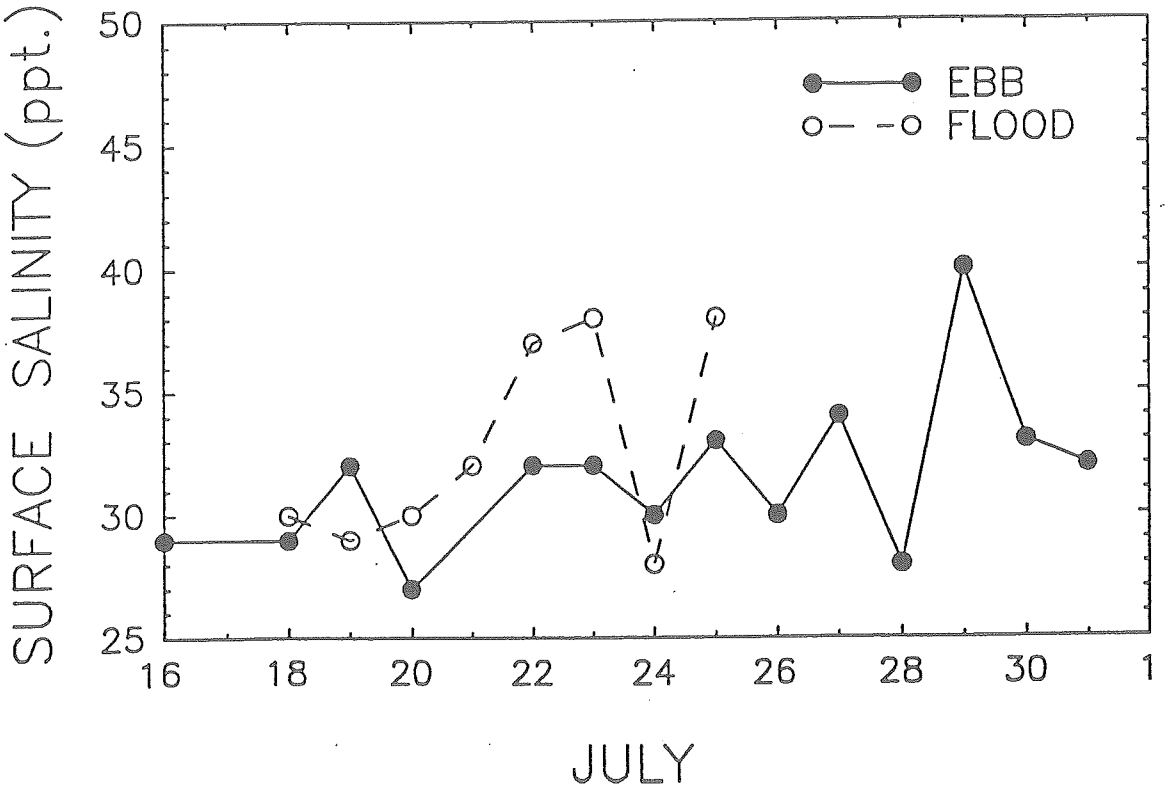

Figure 3.28. Change in salinity of surface pore fluid (scraping) versus date of sampling.

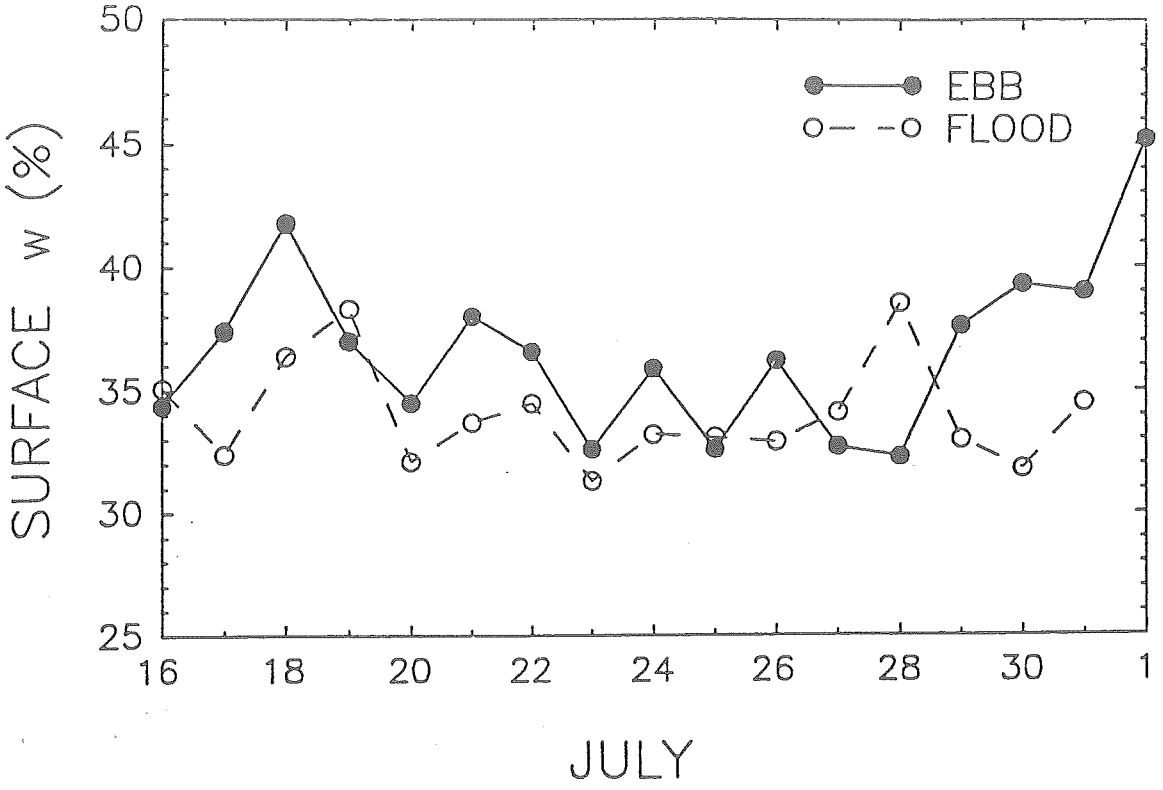

Figure 3.29. Change in surface water content (uncorrected for salinity) versus date of sampling.

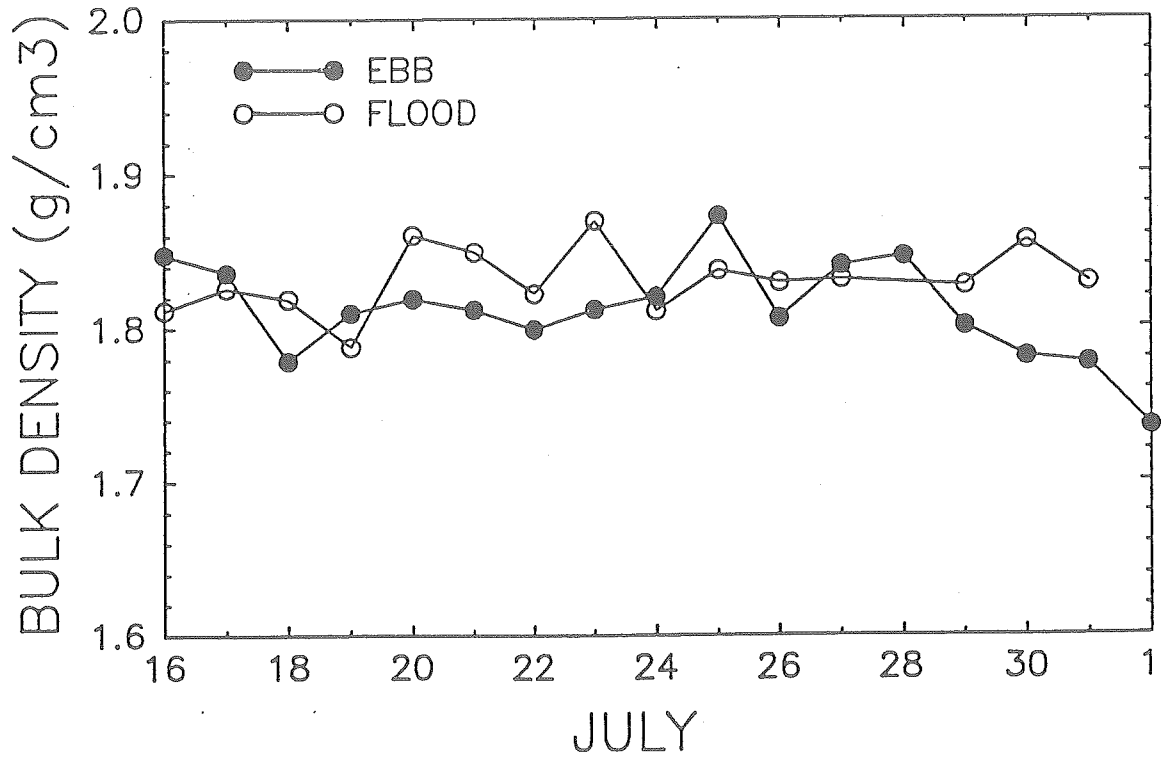

Figure 3.30. Change in surface bulk density versus date of sampling.

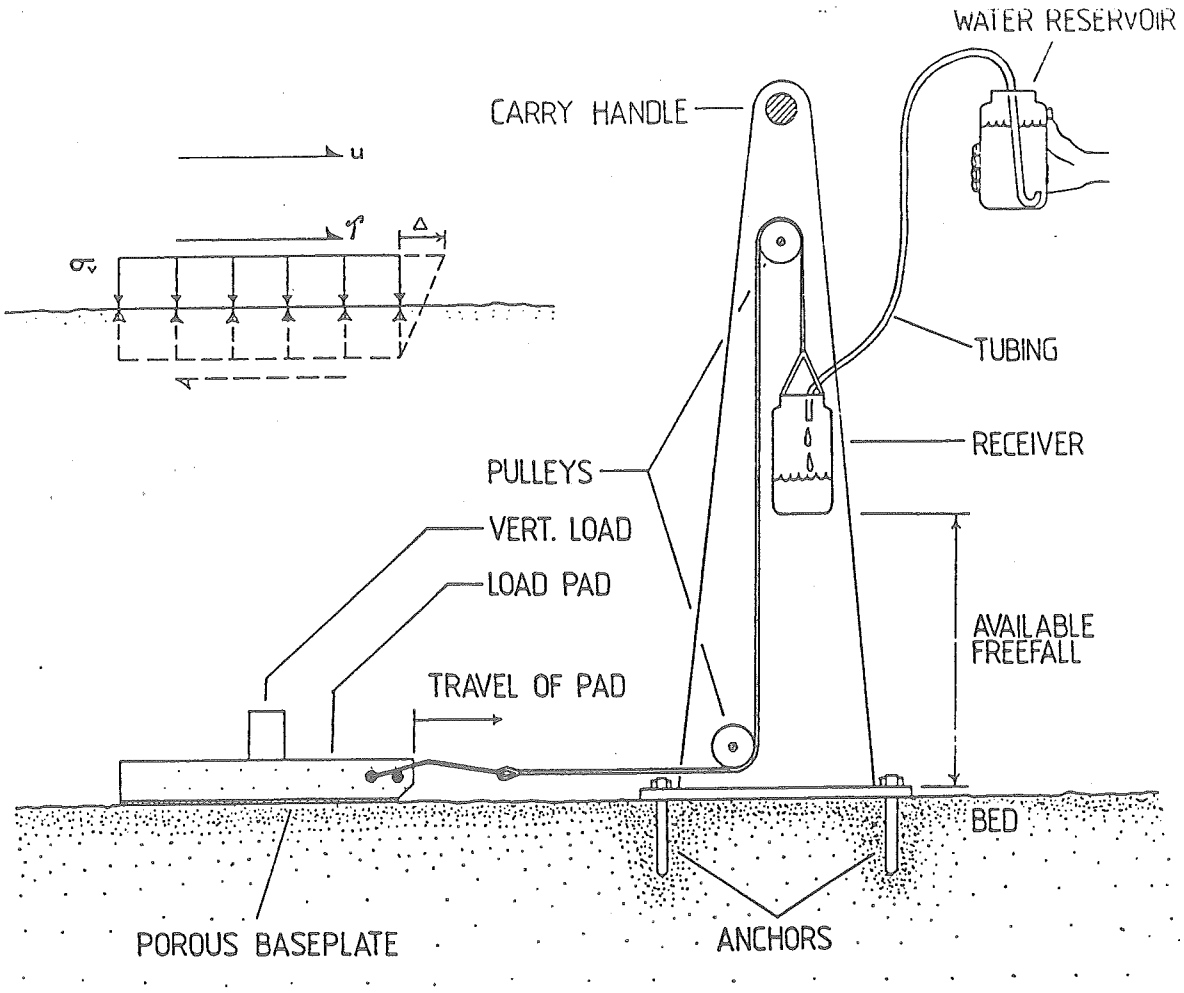

Figure 3.31. Diagram showing the INSIST apparatus: note the vertical lead weight applied to the pad and the method of increasing the shear stress; also the inset showing the stress application where Δ is the horizontal displacement of the pad, σ_v is the vertical stress, τ is the shear stress, and u is the flow velocity above the bed which is being simulated by the INSIST approach.

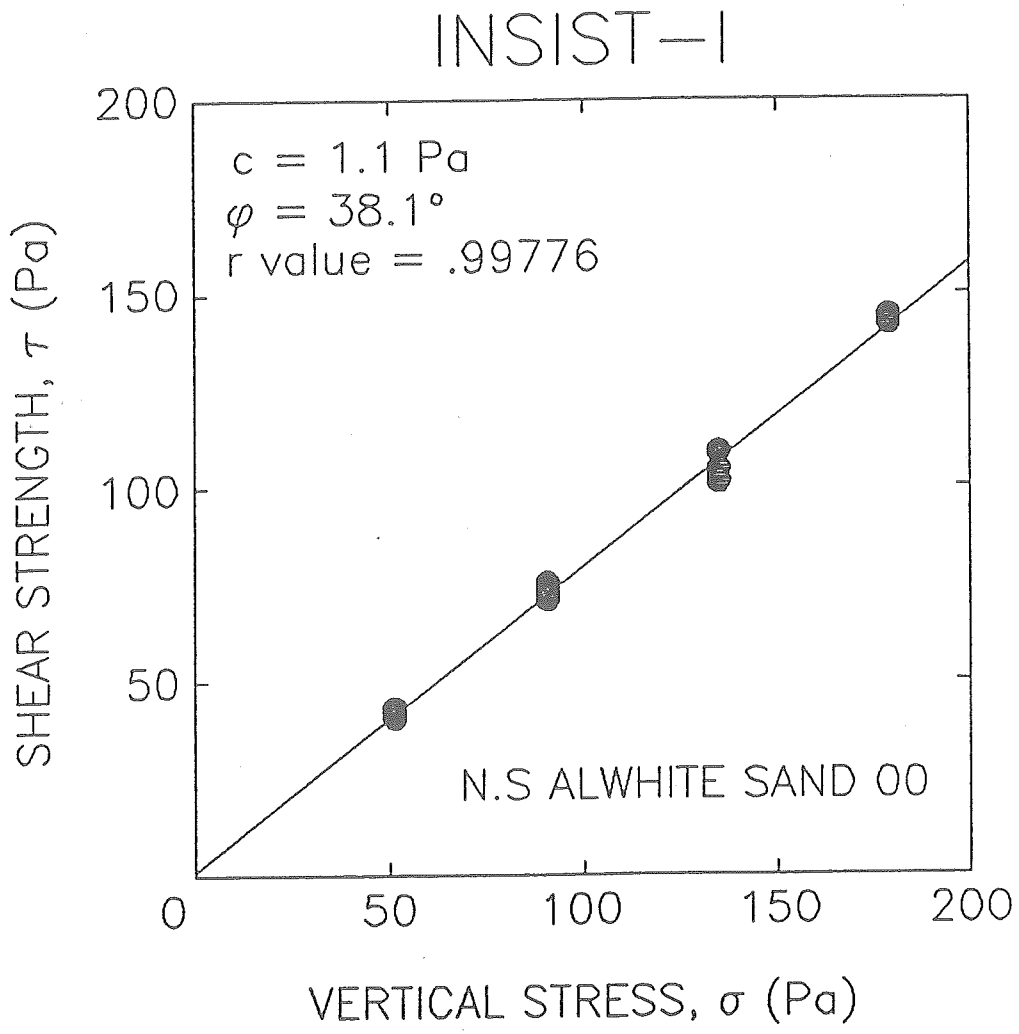

Figure 3.32. An INSIST calibration failure envelope for a cohesionless well-rounded commercial blasting sand showing the high level of accuracy of the apparatus.

Table 3.6. Key site information summary for test sites

Date	Site	Exposure Time	Off Site Time	Elasped Time (hrs.)	Solar Flux (kJ/m^3)	Weather Notes
Control Sites						
15	1	1345	1500	1.25	--	SUNNY
15	2	1400	1700	3.00	--	SUNNY
16	3	1505	1820	3.25	3305	CLOUDY
17	2	1535	1910	3.58	442	HEAVY RAIN
18	1	1605	1910	3.08	5901	SUNNY
19	2	1700	1935	2.58	3903	SUNNY
20	3	1800	2020	2.33	966	RAINING
21	2	0550	1220	7.50	7198	PARTLY SUNNY
22	1	0635	1200	5.42	7916	PARTLY SUNNY
23	2	0725	1330	6.08	12634	SUNNY
24	3	0840	1250	4.17	9213	SUNNY
25	2	0910	1535	6.42	13368	SUNNY & WINDY
26	1	1005	1440	4.58	11992	SUNNY
27	2	1115	1650	5.58	10776	SHOWERS
28	3	1250	1610	3.33	2151	LIGHT RAIN
29	2	1335	1800	4.42	12516	SUNNY & WINDY
30	1	1430	1800	3.50	8299	SUNNY & WINDY
31	2	1540	1845	3.08	6414	SUNNY
1	FISH*	1635	1955	3.34	3563	SUNNY
Poisoned Sites						
23	2FORM	0725	1330	6.08	12634	SUNNY
25	2FORM	0910	1535	6.42	13368	SUNNY & WINDY
27	2FORM	1115	1515	4.00	10110	SHOWERS
29	2DCMU	1335	1730	3.92	11399	SUNNY & WINDY
29	2BOTH	1335	1710	3.58	10655	SUNNY & WINDY
29	2CYAN	1335	1655	3.33	10054	SUNNY & WINDY
1	FISH**	1635	2015	3.67	3646	SUNNY

*FISH refers to the fish exclosure site which is taken to be roughly equivalent to site 3; no index property information is available.

**The poison used at the FISH exclosure site on August 1 was DCMU.

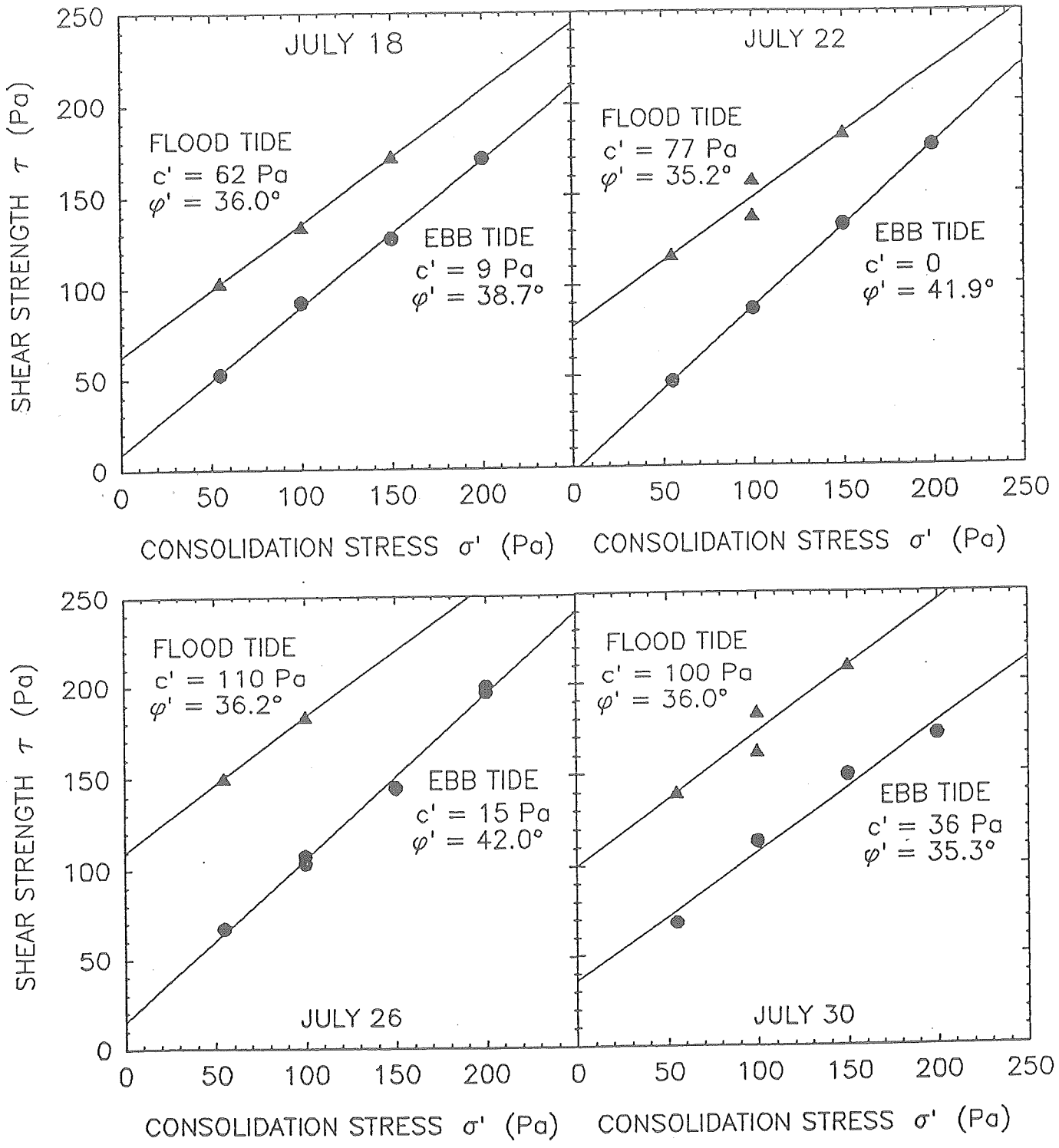

Figure 3.33. Daily INSIST plots for site 1 showing both the ebb and the flood tide failure envelopes.

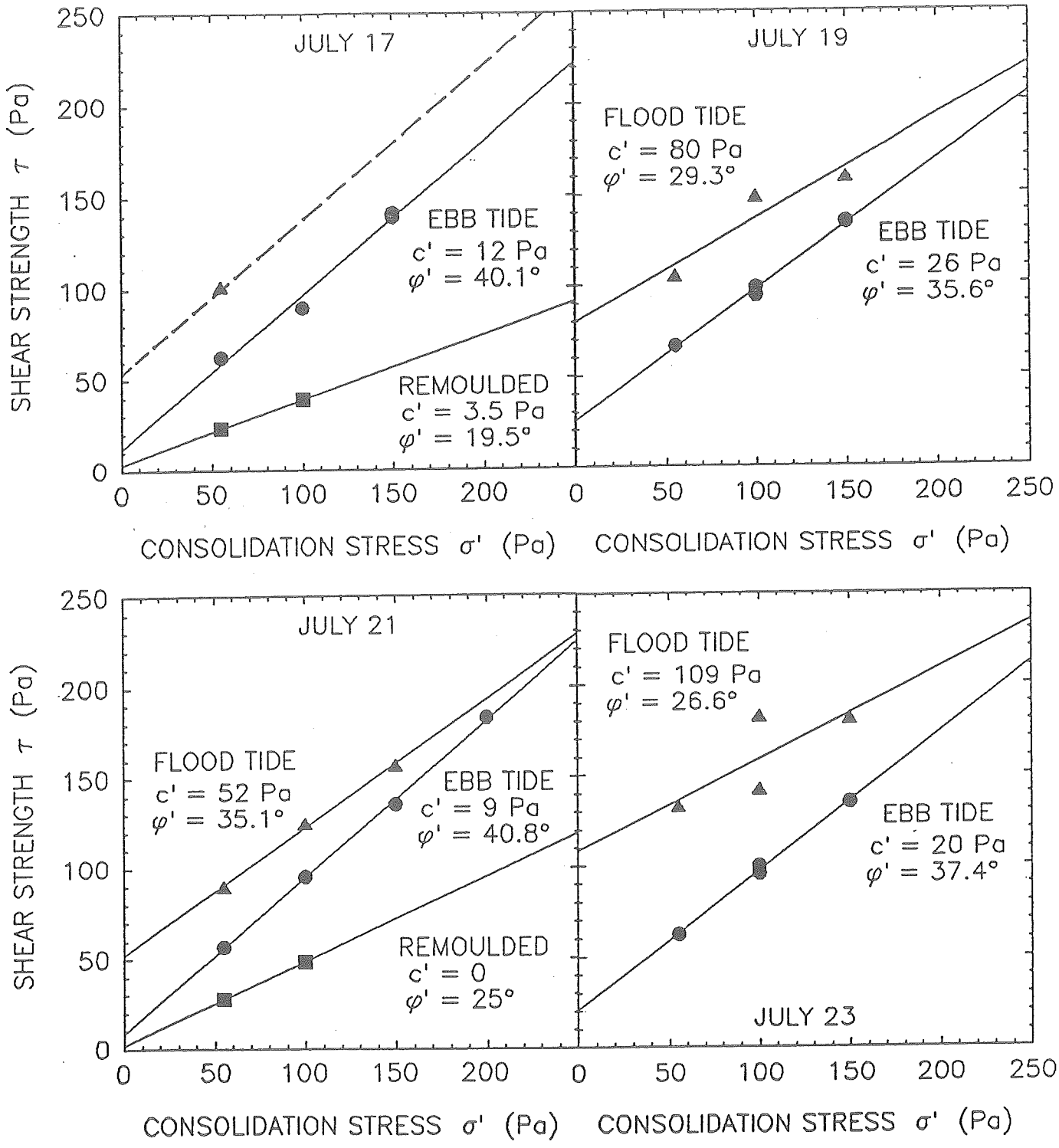

Figure 3.34A. Daily INSIST plots for site 2 showing both the ebb and the flood tide failure envelopes, along with two remoulded tests where all interlocking was removed by reworking the bed to check the minimum possible friction angle (note flood tide data unavailable for July 17 due to poor weather at the site).

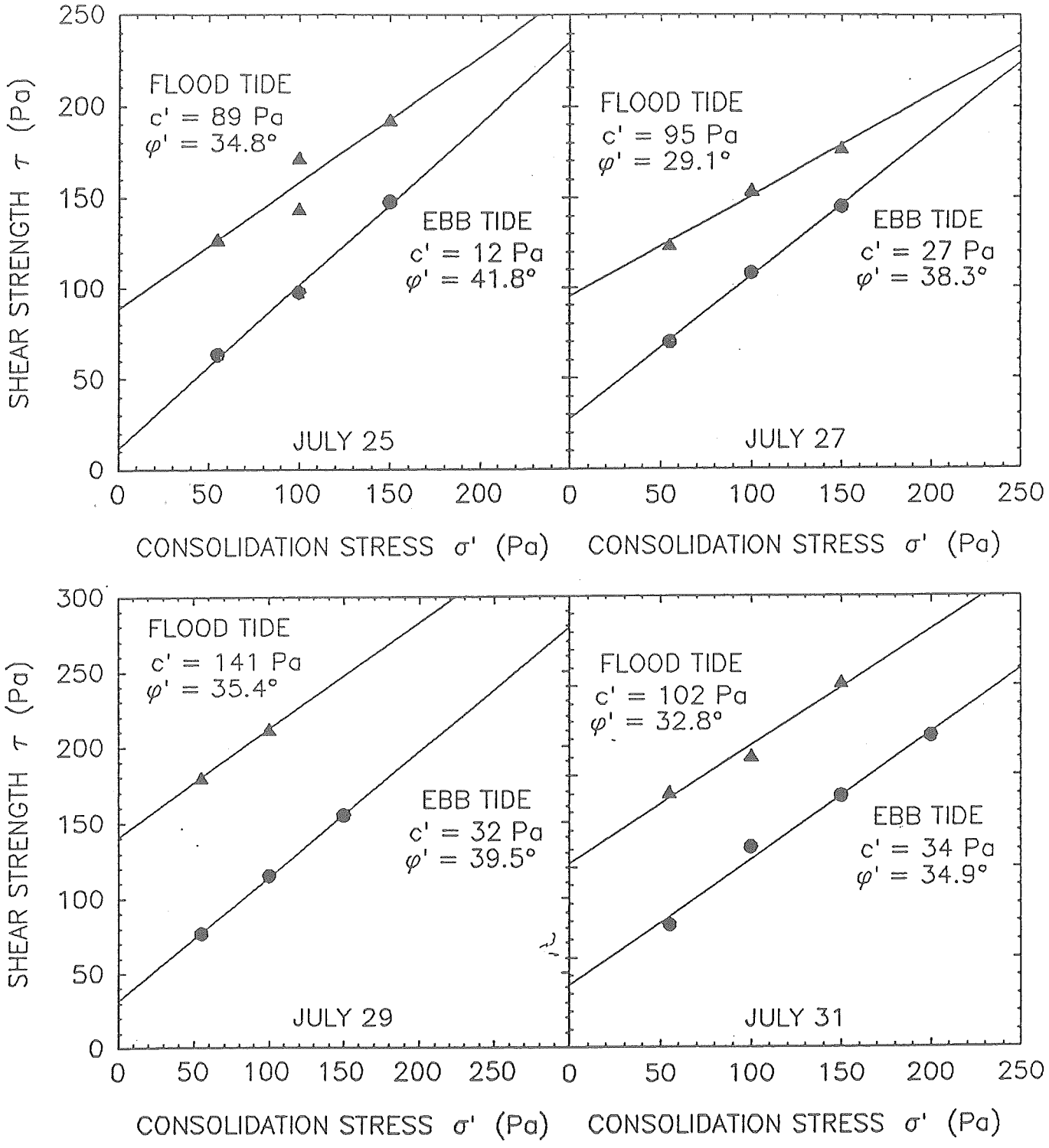

Figure 3.34B. Remaining INSIST plots for site 2 showing both the ebb and the flood tide failure envelopes.

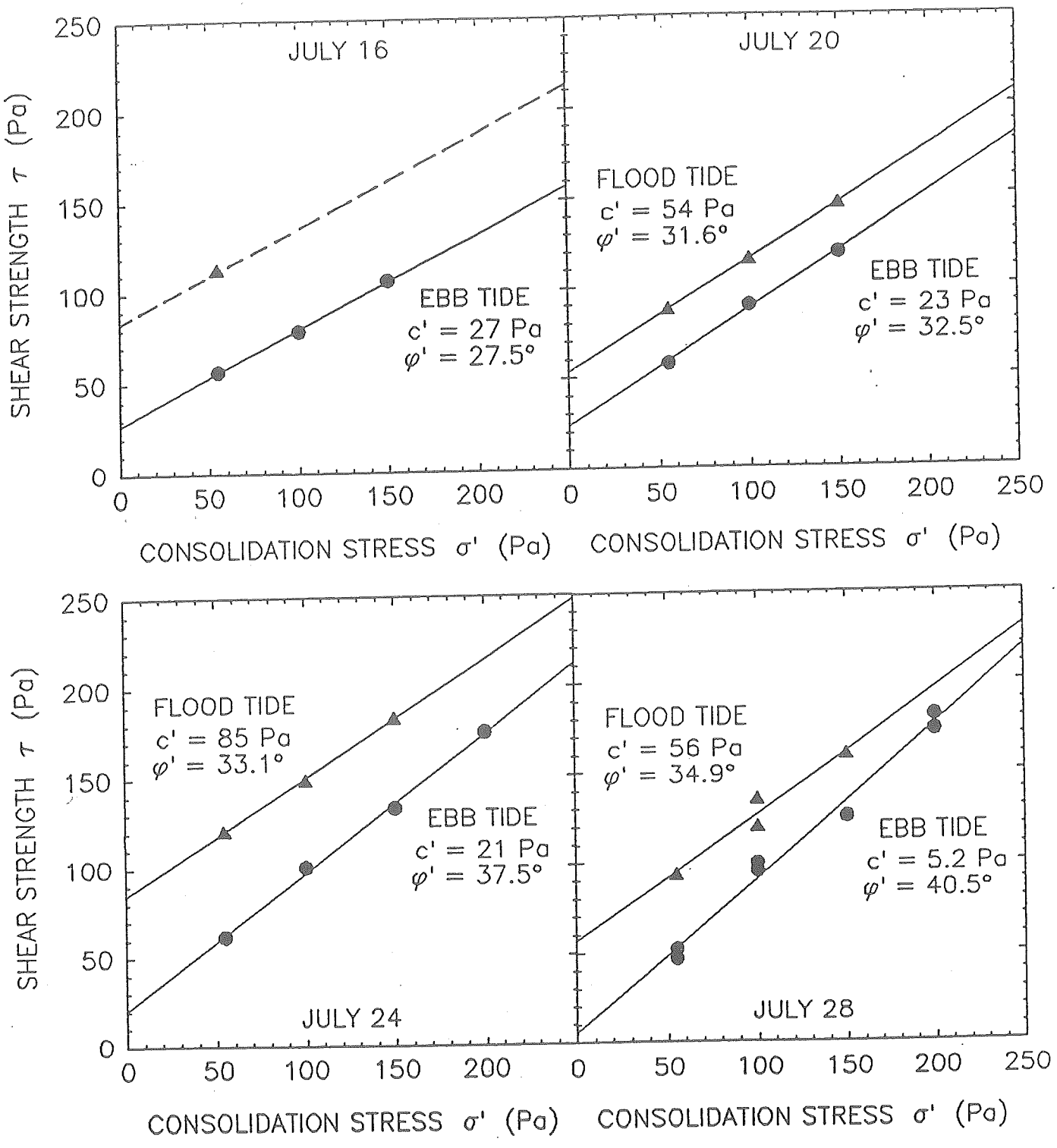

Figure 3.35. Daily INSIST plots for site 3 showing both the ebb and the flood tide failure envelopes (note flood tide data missing for July 16 due to operator fatigue from trying to do too many sites in one day).

INSIST data for sites 1, 2 and 3. The test was also run twice on artificially remoulded sediments to check the minimum possible friction angle. Index properties for both the control and poisoned sites are given in Table 3.7.

Figures 3.36 and 3.37 show time series of cohesion and friction angle, respectively for all sites; the same data are listed in Table 3.8. Note that each drying period resulted in a significant increase in cohesion along with a slight reduction in friction angle. These two observations are not necessarily linked; a decrease in friction angle usually means that the sediment has become looser. Figure 3.30 shows bulk density data following trends opposite to what one would expect based on friction angle data. It is of some importance to realize that the bulk density data in Figure 3.32 are average values over the uppermost 2 cm, whereas the INSIST measurements involve only the uppermost 2 mm. The obvious conclusion would seem to be that cementation, rather than drying (and consolidation), must predominate within the upper 2 mm, leading to a gain in strength, since the trend of reduction in friction angle is consistent over the LISP experiment, except after July 29.

These results could have a bearing on the previously noted trend that water content increased during the latter part of July while strength was also increased, coincident with the disappearance of *Corophium* from the surface of the mudflat. It would seem that the *Corophium* have a major effect in altering the physical characteristics (water content, density and strength) of at least the uppermost few millimetres of sediment, and their absence has the effect of allowing the physical system to return toward an equilibrium condition wherein bedforms are allowed to develop in response to the hydrodynamic stress regime. It is not clear whether the coincident strength increase would completely offset the increase in water content. The Starrs Point mudflat is a very unusual area where long-term increases in water content sometimes occur paradoxically together with increases in cohesion. This change occurs during a decline in numbers and activity of *Corophium,* which plays a significant role in limiting the buildup of biologically-produced cohesion.

Alternatively, long-term increasing silt content could explain these unusual changes since a higher baseline for equilibrium conditions of water content and strength would develop. Figure 3.25 shows a slight increase in silt percentage only at site 2 over the last week of July, but it is difficult to be sure if the trend is real or if it is simply within the range of local variability. Amos et al. (1988) observed an identical trend of increasing fines content together with higher water content and shear strength in their field studies, however they do not break the fine fractions down further in the silt and clay. There did not appear to be significant changes in clay content at any site.

The net effect of poisoning was to allow the emergence of well-defined bedforms with clay deposits in the troughs (e.g., desegregation of fines from the coarse matrix) since there was little or no bioturbation for many tidal cycles. It was also noted that the strength increases each day were most pronounced inside the poisoned areas. This may be due to experimental error since the INSIST device requires a flat surface, which was only available in the space between emergent bedforms where silt and clay had separated from the matrix. Therefore, the INSIST data from the poisoned site are not directly comparable to the rest of the mudflat as the data were derived from the fine fractions where cohesion increases would have been the most dramatic. This would explain why the poisoned sites gained strength faster each day than the control area.

Contrary to their original intention, the poisoning experiments also had no relative usefulness for the latter

Table 3.7. Summary of surface index properties for test sites

Date	Site	WC (%)	Salinity (ppt)	Density (g/cm^3)	WC (%)	Salinity (ppt)	Density (g/cm^3)
Control Sites							
15	1	38.6	--	1.795	30.1	--	1.765
15	2	29.2	--	1.872	30.1	--	1.891
16	3	34.4	29	1.848	35.1	--	1.812
17	2	37.4	22	1.836	32.4	22	1.826
18	1	41.8	29	1.779	36.4	30	1.819
19	2	37.0	32	1.810	38.3	29	1.788
20	3	34.5	27	1.819	32.1	30	1.860
21	2	38.0	--	1.812	33.7	32	1.849
22	1	36.6	32	1.799	34.5	37	1.822
23	2	32.6	32	1.812	31.3	38	1.869
24	3	35.9	30	1.820	33.2	28	1.811
25	2	32.6	33	1.872	33.1	38	1.837
26	1	36.2	30	1.806	32.9	--	1.829
27	2	32.7	34	1.840	34.1	--	1.831
28	3	32.3	28	1.846	9.8	--	--
29	2	37.6	40	1.801	33.0	--	1.827
30	1	39.3	33	1.781	31.8	--	1.856
31	2	39.0	32	1.777	34.5	--	1.829
1	FISH	45.2	--	1.735	--	--	--
Poisoned Data							
23	2FORM	32.6	32	1.848	30.0	--	1.876
25	2FORM	31.2	35	1.882	32.1	--	1.853
27	2FORM	32.1	35	1.850	29.4	--	1.904
29	2DCMU	33.2	--	1.847	33.4	--	1.831
29	2BOTH	32.4	--	1.867	37.0	--	1.795
29	2CYAN	35.5	--	1.818	31.6	--	1.856
1	FISH	45.0	--	1.734	46.6	--	1.707

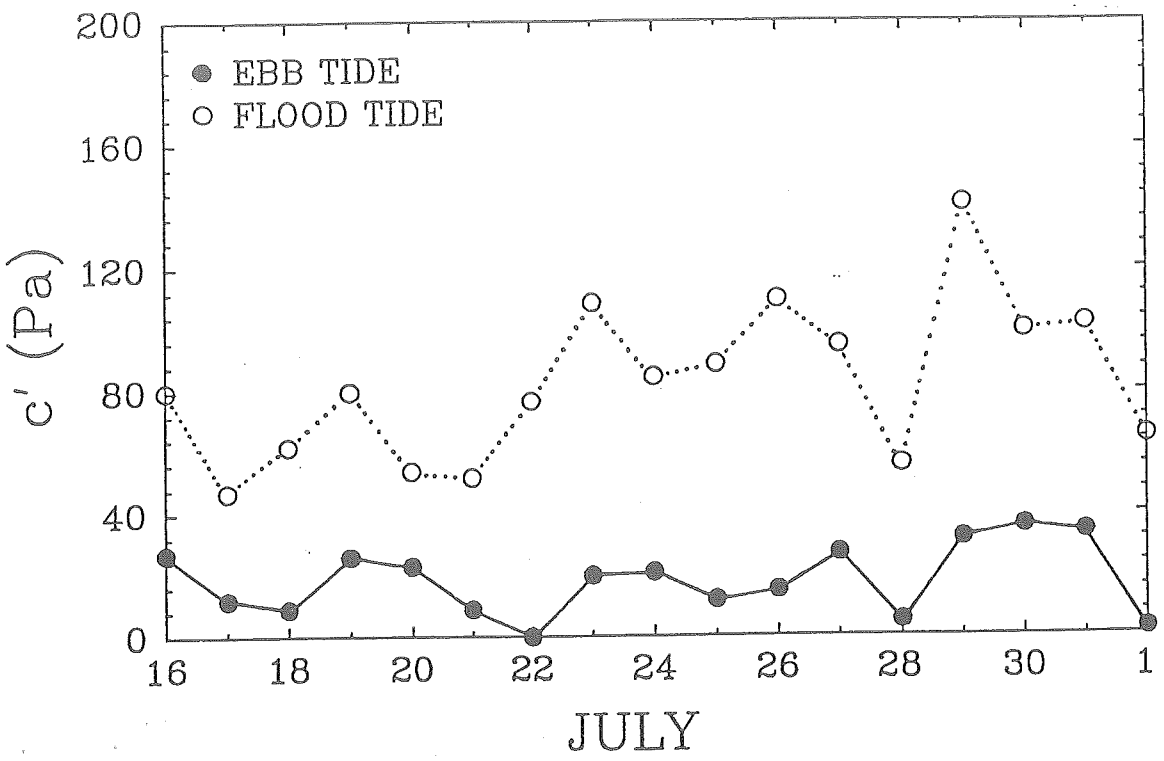

Figure 3.36A. Time series showing the INSIST cohesion buildup for the control sites during each daytime exposure of the mudflat.

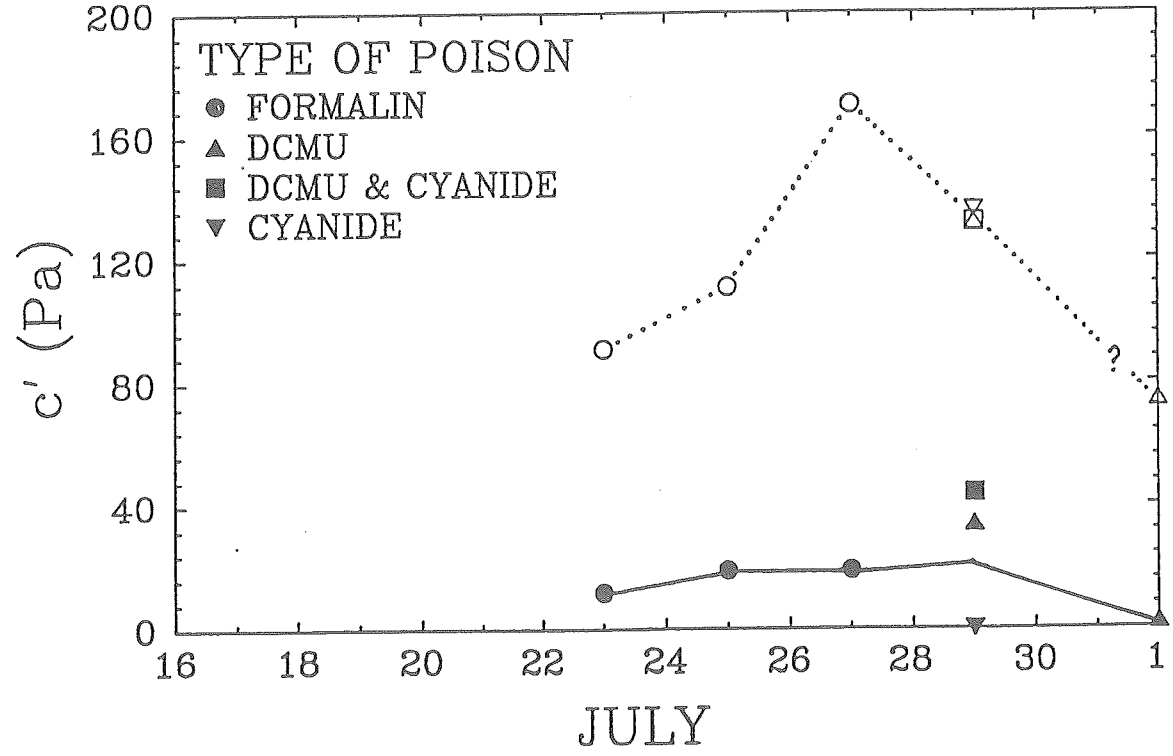

Figure 3.36B. Time series showing the INSIST cohesion buildup for the poisoned areas during each daytime exposure.

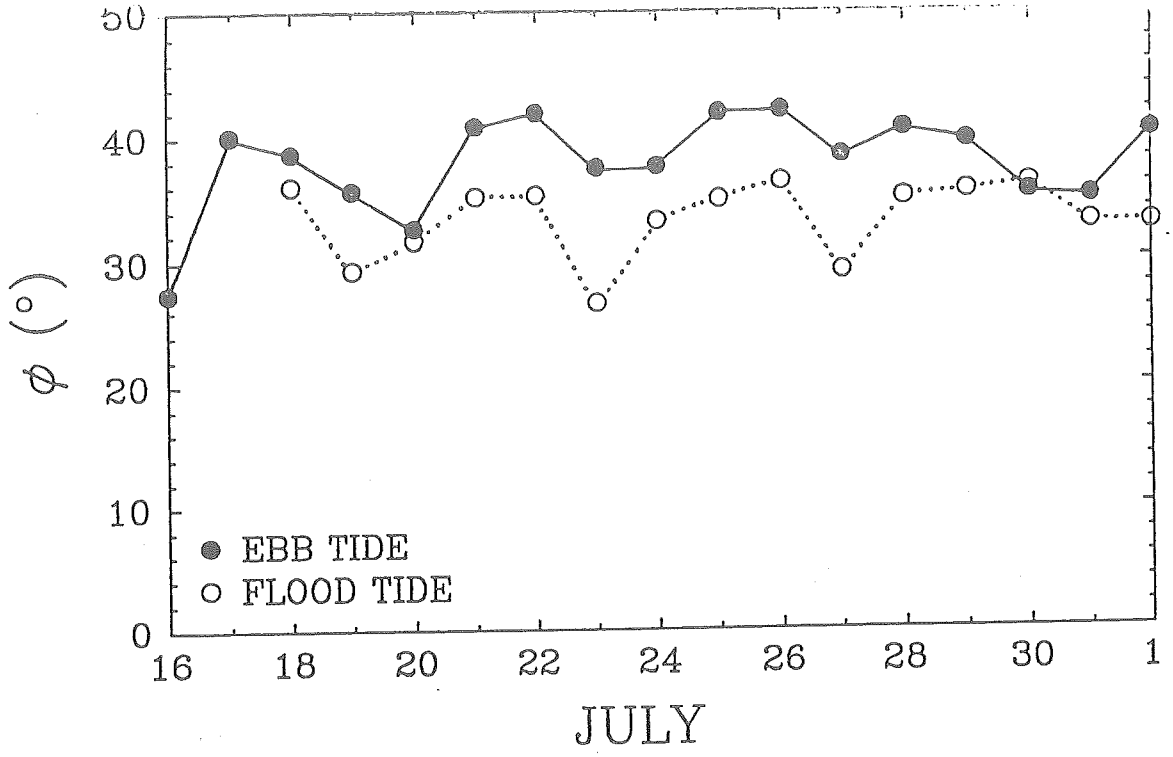

Figure 3.37A. Time series showing the change in friction angle derived from the INSIST failure envelope for the control sites.

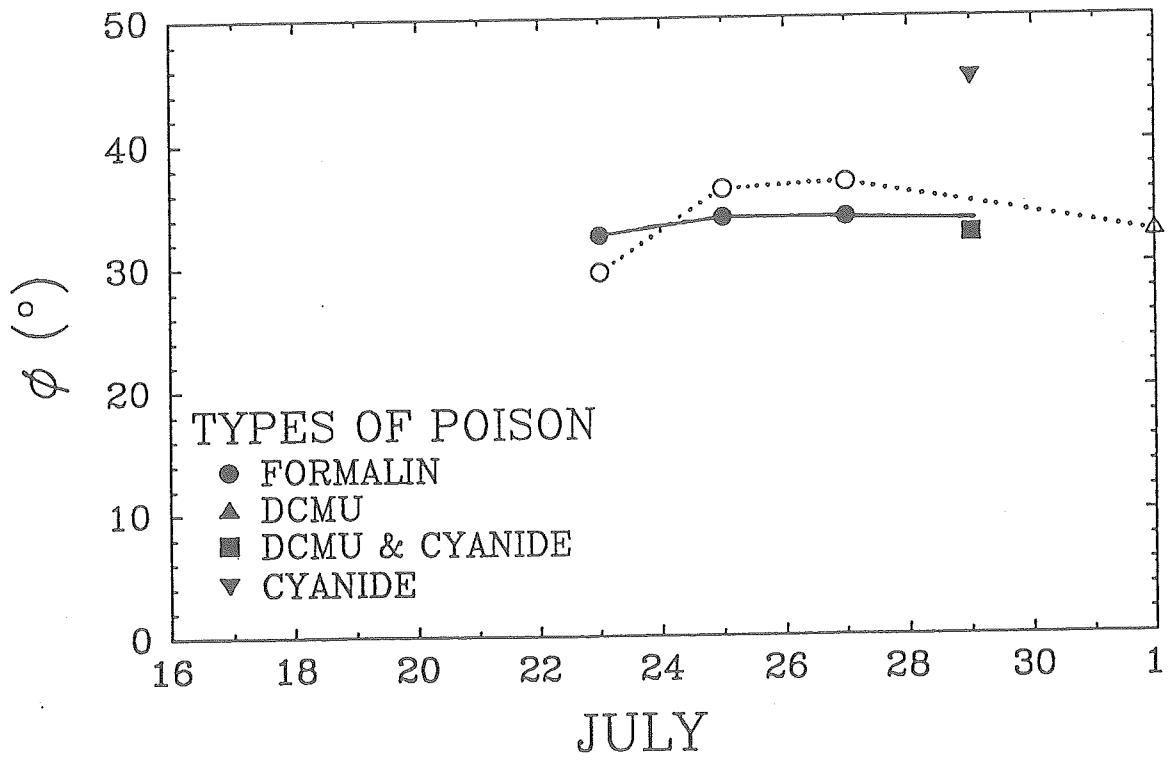

Figure 3.37B. Time series showing the change in friction angle derived from the INSIST failure envelope for the poisoned sites.

Table 3.8. Results from INSIST for all test sites

Date	Site	Cohesion (Pa)	Friction Angle	Cohesion (Pa)	Friction Angle
Control Sites					
16	3	27	27.5	80	--
17	2	12	40.1	47	--
18	1	9	38.7	62	36.0
19	2	26	35.6	80	29.3
20	3	23	32.5	54	31.6
21	2	9	40.8	52	35.1
22	1	0	41.9	77	35.2
23	2	20	37.4	109	26.6
24	3	21	37.5	85	33.1
25	2	12	41.8	89	34.8
26	1	15	42.0	110	36.2
27	2	27	38.3	95	29.1
28	3	5	40.5	56	34.9
29	2	32	39.5	141	35.4
30	1	36	35.3	100	36.0
31	2	34	34.9	102	32.8
1	FISH	2	40.2	65	32.7
Poisoned Sites					
23	2FORM	12	32.5	91	29.5
25	2FORM	19	33.9	111	36.2
27	2FORM	19	33.9	170	36.7
29	2DCMU	34	32.5	132	--
29	2BOTH	44	32.5	132	--
29	2CYAN	0	45.0	136	--
1	FISH	2	--	74	32.7

part of LISP since the control area began to behave in a similar manner as the poisoned sites. However, they did show that the absence of *Corophium* achieved through different methods (natural versus artificial) had the same net effect on physical properties. This is evident from comparison of Figures 3.36a and 3.37a with 3.36b and 3.37b which show the cohesion and friction angle time series for the control sites and poisoned site 2, respectively.

To explore these relationships further, solar radiation as measured by a weather station at the barge (site 2-Fig. 3.38) was used to normalize the strength increase on a daily basis. Figure 3.39 shows that even on rainy days there was still a significant strength gain, reinforcing the conclusion that atmospheric effects are not the entire story.

3.7.5 Subbottom Conditions

Figures 3.40, 3.41 and 3.42 illustrate the index properties at depth for sites 1, 2 and 3; grain size data are listed in Table 3.9. It is noteworthy that for all sites, sand content decreases with depth while clay content increases with depth. Water content decreases with depth, corresponding to increased bulk density. Figures 3.43, 3.44 and 3.45 show undrained strengths deduced from cone tip resistance data which increase with depth to very high levels very quickly, indicating a sharp transition from loose unconsolidated sediment to the heavily overconsolidated material existing below 10 cm. This dense boundary is presumably related to the cyclic loading effect by grounded winter pack ice that exists in the area.

The origin of the higher clay contents and lower sand contents at depth is somewhat puzzling. Either sand is being selectively removed from the system or more clay is being added. In fact, both could actually be occurring due to the presence of *Corophium*, which are known to burrow to 10 cm below the surface and maintain clean burrows by ejecting material into the water column during the flood tide. Daborn (personal communication) has noted that *Corophium* have been known to use clay to cement the walls of their burrows to keep them from collapsing. Faas (1990) has speculated that abandoned burrows could act as small settling tubes, allowing the intrusion of fine-grained material into the substrate. It would appear here again that biological activity plays an important role in this complex system, perhaps even to the point of assisting the stabilization of the mudflat by removing easily-eroded sand sizes from the sedimentary column.

3.7.6 Conclusions

To summarize, the INSIST device provides a new insight into *in situ* surficial spatial and temporal changes in shear strength on intertidal mudflats and allows direct comparison of independent variables to determine which environmental processes play predominant roles in modifying sediment resistance to erosion. The data reported herein are internally consistent, except for the odd increase in ebb water content toward the end of LISP in conjunction with reduced ebb friction angle, while cohesion increased. Strength changes may not be as well linked to atmospheric processes as previously thought in this setting, but may be controlled largely by biological

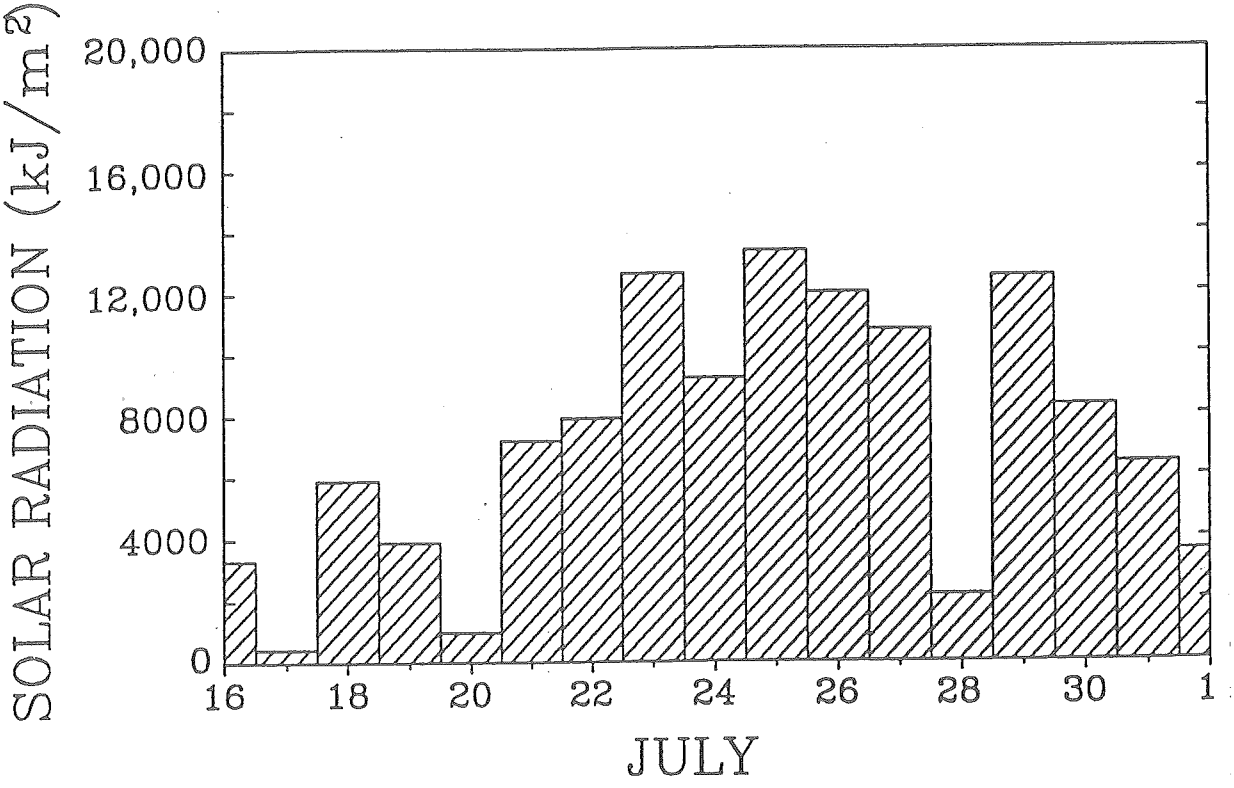

Figure 3.38. Measured solar radiation impacting the study area (barge) for the LISP period (note July 17, 20 and 28 when the sky was overcast and it was raining).

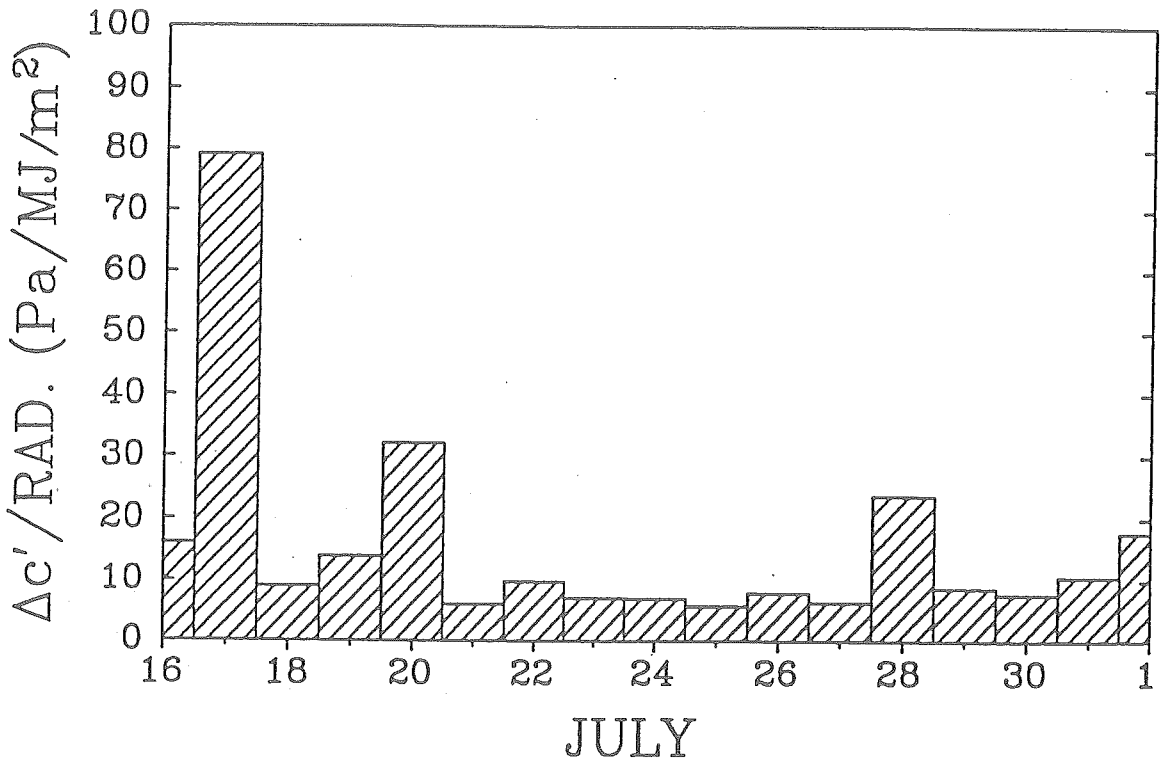

Figure 3.39. Daily INSIST cohesion increase normalized to the amount of solar radiation for the LISP period (note that cohesion increase on the rainy days was not related to drying). It is perhaps noteworthy to add that when it really began to pour, the equipment stopped working, followed soon after by the operator!

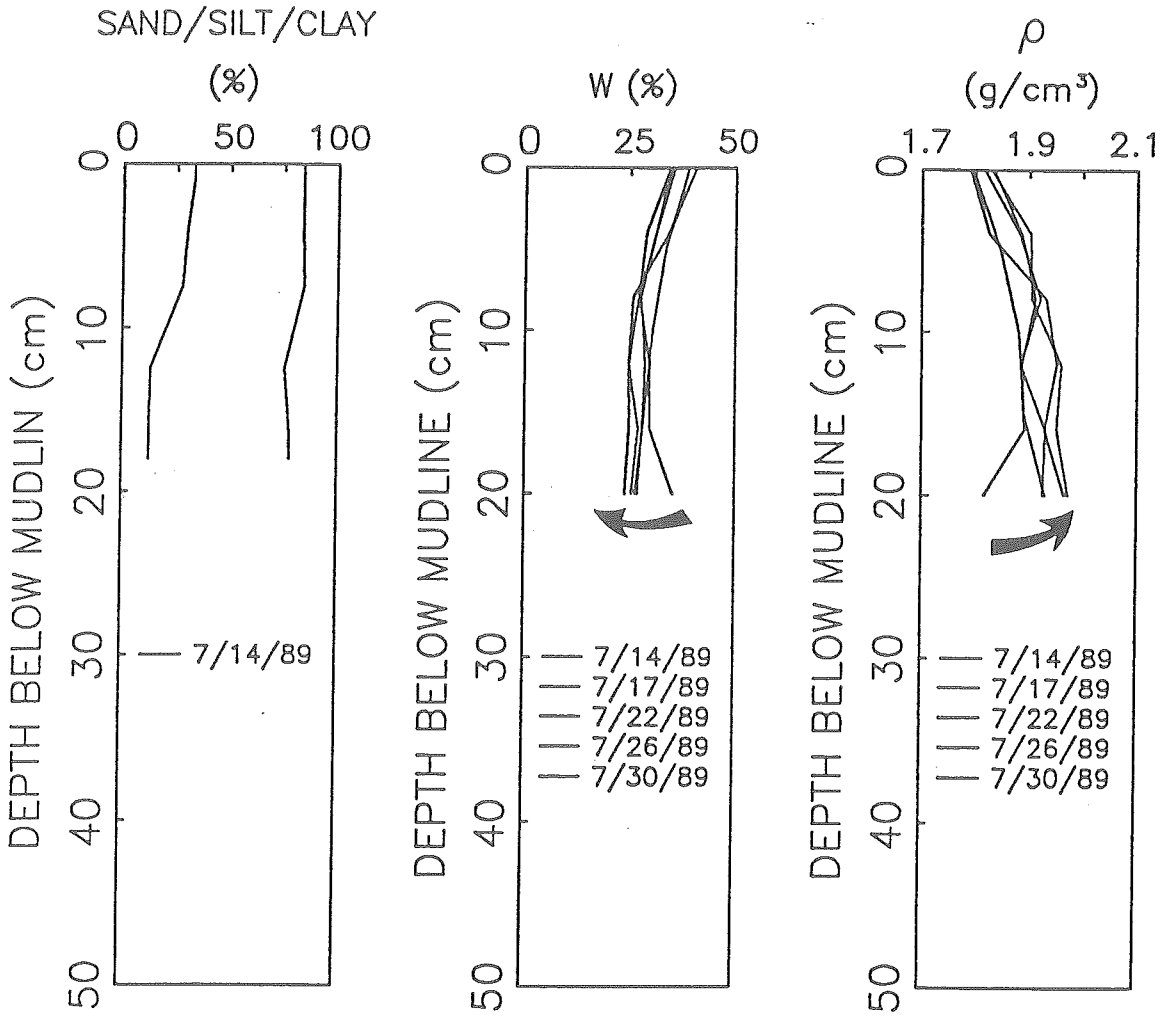

Figure 3.40. Profiles of index properties (grain size distribution, water content and bulk density) for site 1 with test pits dug on the days indicated.

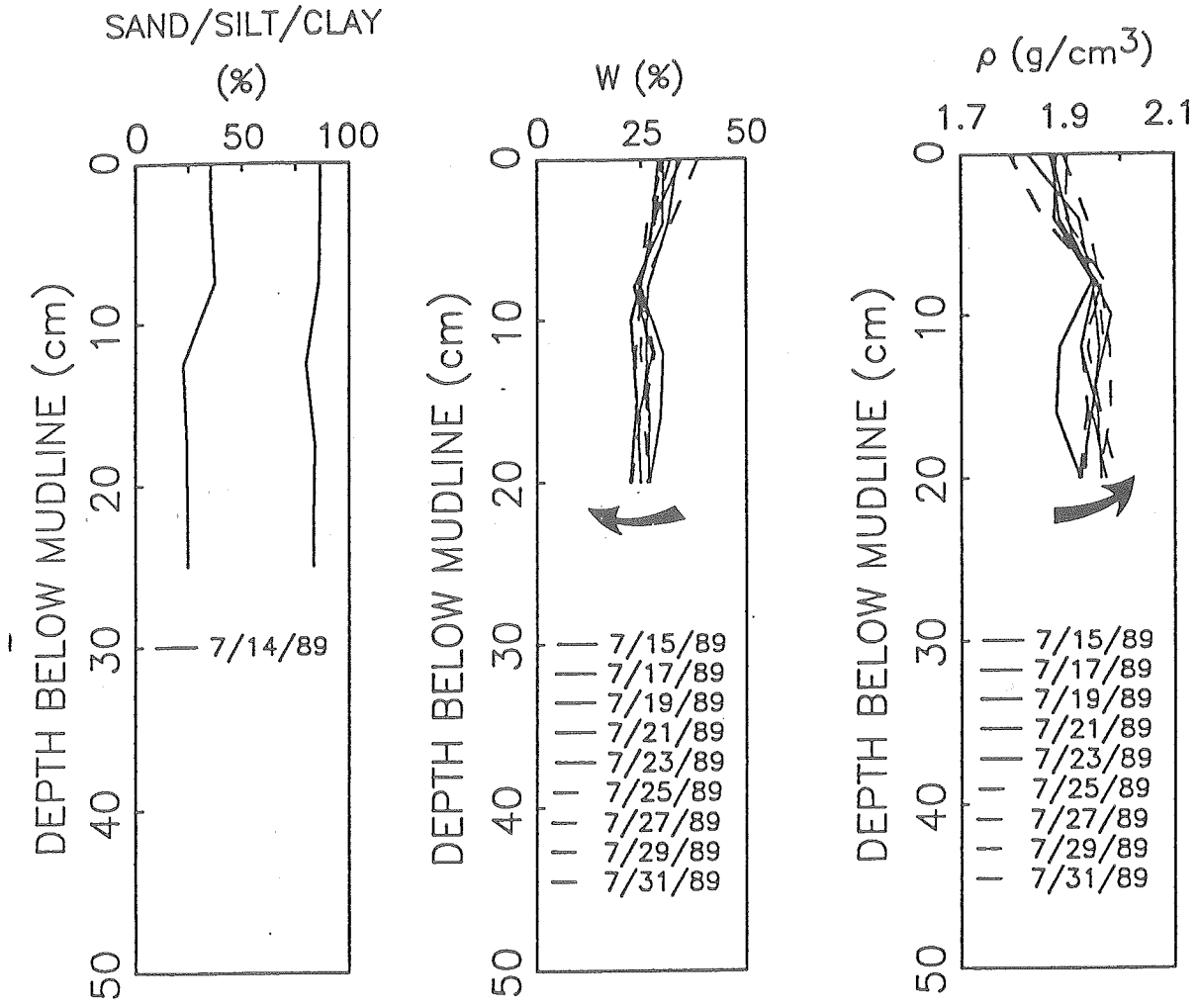

Figure 3.41. Profiles of index properties (grain size distribution, water content and bulk density) for site 2 with test pits dug on the days indicated.

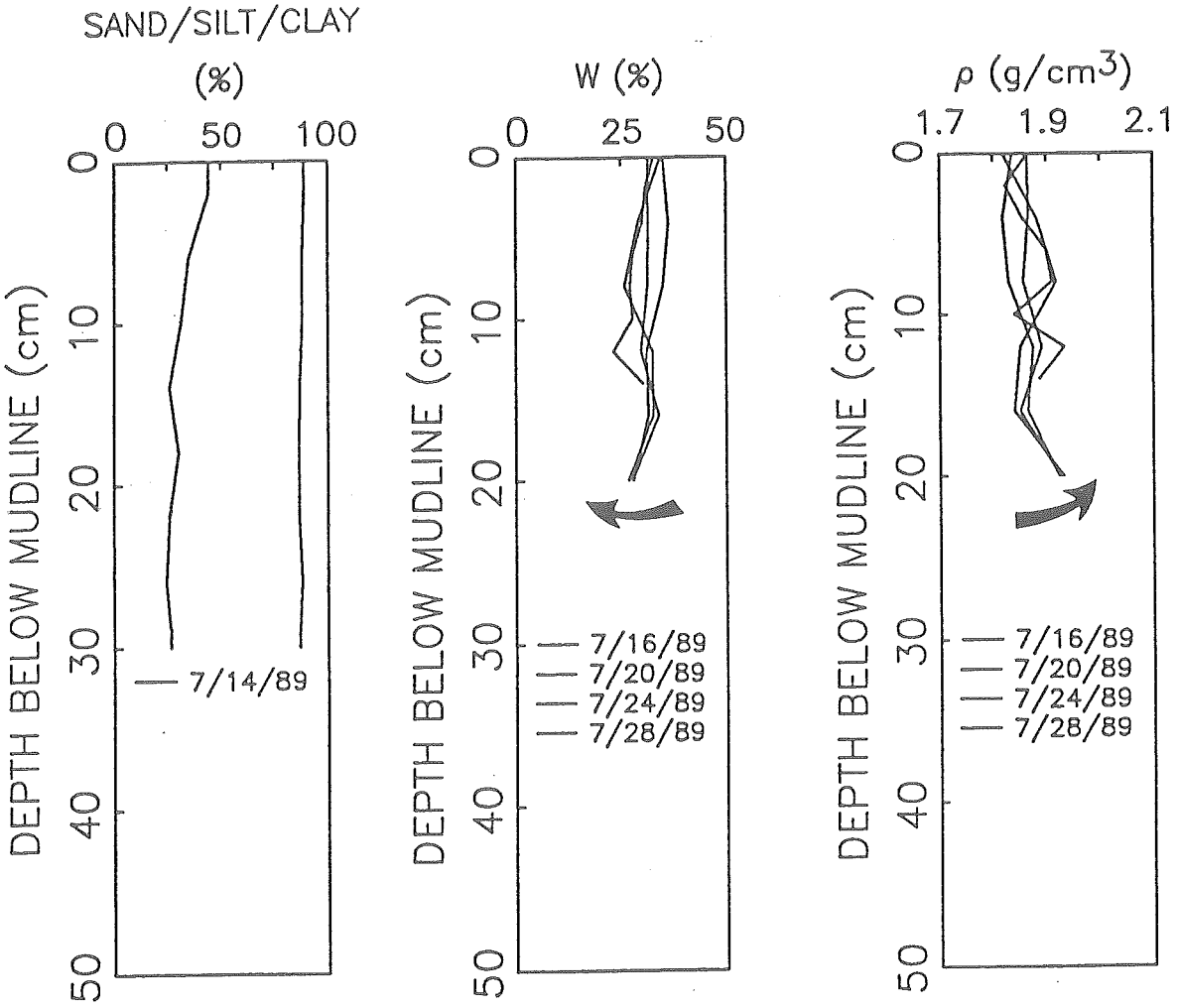

Figure 3.42. Profiles of index properties (grain size distribution, water content and bulk density) for site 3 with test pits dug on the days indicated.

Table 3.9. Summary of grain size distribution with depth for the three test sites

Sample	Date	Site	Depth (cm)	Sand (%)	Silt (%)	Clay (%)
14-1A	14	1	0-1	32.9	51.1	16.0
14-1B	14	1	1-5	30.0	54.0	16.0
14-1C	14	1	5-10	28.0	56.5	15.5
14-1D	14	1	10-15	13.3	62.2	24.5
14-1E	14	1	15-18	13.0	65.0	22.0
14-2A	14	2	0-5	35.5	51.0	13.5
14-2B	14	2	5-11	37.1	48.9	14.0
14-2C	14	2	11-15	22.5	57.5	20.0
14-2D	14	2	15-20	24.4	60.1	15.5
14-2E	14	2	20-25	24.6	58.9	16.5
14-3A	14	3	0-4	44.4	44.6	11.0
14-3B	14	3	4-8	34.9	53.1	12.0
14-3C	14	3	8-12	31.3	56.7	12.0
14-3D	14	3	12-16	26.2	60.8	13.0
14-3E	14	3	16-20	30.4	56.1	13.5
14-3F	14	3	20-24	26.3	60.2	13.5
14-3G	14	3	24-28	24.6	63.4	12.0
14-3H	14	3	28-30	26.8	60.2	13.0
16-3A	16	3	0-5	--	--	--
16-3B	16	3	5-10	50.6	38.4	11.0
16-3C	16	3	10-15	69.0	18.5	12.5
16-3D	16	3	15-20	27.7	57.8	14.5
16-3E	16	3	20-25	26.6	57.4	16.0

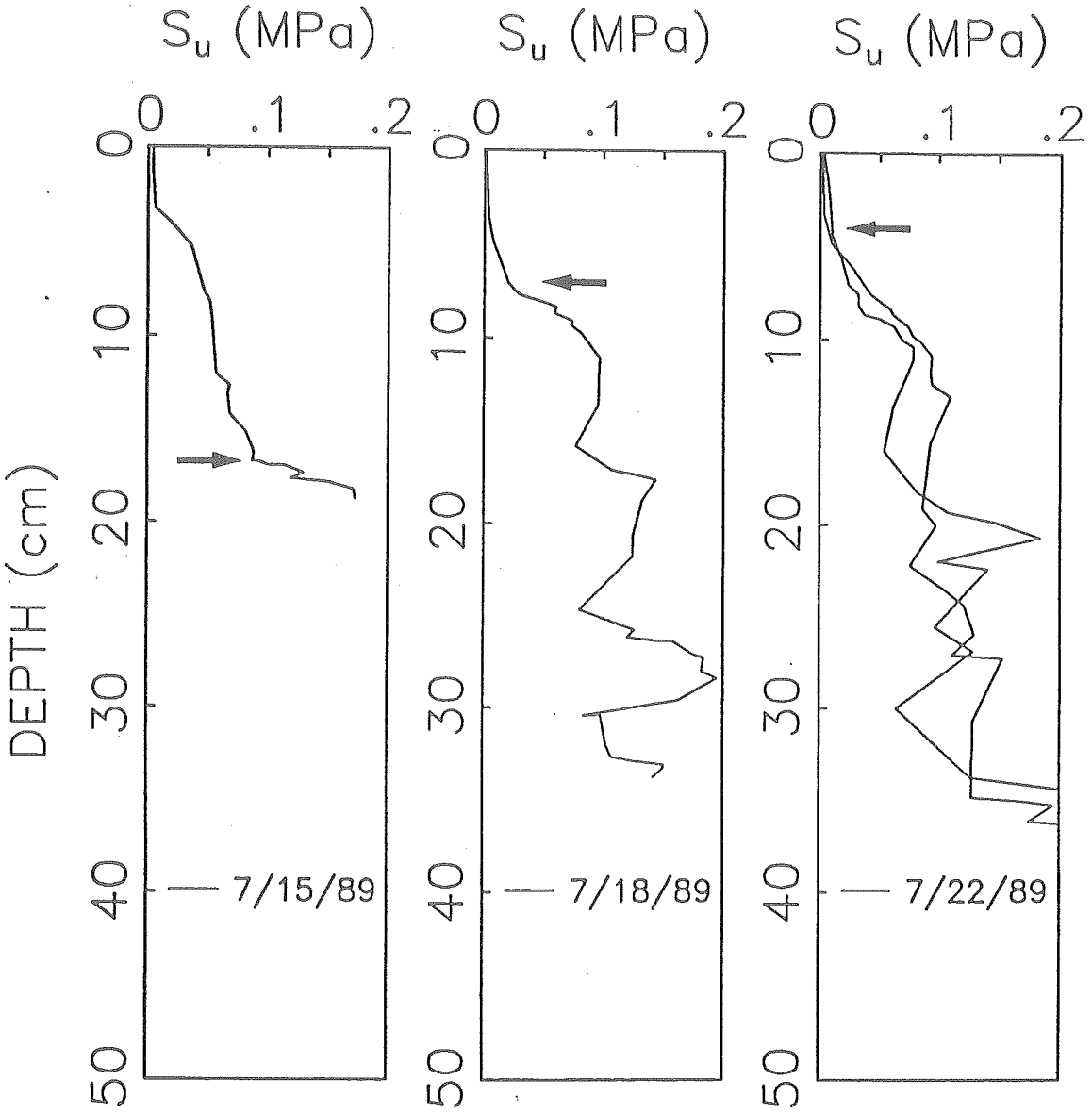

Figure 3.43. Cone penetration records showing undrained strength derived from cone resistance (cone factor of 15) versus depth for site 1. Note the top of the dense stratra occurring from 4 to 16 cm, indicating the highly localized variability and perhaps also indicating the heavily channelized nature of the subbottom conditions.

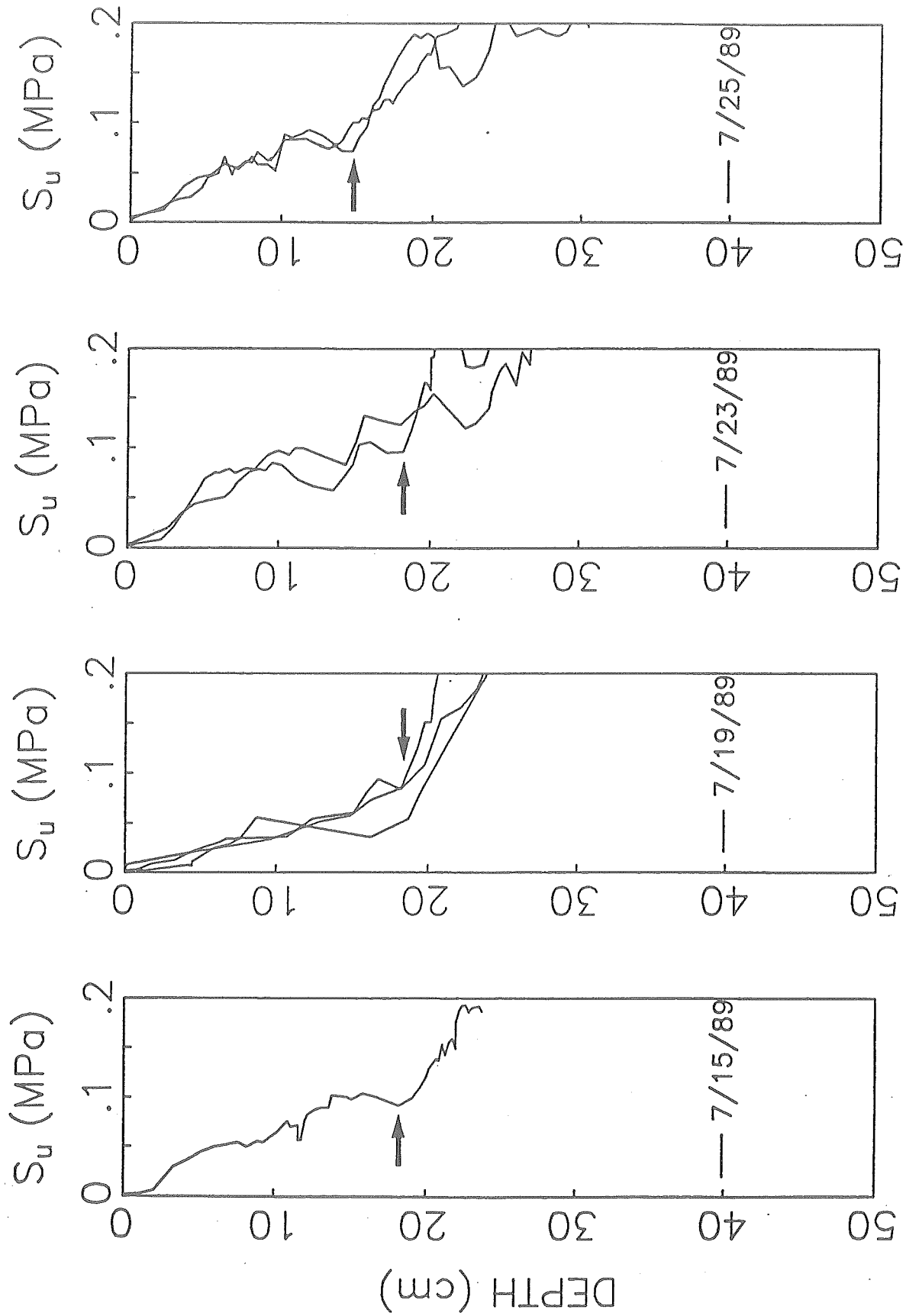

Figure 3.44. Cone penetration records for site 2 showing that the dense layer occurs within a fairly narrow depth range of 15 to 19 cm.

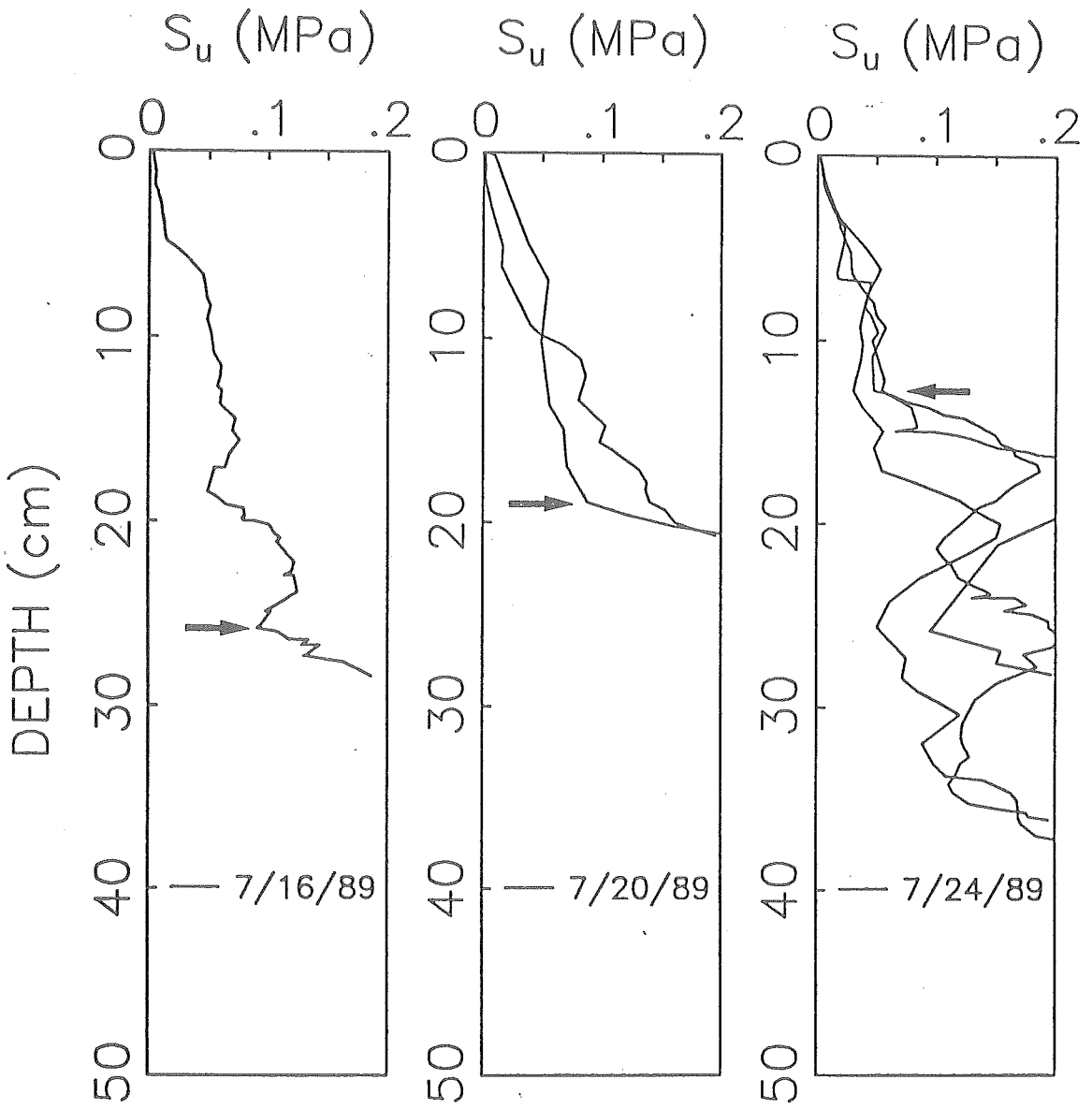

Figure 3.45. Cone penetration records for site 3 showing that the dense layer occurs within a wide depth range of 13 to 26 cm.

activity. Alternatively, an event noted by Amos et al. (1988) may have been repeated in this study, whereby strength increases resulted as a consequence of changing grain size over the long-term. The latter explanation is more satisfying from a geotechnical point of view, since it explains the unusual changes in the index properties occurring at the same time.

Textural changes at depth on Starrs Point seem to indicate that biological activity also affects the stability by selectively ejecting coarse-grained material from the sediment package, resulting in an environment that is more stable under environmental loading and easier for *Corophium* to maintain open burrows. The entire system would appear to be reset by consolidation beneath winter pack ice accumulated on the mudflat, producing very high degrees of overconsolidation. The uppermost 10-20 cm would then be subjected to erosion and redistribution by the ice as it shifts around in response to wind and currents, leading to the development of a softened zone as noted in the test pits and cone penetration tests conducted in this study.

3.8 Erodibility of the Starrs Point Tidal Flat

A central objective of the LISP project was to develop techniques that would enable direct *in situ* measurements of sediment erodibility, recognising that sampling and trans-shipment of sediments to laboratory flumes, as has commonly been done in the past, has the potential for changing critical properties of the sediment. Such samples lose much of their structural organisation, especially where this is the result of biological activities such as growth of benthic algae, or tube-construction and cleaning activities of invertebrates. Holding of such sediments for any length of time leads to death of important biota, decay of organic matter and development of anoxic conditions and anaerobic bacterial flora, which may be critical to the structural organisation of the deposit. Preliminary studies by Amos and Mosher (1985) showed that fine Minas Basin sediments, when carefully removed from the field and examined as soon as possible in a laboratory flume, were much more resistant to erosion than disturbed and remixed sediments of similar grain size that had been used in previous studies.

During LISP 89, a comparative study was conducted between two techniques for *in situ* measurement of erodibility (Amos' 'Sea Carousel' and Paterson's 'Cohesive Shear Meter'). As a form of control, sediment cores were removed from the experimental sites by Dr. J. Grant, rapidly and carefully returned to a laboratory at Dalhousie University (Halifax), and then inserted in a seawater flume for precise study of erodibility. Results from two of these study components are not yet complete. This section provides information on 'Sea Carousel', and summaries of the other two portions of the study.

3.8a Sea Carousel - A Benthic, Annular Flume

CARL L. AMOS

3.8a.1 Introduction

A benthic annular flume (Sea Carousel) has been developed and tested to measure the erodibility *in situ* of cohesive sediments. The flume is equipped with three Optical Backscatter Sensors, a lid rotation switch, and an E.M. flow meter capable of detecting azimuthal and vertical components of flow. Data are logged at rates up to 10.66 Hz. Erodibility is interpreted from the rate of change in suspended sediment concentration detected in the annulus.

Several field flumes have been developed and tested in order to derive realistic *in situ* measures of bed erodibility. A review of these was made by Zeman (1983). Black (1989) more recently described eight flumes developed for field use, including Scoffin's (1968) flow-through flume, Peirce's recirculating annular flume (Peirce et al. 1970) , SEAFLUME (Young, 1977), SEADUCT (Nowell et al. 1985), and Black's own mobile recirculating flume (MORF). Only the SEAFLUME and SEADUCT were capable of submerged remote deployment.

The use of annular flumes over those of other shapes in the study of bed erosion has clear advantages

(Partheniades et al. 1968; Mehta and Partheniades 1979; Creutzberg and Postma 1979; Fukuda and Lick 1980; Lee et al. 1981; Lick 1982; Kusuda and Umita 1982; Burt 1984; Wilkinson and Jones 1988; Sheng and Villaret 1989; Hill et al. 1988; Kuijper et al. 1989; and Maa 1990). These authors argued that a constant channel geometry and infinite flow length results in a fully developed benthic boundary layer—an essential prerequisite to the application of flume-derived bed erosion studies to the natural environment. Furthermore, analyses of the total (radial and tangential) bed stress across an annulus made by Hydraulic Research Limited (1987), Maa (1990) and by T.E.R. Jones (personal communication, 1989) show only minor increases radially. In fact, Maa predicted that the total (radial and tangential) and average bed stresses were within 20% of each other for the central 80% of the annulus. Unfortunately, none of the developed benthic flumes is capable of continuous and remote monitoring of flow character and bed response.

The purposes of this part of the study were :

(1) to develop, build and test an annular benthic flume capable of logging and quantifying flow character and bed response at high (up to 10 Hz) frequencies, to derive the critical shear stress for erosion versus depth within a sediment and to collect field data to help characterize cohesive sediment erodibility in Minas Basin;

(2) to measure bed erosion rate as a function of time and imposed bed stress, the equilibrium suspended sediment concentration as a function of flow velocity and the still-water particle settling rate as a function of sediment concentration.

3.8a.2 Instrumentation and Calibration

System Configuration

Sea Carousel, named after the carousels of Postma (1967) and Hydraulic Research Limited (Burt 1984), is an annular, benthic flume designed for field use in intertidal and subtidal settings. The carousel is 1.0 m in radius with an annulus 0.15 m wide and 0.25 m high (Fig. 3.46). It weighs approximately 150 kg in air and 40 kg in water and is made entirely of aluminium. Flow in the annulus is induced by rotating a moveable lid that is driven by a 0.5 hp DC motor powered from the surface. Eight small paddles, spaced equidistantly beneath the lid, serve to induce a flow of water in the annulus. The width of the annulus (D) was optimized at 0.15 m to give a relative roughness (e/D) $\approx$ 0.004 (where the wall roughness, e $\approx$ 0.0006 m; after Shames 1962). The water depth in the annulus was minimized to 0.25 m to ensure conditions for Nikuradse's "rough-pipe zone of flow" wherein changes in wall friction factor with changes in Reynold's number are at a minimum (Shames 1962).

A schematic diagram of the Sea Carousel configuration is shown in Figure 3.47. It is equipped with three Optical Backscatter Sensors (OBS's; Downing 1983). Two of these are located non-intrusively on the inner wall of the annulus at heights of 0.03 and 0.18 m above the skirt (the skirt is a horizontal flange situated around the outer wall of the annulus 0.04 m above the base; it was designed to standardize penetration of the flume into the seabed; cf. Fig. 3.46). The third OBS detects ambient particle concentration in the annulus at a height of 0.3 m

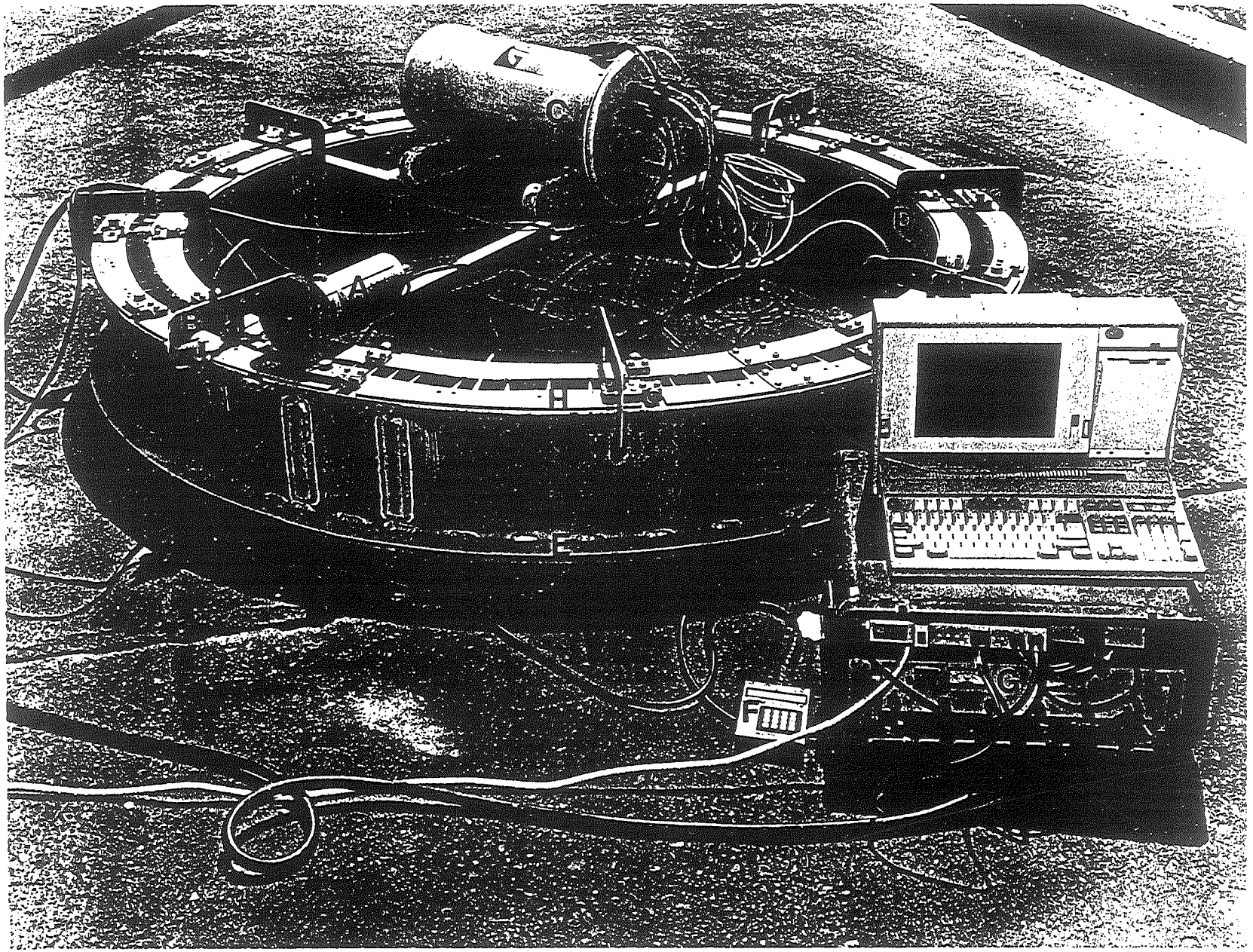

Figure 3.46. The Sea Carousel System. (A) Underwater Motor; (B) Magnetic Read Switch; (C) Underwater Pod; (D) Re-inforcing Gusset; (E) Bed Level Flange; (F) Keyboard to Data Logger; (G) Power Supply to Motor; (H) Rotating Lid.

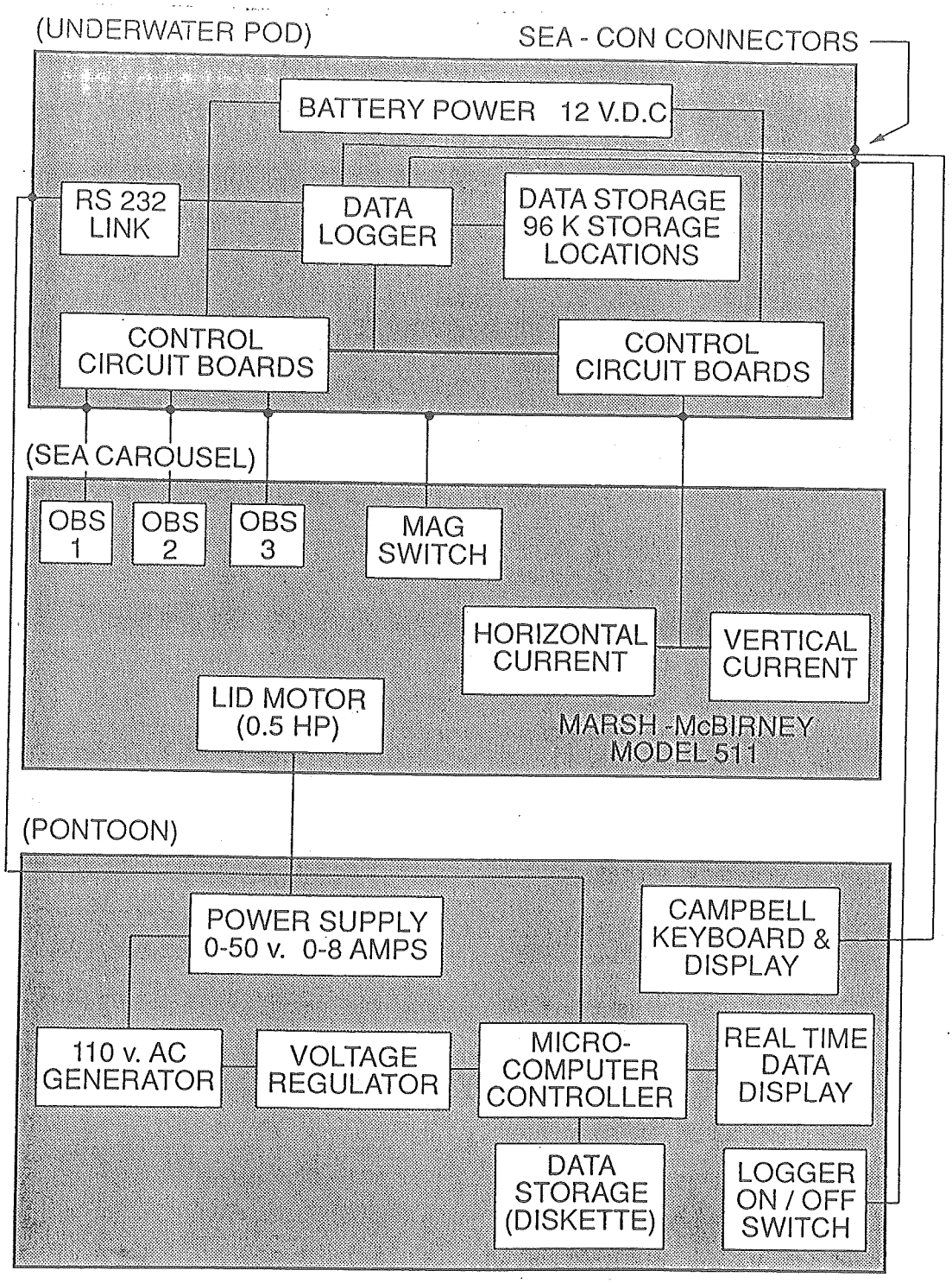

Figure 3.47. A schematic diagram of the electronic and electrical layout of Sea Carousel.

above the bed or it may be used to detect internal sediment concentration at a height midway between the other two. The OBS sensors give linear responses to particle concentration for both mud and sand over a concentration range of 0.1 to 50 $g.L^{-1}$ (Downing and Beach 1989). They are unaffected by flows below 1.5 $m.s^{-1}$ and are stable through time. A sampling port is situated in the outer wall of the annulus at a height of 0.2 m above the skirt through which water samples can be drawn to calibrate the three sensors under well mixed conditions.

A Marsh/McBirney current meter (model 511) is located on the centreline of the annulus at a height of 0.16 m above the skirt. It was modified to detect the instantaneous azimuthal and vertical components of flow within the annulus (U_y and U_w respectively). Mean tangential lid rotation ($\overline{U}_r$) is detected through a magnetic reed switch which is triggered by the passage of 12 magnets spaced equidistantly around the lid. Controller boards for each sensor and the necessary power (12 VDC) are derived from an underwater pod located inside the annulus. Output voltages from all sensors are digitized and transformed to scientific units on a Campbell Scientific CR10 data logger and stored on a Campbell Scientific SM192 storage module (storage capacity of 96,000 data values), also located in the underwater pod. The data logger is interrogated and programmed from the surface using a microcomputer linked to the data logger through an RS232 interface. Maximum sampling rate of all channels is approximately 2Hz, whereas U_y and U_w may be logged at rates up to 10.66 Hz. All channels may be monitored and displayed on the surface computer allowing the operator to "drive" the experiment in an interactive mode. A "stress profile through time" is created by varying the power supplied to the underwater motor between 50 and 250 watts via a surface power supply. The data stored from each deployment may be downloaded remotely through the RS232 cable at the end of each experiment and the storage module initialized.

Current Velocity Measures and Friction Velocity

Flume Reynold's numbers (R_e) for $0.1 > Uy > 0.5$ $m.s^{-1}$ are $2.3 \times 10^4 > Re > 1.1 \times 10^5$ calculated by :

$$R_e = (\rho U y R_h)/\mu \qquad (1)$$

where the fluid density $\rho = 1026$ $kg.m^{-3}$, the absolute viscosity μ is normalized to $10^oC = 0.0013$ $kg.m^{-1}.s^{-1}$, and the flume hydraulic radius $R_h = 37.5$ mm. Eroding flows are thus considered fully turbulent. Variations in Reynold's number within this range result in a 3% variation only in the wall boundary layer velocity profile, and so time variations in wall effects on our flow measurements are ignored. Azimuthal velocity profiles carried out by Fukuda and Lick (1980) in an annular flume showed that the thickness of the viscous sub-layer (δ') is defined by the relationship :

$$\rho \overline{U}_* \delta'/\mu \approx 12 \qquad (2)$$

where $\overline{U}_*$ is the time-averaged friction velocity. The thickness of the inner buffer layer or logarithmic region over which "law of the wall" can be expected to apply is defined by Gust's (1976) observations as :

$$\rho\overline{U}_*\delta'/\mu \approx 300 \qquad (3)$$

The predicted thicknesses of the benthic viscous sub-layer and the inner buffer layer in the flume for $\overline{U}_* =$ 16 mm.s^{-1} (a typical friction velocity for erosion; Nowell et al. 1981) are 0.9 mm and 25.2 mm respectively. If we approximate a typical mudflat roughness to the floc diameter of material forming it (Yingst and Rhoads 1978) : 0.03 mm (Hildebrand et al. 1980) then bed erosion would begin under dynamically smooth turbulent flow conditions. Measurements of the viscous sub-layer made by Gust (1976) and Buchholtz-Ten Brink et al. (1989) verify this, and show that turbidity expands this layer by a factor of 2 at 500 mg.L^{-1} and 3 at 10 g.L^{-1}. It was not physically possible to measure flow velocity within the inner buffer layer. However, the majority of the flume is expected to be occupied by the turbulent outer layer where time-averaged velocity, U, is a function of the velocity-defect law and so is independent of turbulent scales, absolute viscosity and bed roughness :

$$(\overline{U}_r - \overline{U}_y)/\overline{U}_* = f(y/d) \qquad (4)$$

where y is the height of the measurement of $\overline{U}_y$ and d is flow depth. From direct measures of U_* (see next section) the constant f was evaluated at 5.94 ($\pm$0.35) and so the centreline velocity profile for this region may be derived. The velocity profile for the centreline velocity ($\overline{U}_y$) in the inner buffer layer may be approximated by :

$$\overline{U}_y/\overline{U}_* = 2.5\ \mathrm{Ln}(\rho\overline{U}_*y/\mu) + C_2 \qquad (5)$$

C_2 is evaluated to match results from equation 7 for y set at the height of the inner buffer layer (derived in equation 2). The velocity in the viscous sub-layer is derived from :

$$\overline{U}_y/\overline{U}_* = (\rho\overline{U}_*y)/\mu \qquad (6)$$

where $\overline{U}_y$ is the azimuthal flow for y at the top of the viscous sub-layer (from equations 1 and 4). Finally, the resulting time-averaged bed stress may be determined from the relationship :

$$\tau o = \rho\overline{U}_*^2 \qquad (7)$$

3.8a.3 Methodology

Laboratory Calibration

The sensors on Sea Carousel were calibrated *in situ* in a saline water-filled test tank using known concentrations of Minas Basin mud. The verification of lid rotation speed was carried out by timing ten revolutions of the lid at a range of speeds. The current meter was calibrated in a test tow tank at Bedford Institute of Oceanography. The meter was also tested in place against a Nixon impeller meter to determine effects of

electric field distortions derived from the structure and operation of the system. Further tests were made to evaluate the effects of temperature and salinity on flow character by driving Sea Carousel in a test tank over a range of temperatures, salinities and sediment concentrations and logging the azimuthal and vertical components of current velocity at 10.66 Hz.

Total U_* was measured at a series of differing flow velocities at five positions radially across the annulus using an omni-directional, flush-mounted, hot-film sensor of Gust (1988) embedded in the base of a smooth fibre glass test tank. Voltage output of the hot-film sensor was calibrated directly to friction velocity which was determined from the pressure gradient in pipe flow (J. Grant - unpublished data). No attempt was made to resolve bed stress into radial and azimuthal components.

Field Deployment

The method used to collect information on bed erosion and erosion rates is similar to that proposed by Mehta and Partheniades (1982), Thorn and Parsons (1980), Kuijper et al. (1989) and Sheng and Villaret (1989). That is, to increase nearbed flow and hence bed stress in steps through time and to hold the bed stress constant between each step (Δt) of 10 to 20 minutes. Thereafter, lid rotation is decremented in order to monitor deposition rates (W_s) as a function of flow velocity and concentration, and the equilibrium concentration at each flow velocity. Lid rotation, azimuthal velocity, vertical velocity, and the three measures of suspended sediment concentration were sampled and logged at 1 Hz. Time series of each parameter were generated after time-averaging (20 second) and despiking the data between 2 standard deviations of the 20 second mean values. Transforms of velocity to bed stress were carried out based on the calibration results above and assuming a smooth bed. Total suspended mass (M) was computed each 20 seconds from $M = V/d \int_0^z S\, \partial z$, where V is the annulus volume (0.218 m^3), S is the mean suspended sediment concentration, and d is the height of the annulus above the bed (0.26 m). The erosion rate was determined from the differential concentration ($E \propto \Delta S/\Delta t$) of successive 20-second time-averaged measures of S. The depth of erosion (z) was estimated as $z = M/A\rho s$, where A is the annulus area (0.873 m^2) and ρs is the measured sediment bulk density (in the case presented $\rho s = 1850$ kg.m^{-3}; Christian et al. 1990). Surface critical shear stress is determined following Mehta and Partheniades (1982) and Mehta et al. (1982), i.e., by assuming that the measured bed stress is equivalent to the aggregate shear strength at the depth in the sediment at which erosion ceases. The surface critical shear stress (τ_c) is derived by extrapolation of the least squares best-fit line to the surface. This method can only be used under conditions of Type I erosion. Under other conditions, τ_c may be derived by examining erosion rate as a function of applied bed stress on a series of fresh surfaces. τ_c is found from the zero intercept of erosion of a least squares regression line of the two variables.

Data Processing

Data from the Sea Carousel sensors are logged by the Campbell CR10 data logger and stored on a Campbell SM72 at 1 Hz for the duration of each experiment. The channels logged are as follows :

(1) OBS1 voltage
(2) OBS2 voltage
(3) OBS3 voltage
(4) vertical component of flow
(5) azimuthal component of flow
(6) lid rotation

A time stamp is placed in the record at 10-minute intervals. This time stamp contains the julian day and the time (AST; hh:mm). The raw data file is backed up to diskette at the end of each experiment and the storage module initialized for the next experiment. These data are then processed using a series of basic programs (PROC1 - PROC4) in the following fashion :

(1) read time stamp and strip out CR10 code
(2) read each sequential record (6 variables) over time average interval and strip out CR10 code
(3) despike data between ±2 standard deviations
(4) time average each smoothed channel
(5) transform OBS voltage to sediment concentration ($mg.L^{-1}$)
(6) transform E.M. voltage to velocities ($m.s^{-1}$)
(7) compute dispersed mass and eroded mass (kg)
(8) correct eroded mass for dispersion
(9) determine eroded depth from eroded mass (kg)
(10) compute friction velocity ($m.s^{-1}$) and bed stress (Pa)
(11) write day, time, OBS1, OBS2, OBS3, vertical velocity, azimuthal velocity, lid rotation, eroded mass, erosion rate, eroded depth, friction velocity and bed stress for each time-averaged interval.

The processed data file is imported into a plot package (SIGMAPLO) and a time-series of each parameter produced.

3.8a.4 Results

Laboratory Calibration

Calibrations of the three OBS sensors were carried out by sampling flume water from the sample port during operation. Sediment concentration is derived by vacuum filtration and determined gravimetrically. The linear functions for the calibration of the three sensors to Bay of Fundy mud are :

$OBS1 = 2.16(voltage) - 89$ ($mg.L^{-1}$; $r = 0.98$; $n = 5$) (8)
$OBS2 = 2.72(voltage)$ ($mg.L^{-1}$; $r = 0.98$; $n = 5$) (9)
$OBS3 = 1.98(voltage) - 87$ ($mg.L^{-1}$; $r = 0.98$; $n = 5$) (10)

All OBS's yielded similar slopes in the correlation function, but varied in the offsets (Fig. 3.48). The relationship for the ambient OBS (2) passes through the origin, whereas the other two register backscatter when the suspended sediment concentration is zero. This suggests that OBS1 and OBS3 are affected through backscatter from the opposite flume wall.

A time series of an experiment to relate lid rotation, azimuthal velocity and vertical velocity is shown in Figure 3.49. Lid rotation was increased to a maximum of 0.9 $m.s^{-1}$ from rest, then decreased to rest over a 25-minute period. Data were recorded at 1 Hz and time-averaged over 10 seconds. No apparent long-term drift in lid rotation occurred nor is there evidence of excessive signal noise. Lid rotation was accurate to $\pm 4\%$. Azimuthal current was stable and showed a clear relationship to lid rotation. This relationship is linear over the entire test range and results in a velocity defect of :

$$\overline{U}_y = 0.574\overline{U}_r + 0.025 \ (m.s^{-1};\ r = 0.96;\ n = 180) \qquad (11)$$

The relationship is unaffected by changes in suspended sediment concentration (up to 208 $mg.L^{-1}$; Fig. 3.50A) or temperature (between 4.5° and 18°C; Fig. 3.50B). It is however affected by salinity. Measures of U_y are consistently 0.05 to 0.1 $m.s^{-1}$ greater in saline water (34 ‰) than in brackish water (0.16 ‰). This offset is presumably the result of changes in response of the E.M. flow meter over the range in salinities tested. The vertical current is positive (downward flowing) in all cases and is weakly correlated with U_y ($r = 0.85$; $n = 180$). Day to day variations in the zero offset of the E.M. meter were up to ± 0.05 $m.s^{-1}$. Still water calibrations are therefore necessary prior to each experiment.

High-frequency (10.66 Hz) sampling of U_y and U_w was undertaken to evaluate system noise and the turbulent structure in the annulus (salinity = 34 ‰; temperature = 4.5° and 18°C). An example of the still-water signals is shown in Figure 3.51. A zero-offset of approximately 0.01 $m.s^{-1}$ is apparent in the azimuthal velocity due to sensor drift with time. Also, fluctuations in both components of velocity were detected with an amplitude standard deviation of 6×10^{-6} $m.s^{-1}$. Spectral analysis (FFT) of these signals (Fig. 3.52A) showed a relatively flat spectrum typical of white noise in the macroturbulent range and energy dissipation in the inertial sub-range.

The turbulent character of the flow was determined over a wide range of lid rotations and lid accelerations. Examples of annulus flow from still water conditions to a speed of approximately 0.4 $m.s^{-1}$ are shown for 4.5° and 18°C salt water in Figures 3.53A and 3.53B respectively. The turbulent fluctuations in velocity are evident in both cases. Also, the amplitudes of the fluctuations are much larger in the warm water test. The current speed standard deviation for the time-series ($3 - 4 \times 10^{-4}$ $m.s^{-1}$) showed only a weak relationship to U_y and no apparent relationship to current acceleration or deceleration. This implies that the flow turbulence generated by paddle rotation is not enhanced during changes in rotation speed. Spectral analysis of U_y reveals an orderly structure to flow microturbulence. Figure 3.52B shows spectral density plotted against wave number for a mean speed of 0.42 $m.s^{-1}$. Notice that the energy density within the inertial subrange (wave number(k) > 15) decreases monotonically with a slope of -5/3. This slope is typical of microturbulent energy dissipation found in many flumes and in the benthic boundary layer of open marine environments and suggests normal viscous dissipation

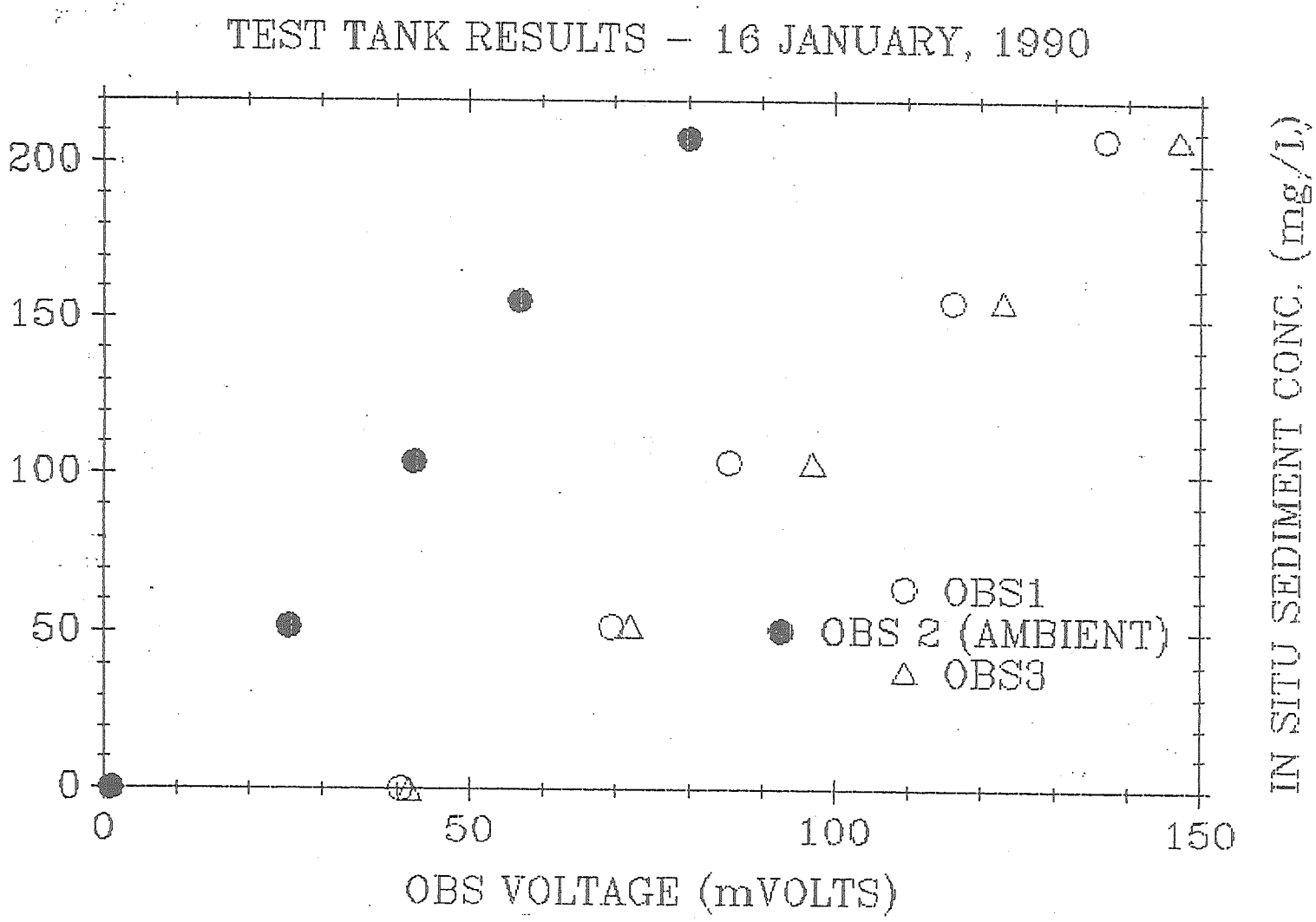

Figure 3.48. Calibration results of the three Optical Backscatter Sensors used in Sea Carousel. Notice the offset in the two sensors (OBS 1 and 3) located inside the annulus. This is presumed to be due to backscattering off the far wall of the annulus.

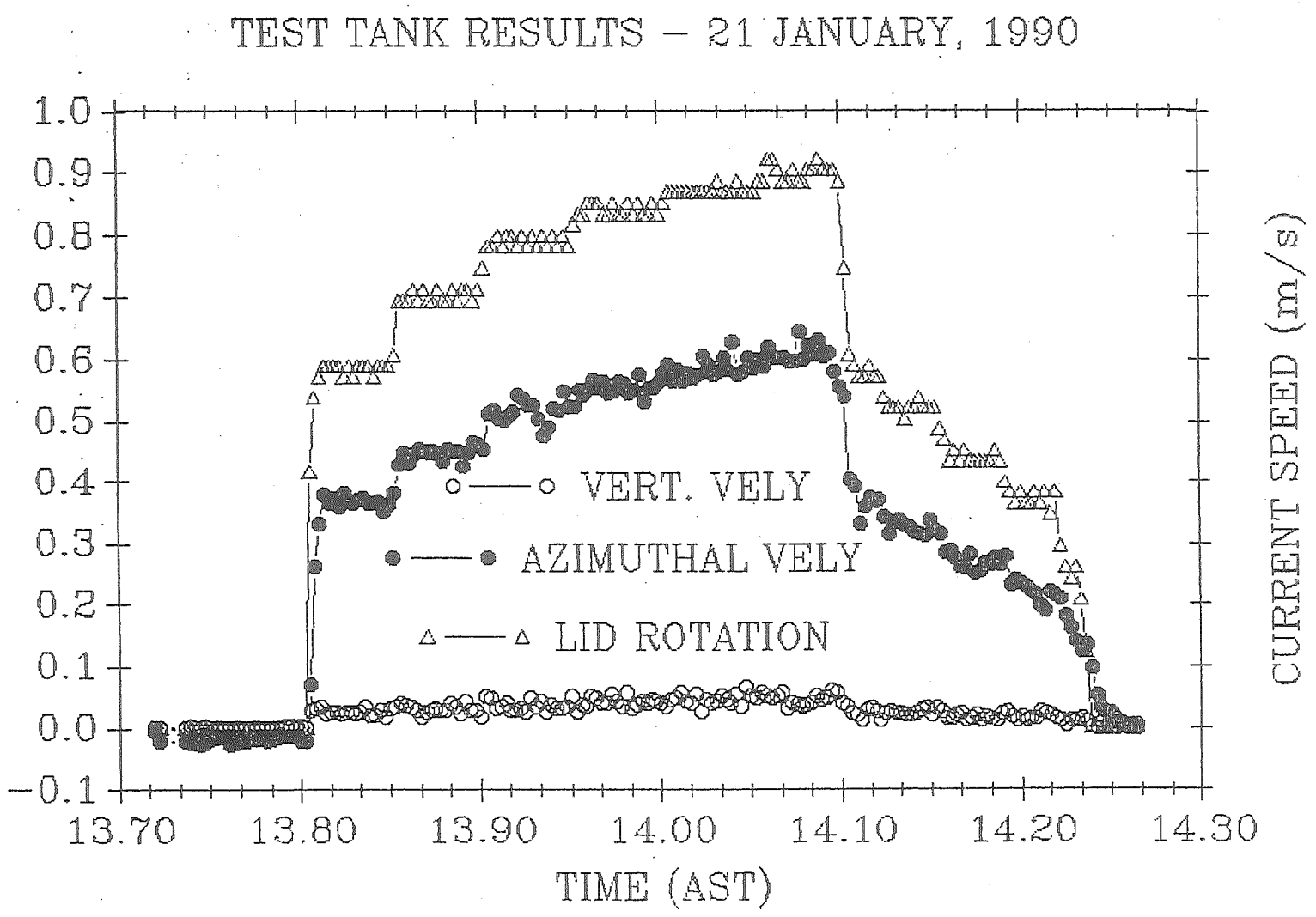

Figure 3.49. A time-series of lid rotation, azimuthal flow and vertical flow during a test of Sea Carousel. The data have been time-averaged over ten seconds and despiked at ± 2 standard deviations. In most experiments lid rotation was increased and subsequently decreased in a series of steps.

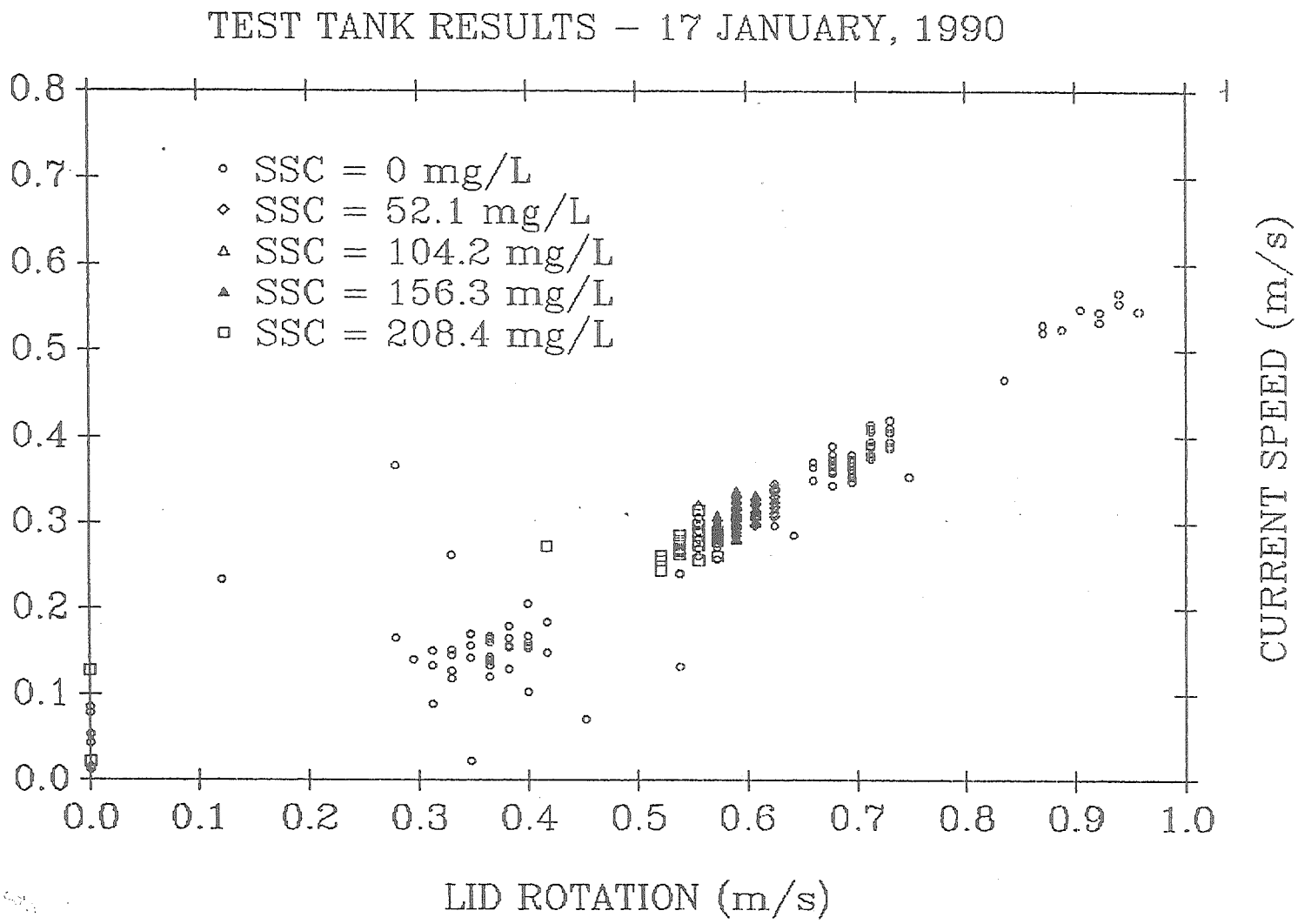

Figure 3.50A. A scattergram of lid rotation versus azimuthal current speed for a range of sediment concentrations ($0 < S < 208$ mg.L^{-1}; salinity = 0.16 ‰). There is a strong relationship between the two variables irrespective of S. The scatter at low rotation and the zero-flow offset of the E.M. flow meter are evident.

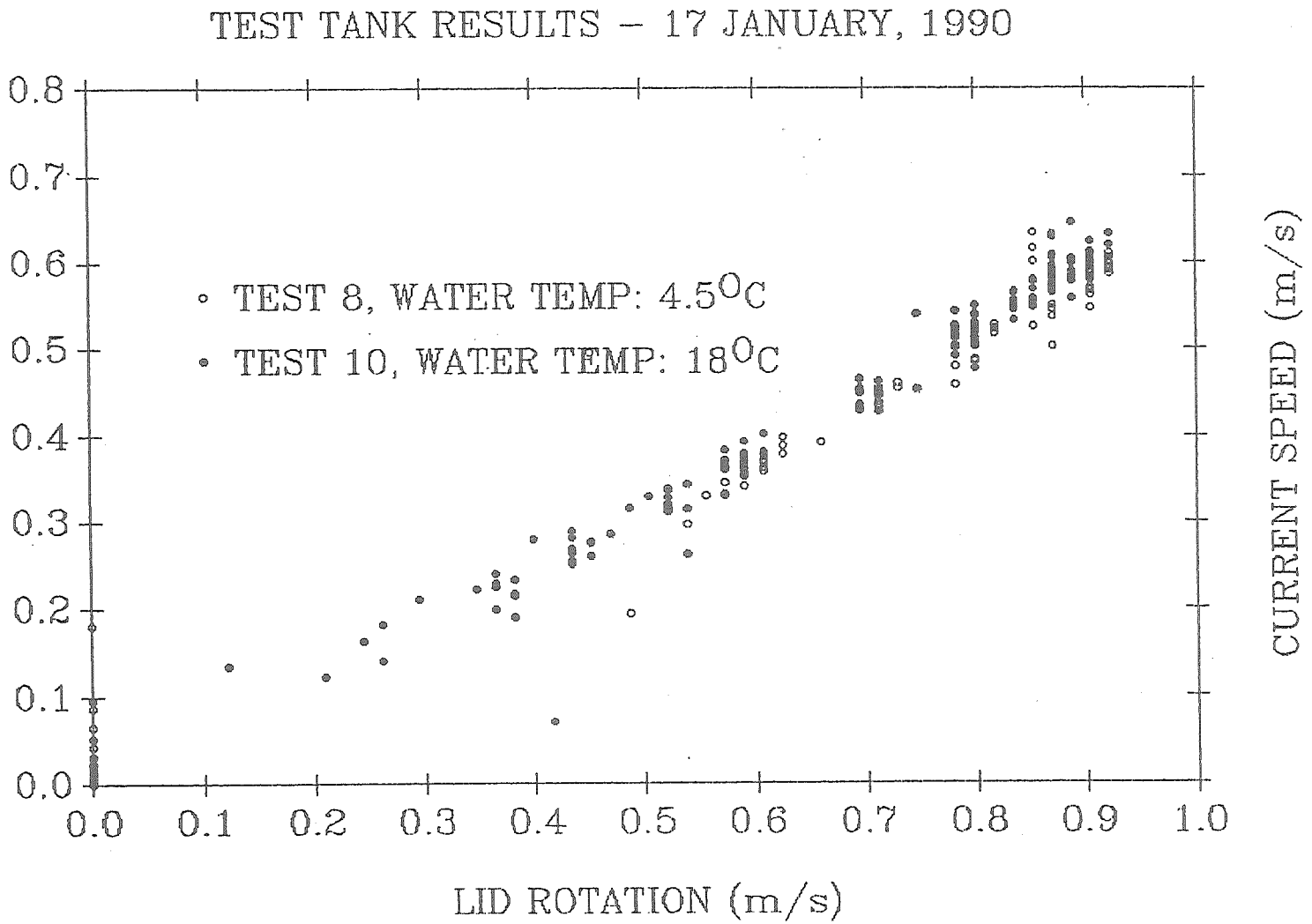

3.50B.A scattergram of lid rotation versus azimuthal current speed for two water temperatures (4.5° and 18°C; salinity = 34 ‰). Water temperature has little effect on the relationship of the two variables.

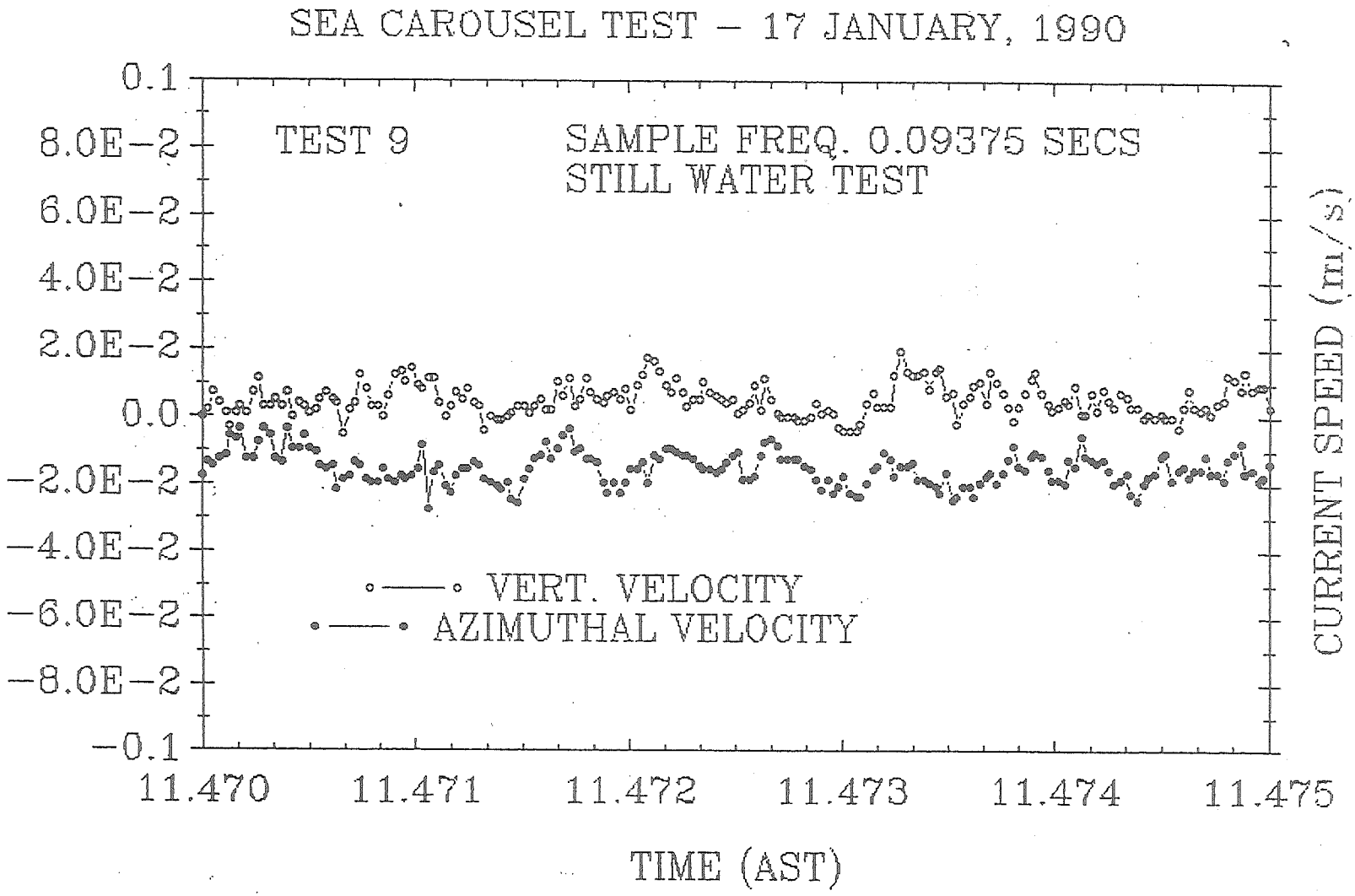

Figure 3.51. A time-series of unfiltered measurements of azimuthal and vertical flows during a "still-water" test (water temperature = 4.5°C; salinity = 34 ‰). The currents were sampled at 10.66 Hz. Note the time-variability of both currents of an approximate amplitude of ± 0.01 $m.s^{-1}$, and the offset of the azimuthal current. Offset is corrected by a still water test in advance of each experiment.

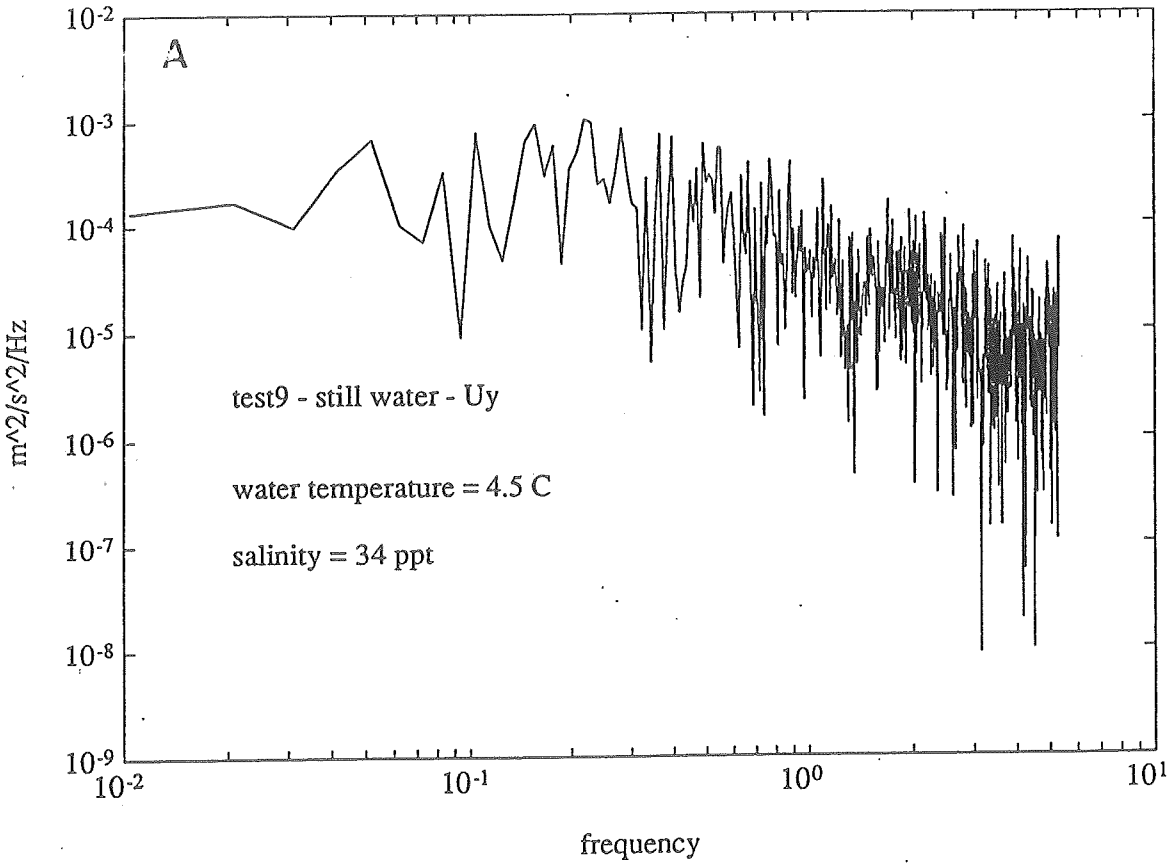

Figure 3.52A. The log spectral density from the fast Fourier transform of the raw record of azimuthal flow illustrated in Figure 6 plotted against log frequency. Notice the relatively flat spectrum in the macroturbulent range and the energy dissipation in the microturbulent range.

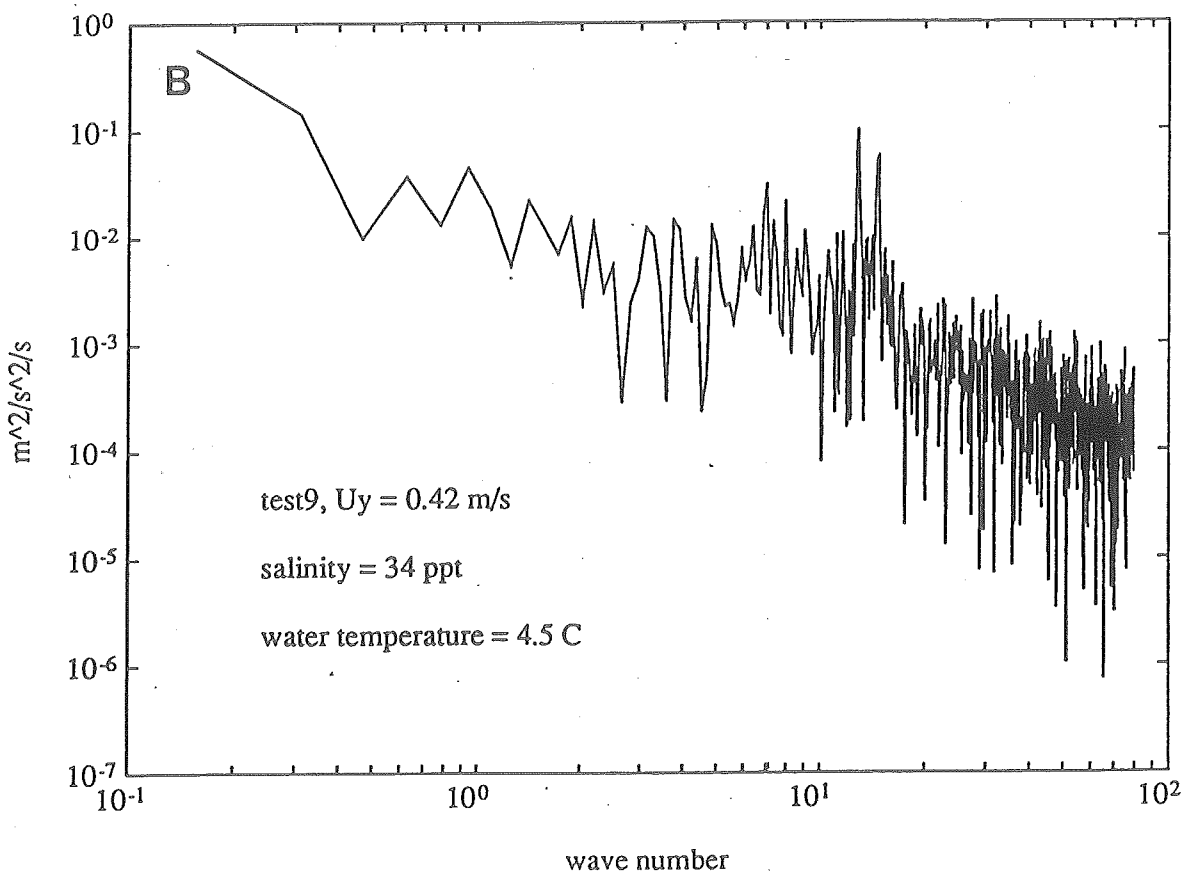

Figure 3.52B. The log spectral density from the fast Fourier transform of azimuthal flow illustrated between 11.55 and 11.56 AST of Figure 8A (Uy = 0.42 $m.s^{-1}$) plotted against log wave number. Spectral energy drops with increasing frequency with a slope of -5/3. A peak in the spectrum at k = 14 is correlated with paddle rotation. A peak at k = 7 is interpreted as lid eccentricity.

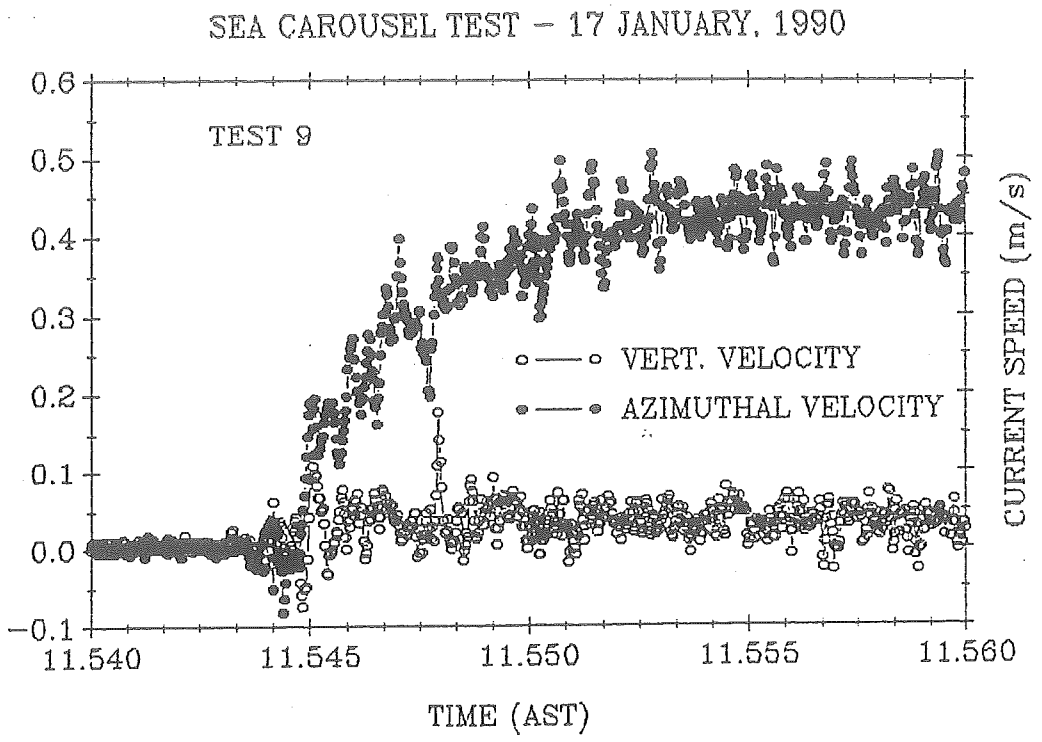

Figure 3.53A. A time-series of unfiltered measurements of azimuthal and vertical flows during acceleration from still water (water temperature = 4.5°C; salinity = 34 ‰). Analysis of signal variance over 20 second increments shows no relationship with flow acceleration or deceleration.

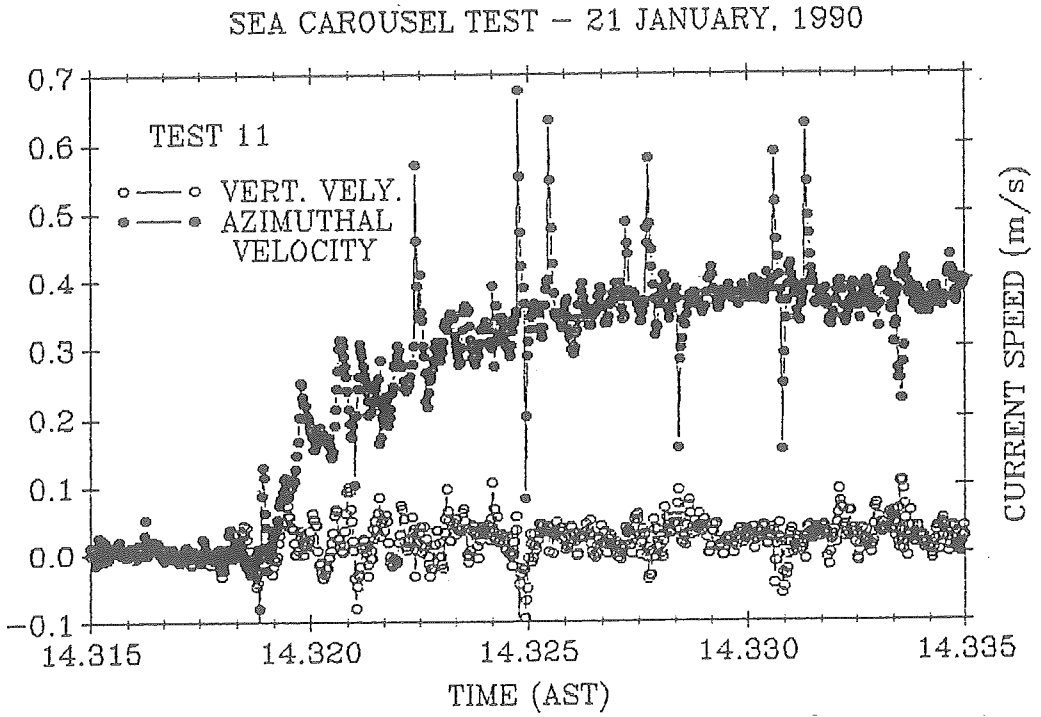

Figure 3.53B. A time-series of unfiltered measurements of azimuthal and vertical flows during acceleration from still water (water temperature = 18.0°C; salinity = 34 ‰). Notice the low frequency instabilities during flow acceleration to 0.4 $m.s^{-1}$ and the propagation of high amplitude turbulent fluctuations that appear coherent in the velocity measures. At these temperatures, changes in flow rate should be restricted to ± 0.1 $m.s^{-1}$ to minimize generation of flow instabilities.

of energy (West et al. 1986). The paddle wave number for an azimuthal current speed of 0.42 $m.s^{-1}$ is 14. Notice that there is a narrow peak in the energy density at this frequency. This indicates that the paddles generate measurable turbulence, but not at frequencies where viscous dissipation takes place. A second peak in the spectrum at k = 7 corresponds to 1/2 the frequency of paddle passage and may be related to eccentricity of lid rotation. The majority of the energy of the flow is found at wave numbers less than 10, i.e., within macroturbulent events. These events are controlled by the geometry of the flume and by time variations in paddle rotation. The illustrated spectrum was consistent for all water salinities and temperatures tested.

The measurements of friction velocity with time revealed significant variance even at constant flows. This may be related to turbulent eddies generated by paddle rotation. Figure 3.54 shows results recorded .05 m from the outer wall at four different values of $\overline{U}_y$. There is considerable overlap in friction velocity for different flow rates indicating a non-steady bed stress. The mean deviation in friction velocity (0.1 to 2.0%) shows no relationship to its mean value. However, the time-averaged friction velocity yielded stable results that illustrated a variation in bed stress radially across the annulus. Figure 3.55 illustrates measurements of time-averaged friction velocity across the annulus for four differing values of $\overline{U}_y$. Notice that the cross-channel gradient in friction velocity increases with azimuthal current speed. This gradient (expressed as standard error bars in Figure 3.56) is linearly related to $\overline{U}_y$ and goes to zero at $\overline{U}_y = 0.32$ $m.s^{-1}$. Below this value, the friction velocity is considered to be constant across the floor of the flume. The root-mean-square value of the time-averaged, cross channel friction velocity ($\overline{U}_*$ rms) is used as the standard hydrodynamic measure in this study above a $\overline{U}_y = 0.32$ $m.s^{-1}$. The strong relationship of $\overline{U}_*$ rms to $\overline{U}_y$ is shown in Figure 3.56 and is in the form :

$$\overline{U}_* \text{ rms} = 0.0167 + 0.097\,\overline{U}_y \ (m.s^{-1};\ r = 0.98) \qquad (12)$$

By manipulation of the quadratic stress law (equation 17), a drag coefficient (C_d) relating $\overline{U}_y$ and $\overline{U}_*$ is derived :

$$\overline{U}^* = \sqrt{\tau/\rho} \qquad (13)$$

and :

$$\tau = C_d \rho \overline{U}_y 2 \qquad (14)$$

This results in a value of $C_d = 4.0 \times 10^{-2}$ and a corresponding $C_d 100$ of 1.3×10^{-3}. This latter coefficient, according to Sternberg (1972), falls within the limits detected over flat bed in his field observations.

The relationship $[(\overline{U}_r - \overline{U}_y)/\overline{U}_*]$ seen in equation 7 was not constant, but resulted in a value f which increased systematically with $\overline{U}_y$ from 6.88 to 7.81. A mean value for f of 7.21 (±0.43) may be used to construct a velocity profile in the outer layer. Solving $\overline{U}_y$ at the top of the inner buffer layer (y = 20 mm) yields unrealistically low values (0.036 to 0.04 $m.s^{-1}$) in equation 7. This indicates that the azimuthal velocity-defect in Sea Carousel ($\overline{U}_r - \overline{U}_y$) is unusually large and cannot be used to define the velocity gradient. Burt (1984) shows measurements of

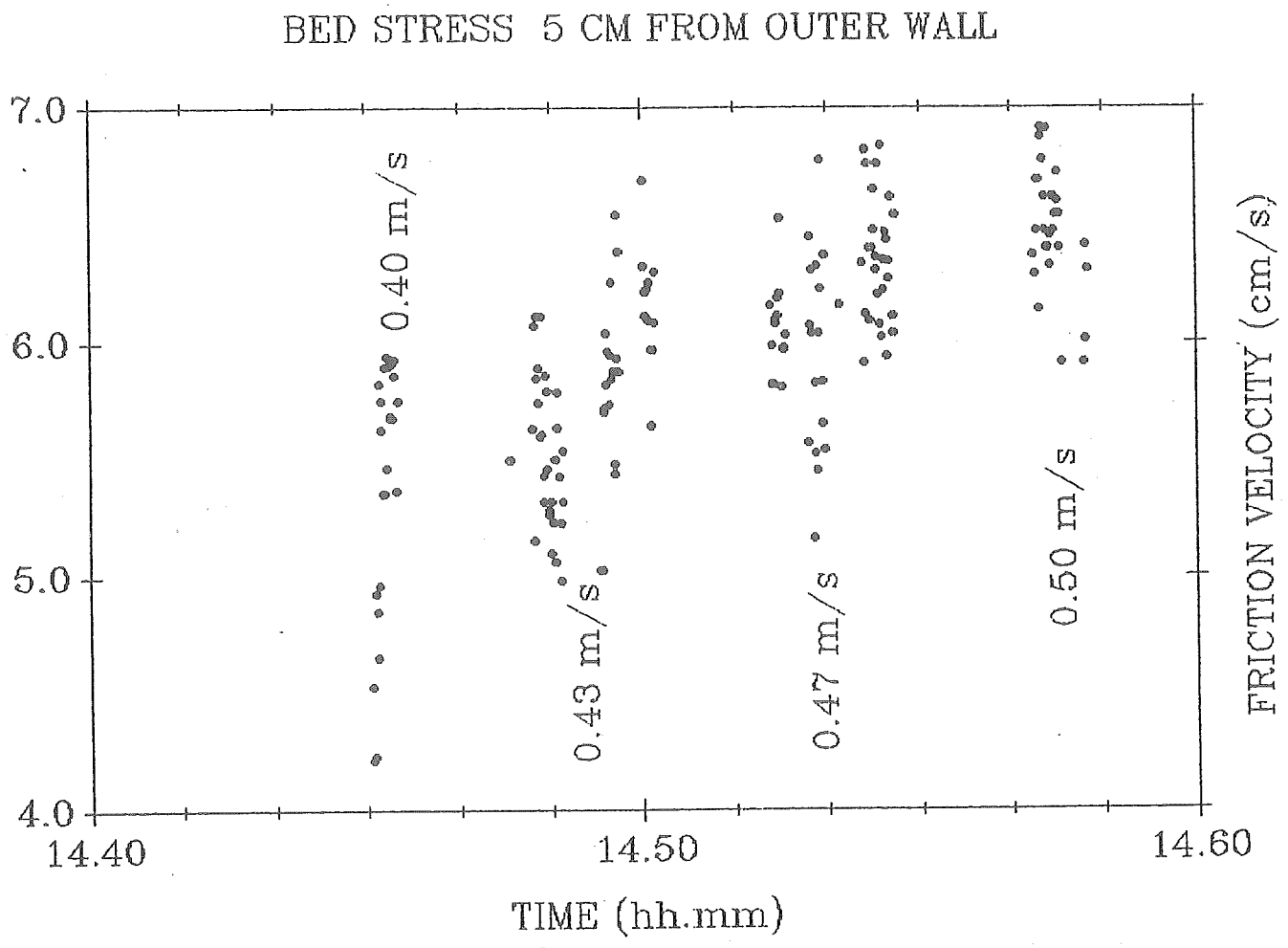

Figure 3.54. A scattergram of total (azimuthal and radial) friction velocity measured at 1 Hz using the bottom-mounted hot-film sensor of Gust (1988). The figure shows results recorded at four different azimuthal velocities ($0.40 < U_y < 0.50$ m.s^{-1}). Flow in each case was allowed to stabilize for 60 seconds before recording. Notice the time-variability in friction velocity ($\pm$ 0.005 m.s^{-1}).

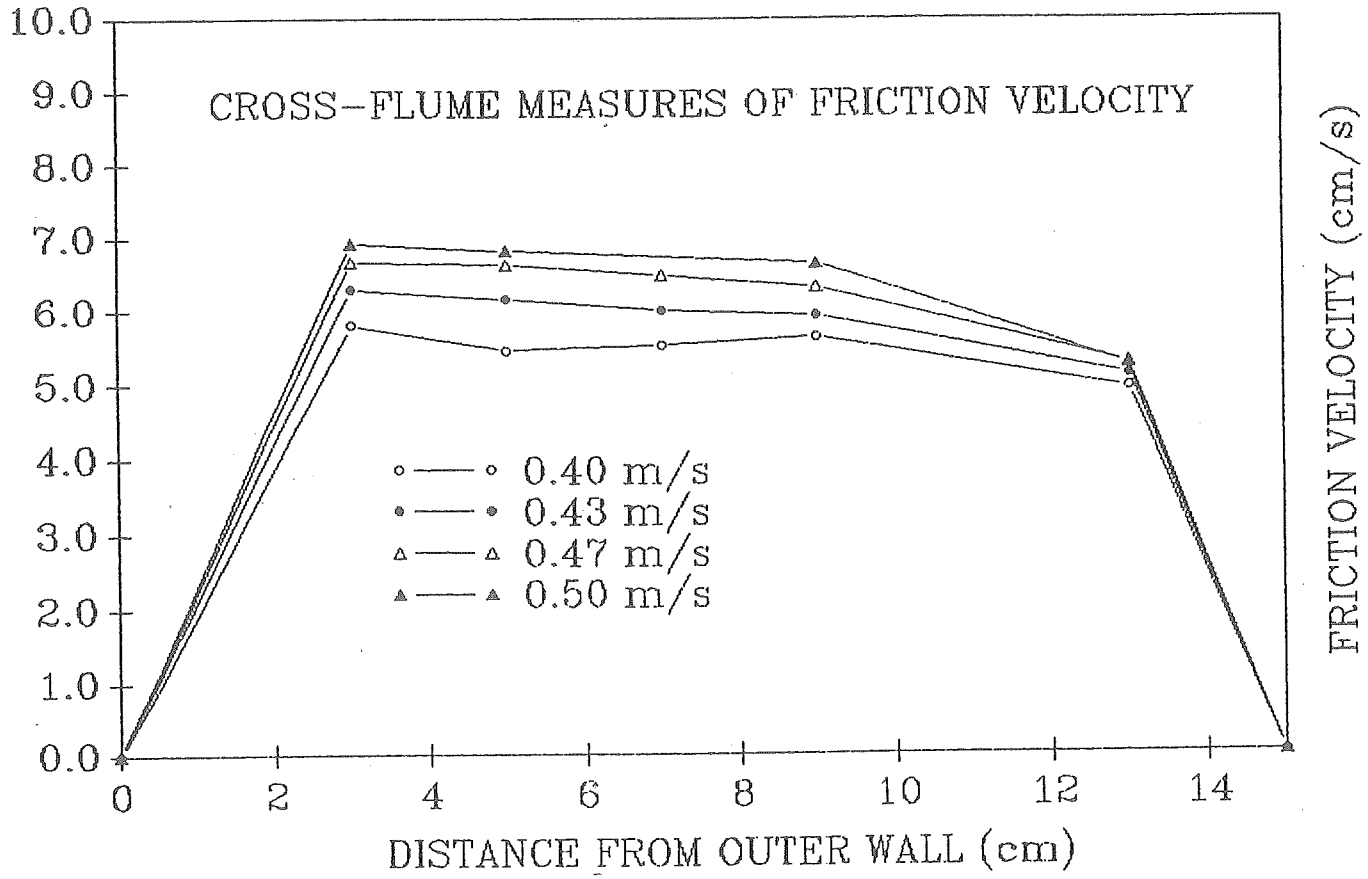

Figure 3.55. Cross-flume measurements of total friction velocity at four levels of azimuthal flow. Notice the systematic radial increase which appears to be linear with radius. The radial increase is strongly correlated with azimuthal velocity and goes to zero for $U_y < 0.32$ m.s^{-1}.

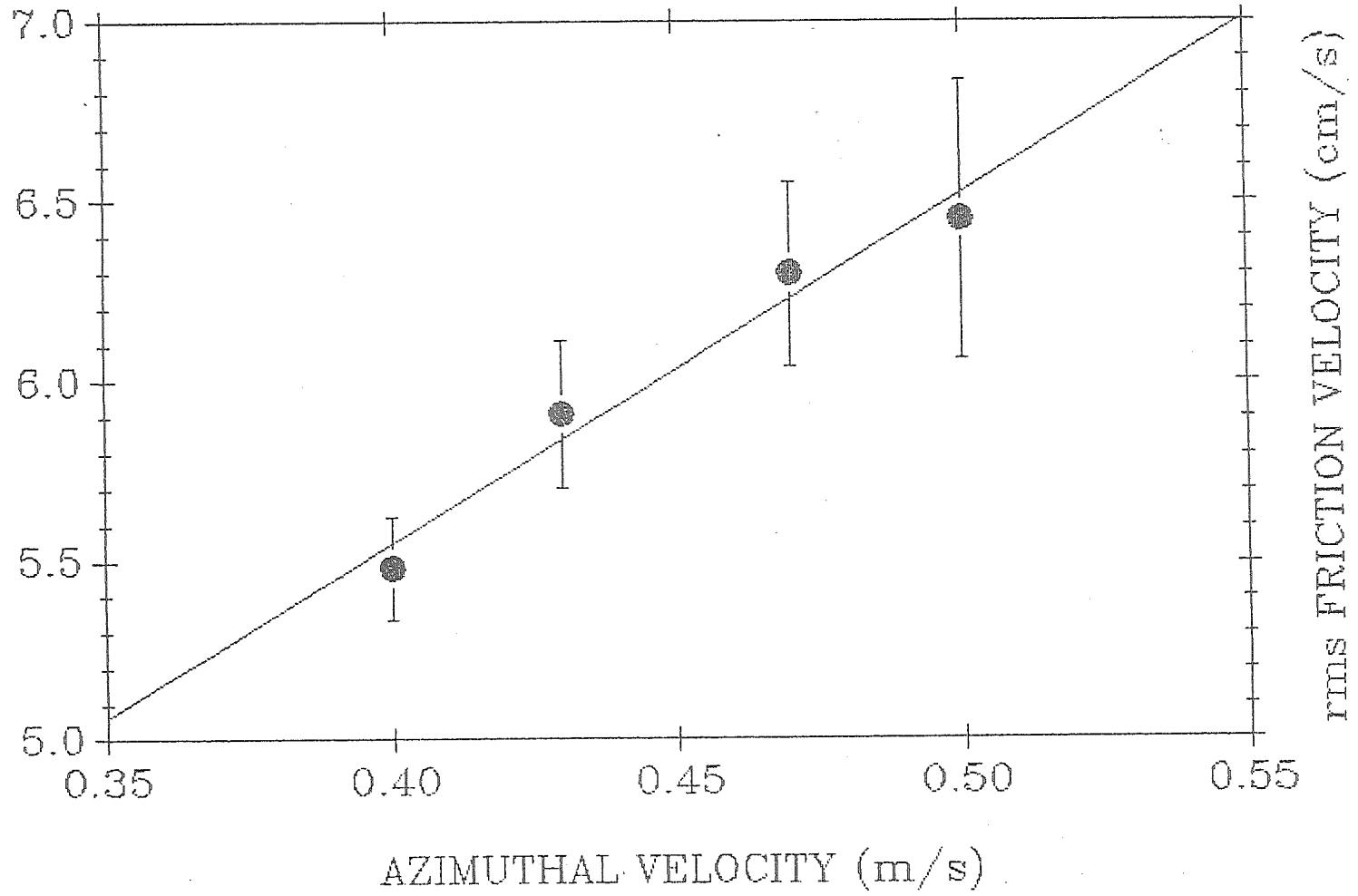

Figure 3.56. A plot of the rms value of total friction velocity for the four azimuthal flows shown in Figure 3.55. The standard errors of these values are also shown and are a measure of the radial change in friction velocity. Notice the decrease in standard error with azimuthal velocity.

velocity in an annular flume which demonstrate a near constant net flow with depth through the outer layer due, in part, to radial circulations. We anticipate the existence of strong radial component to $\overline{U}_y$ in Sea Carousel that was not measured in this study.

The effects of suspended sediment concentration on the time-averaged friction velocity near the centre of the annulus were evaluated at a constant $\overline{U}_y$ (0.43 $m.s^{-1}$). Sensor drift during the experiment was eliminated by a still-water test before and after the experiment. Results of tests at five differing concentrations (in $mg.L^{-1}$) are illustrated in Figure 3.57. A clear decrease in friction velocity was detected over the concentration range following the exponential form :

$$\overline{U}_*(S) = \overline{U}_*(0) \times 10^{[-1.76E-4(S)]} \qquad (r = 0.91) \qquad (15)$$

The friction velocity derived from equation 15 is for clear seawater and is corrected for suspended sediment concentration using equation 18.

Dispersion of suspended sediment out of the rotating annulus was observed to take place during submerged deployments of Sea Carousel. Dispersion results from exchanges of water mass between the annulus (at concentration S_1) and the open marine environment (at concentration S_o) where $S1 \neq So$. The rate of diffusion of mass (M) may be defined per unit cross-section area as :

$$\partial M/\partial t = - \delta \, \partial S/\partial x \qquad (16)$$

where δ is the coefficient of diffusivity (L^2T^{-1}) and x is a typical horizontal length scale, which in our case is unknown. Similarly, the change in mass in Sea Carousel may be defined as :

$$\partial M/\partial t = - \delta \, \partial S/\partial x \, \varepsilon/V \qquad (17)$$

where A is the area over which diffusion takes place (0.012 m^2), V is the volume of Sea Carousel (0.218 m^3), and ε is an efficiency term dependent on the azimuthal velocity ($\varepsilon \propto Uy$). Measurements of $\partial M/\partial t$ at different constant azimuthal velocities yield a concentration half-life ($S_{1/2}$) of 2400 seconds and setting $\varepsilon = \overline{U}_y$ the quotient ($- \partial A/\partial x$) is derived :

$$\partial M = - 3.3 \times 10^{-3}(S_1 - S_o) \, \varepsilon \, \partial t \qquad (18)$$

The loss of mass through dispersion, calculated using equation 18, is added to measured annulus mass (SV) to derive a measure of the total mass.

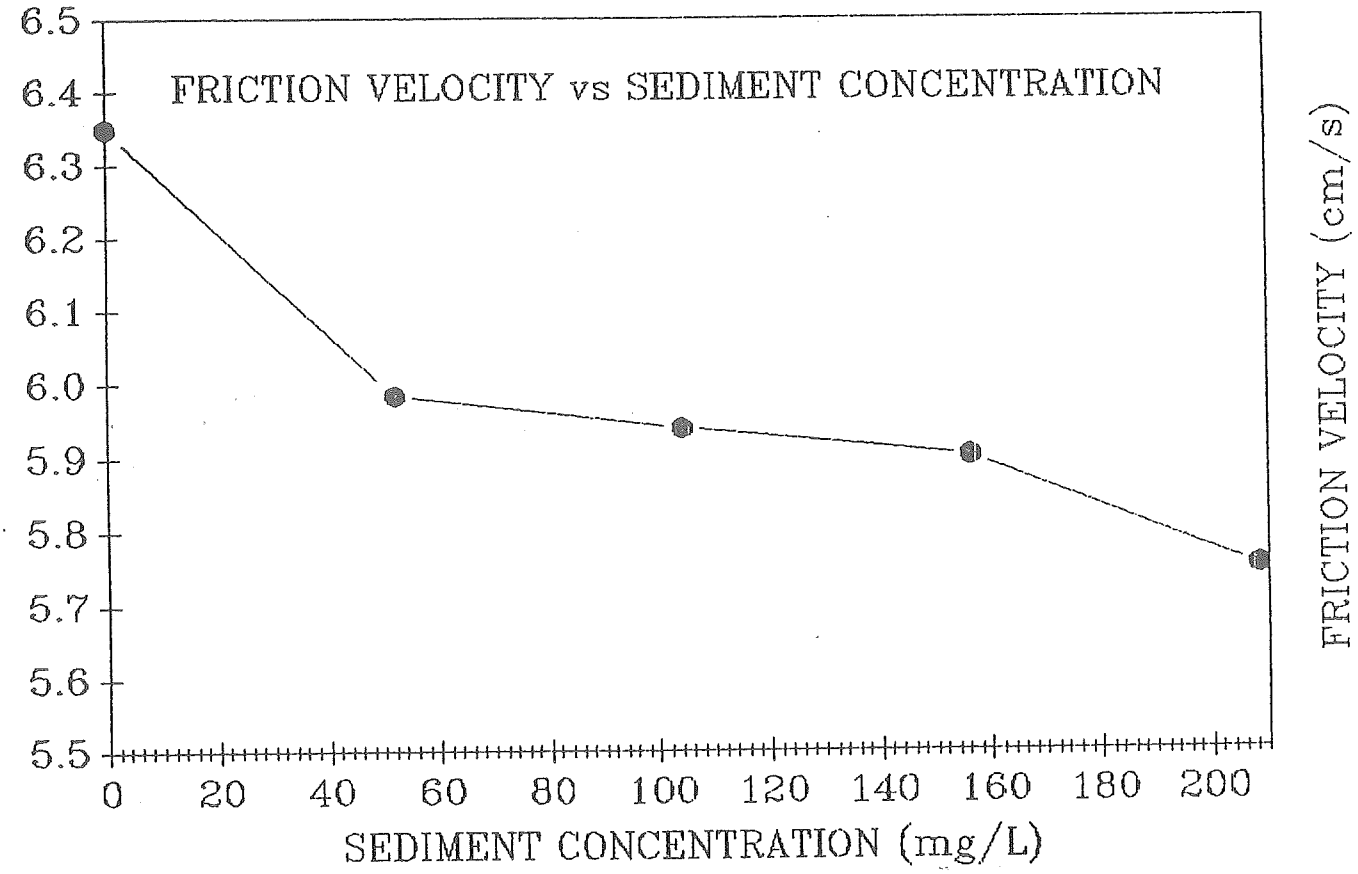

Figure 3.57. A plot of the measured total friction velocity at a constant azimuthal flow of 0.48 $m.s^{-1}$ and for five different suspended sediment concentrations. Notice the significant decrease in U_* with S particularly for the range $0 < S < 50$ $mg.L^{-1}$.

Field Calibration

The Sea Carousel has been deployed in both submerged and subaerial (intertidal) settings (see Table 3.10). In subaerial cases, the flume was deployed in 0.5 m of water on an ebbing tide. Experiments were started once the tide had exposed the annulus leaving a portion of the ebbing tidal water trapped within the annulus. In submerged cases, experiments were carried out from a moored boat, with the flume being deployed from the boat. The results for two experiments are discussed in detail : one from a subaerial deployment on an intertidal mudflat in Bay of Fundy and the second from a submerged deployment over a mudflat in the same estuary. In the first case, a 1.6 hour experiment was carried out, during which time erosion and subsequent deposition of bottom sediment were detected. Azimuthal current speed was accelerated in three steps from 0.3 to 0.9 $m.s^{-1}$ and subsequently decelerated in three steps to still water between 17.5 and 19.1 AST (Fig. 3.58A). The measured changes in suspended sediment concentration (from the three OBS's) in the flume are illustrated in Figure 3.58B. A rapid and dramatic increase in S was detected at the initial increase in current (17.65 AST). The increase in S was asymptotic with time and exhibited the character of "Type I" , "aggregate-by-aggregate", or "surface" erosion (Mehta and Partheniades 1979; Mehta et al. 1982). Subsequent increases in lid rotation were paralleled by increases in S to a limit of 3500 $mg.L^{-1}$ at a lid rotation of 1.4 $m.s^{-1}$, whereupon aeration of the annulus and water losses resulted from centrifugal effects. The water column of the annulus was well mixed below 2000 $mg.L^{-1}$ but showed sediment stratification above this value (OBS3, Fig. 3.58B). The three decreases in current velocity led in each case to an exponentially-decreasing S to equilibrium values (S1(OBS2) = 2200 $mg.L^{-1}$, S2(OBS2) = 1400 $mg.L^{-1}$ and still water S = 0 $mg.L^{-1}$).

The rate of change of S with time is illustrated in Figure 3.58C in terms of an erosion rate. The peak at 17.65 AST is evident and has a value of $5.0E^{-3}$ $kg.m^{-2}.s^{-1}$. This peak occurs within 30 seconds of the onset of the current acceleration and decreases with time in an exponentially-decaying fashion to an approximate value of $1E^{-4}$ $kg.m^{-2}.s^{-1}$. Settling during annulus aeration shows a high degree of scatter (S1). By contrast, subsequent settling increases to a maximum within 2 minutes of reduction of current velocity to a maximum of $2.5E^{-3}$ $kg.m^{-2}.s^{-1}$. Note that the short-time-variability in S appears less during periods of deposition than during periods of erosion.

The mass eroded from the bed during the course of the experiment was 0.7 kg. This corresponds to a mean depth of bed erosion of 0.4 mm (Fig. 3.58D; sediment mass was converted to volume using a sediment bulk density courtesy of H. Christian - unpublished data, 1989). The termination of the deployment (19.1 AST) at a predicted eroded mass and depth of erosion of zero for S $\approx$ 0 $mg.L^{-1}$ indicates conservation of mass in the computational procedure.

A 1.8-hour submerged deployment of Sea Carousel took place on an intertidal mudflat in Minas Basin on 16 July 1989. The velocity time series of the deployment is shown in Figure 3.59A. Lid rotation was increased in 9 steps of equal power output. Associated increases in azimuthal and vertical (downward-directed) velocity are apparent. The time-series of S (corrected for diffusion) is shown in Figure 3.59B (all three OBS's were used in the annulus). Note that erosion appears to take place at all velocities and that both Type I and Type II (the latter termed "mass erosion" by Mehta and Partheniades 1982) are evident. There is no clear evidence of

Table 3.10. Sea Carousel deployments

Date	Time (AST)	Location
8 May, 89	1724-1845	Oak I. Marsh, Annapolis Basin
10 May, 89	0842-0910	Thorne Cave, Annapolis Basin
12 May, 89	0954-1200	Queen Anne Marsh, Annapolis Basin
15 July, 89	0755-1115	ST. 1, Minas Basin
16 July, 89	1035-1355	ST. 3, Minas Basin
17 July, 89	0927-1220	ST. 2, Minas Basin
19 July, 89	1053-1538	ST. 2, Minas Basin
20 July, 89	1113-1552	ST. 3, Minas Basin
21 July, 89	1213-1600	ST. 2, Minas Basin
22 July, 89	1325-1650	ST. 1, Minas Basin
23 July, 89	1404-1615	ST. 2, Minas Basin
24 July, 89	1455-1731	ST. 3, Minas Basin
25 July, 89	1814-2018	ST. 2, Minas Basin
26 July, 89	0628-0832	ST. 1, Minas Basin
27 July, 89	0703-0949	ST. 2, Minas Basin
27 July, 89	1731-1656	Poison Site, Minas Basin
30 July, 89	1210-1300	ST. 1, Minas Basin
31 July, 89	0910-1150	ST. 2, Minas Basin
1 Aug, 89	1000-1240	ST. 2, Minas Basin
2 Aug, 89	1042-1228	ST. 2, Minas Basin

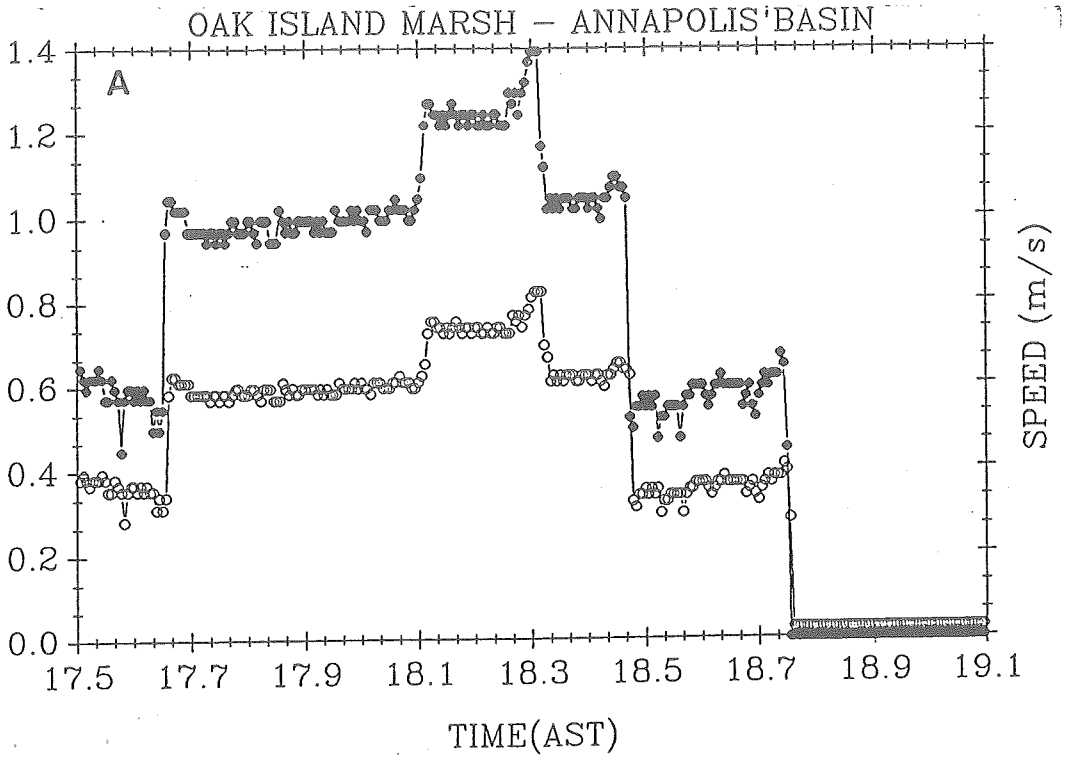

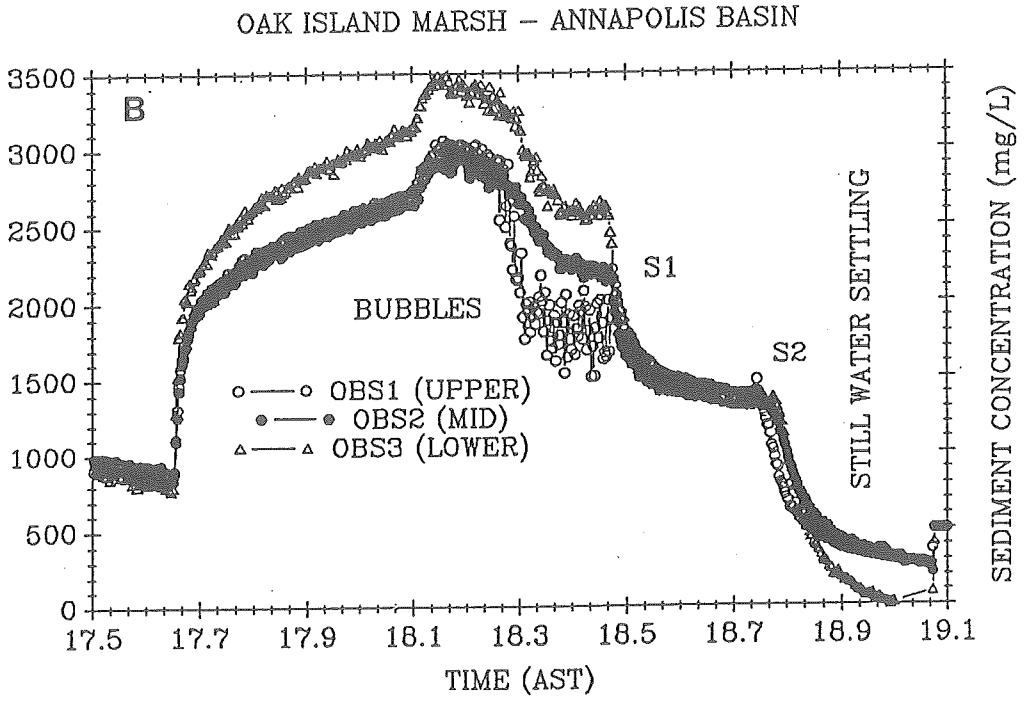

Figure 3.58. A time-series of Sea Carousel measurements made during an intertidal, subaerial deployment on a mudflat in the Bay of Fundy during a 1.6 hour experiment. (A). Measured lid rotation and predicted azimuthal current. (B). Suspended sediment concentration indicated by the upper (OBS1) mid (OBS2) and lower (OBS3) Optical Backscatter Sensors. S1 and S2 are equilibrium concentrations for U_y of 0.6 and 0.4 $m.s^{-1}$ respectively.

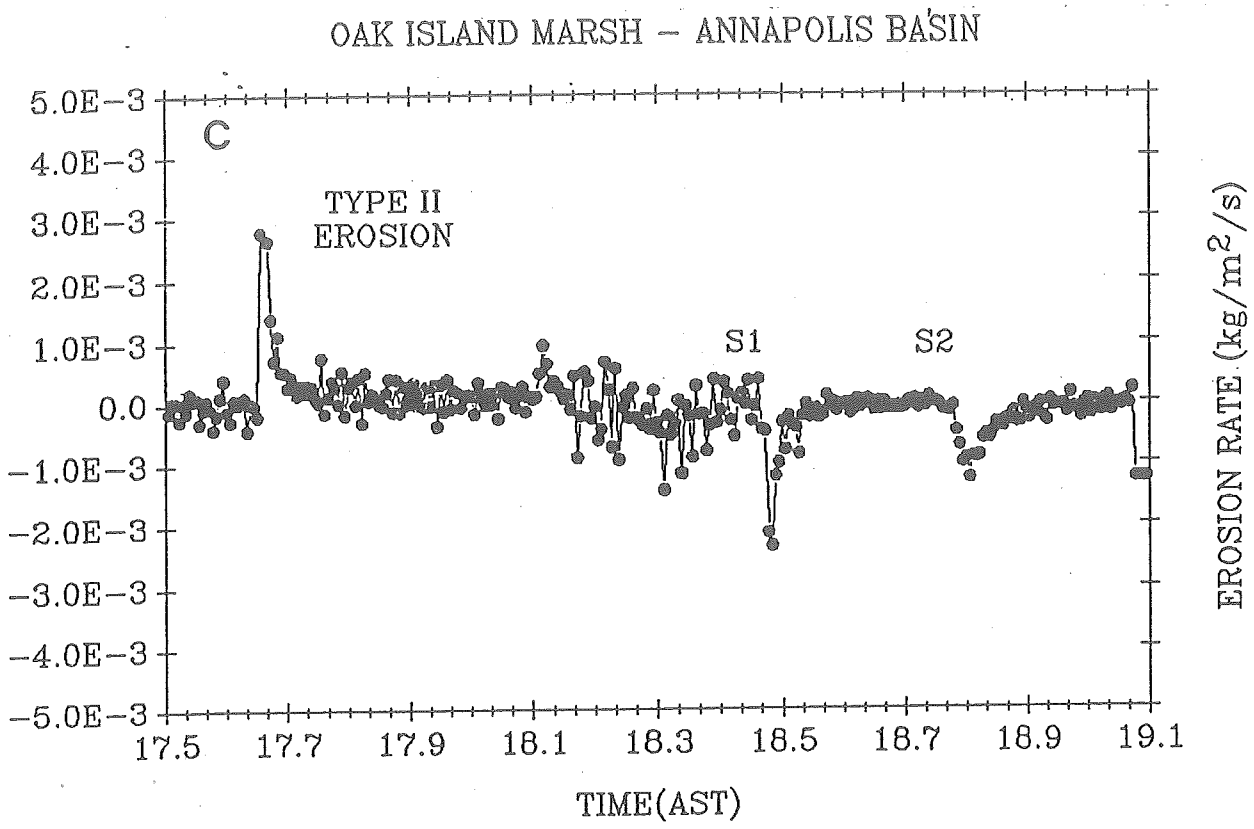

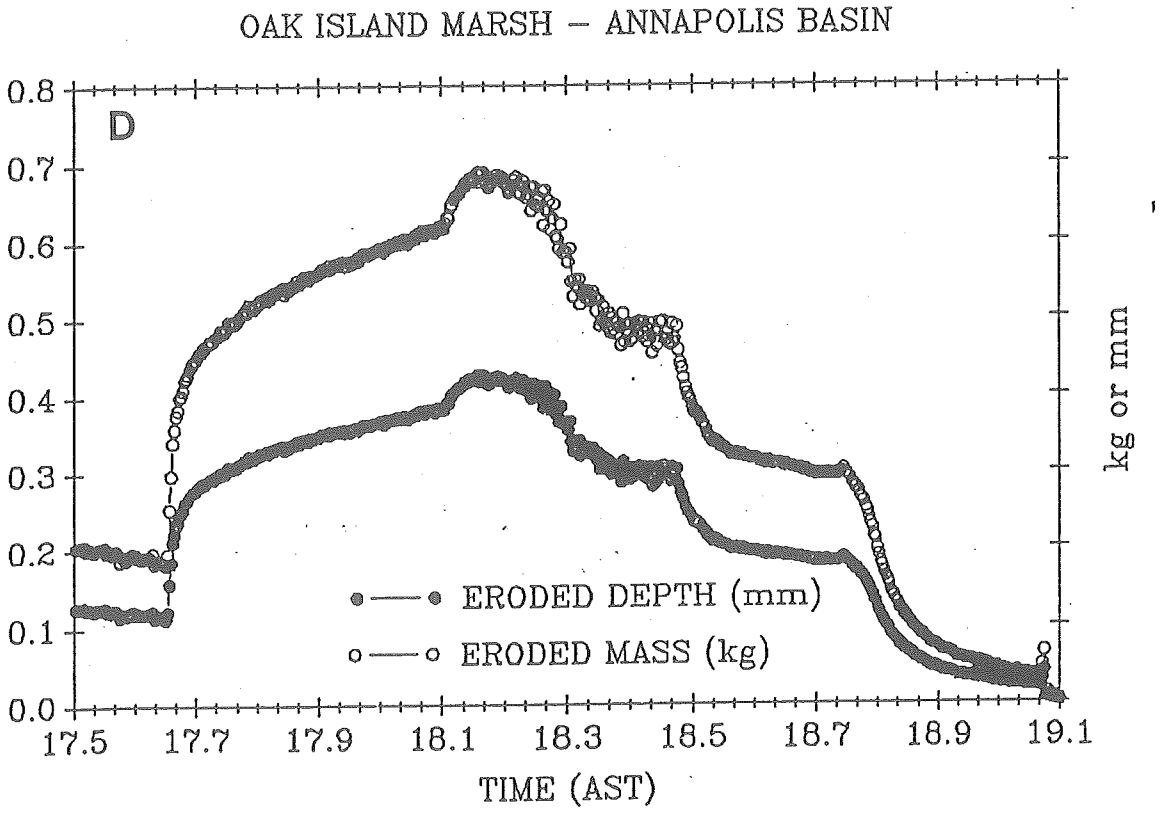

Figure 3.58 Cont. (C). Erosion/deposition rate calculated from the rate of change in S ($\Delta S/\Delta t$). (D). Eroded depth and eroded mass calculated from depth-integration of sediment concentration.

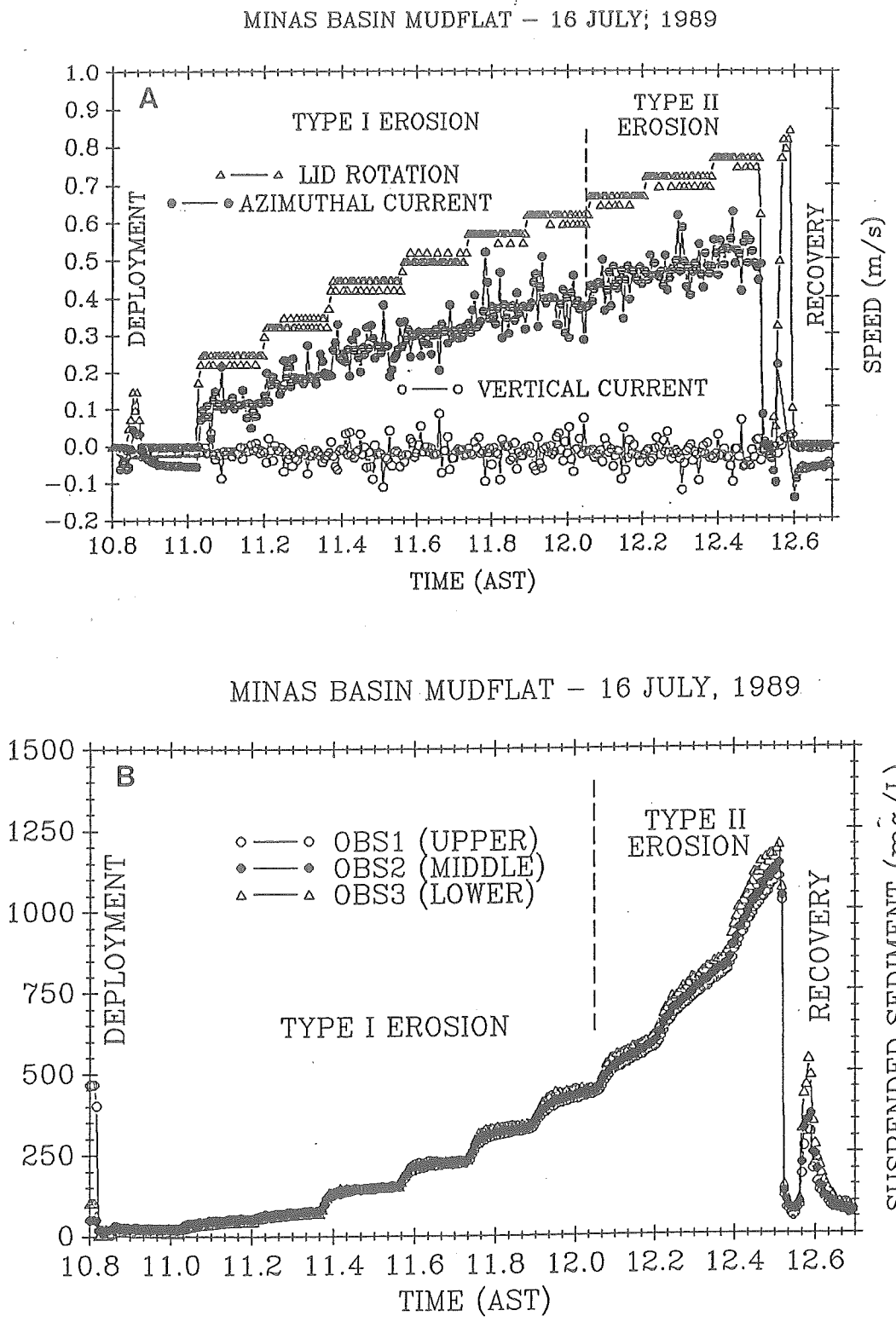

Figure 3.59. A time-series of Sea Carousel measurements made during an intertidal, submarine deployment on a mudflat in the Bay of Fundy during a 1.8 hour experiment. (A). Measured lid rotation, azimuthal current and vertical current in nine increments of increasing lid rotation. (B). Corrected suspended sediment concentration measured by the three OBS's. Notice that stratification is becoming evident under Type II erosion.

stratification in S until 12.4 AST whereupon an increase with depth became apparent. Type I erosion typifies flows where $U_y < 0.45$ m.s^{-1}; Type II erosion prevails at stronger flows. Bed erosion is more clearly demonstrated by reference to Figure 3.59C. Here, a rapid peaking in erosion rate within 30 seconds of flow acceleration is evident in the 7 highest of the 9 flow accelerations. Type I peak erosion rate is approximately 2.0E^{-4} kg.m^{-2}.s^{-1} and does not appear correlated with azimuthal velocity. Also the rate of erosion drops quickly back towards zero in an exponentially decaying fashion. Type II peak erosion rate shows an increase with $\overline{U}_y$. This peak is less clearly developed and drops back towards a constant erosion rate that also increases with $\overline{U}_y$. The scatter of the background signal of Type II erosion is significantly greater than for Type I erosion (Fig. 3.59C).

The observed trends in S for the two presented field experiments follow closely trends observed in the laboratory (Owen 1977; Lee et al. 1981; Kusuda and Umita 1982; Mehta and Partheniades 1982; Thorn and Parsons 1980). Type I erosion is clearly evident in Figure 3.58B during flow acceleration together with subsequent exponentially-decaying settling rates during decelerating phases. Peak erosion rate is 2.9 x 10^{-3} kg.m^{-2}.s^{-1}. It occurs within 20 seconds of flow acceleration and lasts for less than 40 seconds (Fig. 3.58C). This rate is within the range of 0.5 to 5.0 x 10^{-3}kg.m^{-2}.s^{-1} reported by Ariathurai and Arulanandan (1978) from laboratory experiments in an annular flume.

The equilibrium concentrations (S1 and S2; Fig. 3.58B) are linearly related to azimuthal velocity by the expression $S = 4.16 \times 103(\overline{U}_y)$. Deposition rate is observed to be time variable, maximizing within 1 minute of velocity reduction to 2.0 x 10^{-3} kg.m^{-2}.s^{-1}. Equilibrium conditions were reached within 4 minutes of flow deceleration. Still water deposition rate peaked at 1.4 x 10^{-3}kg.m^{-2}.s^{-1} and also dropped off exponentially with time.

Type I and Type II erosion are apparent in our second field example (Fig. 3.59B). Insofar as our sediments are naturally deposited, the observed trends cannot be artifacts of bed preparation in the laboratory. Peak erosion rates for Type I erosion vary between 1.5 and 2.5 x 10^{-4}kg.m^{-2}.s^{-1}. These values are similar to the erosion rate of 3.3 x 10^{-4} kg.m^{-2}.s^{-1}reported by Kusuda and Umita (1982). Remember that actual values of S in our test were decreasing through time due to dispersion yet this trend appears to have no effect on E. Our observations, therefore, support the proposal of Mehta and Partheniades (1982) that there is a physical difference in the erosion process between Type I and Type II erosion that is independent of S. This conclusion is also evident in the difference between the scatter of the Type I and Type II time-series of erosion rate shown in Figure 3.59C. Notice that Type I erosion shows the characteristics of rapid initial erosion rate followed by an exponential decay to zero, as predicted by Sheng and Villaret (1989). We conclude, therefore, that Type I erosion results from aggregate-by-aggregate surface erosion that takes place in an ordered fashion. By contrast, Type II erosion we agree, results from mass wasting of the bed that takes place in quantum releases of bed material. This process is termed "slacking" by Partheniades and Paaswell (1970) and "flacking" by Lee et al. (1981). The observed scatter in erosion rate cannot be explained in terms of long-time variability of bed stress, which appears to be less under Type II than under Type I erosion (Fig. 3.59D). The observed radial increase in bed stress may in part explain, however, the presence of Type II erosion observed at high flows.

Erosion resistance of Minas Basin sediment is plotted against depth in Figure 3.60. As can be seen, there

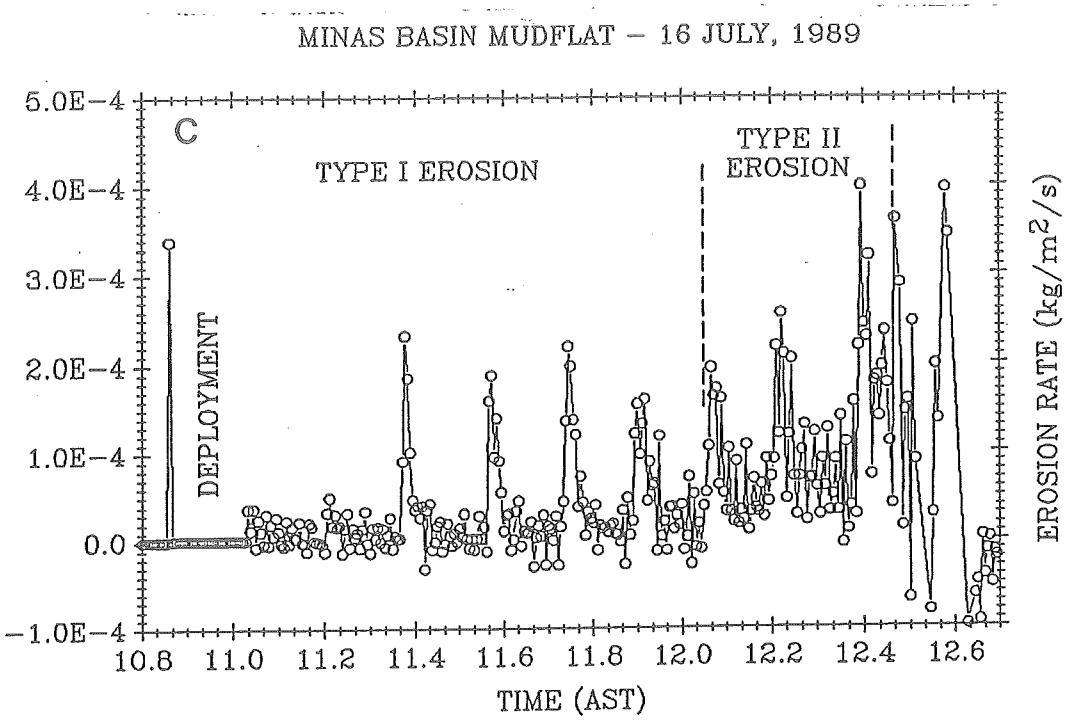

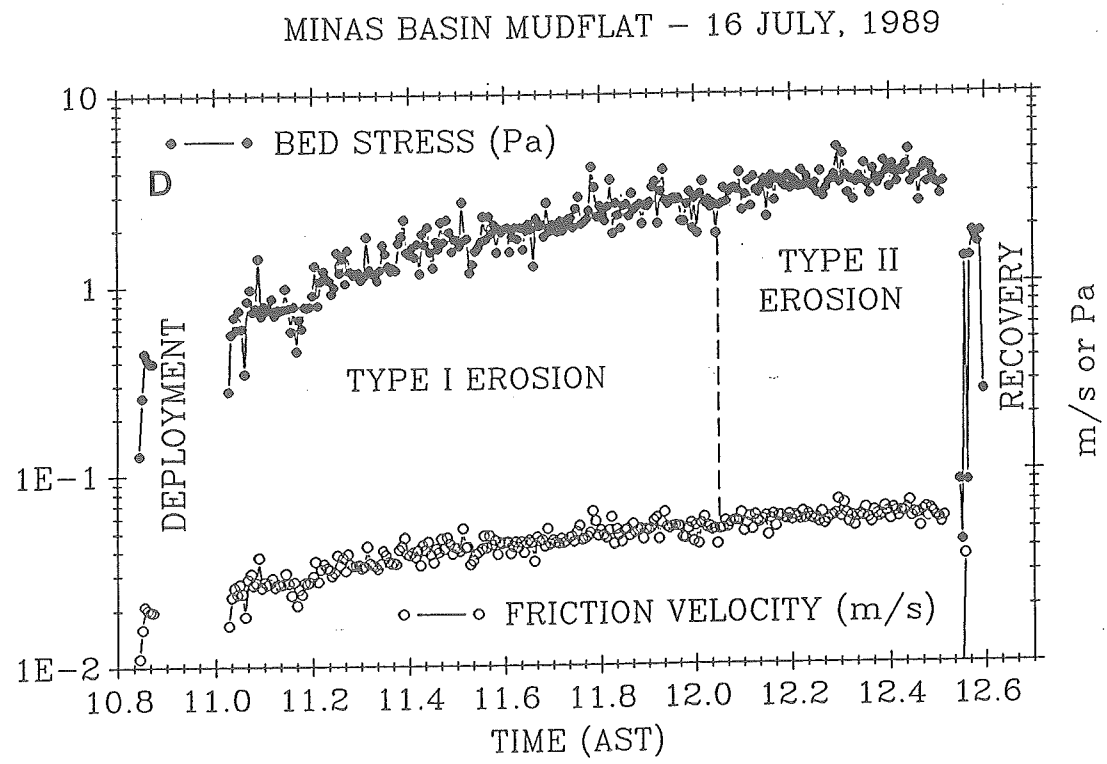

Figure 3.59 Cont. (C). Erosion rate calculated from $\Delta S/\Delta t$. Notice the rapid peak in erosion upon flow acceleration and the exponential decay of this rate thereafter. Also notice the difference in erosion rates between Type I and Type II erosion. The scatter in Type II erosion is evident. (D). Bed stress and friction velocity. Notice the apparent decrease in scatter of the time-series under Type II erosion. This corresponds to the development of sediment stratification evident in (3.59B).

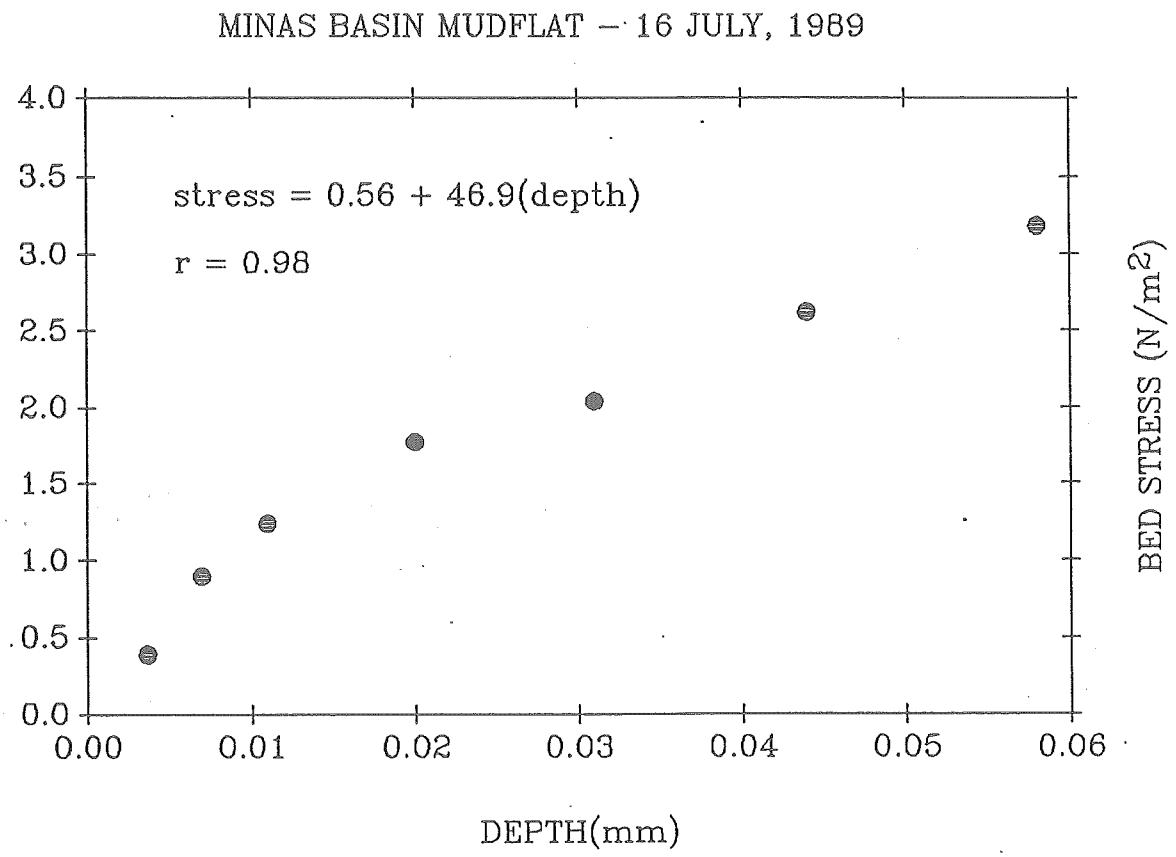

Figure 3.60. Depth of erosion versus the time-averaged bed stress at which erosion ceases under Type I erosion of the submarine deployment in Minas Basin. Notice that equilibrium stress increases linearly with depth below 0.01 mm and has an intercept of 0.56 $N.m^{-2}$. Compare this value to a range in critical values of 0.21-0.98 $N.m^{-2}$ derived from visual observations of erosion by Grant et al. (1990). Above 0.01 mm, however, data points appear to curve through the origin. The inference would be that this sediment has no time-averaged critical yield strength. We propose that this is due to fluctuations in instantaneous bed stress some of which exceed the critical threshold even when $\tau < \tau_c$.

appears to be no critical value for erosion despite a measurable cohesion and yield strength at this site (Christian et al. 1990; Grant et al. 1990). The best-fit regression line shows a linearly increasing erosion resistance versus depth below 0.01 mm that yields an intercept of 0.56 $N.m^{-2}$. This value is analogous to the Bingham yield strength as derived by Otsubo and Muraoka (1988) that they suggest is larger than the critical value for bed erosion. The curve we present is qualitatively similar to the one presented by Dyer (1989), although we see no clear relationship to the oxic/anoxic boundary.

3.8a.5 LISP Results

Twenty deployments of Sea Carousel were undertaken during the course of the LISP study. Three were made in Annapolis Basin and seventeen at the LISP site in Minas Basin. Good results were obtained at all but one of the deployments.

Annapolis Basin Survey

Three deployments of Sea Carousel were undertaken in Annapolis Basin (see Table 3.10 and Part 1). All three deployments were made on intertidal mudflats during sub-aerial exposure. Oak Island and Thorne Cove mudflats were known to be sites of significant clam mortality. Queen Anne Marsh, by contrast, had a normal clam community. Differences in the stability of the mudflats were evident. Figure 3.61 shows the critical (erosion) bed shear strength versus depth for the three sites. Notice that the surface critical shear stress for erosion is constant at approximately 0.5 Pa. This value is typical of soft, newly deposited muds. Also note that the strength of Queen Anne mudflat sediments increases more rapidly with depth than does that of Oak Island sediment. The interpretation is that Queen Anne marsh is less susceptible to resuspension that is Oak Island. Suspended solids concentration over Oak Island mudflats is likely to be greater during super-critical events than at Queen Anne Marsh by a factor of 2-3.

Minas Basin Survey

Twelve successful deployments of Sea Carousel were made on the Starrs Point mudflat, Minas Basin between 15 July and 2 August, 1989 : four at station 1, six at station 2 and two at station 3. Station 3 was abandoned early in the experiment due to the disruptive effects of worm diggers in the region.

A synthesis of the results is shown in Figure 3.62. The figure shows surface sediment strength given in terms of the flow velocity 0.2 m above the bed. Notice that there is a general decrease in critical erosion velocity seawards, from approximately 0.26 $m.s^{-1}$ at station 1 to 0.14 $m.s^{-1}$ at station 3. Also note that there is no clear trend in the critical erosion velocity with time for stations 1 and 3. There is, however, a significant trend at station 2. Here, an overall increase in erosion velocity from 0.19 $m.s^{-1}$ to 0.28 $m.s^{-1}$ was observed to take place throughout the end of July and early August. The most significant changes took place during the period 30 July - 2 August

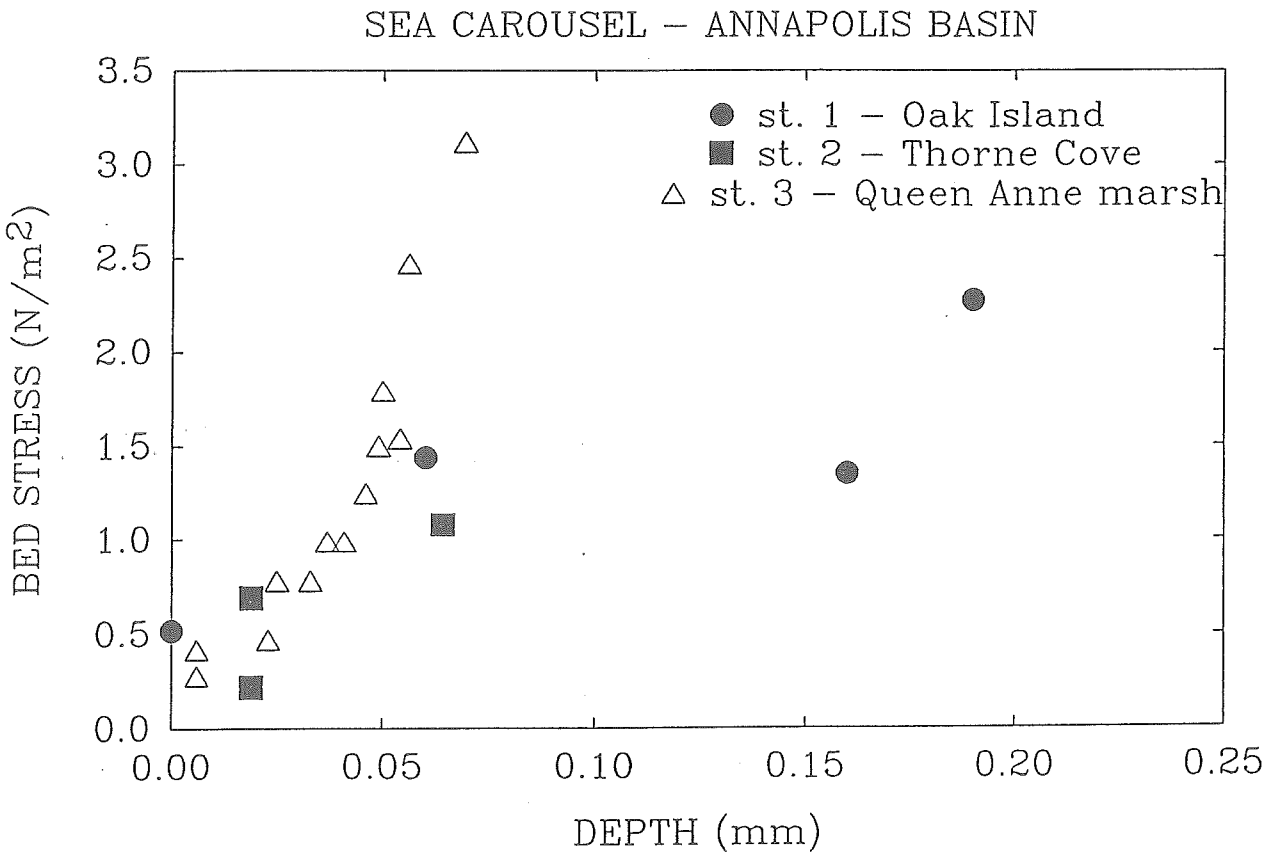

Figure 3.61: The critical bed shear stress for erosion plotted against depth within the sediment for the three sites analysed in Annapolis Basin : Oak Island, Thorne Cove and Queen Anne Marsh. Notice the significant difference in strengths with depth despite similarities at the surface.

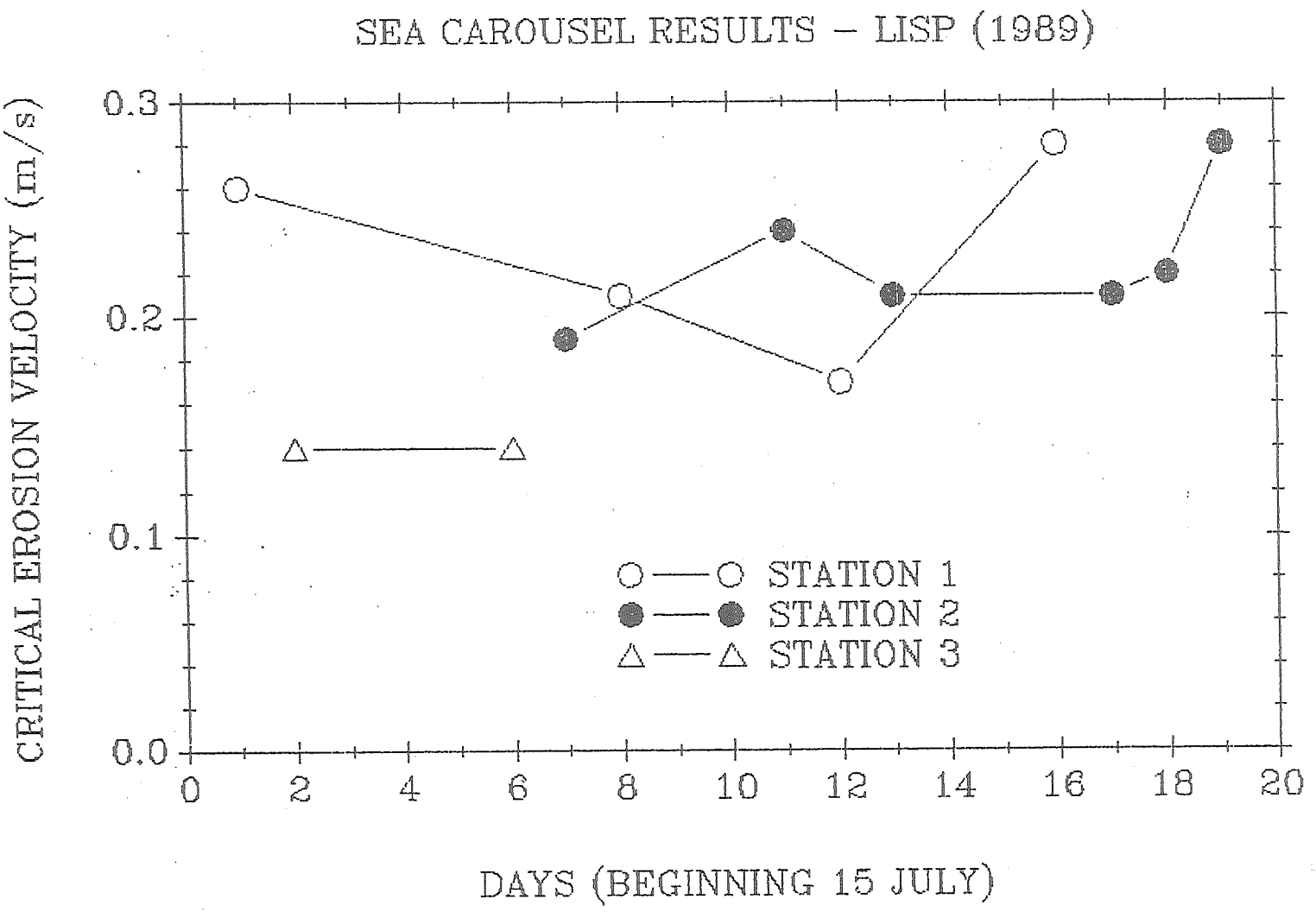

Figure 3.62. A time-series of surface critical erosion velocity (at a height of 0.2 m above the bed) for stations 1, 2 and 3 at Starr's Point, Minas Basin. Notice the systematic increase in strength at station 2 and the differences in strength between the stations. This indicates that bed strength varies both spatially and with time.

1989. These changes could not be correlated with solar radiation, rainfall, tidal range or tidal exposure.

Figure 3.63 shows the slope of the sediment strength increase with depth plotted for the same time-series as shown in Figure 3.62. No clear trends in results from stations 1 and 3 are evident. Again station 2 shows a consistent increase in slope with time, corresponding to the increase in surface strength. The peak in this trend, however, occurs before the peak in surface strength. The inference from these data is that sediment strength varies both spatially and with time by a factor of between 2 and 3 for the surface and by a factor of between 5 and 30 for strength change with depth. The results clearly show that single values of critical erosion velocity of natural mudflats are over-simplifications of reality.

3.8a.6 Conclusions

This paper describes the benthic flume Sea Carousel which was developed for the evaluation of erodibility of muds in intertidal or submerged settings. The system developed is an operational success although a number of improvements and refinements appear necessary. The major points of conclusion of the study are :

(1) Sea Carousel has been deployed 27 times in subaerial and submerged settings in a variety of manners. Results on mudflat stability were obtained on 25 occasions.

(2) Sea Carousel is best deployed and operated in submerged settings (even when studying intertidal flats) in order to minimize mudflat disturbance, water losses and aeration of the annulus.

(3) There is a consistent and linear relationship between lid rotation and azimuthal current speed for a salt water (34 ‰) temperature range of 4.5° to 18°C and for a range in S up to 208 mg.L^{-1}. Changes in salinity (from 34 to 0.16 ‰) result in a decrease in measured U_y by a constant 0.05 m.s^{-1}. This appears due to changes in sensor response.

(4) Spectral analysis of burst-sampled currents in the annulus showed that microturbulence structure is similar to that measured in the field. That is, the energy density falls off with frequency in proportion to -5/3. There is evidence of energy input at the frequency of paddle rotation. This appears to have no effect on the microturbulent structure.

(5) Instantaneous bed friction velocity shows a high degree of time variability at all tested current speeds. Systematic results were obtained by time-averaging measures of friction velocity over 60 seconds. The results showed that when $\overline{U}_y > 0.32$ m.s^{-1} friction velocity increased radially across the annulus. This increase is linear and in proportion to ($\overline{U}_y$ - 0.32 m.s^{-1}). The rms value of the spatially varying friction velocity showed a high correlation with azimuthal velocity in the form :
$\overline{U}_*$ rms = 0.0167 + 0.097 $\overline{U}_y$ (m.s^{-1}; r = 0.98)

(6) Friction velocity was determined to decrease with increases in S over a range 0 < S < 208 mg.L^{-1}. The relationship follows the function :
$\overline{U}_*(S) = \overline{U}_*(0).10^{[-1.76E\text{-}4(S)]}$ (m.s^{-1}; r = 0.91)

(7) Subaerial deployments of Sea Carousel resulted in substrate disturbance, water losses and aeration of the

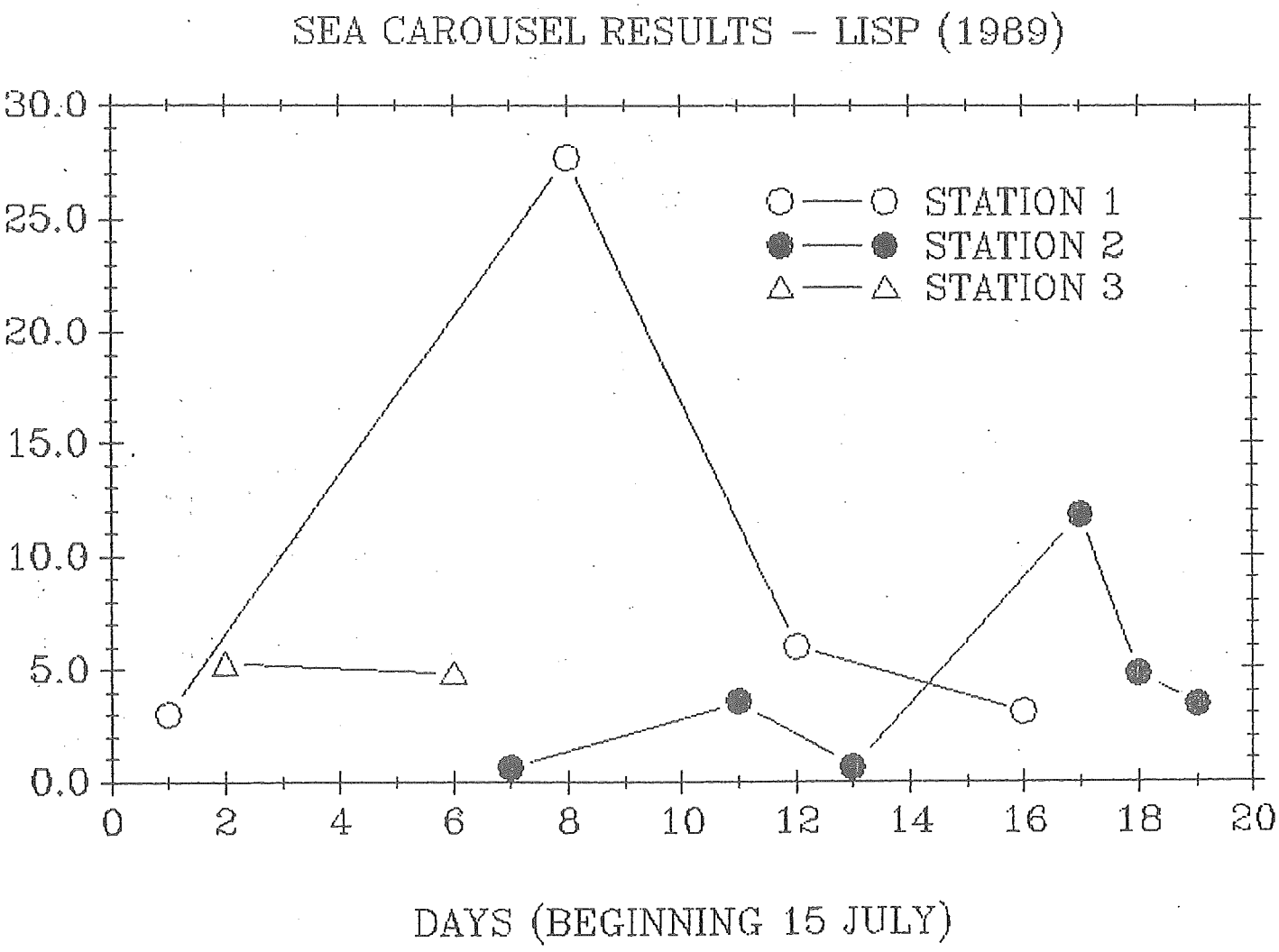

Figure 3.63. The slope (in reciprocal seconds) of the increase in bed strength with depth for the Minas Basin Sea Carousel deployments. Notice the temporal changes in slope at station 1, and the systematic increase at station 2.

annulus. However, good results were obtained on erosion rates and settling rates at low flow rates.

(8) Submerged deployments of Sea Carousel resulted in little seabed disturbance. Dispersion of turbid water from the annulus was detected with a resulting suspended sediment concentration half-life of 2400 seconds. Time-series of S must be corrected by this dispersion rate in order to determine true S and subsequent erosion rates.

(9) Notwithstanding conclusion 8, consistent and systematic trends in S and erosion rate were produced. These results showed that both Type I and Type II erosion of Mehta and Partheniades (1982) could be detected. In the former case, erosion rate peaked within 40 seconds of current acceleration and dropped in an exponentially-decaying fashion to zero. In the latter case, a similar, but less well-developed peak in erosion rate was measured but the decay was less clearly defined and the time-variability in erosion was large.

3.8a.7 Acknowledgements

This paper is the result of a strong team effort. Our thanks go to : R. Vine who produced mechanical designs and machine drawings from rough notes; J. Horne who built Sea Carousel and made numerous suggestions to help improve operation; A. Atkinson who interfaced and installed the electronic and electrical system; B.F. Long (INRS-Oceanologie) who supplied us with the underwater pod; A. Robertson who built the launch pontoon and helped with deployment; F. Jodrey who provided laboratory support during calibration; and H. Christian who provided geotechnical input into data interpretation. This section was reviewed by D. Gillespie and D. Willis.

3.8a.8 Notation

A	area of annulus footprint, m^2
C_d	dimensionless drag coefficient
d	depth of flow, m
D	annulus width, m
e	flume wall roughness scale, m
E	bed mass erosion rate, $kg.m^{-2}.s^{-1}$
M	sediment mass, kg
R_h	flume hydraulic radius, m
S	suspended sediment mass concentration, $mg.L^{-1}$
U_r	lid rotation speed, $m.s^{-1}$
U_y	azimuthal current speed, $m.s^{-1}$
U_w	vertical current speed, $m.s^{-1}$
U_*	friction velocity, $mm.s^{-1}$
V	annulus volume, m^3

y	height above seabed, m
z	depth within sediment, m
δ	dimensionless coefficient of diffusivity
δ'	thickness of viscous sub-layer, mm
ε	dimensionless efficiency factor
τ_o	applied bed shear stress, $N.m^{-2}$
τ_c	critical shear stress for bed erosion, $N.m^{-2}$
ρ_s	sediment density, $kg.m^{-3}$
ρ	fluid density, $kg.m^{-3}$
$\propto,\eta$	coefficients of proportionality
θ	dimensionless bed shear stress
μ	absolute fluid viscosity, $kg.m^{-1}.s^{-1}$

3.8b Biological Effects on Surface Cohesion

DAVID M. PATERSON

3.8b.1 Introduction

This portion of LISP 89 was directed at examining the changes in the erodibility of intertidal experiments over individual exposure periods, and particularly to examine possible biological influences on the erosion threshold of those sediments. It thus transcends the boundaries between sedimentology and biology. Dr. Paterson measured the surface erodibility, the chlorophyll *a* content and mucopolysaccharide concentrations of the surface sediments. These latter carbohydrates are extra-cellular products of benthic diatoms and other algae, and are thought to have an influence upon sediment erosion thresholds. The initial objective of this portion of the study was to examine the variables at different elevations on the mudflat (i.e., the original LISP stations), over the experimental period, however the poisoning of a site was a good opportunity to examine biological effects in greater detail, and therefore most effort was concentrated on the mid-tidal station near the barge, where an experimental plot was poisoned with formaldehyde. An adjacent untouched site was used as a control to examine the effect of the poison on sediment behaviour.

3.8b.2 Materials and Methods

Chlorophyll *a* , Water Content and Soluble Carbohydrate

The top 2 mm of three sediment cores were combined into each single sample to reduce the effect of natural patchiness on the sampling procedure. Three replicate samples were taken at each sample time. The samples were frozen and stored before analysis. Chlorophyll *a* analysis was based on Jensen (1978) and carbohydrate analysis on the method described by Kochert (1978). Surface scrapes of sediment were collected, wet-weighed, dried in a vacuum oven at 55°C overnight and reweighed to determine water content.

Sediment Erodibility

The erodibility of the surface of the sediment was measured using a 'Cohesive Strength Meter' (CSM - Paterson 1989), which functions by the firing of a pulse of water at 90° to the surface of the sediment, and recording the opacity of the water just above the sediment. An improvement from the described version was that a data logger has been incorporated into the system to record the transmission of light in the test chamber above the sediment. The sensitivity of the device was also increased for work in the Bay of Fundy by lowering the pressure initiating the water pulse to a minimum of 1.3 KPa. An initial attempt to record the surface shear within the test chamber (facilities courtesy of Dr. J. Grant) was unsuccessful because the pulse event (0.2 s) was too short to be accurately measured. Calibration of the device is to be carried out by Hydraulics Research Laboratories (U.K.).

3.8b.3 Results and Discussion

Measurements were carried out between 18 and 27 July. Sediment water content (expressed as a percent of fresh weight) varied rather little during any single exposure period (Fig. 3.64), indicating that evaporation from the tidal flat during the daytime exposure did not really dehydrate the sediment to any measurable extent; hence changes in erodibility during a single exposure period are not entirely due to evaporation effects. Higher water contents on 18, 25 and 27 July were not associated with precipitation during the exposure period, since none was recorded on those dates. In fact, these were days of relatively higher radiation (cf. Fig. 3.38 above), but followed days when rainfall was recorded at the Barge (Fig. 3.68 below).

At the beginning of the experimental period the tidal flats were heavily colonized by the amphipod *Corophium volutator* which showed visible evidence of sediment reworking. Towards the end of the study period the numbers of *C. volutator* were apparently greatly reduced (cf. Section 3.10), because of grazing activities of sandpipers and other predators, and because of changes in the behaviour of *Corophium* when these predators were present. Diatoms were generally low in density at the start of the study period, but became more abundant toward the end. This may be correlated with reduction in the numbers of *C. volutator*, which feeds by sifting through surface sediments. *Corophium* was immediately affected by poisoning with formalin, the animals quickly coming out of their burrows and often dying on the surface. For several days after the poisoning there was no successful immigration by *Corophium* into the poisoned area; those animals which did stray into the site either died there or left without burrowing. Microscopic examination of the sediments revealed that diatoms ceased movement following poisoning, and although cell contents were evident (formalin is an effective fixative), there was no evidence of physiological activity such as cytoplasmic streaming.

The concentration of chlorophyll *a* was fairly consistent between stations until 23 July, from which time sampling was confined to the poison and control sites near the Barge. The levels of chlorophyll *a* in the sediment reflect a gradual increase in diatom density (Fig. 3.65). One experimental site was sprayed with 4 L of formalin on 22 July; on the following day, chlorophyll *a* levels were similar on both poisoned and control areas, but as time progressed the disparity between the control and poison sites grew until by 27 July there was almost twice as much chlorophyll *a* in the control area than in both the poisoned site and the control site on earlier days. The continued presence of chlorophyll in the poisoned area may be explained since the formalin acts as a fixative, and because there were no grazers present to remove the diatoms that had been killed. A slight increase in chlorophyll on 27 July in the poisoned area may represent the initial stages of recovery of the diatom flora. In previous studies, benthic algal populations have started to recover within 4-7 days following elimination by formalin (G. Daborn - unpublished data).

Carbohydrate concentrations were lowest at the most seaward station (site 3), but comparable at sites 1 and 2. This may reflect the longer period of immersion at site 3, since there is less time for accumulation of soluble carbohydrates during exposure, and a correspondingly longer time for hydration. If cohesion from carbohydrates does affect critical erosion velocities, then this is another factor that will tend to make more seaward sites

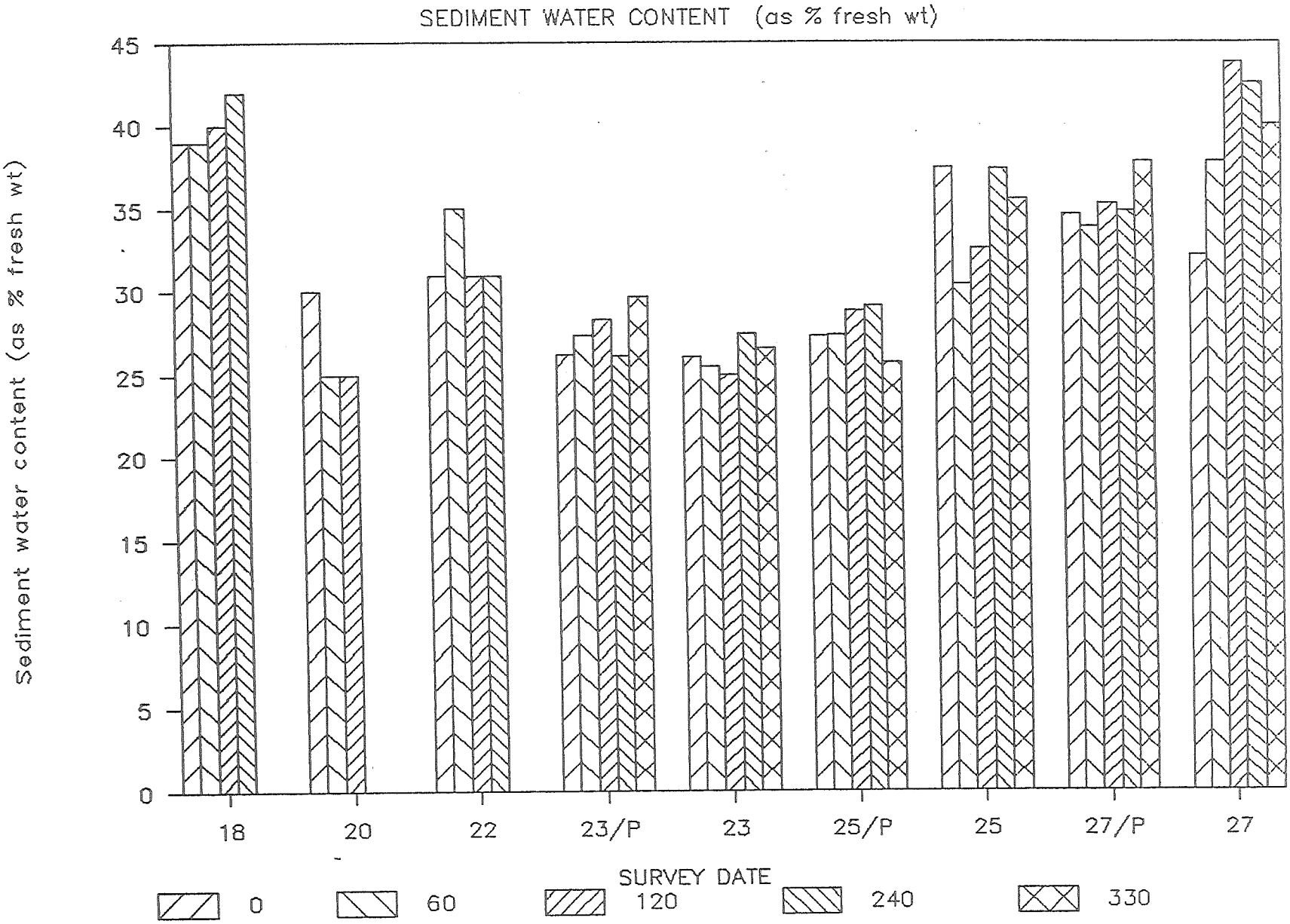

Figure 3.64. Water Content of Surface Sediments, July 1989. 0, 60, 120, 240, 330 - Time (minutes) of subaerial exposure. P - experimental site poisoned on 22 July.

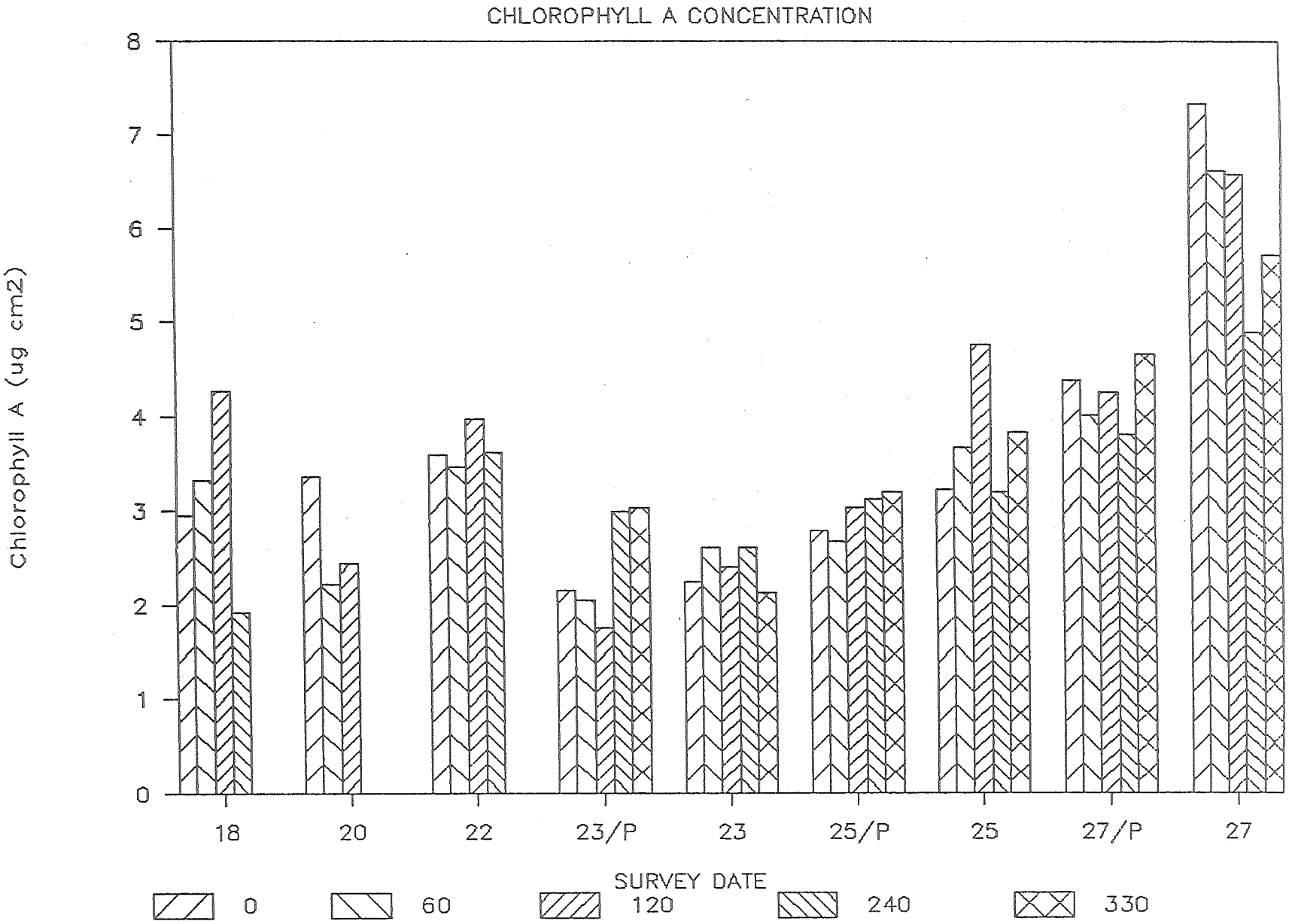

Figure 3.65. Chlorophyll *a* Concentration in Surficial Sediments, July 1989.

more prone to erosion, especially under the influence of higher current velocities (Section 3.5). However, this station also has a somewhat coarser sediment composition (cf. Section 3.6).

A dramatic effect on carbohydrate concentration was caused by poisoning of the sediment (Fig. 3.66). This suggests that soluble carbohydrate concentrations are a better index of biological activity than chlorophyll content, although it is somewhat less specific. The reduction in carbohydrate production confirms that the diatoms which produce soluble carbohydrates as part of their locomotive mechanism were physiologically inactive. The greatest reduction in soluble carbohydrate was noted two days after poisoning, which may reflect the time required for hydration of some less labile compounds. A further two days later there was evidence of a recovery of the community, as with the chlorophyll values. Microscopic analysis of sediment samples is continuing in order to confirm this interpretation.

The sediments of the Starrs Point tidal flat exhibited very little cohesion compared with cohesive sediments in the Severn Estuary (U.K.). The Southern Bight substrates displayed a "silty-sand" type of behaviour within the CSM, with no demonstrable point of "incipient scour" (Dunn 1959). Some cohesion was present, as shown in Figure 3.67, since drying or repacking of sediment particles during the tidal exposure period led to a decrease in the amount of sediment that was eroded by the CSM pulse as tidal exposure progressed. This is demonstrated in Figure 3.67 by the trend of the bars to decrease from left to right for each experiment. A rain shower during the experiment on 27 July (arrow in Fig. 3.67) caused the trend to reverse, indicating the transient nature of this cohesion, but the cohesion returned after a further drying period. On rare occasions, cohesion developed sufficiently for the sediment surface to behave as a cohesive sediment, with a measurable yield stress built up by the end of the experiment. The decrease in erodibility of the poisoned site on 23 and 25 July was less than that on the control area; presumably this decrease is attributable primarily to atmospheric effects, whereas on the control area diatom growth and release of carbohydrates are contributory factors also. This may be the first evidence of a sediment behaving both as cohesionless and cohesive in response to biological factors. These results in many ways are similar to those obtained with 'INSIST' (cf. Section 3.7).

Comparison of Figures 3.65 - 3.67 indicates that chlorophyll *a* and carbohydrate concentrations increased with time during the LISP study, and that as this occurred the sediment became harder to erode. There is a residual build-up of cohesion from tide to tide, although this may be dependent upon meteorological conditions such as insolation and rainfall, as well as biological changes. The decrease in erodibility measured by the CSM toward the end of the LISP study echoes similar results with both 'INSIST' and 'Sea Carousel'. There can be little doubt that the change is real.

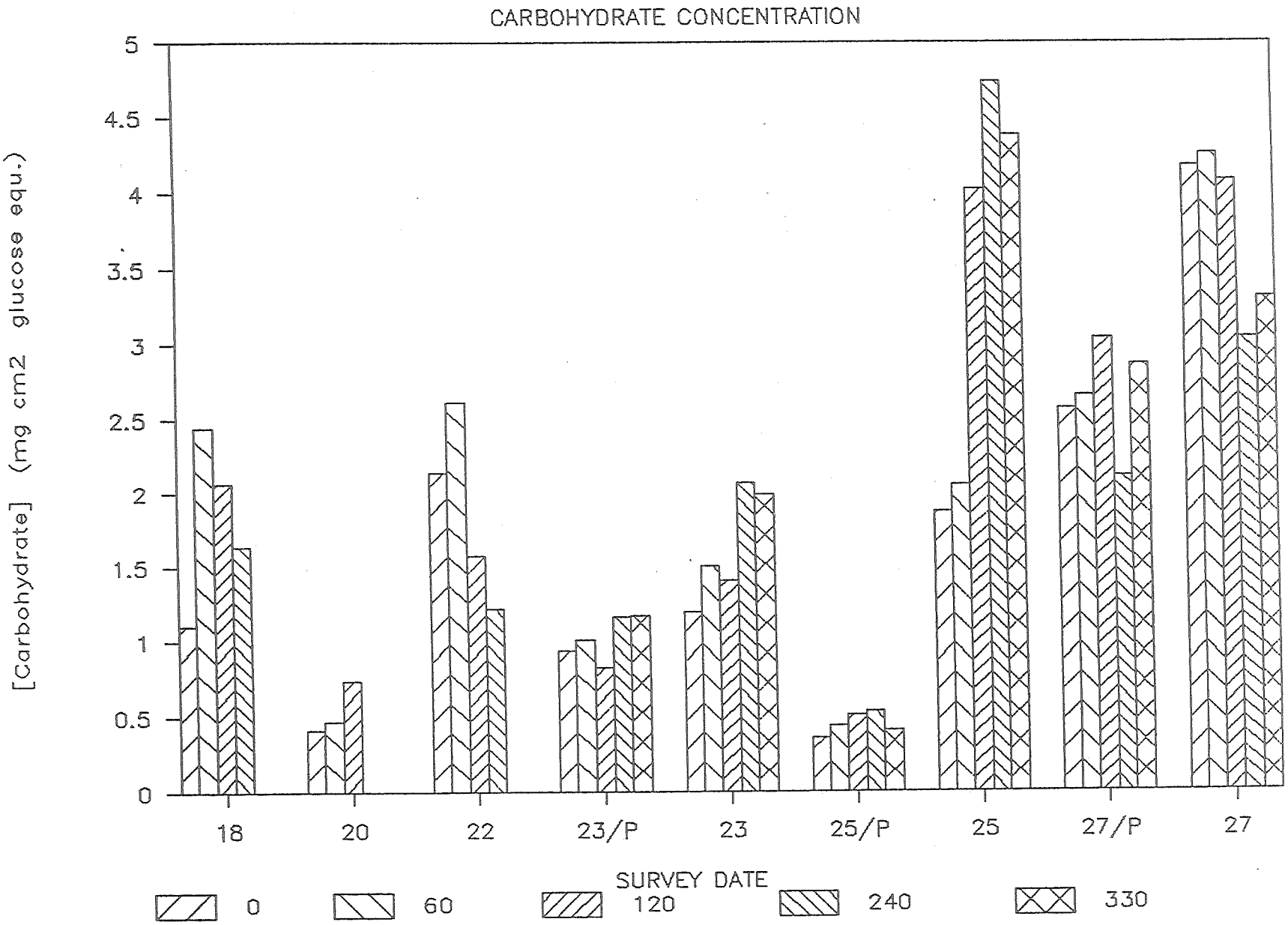

Figure 3.66. Soluble Carbohydrate Concentrations in Surficial Sediments, July 1989.

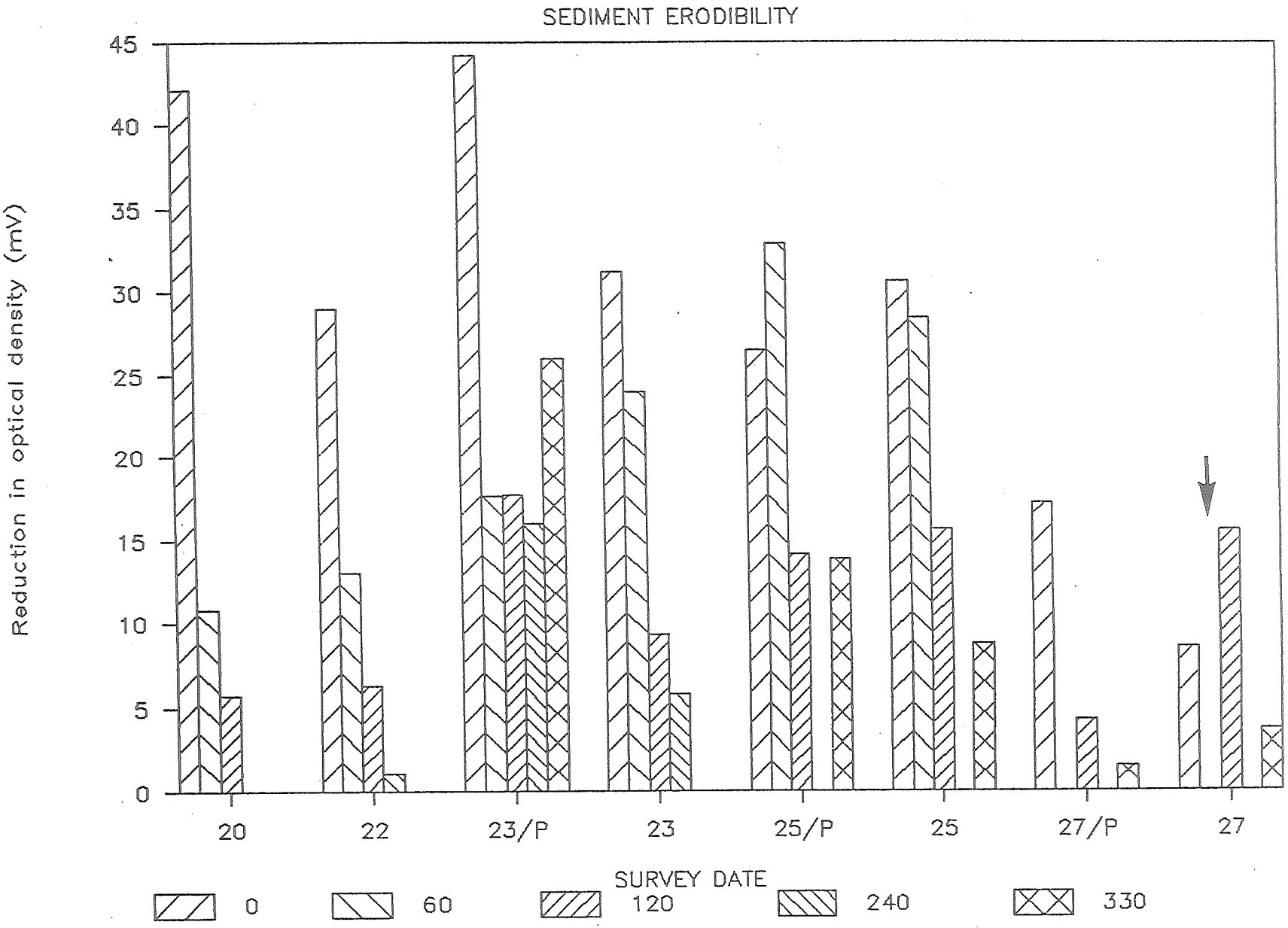

Figure 3.67. Sediment Erodibility determined using CSM.

3.8c Laboratory Flume Studies of Sediment Erodibility

GRAHAM R. DABORN

In order to provide a comparison between information on erodibility of intertidal sediments obtained by the *in situ* techniques described above, and the more traditional procedure of removing sediments to a laboratory flume, Dr. J. Grant collected sediment cores from the Starrs Point tidal flat during low water and returned them to Dalhousie University with as little disturbance and delay as possible. Full results of this portion of the study are not yet available. However, a number of observations have been passed on relating to the overall conclusions of the study.

Sediment cores were inserted into a laboratory flume and subjected to controlled flows of sea water. The flume arrangement permitted detection of both bedflow and resuspension of surface sediments, and also close observation. Every effort was made to minimise disturbance of the core and its biotic contents. A major observation made during the experiments was that much or most of the sediments resuspended during a run were the result of *Corophium* activity, particularly the process of cleaning out fine sediment from their tubes. This was evident from the periodic expulsion of clouds of fine sediment from each burrow. It seems probable that this activity is a consequence of the inevitable disturbance resulting from transshipment of the core from the field to the laboratory, a process that inevitably took more than a couple of hours. During this time it is presumed that the *Corophium* in the core would have remained relatively inactive, so that sediments suspended in the water in the tubes would tend to settle out, and perhaps some of the surficial sediments might fall into open burrows as a result of vibration. When the cores were recovered with flowing water, the occupants of the burrow would then expel accumulated silt as part of normal activity. It is probable that such a sequence occurs following every flood in the field, and therefore that 'housecleaning' activities of *Corophium* are a contributor of fine sediment resuspended on the flood. However it is not possible to ascertain at this time the extent to which the necessity for such clearing was increased as a result of the disturbance associated with removing the cores to the laboratory. It seems appropriate to view these observations as further evidence that accurate understanding of the factors controlling erodibility of finer sediments cannot be achieved without *in situ* measurements.

Tubicolous animals such as *Corophium* may play a different role as a result of the construction of their tubes, which are composed of selected sediment particles 'glued' together by exudates of the animals themselves. Following each experiment the cores were examined carefully, and the number of *Corophium* burrows counted. Results are shown in Figure 3.68. It is evident from this data set that the erosion rate under specified conditions is inversely proportional to the number of juvenile *Corophium* burrows in the core. Construction of burrows appears to be an important factor in stabilising the sediment against the erosive tendency of flowing water. These observations are entirely compatible with the inference that an increase in resistance to erosion detected with 'Sea Carousel', 'INSIST' and the 'CSM' during the last part of July and early August was related to the decline in abundance of *Corophium* in the study plots.

Analysis of these data is continuing.

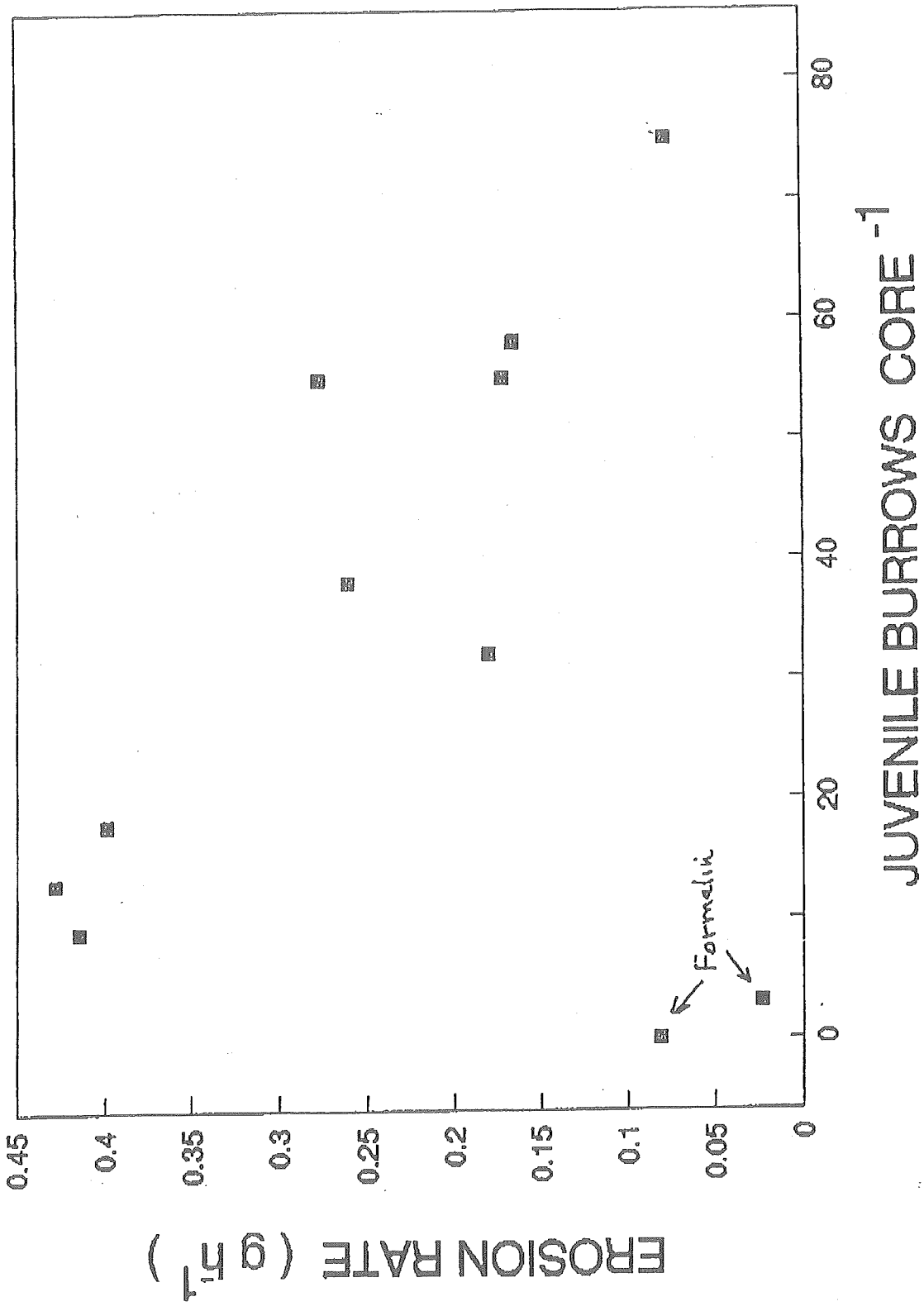

Figure 3.68. Effect of *Corophium* burrows on erosion rate of Starrs Point sediment cores analysed in a laboratory flume.

3.9 Air-Sea-Land Interactions

MARIA CINTIA PICCOLO, GERARDO M.E. PERILLO and GRAHAM R. DABORN

The main objective of this portion of the study was to determine the atmospheric conditions prevalent during experimental studies on the Starrs Point tidal flat in order to examine their influence on changing properties of the sediment. Weather data were obtained from a recording weather station on the Barge from 13 July to 9 August; from 28 June to 13 July it was located on the dyke near Willowbank Farms, southwest of the Barge site.

Results of the measurements are shown in Figure 3.69. Full analysis of the data, and correlation with changing sediment properties is still to be carried out. All major weather events that were considered potentially important in affecting sediment strength were encountered during the study, including : warm sunny days with little or no wind (21, 23, 31 July); heavy rainfall over the flat occurring during exposure periods (20, 26 July) and when the site was flooded (27/28 July); dry days with strong winds (22 July). Maximum wind speeds recorded during the experimental period (15 July-2 August) were 7.5 to 8.5 $m.s^{-1}$. Maximum hourly air temperature (averaged from 1 min readings) was 30.7°C, recorded on 26 July when the mudflat at the Barge site had been exposed for about 5 hours.

Examination of SPM values during strong wind events (e.g., 0900-1030 h 28 July) indicates that even with water depths of 5+ m, surface SPM values could increase somewhat (16 to 22 $mg.L^{-1}$) as a result of wind-induced mixing associated with winds of 7-8 $m.s^{-1}$.

Weather data recorded at the Kentville Research Station between 26 June and 8 August were obtained, courtesy of Ed Reed (Agriculture Canada). These data were recorded on strip charts, and are to be read and processed by M.C. Piccolo in Argentina for cross-correlation with the data from the recording weather station at the Barge. Daily weather maps for the same period have been provided by the Atmospheric Environment Service.

Total solar radiation was measured at the Barge using a LI-200S pyranometer, with data recorded on a datalogger. Results are shown in Figures 3.70 and 3.71. Maximum hourly radiation values were reasonably similar on most days, between 2500 and 3500 $KJ.m^{-2}.h^{-1}$, with low values on the rainfall days of 17, 20 and 28 July (Fig. 3.70). Total daily radiation was somewhat more variable (Fig. 3.71). From the point of view of impact of irradiation on sediment properties, however, the more relevant variable is the amount of radiation falling on the tidal flat during the period of exposure, as described in sections 3.7 and 3.8 above.

During the study, temperatures of the air, water and sediments were monitored continuously using the thermistor chain established near the Barge. Thermistors were located at 5, 10, 25 and 50 cm below the sediment surface, and at 5, 30 and 130 cm above the surface of the flat. An extra thermistor lying initially at the surface was buried naturally by accumulation of 1 cm of sediment during the course of the experiment. Data from the thermistor chain were sampled every 10 minutes.

Assuming that sediment temperature varied as a sinusoidal function of time, thermal diffusivity (k) was determined from a wave amplitude-depth relationship :

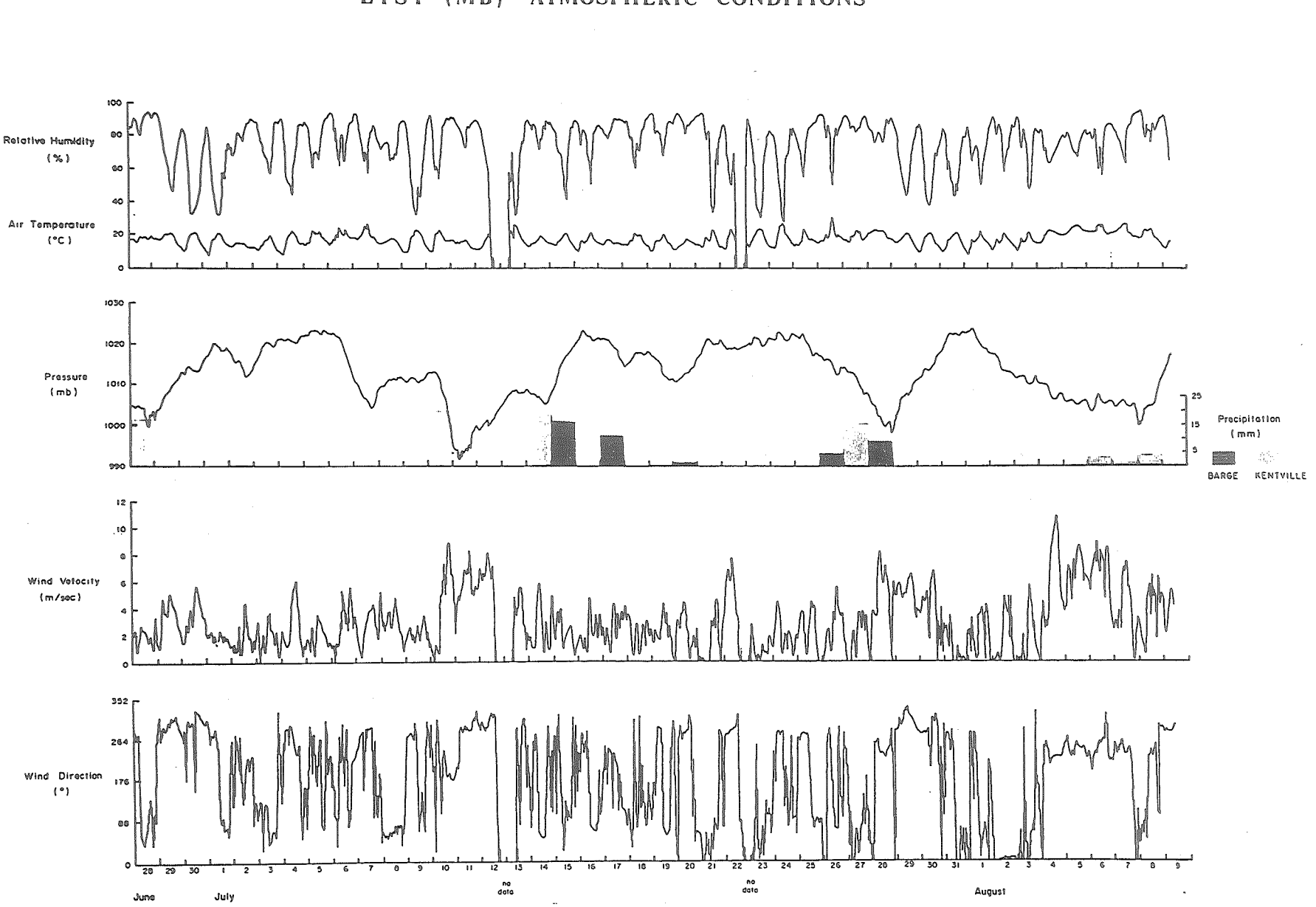

Figure 3.69. Weather data recorded at Starrs Point June - August 1989.

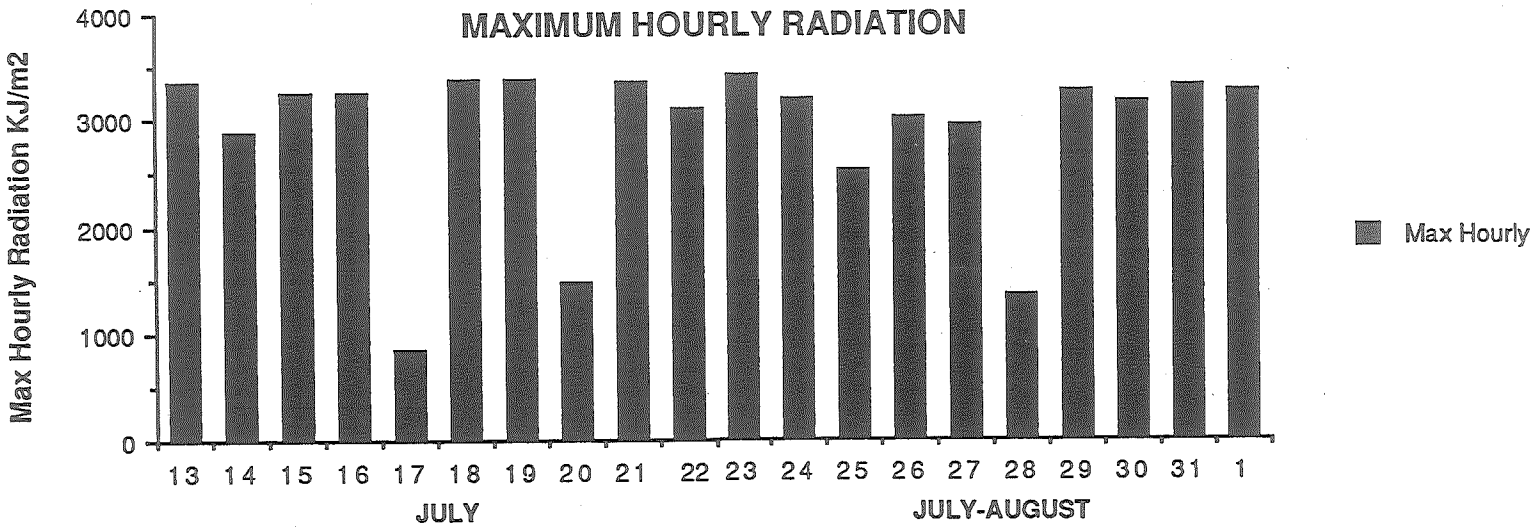

Figure 3.70. Maximum hourly radiation recorded at Barge site 13 July - 1 August 1989.

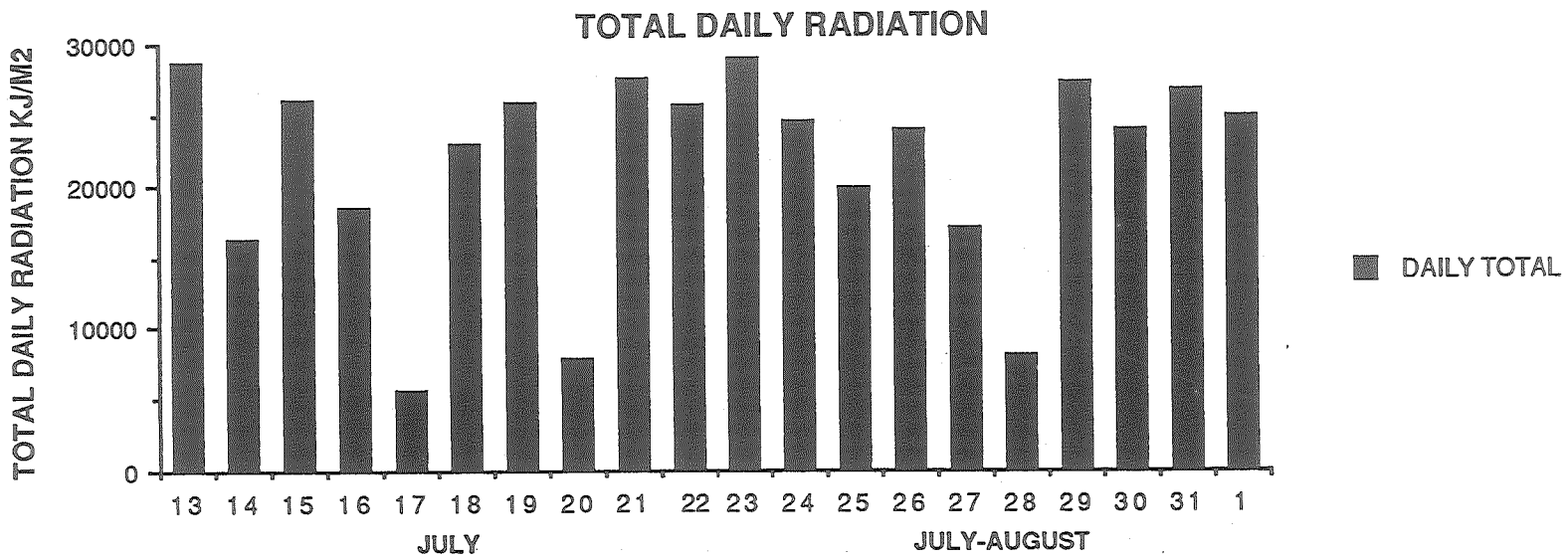

Figure 3.71. Total daily radiation recorded at the Barge site 13 July - 1 August 1989.

$$k = \frac{pi \ (Z_1 - Z_2)^2}{P \cdot \ln (A_1/A_2)} \qquad (1)$$

where A_1 and A_2 are the amplitudes, and P the period of oscillation (12 h). The mean value estimated between 0.01 m and 0.05 m was $0.848 \cdot 10^{-6}$ $m^2.s^{-1}$. This compares favourably with the estimates of Harrison and Phizacklea (1987) for muddy sediments elsewhere. Table 3.11 shows values of k for different sediment layers.

The analysis of the time lag between temperature waves at different depths gives an idea of the real diffusivity. With the mean time lags between diurnal temperature waves and the field temperature, diffusivity was again estimated, using Equation 2 :

$$k = \frac{P (Z_1 - Z_2)^2}{4 \ pi \ (\Delta t)^2} \qquad (2)$$

The field thermal diffusivity between 0.01 and 0.25 m is greater than that calculated under non-tidal conditions of molecular heat diffusion. The increase is the result of the exchange of water-borne heat across the sediment-water interface, and its rapid transfer through non-capillary pore spaces in the sediment during inundation. As indicated in sedimentological and biological components of LISP, the activities of burrowing and foraging animals are undoubtedly significant influences on the rate of heat transfer between water and sediment.

The magnitude and rate of heat exchange during tidal inundation is dependent upon the relative temperature of the sediment and the incoming water layer. The net result of tidal inundation during daylight hours, especially after noon, is a very sharp fall in temperature, the magnitude of which is very closely related to the timing of tidal water movements. The greatest fall in sediment temperature at 0.01 m depth occurred during a late afternoon flooding.

The effect of the tidal inundation (bimodal wave) is evident up to 0.10 m. A small temperature variation, less than 1°C, is found at 0.50 m depth. Some of this difference might be due to observation error. Vertical gradients were stronger from the surface to 0.05 m. The effect of flooding on the 0.01-0.05 m and 0.05-0.10 m layers was to reduce temperature gradients almost to an isothermal state, while in the 0.10-0.25 m and 0.25-0.50 m layers there was a residual thermal stratification.

Power spectra of the air temperatures at different heights and sediment temperatures at 0.01 m depth show a maximum peak at 213 minutes. At 0.05 and 0.50 m depth levels the maximum peaks were found at 256 minutes, while at 0.10 and 0.25 peaks were at 320 and 33 minutes. The spectrum of thermal waves at 0.05 and 0.25 m presented peaks at 80 and 40 minutes, respectively.

Table 3.11. Mean Time Lags and Thermal Diffusivities for Different Sediment Layers, Starrs Point Tidal Flat

Z (m)	Mean Time Lag (min)	k (Eq. 1)	k (Eq. 2)
0.01 - 0.05	60	0.848	0.27
0.05 - 0.10	60	1.326	0.77
0.10 - 0.25	140	2.179	1.66
0.25 - 0.50	270	1.638	1.57
0.05 - 0.50	500	1.546	1.46
0.05 - 0.25	210	1.732	1.33

The results of the heat balance study can be summarised as follows :

(1) The latent heat flux is by far the most important component in redistributing the net solar radiation;

(2) The sensible heat flux is comparable in magnitude to the ground heat flux;

(3) The comparison of different methods to calculate evaporation resulted in similar values, therefore conventional meteorological measurements may be used to calculate the evaporation during exposure hours.

3.10 Primary Production Studies

DAVID PATERSON and MICHAEL BRYLINSKY

3.10.1 Introduction

A number of studies (e.g., Holland et al. 1974; Coles 1979; Zeman 1983; Paterson 1989) have indicated that the production and growth of benthic diatoms may play a significant role in the stabilisation of sediments as a result of the production of sediment-binding carbohydrates. As part of the holistic approach to LISP 89, an attempt was made to measure the productivity of benthic diatoms, and to relate the chlorophyll and carbohydrate concentrations found within surficial sediments to primary production processes and, ultimately, to sediment stability. Initially, a number of measurements were made to determine if any significant differences existed between the three major study sites in terms of the biomass and production of benthic diatoms. As the study progressed, attention was directed toward determining the short-term impact of plant and animal activity on sediment characteristics. These studies were carried out using various types of selective metabolic inhibitors, the effectiveness of which was monitored by photosynthesis and respiration measurements.

3.10.2 Methods

Photosynthesis and Respiration

In situ measurements of photosynthesis and respiration were made by measuring the change in oxygen concentration in light and dark 5 cm diameter plexiglass cores. The cores were inserted into the sediment to a depth of 5 cm and filled with 0.45 µm filtered seawater that was previously purged with nitrogen gas to reduce the initial oxygen level to about 20 percent saturation. Incubations lasted between 0.75 and 1.25 hours. Changes in oxygen concentration were determined using a micro-Winkler procedure.

Chlorophyll *a* and Dissolved Carbohydrate

Samples for chlorophyll *a* and dissolved carbohydrate determinations were collected in triplicate using a 1.2 cm diameter plexiglass core. The top 5 mm of sediment was collected and stored frozen until analysis. Chlorophyll *a* analysis followed the procedure described by Jensen (1978) and carbohydrate analysis followed the procedure described by Kochert (1978).

3.10.3 Results

Site Comparisons

On 24 July photosynthesis and respiration measurements were made simultaneously at each of the three main study sites. Chlorophyll *a* and dissolved carbohydrate determinations were also made at each site. The results

are presented in Figure 3.72. In general, photosynthetic rates were greatest at the middle station, lowest at the seaward station and intermediate at the landward station. Respiration rates, however, varied little among stations. Chlorophyll *a* concentrations were about equal at the landward and middle stations and lowest at the seaward station. Dissolved carbohydrate concentrations showed a decrease as one moved seaward. These observations suggest that the most seaward station is the least photosynthetically active and, as a result, is lowest in both the biomass of benthic diatoms and the concentration of dissolved carbohydrates. This difference is most likely a result of its shorter exposure period, and larger grain size.

There was no obvious relationship between respiration rates and the biomass of macroinvertebrates contained within the cores, suggesting that most respiratory activity is due to sediment microorganisms.

Metabolic Measurements at the Barge Poisoned and Control Sites

As an aid in interpreting the time course of recovery of biological activity at the Poisoned site (described in Section 3.8b), a series of metabolic measurements were made at this site beginning on 23 July, five days after initial application of the poison, and continuing at two day intervals to 29 July. Figure 3.73 shows the change in photosynthesis and respiration occurring during this period at the Poisoned site and its Control. On 23 July photosynthesis and respiration rates were essentially equal to zero indicating that the poison was still having a significant effect on biological processes. By July 27 photosynthetic rates increased greatly and were equal to those of the nearby Control site. Respiration rates, however, were still below those of the Control suggesting that the animal component had not recovered to the same extent as the benthic diatoms.

Dissolved Carbohydrate Production and Sediment Shear Strength

In an attempt to demonstrate a direct relationship between dissolved carbohydrate concentration and sediment shear strength the following experiment was carried out on 8 August. An undisturbed area of the mudflat located in close proximity to the Barge was divided into a control and experimental area. The experimental area was treated with DCMU immediately after exposure to inhibit photosynthesis. At hourly intervals sediment samples were taken for dissolved carbohydrate analysis, and a measure of sediment shear strength was made. Sediment shear strength was measured in relative terms by determining the amount of weight required to move a weighted shear plate (of the type used in the INSIST apparatus - see Section 3.7). The experiment lasted for about 5 hrs. The results, presented in Figure 3.74, were contrary to what was expected. Although dissolved carbohydrate concentrations increased considerably with time at the control site, and remained relatively constant at the poisoned site, the increase in shear strength was considerably greater at the poisoned site. These results suggest that the production of dissolved carbohydrates may actually decrease sediment shear strength, at least over short time periods.

An additional experiment, based on an observation made earlier in the project by H. Christian, was performed to determine the affect of flooding on the observed increase in shear strength during exposure. A 1 m^2 area at

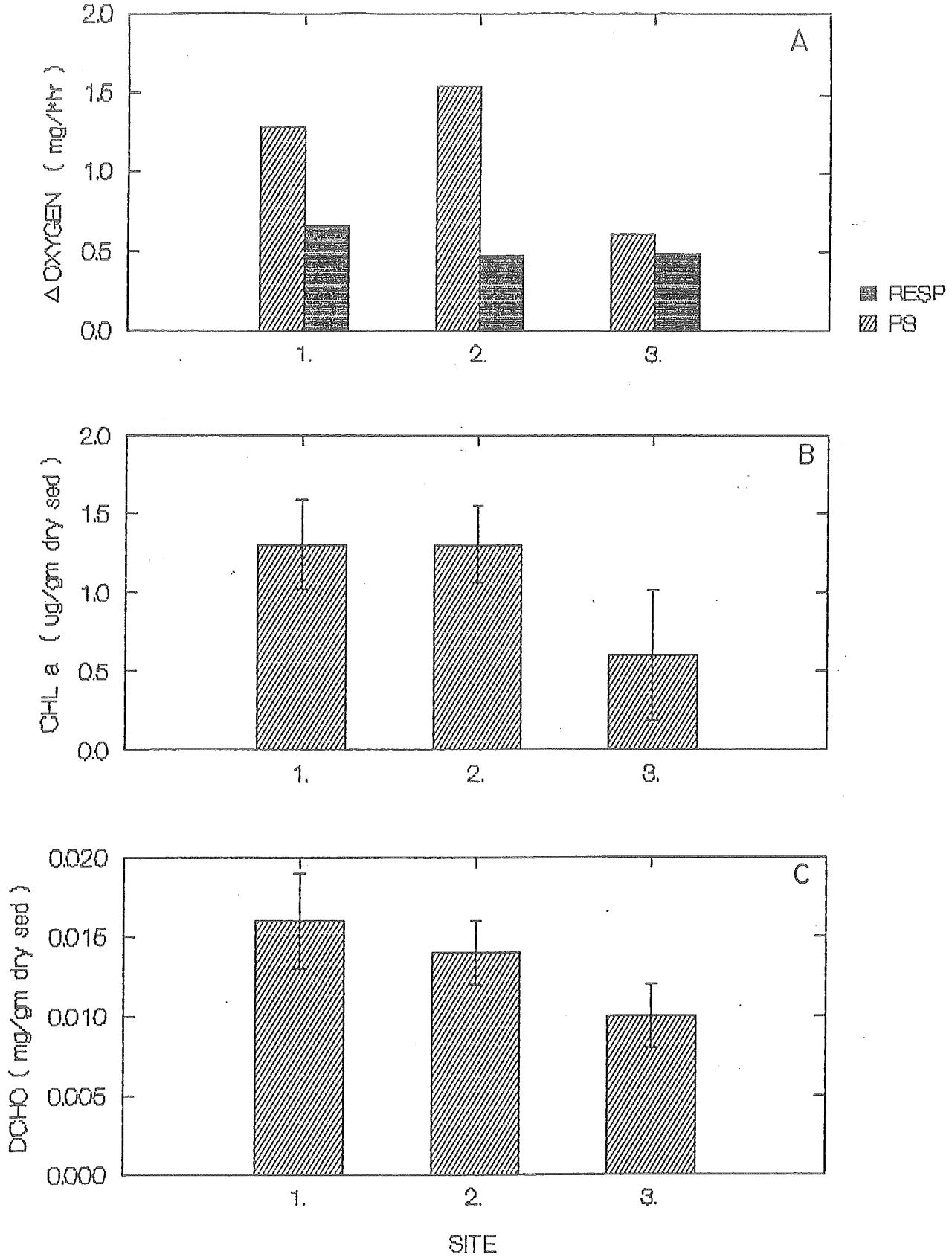

Figure 3.72. Comparison of sites (1 = shoreward, 2 = midflat, 3 = seaward) in terms of (A) photosynthesis and respiration; (B) chlorophyll *a* concentration and; (C) dissolved carbohydrate concentration. Error bars are one standard error of the mean.

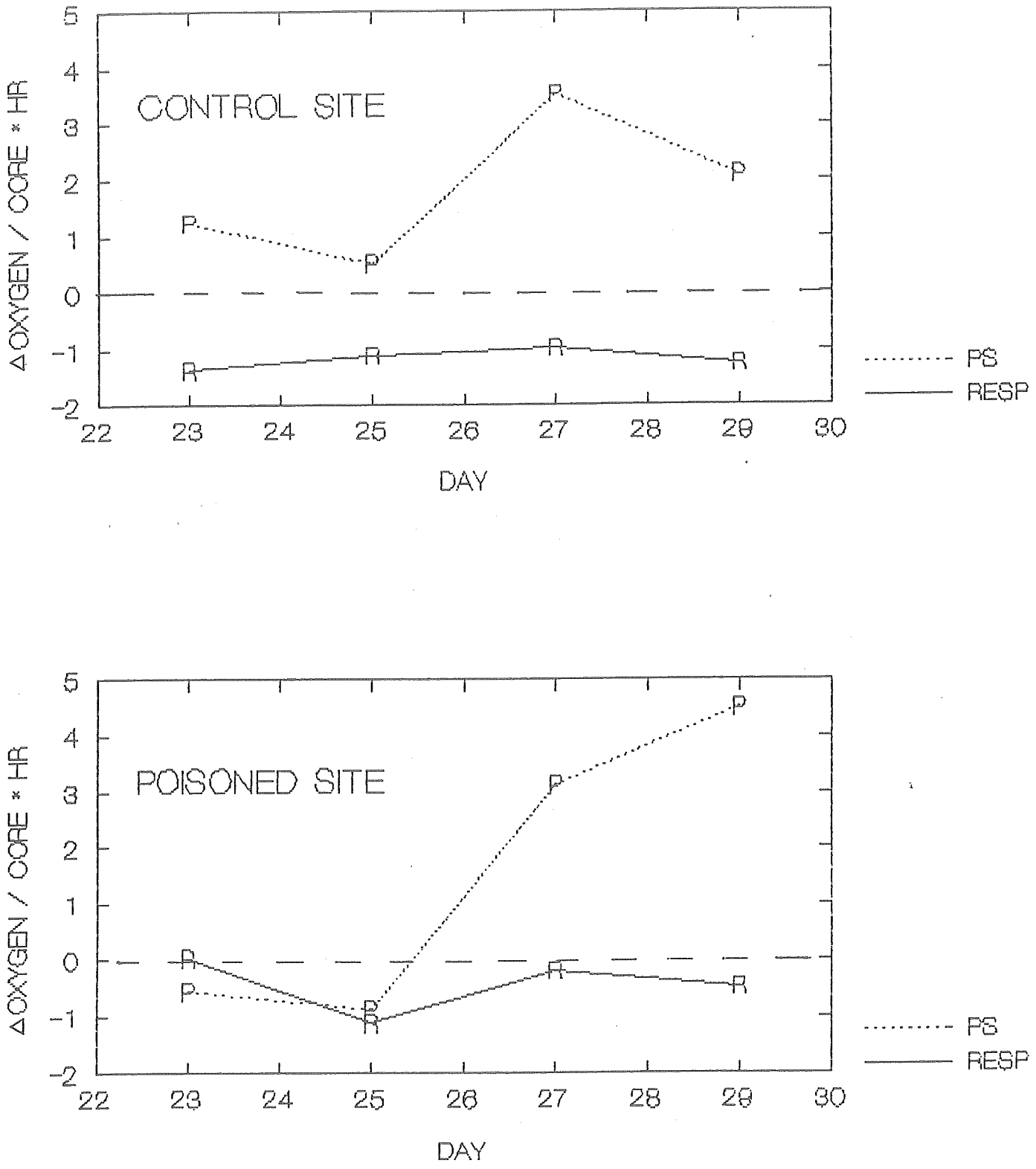

Figure 3.73. Time course of photosynthesis and respiration at the Poisoned and Control sites.

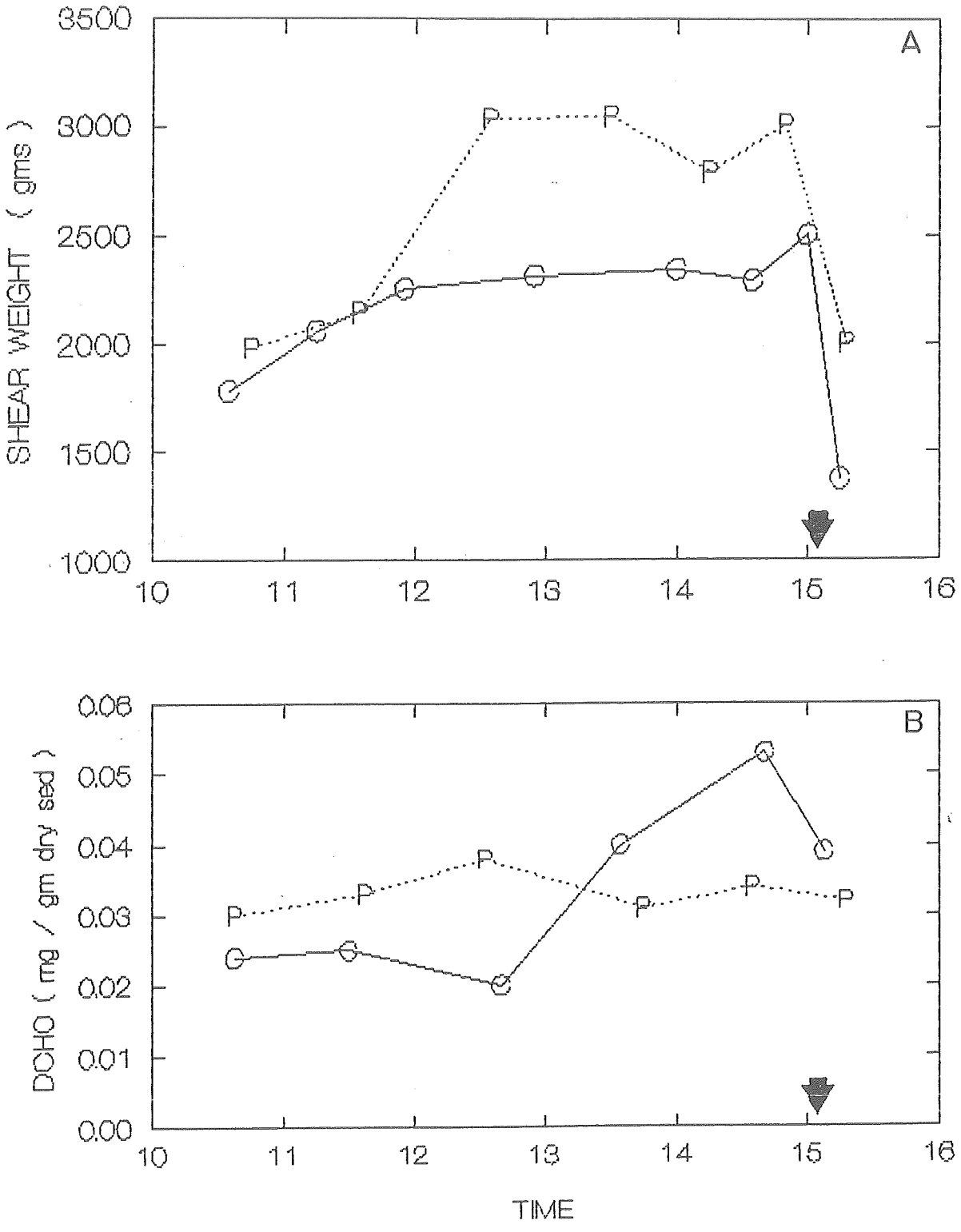

Figure 3.74. Time course of changes in (A) shear strength and (B) dissolved carbohydrate concentration at the Poisoned (···P···) and Control (--C--) sites. Arrow indicates time at which flooding experiment occurred.

each site was dammed, flooded for about 5 min, then allowed to drain for another 5 min after which a shear strength measurement was made. At both the control and poisoned site shear strength declined considerably (Figure 3.74A).

Observations on the Use of Metabolic Inhibitors

During the course of the LISP project a number of experiments were carried out using metabolic inhibitors. The intent was to selectively inhibit either photosynthesis and/or animal activity and to determine what affect, if any, this inhibition has on various sediment characteristics. The inhibitor used to prevent photosynthesis by benthic diatoms was DCMU, a common herbicide. Sodium cyanide was employed to inhibit animal activity. Initially the inhibitors were applied to the sediment surface one day prior to making measurements. It was soon discovered, however, that both of these inhibitors, although effective immediately after application, completely lose their affect after one or two tidal periods. Measurements of metabolic activity showed no difference between control and treated sites one day after application of the inhibitors.

3.11 Animal-Sediment Interactions

GRAHAM R. DABORN

Participants :
G.R. Daborn, D.L. Amirault, P. Crawford-Kellock, M. Shaffelburg

3.11.1 Introduction

The intricate relationship between sediment characteristics and the fauna inhabiting particular sediments has been the subject of study for many decades. Traditionally, species-specific patterns of distribution have been interpreted as responses to preferred substrate types (e.g., Meadows 1964a, b), a view that underlies formal classifications such as those of Peterson (1913). Such classifications are still in use today (e.g., Warwick and Uncles 1980; Davidson et al. 1991), especially where large and complex coastal or estuarine systems are studied (i.e., where substrate type varies considerably).

In recent years, the converse relationship—that sediment properties are modified by the organisms inhabiting them—has received much attention. Benthic macrofauna have been found to exert destabilising effects on sediments through bioturbation (e.g., Gray 1974; Eckman et al. 1981; Nowell et al. 1981; McCall and Tevesz 1982; Meadows and Tait 1985; Meadows and Tufail 1986), or by increasing bed roughness (e.g., Carey 1983; Luckenbach 1986). More subtle effects such as the modification of pore water chemistry (e.g., Aller 1978) and grain size or geotechnical features (Grant 1981; Meadows and Tait 1985, 1989) have also been investigated. These complex interrelationships are to some extent amenable to laboratory experimentation. However, full understanding of the role of benthic fauna on sediment properties needs to be based on field experiments and observations conducted over time scales that are relevant to biological processes.

During the initial study of Starrs Point tidal flat in 1984, the significant changes in the apparent strength of the sediment were attributed primarily to the effects of subaerial exposure (Amos et al. 1988). It was also recognised, however, that the activities of the benthic fauna, especially the numerically dominant *Corophium volutator* and *Heteromastus filiformis*, probably played an important role. For example, poisoning of the tidal flat eliminated both species initially, but *Corophium* recolonised more rapidly after the poison had washed out of the sediment, and ultimately became more abundant in the treated sites than in untreated control areas. The greater number of *Corophium* led to a decrease in both biomass and productivity (as measured by chlorophyll levels in the sediment) of benthic diatoms in treated areas. These observations suggested that *Corophium* was an effective colonizing species that responded favourably to sediment disturbance. For this reason, three separate experiments were conducted to examine the responses of macroinvertebrates (a) to rapid sediment deposition, (b) to exclusion of predators, and also the response of the sediment to elimination of benthic organisms.

3.11.2 Experimental Plots and Methods

Four experimental plots were established in an area 300-350 m seaward of the Barge (Fig. 3.3) at elevations of -8.07 to -8.25 m below HWST (Table 3.2). Two of the sites, a **Control** and a **Poisoned** site, were 3 x 3 m squares marked out with wooden corner stakes and roped off to restrict interference. A third 3 x 3 m site formed a **Sedimentation Enclosure**, and consisted of 2.5 m high walls constructed of 1 cm diam. reinforcing bar ('rebar') on three sides. The three seaward walls were covered with tarpauline sheets into which lunate holes had been cut to diminish resistance to wind and current. The landward side was left without a wall. The effect of the semi-enclosed volume was to reduce ebb current velocities to some extent, and therefore to induce sediment deposition on each tide. The fourth experimental plot (the **Predator Exclosure**) was a 2 x 4 m area defined by 1 cm diam. 'rebar' frames tied together and covered on all sides and the top with 1 cm mesh screening. A control enclosure of the same dimensions and construction but without the screening (called **Fish Control** to distinguish it from the open **Control** area), was established immediately adjacent to the **Predator Exclosure**. All sites were set up on 11 July 1989 (JD 192) in order to allow time for sediment disturbed during construction to recover.

Each experimental plot was provided with a pair of depth marker posts for monitoring bed level. These consisted of 1 cm diam. 'rebar' driven to the same depth in the sediment, 70 cm apart. On each visit the distance from the sediment surface to a jig mounted on the top of the two marker posts was measured using a steel tape. The jig had two liquid levels mounted at right angles to each other to ensure that it lay horizontal at the time of measurement. Sediment cores (volume 2 cm^3, area 1 cm^2) were taken for chlorophyll analysis, and macroinvertebrate populations were monitored using a core sampler with an area of 40.7 cm^2. Faunal samples were sieved through a 400 μm mesh screen. All samples were taken in triplicate and analysed separately.

3.11.3 Effects of En-/Exclosures

All enclosure/exclosure structures in an intertidal zone present problems because of their pleiotropic effect on environmental processes. It was expected that each enclosure would induce some additional deposition of sediment, and consequently, bed level was monitored in each area. For reasons outlined below, the Sedimentation Enclosure was not effectively monitored; results of bed level measurements on the other experimental plots are shown in Figure 3.75, expressed as changes in bed level relative to that on the day of establishment (JD 192).

During the first week (JD 192-199), bed level on the Control plot was lowered approximately 11 mm; it then began to rise, gaining 7 mm during the next week, before losing another 6 mm between JD 206 and 211. When measured on 2 August (JD 214) it had begun to rise again. This oscillation in bed level, although measured only at a single point, is similar to results obtained in the previous study (Amos et al. 1988). It is apparently not a response to increased current velocities during spring tides, because it is out of phase : the initial loss occurred during neap tides, the accretionary phase over the springs (JD 199-206), and the next losses over the subsequent

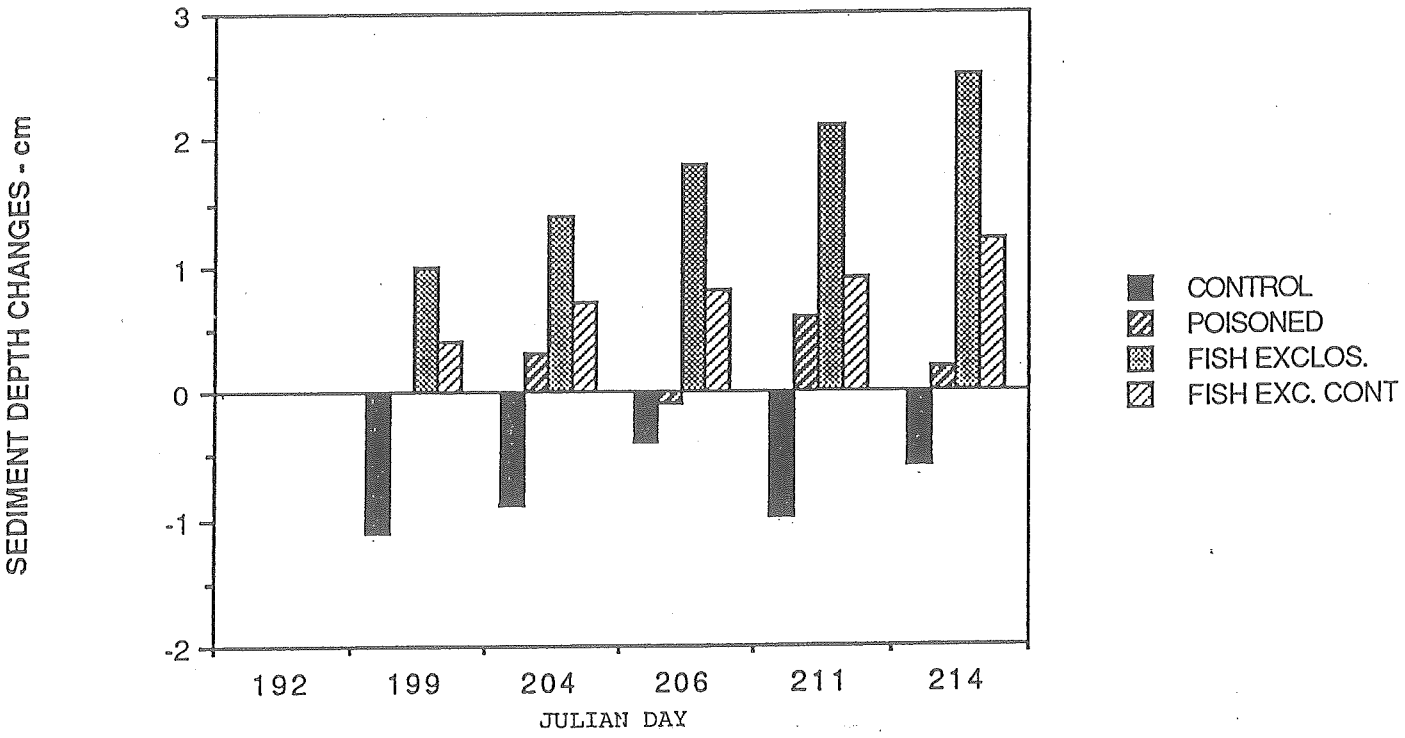

Figure 3.75. Relative changes in bed level in experimental plots following establishment on day 192.

neaps (cf. Fig. 3.5). Nor does wind velocity provide an adequate explanation : although winds were persistently strong between 27 and 31 July (JD 208-212) when bed level decreased, it was very calm during initial measurements when similar losses occurred (cf. Fig. 3.69). It is possible that bed level does oscillate as a result of tidal forcing, as with coarser sediments such as sands, but that this effect is not visible in these clay-containing silts because of a smaller vertical scale and extensive bioturbation. Alternatively, the accretion events might be related to increased sediment mobilization during spring tides, although this would not explain the accelerated erosion on the neaps, nor the lack of phase between the Control and Poisoned plots. Observations on the Poisoned plot showed that these silts quickly develop rippled features when biological processes are interrupted, indicating once again that bioturbation and biocohesion represent critical factors influencing sediment properties.

The Poisoned plot exhibited similar oscillations in bed level, although these were precisely out of phase with the Control plot (Fig. 3.75), and thus were more in phase with the spring-neap cycle. The dramatic effects of poisoning are described below.

Bed levels in the Predator Exclosure and its control (Fish Control) both rose steadily during the experiment, the unscreened Fish Control plot accumulating 12 mm by 2 August, and the screened exclosure 25 mm (Fig. 3.75). There was no comparable oscillation of bed level in these two plots as in the open plots, perhaps because of their construction : both exclosures were surrounded by wooden foot boards approximately 5 cm thick, installed to prevent disturbance of the plot during sampling. These would have prevented any bedload movement that was occurring on the flat itself from affecting these experimental areas. Screening to exclude fish and other predators resulted in greater sediment deposition. As indicated below, this induced sedimentation in itself is unlikely to have had significant effects upon the fauna, although the lower light intensity within the screened area may have had a variety of effects on both the benthic flora and fauna.

Sediment samples from the experimental plots were analysed for photopigments on each sample day to determine whether there were distinct effects on the primary producers. Results are shown in Figure 3.76A and B. Each value shown is a mean of three samples. There are no obvious patterns in these results, although chlorophyll concentrations in control areas analysed for other projects were significantly higher toward the end of July.

3.11.4 Sedimentation Experiment

The objective of this experiment was to examine the effects of relatively rapid sediment deposition on : (a) the properties of the surface sediment, and (b) the fauna of the tidal flat. It was hypothesised that :

(1) Rapid sedimentation would eliminate the macrofauna at first. Subsequent faunal development would be dominated by *Corophium volutator*, which is a good coloniser of disturbed sediments.
(2) Rapid sedimentation will prevent effective diatom growth and productivity, leading to declines in surface chlorophyll. When sediment stabilises, and before the return of *Corophium*, diatom abundance and

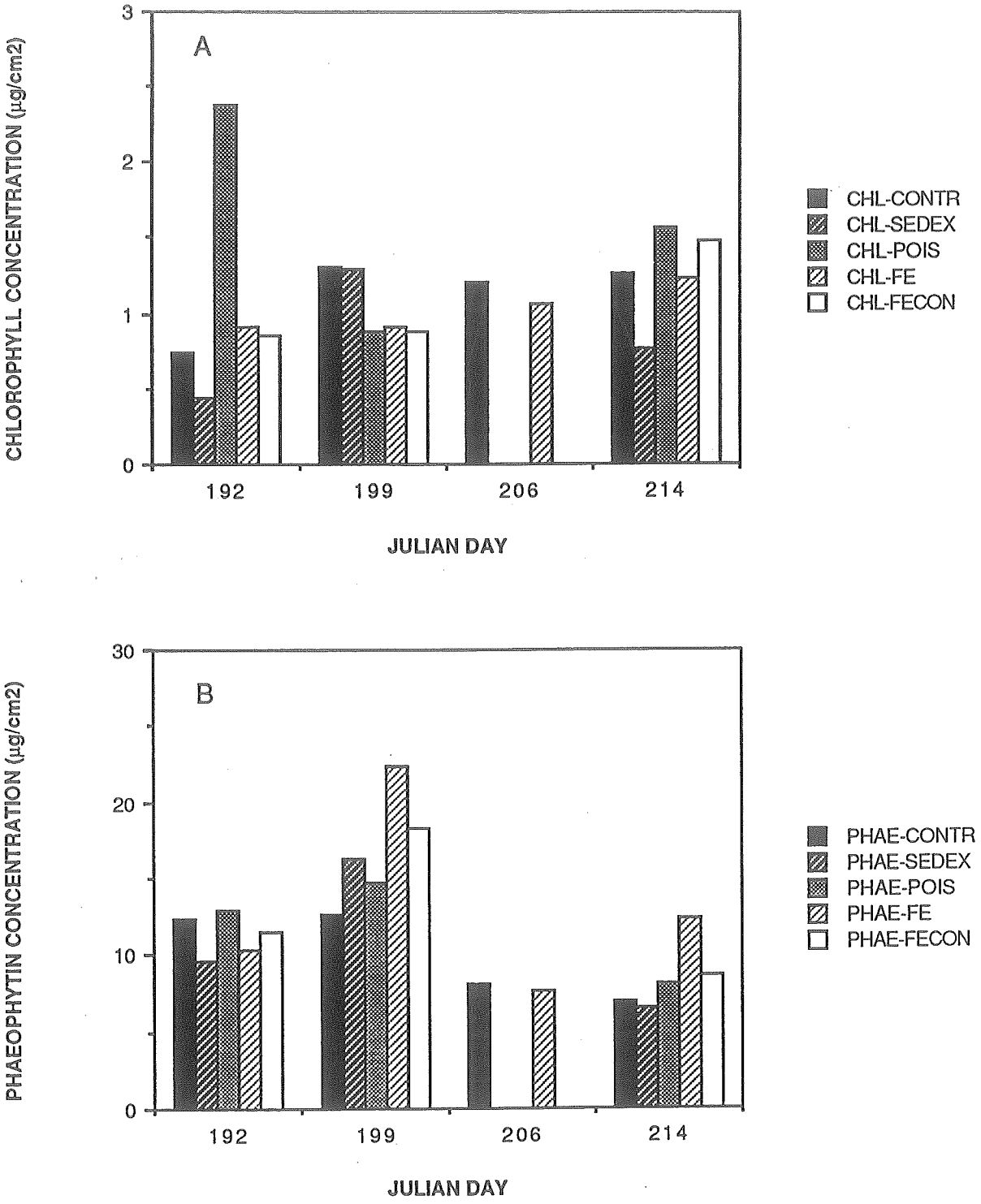

Figure 3.76. Chlorophyll and phaeophytin concentrations in experimental plots. Each value is the mean of 3 replicate samples.

hence chlorophyll levels should increase; when the *Corophium* were reestablished, diatom populations should be reduced below the level of the Control plot.

(3) Absence of bioturbation during the initial accretionary phase should lead to an increase in the fine sediment fraction of surface sediments.

The Sedimentation Enclosure (SEDEX) was set up on 11 July 1989 (JD192) and allowed to continue for 31 days (60 tides). During this time, the tarpauline walls induced a substantial, but uneven deposition of sediment; accretion was considerable in the middle of the plot, but each wall also caused accelerated erosion along the base, and at the corners. Consequently, the initially level plot was converted through time into a mound in which the centre was at least 20 cm above the original level, while the periphery was 5-10 cm below. Unfortunately, the depth marker posts installed to monitor accumulation were established on what became the slope of the mound, and by 2 August continued erosion along one wall had caused one of the posts to move. The depth measurements were therefore considered invalid, and are not shown on Figure 3.75.

Observations during the course of the experiment suggested that deposition of new sediment had an initial effect on all fauna, and the varying conditions within the enclosure were reflected in differences in the degree of bioturbation. For example, on 23 July (JD 204, 13 days after set up) it was noted that the slopes of the mound were heavily bioturbated like the Control plot, with numerous *Corophium* holes apparent and numbers of *Corophium* crawling about. On top of the mound, however, the sediment was relatively smooth and slightly rippled, and although *Corophium* trails were also evident here, there were no burrows visible. By 30 July (JD 211) *Corophium* holes were abundant all over the surface, and many *Corophium* were seen crawling about (albeit very slowly because of the low air temperature on that date). Although at this time *Corophium* abundance was declining over the mudflat as a whole, it was noticeable that relatively large numbers of animals were visible at the surface within and around the SEDEX, where no bird footprints were seen. This reinforces the interpretation of the observations that with the arrival of migratory shorebirds, visible *Corophium* activity at the surface was much decreased.

Numbers of *Corophium* and polychaetes (mostly *Heteromastus*) during the sedimentation experiment are shown in Figure 3.77A and B. Values shown are means of three samples; estimated abundance per m^2 can be obtained by multiplying the mean value by 245.6. Values for samples from the adjacent Control plot are also given. It is apparent that SEDEX *Corophium* numbers were not significantly different from those in the Control area (Fig. 3.77A), either on any given date, or for all dates combined (Wilcoxon Paired Sample Tests, $T' = 4$, $p > 0.05$). In contrast, polychaete numbers were lower in SEDEX than the Control for all days except 30 July (JD 211), although high between-sample variability in polychaete numbers resulted in these daily differences also being non-significant, except for 25 July (JD 206). Overall, polychaete abundance was significantly lower than that in the Control plot (Wilcoxon Paired Sample Test, $T' = 12$, $p < 0.05$).

These data indicate that whereas *Corophium* was unaffected by the rate of new sediment accumulating in the enclosure, polychaetes were negatively affected. Thus, the first hypothesis is rejected with regard to *Corophium*, but accepted for the polychaetes. A possible secondary effect, that sediment deposition might have

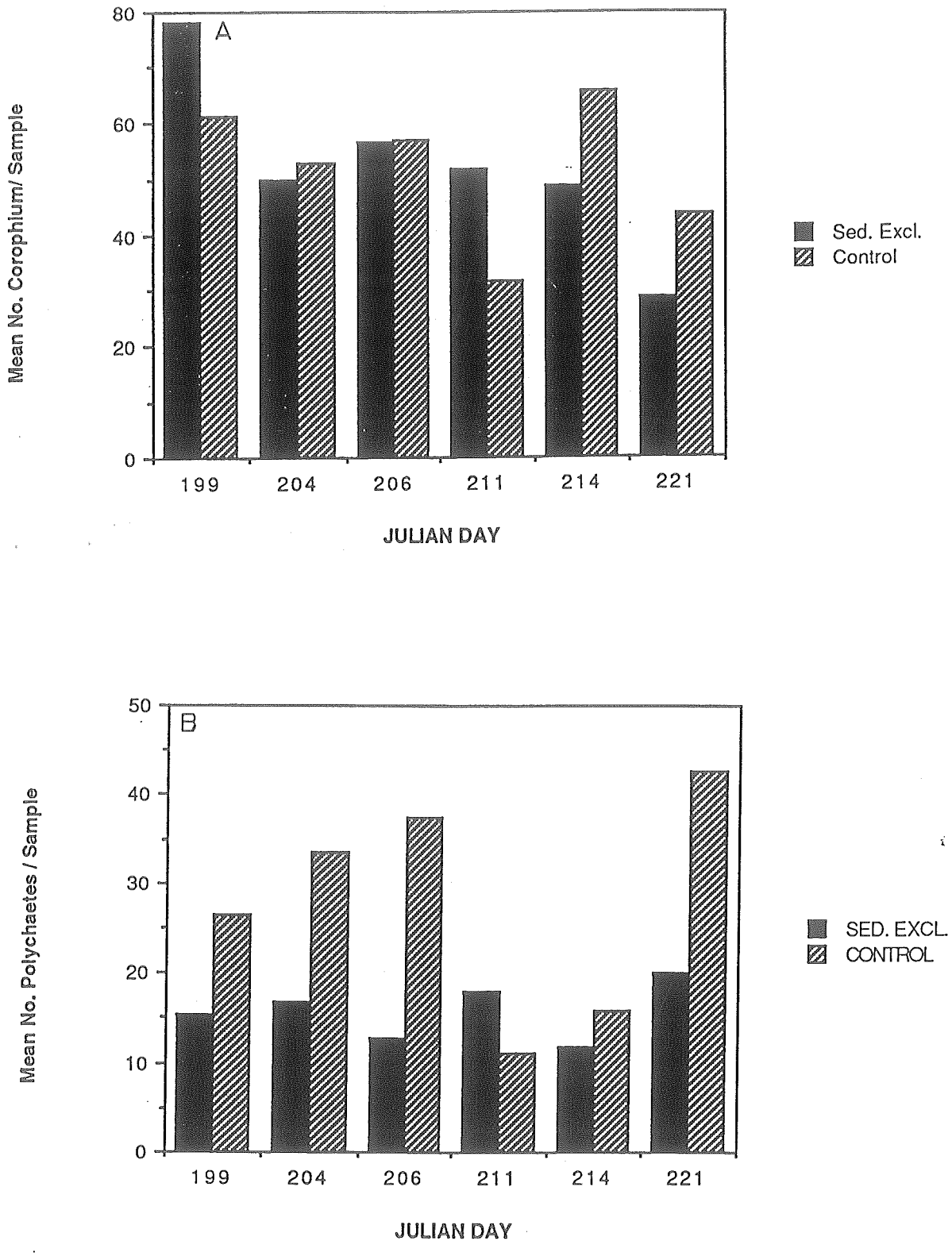

Figure 3.77. Mean number of A *Corophium*, B polychaetes in sediment enclosure and control plot during LISP experiment. Each mean is an average of 3 replicate samples.

differential effects on *Corophium* of different ages or sizes, was examined through comparison of length-frequency distributions in the SEDEX and Control plots. Distributions are shown in Figure 3.78A-F.

Length-frequency distributions were bimodal throughout the study, with modes at 3-5 and 7-9 mm representing the two principal cohorts of the year (cf. Gratto 1979; McCurdy 1979; Boates 1980). There appears to be no significant difference between the patterns of distribution in the SEDEX and Control plots during the first two weeks of the study (JD 199-211), indicating that none of the *Corophium* size classes were negatively affected by the rapid deposition of new sediment. In August (JD 214-221), however, the larger cohort (>7 mm) declined in prominence, especially in the Control (Fig. 3.78E, F). This was probably a consequence of increased mortality associated with the arrival of migratory shorebirds.

On the basis of these results, it may be concluded that *Corophium* of all sizes are tolerant of sediment deposition at rates such as those induced by the sedimentation enclosure. Polychaetes, however, are less tolerant. These conclusions are significant in relation to the effects of the Predator Exclosure and Fish Control site.

3.11.5 Poisoning Experiment

The objective of this experiment was to examine the effects on sediment characteristics of terminating biological processes by a one-time application of a biocide, and allowing the treated area to recover. Previous observations showed that repeated biweekly poisoning of plots on this tidal flat resulted in colonisation of the plots by *Corophium* after about a week and a half, with consequent reduction in benthic diatom production (Daborn - unpublished data). In this experiment we were interested in determining the role of biological processes in influencing surficial sediment features, and also the process of recovery following poisoning. The experimental area was treated with 4 L of 100% formalin solution on the evening of 18 July (JD 199), just after sampling for that day. Observations of sediment features and sampling for biological parameters were carried out at intervals during the next three weeks as with the SEDEX and Control plots. For this portion of the study, the nearby Control plot was considered an appropriate reference for both the SEDEX and Poisoned sites.

On the morning of 22 July, just seven tides following treatment, the Poisoned site had a strongly rippled surface that easily distinguished it from the bioturbated surface that was characteristic of the site before treatment and typical of the rest of the surrounding mudflat (Fig. 3.79A, B). The only evidence of biological activity were trails of *Corophium* individuals that had entered the treated area from the surrounding flat and then moved in a spiral pattern as they attempted to escape the residual toxin retained within the sediment; such animals generally died within the Poisoned plot. The ripples were prominent, 3-5 mm high, and oriented in the flood direction, and the troughs commonly contained finer sediment that had presumably settled during the last phase of the previous ebb. By the next day (23 July, JD 204), *Corophium* trails originating outside the treatment area, and extending inward were usually more or less straight, several of them were still being made by wandering *Corophium* which showed no obvious signs of distress, and there were few signs of the spiral trails that I assume are associated with dying animals. It may be concluded that by this time (nine tides), almost all of the formalin had been washed out of the surface sediments, although some probably remained at greater depth. On the

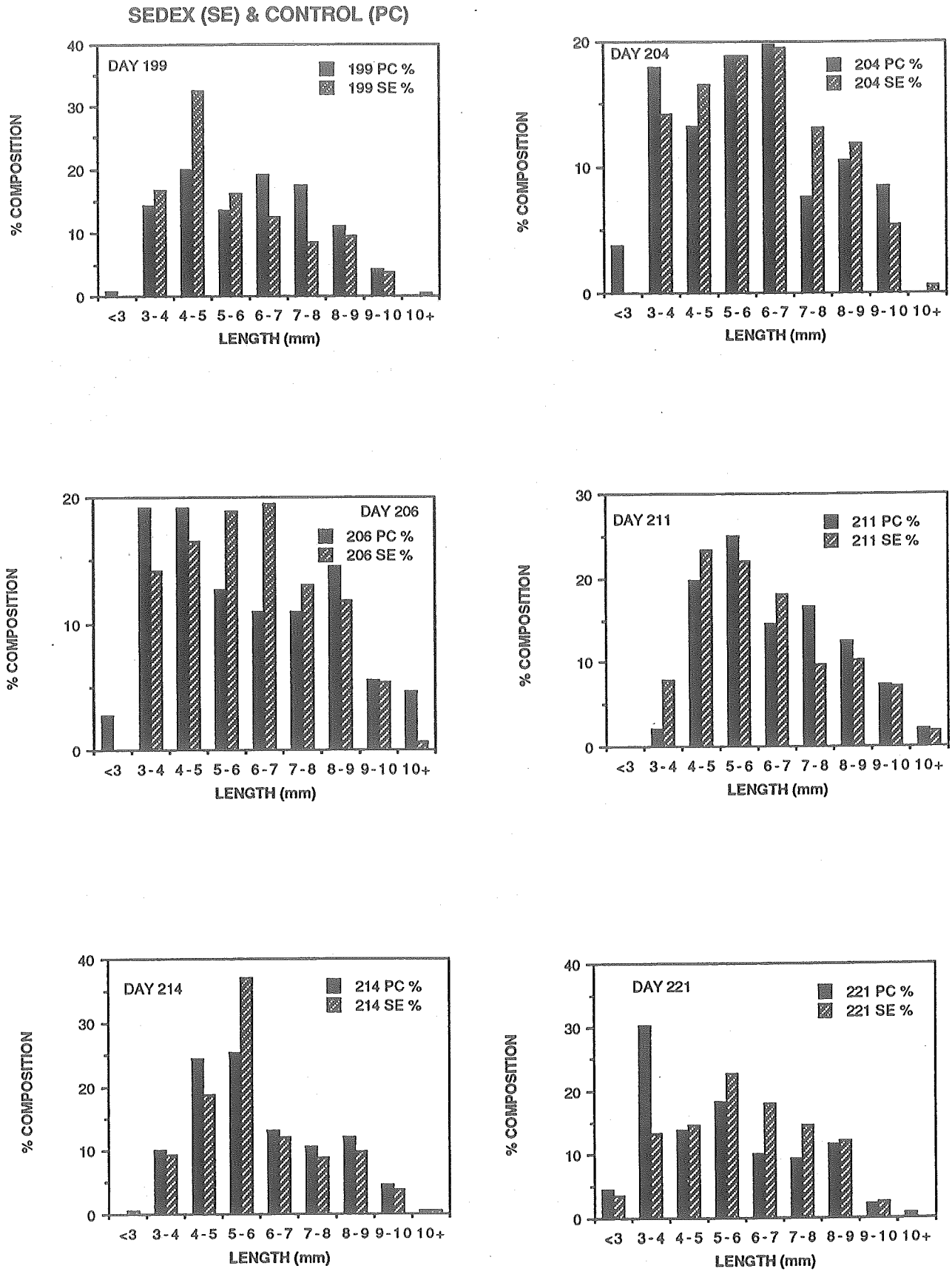

Figure 3.78. Length frequency distributions of *Corophium volutator* in Sediment Enclosure (SE) and Control Plot (PC) during LISP experiment.

BIOTURBATED SURFACE (Control)

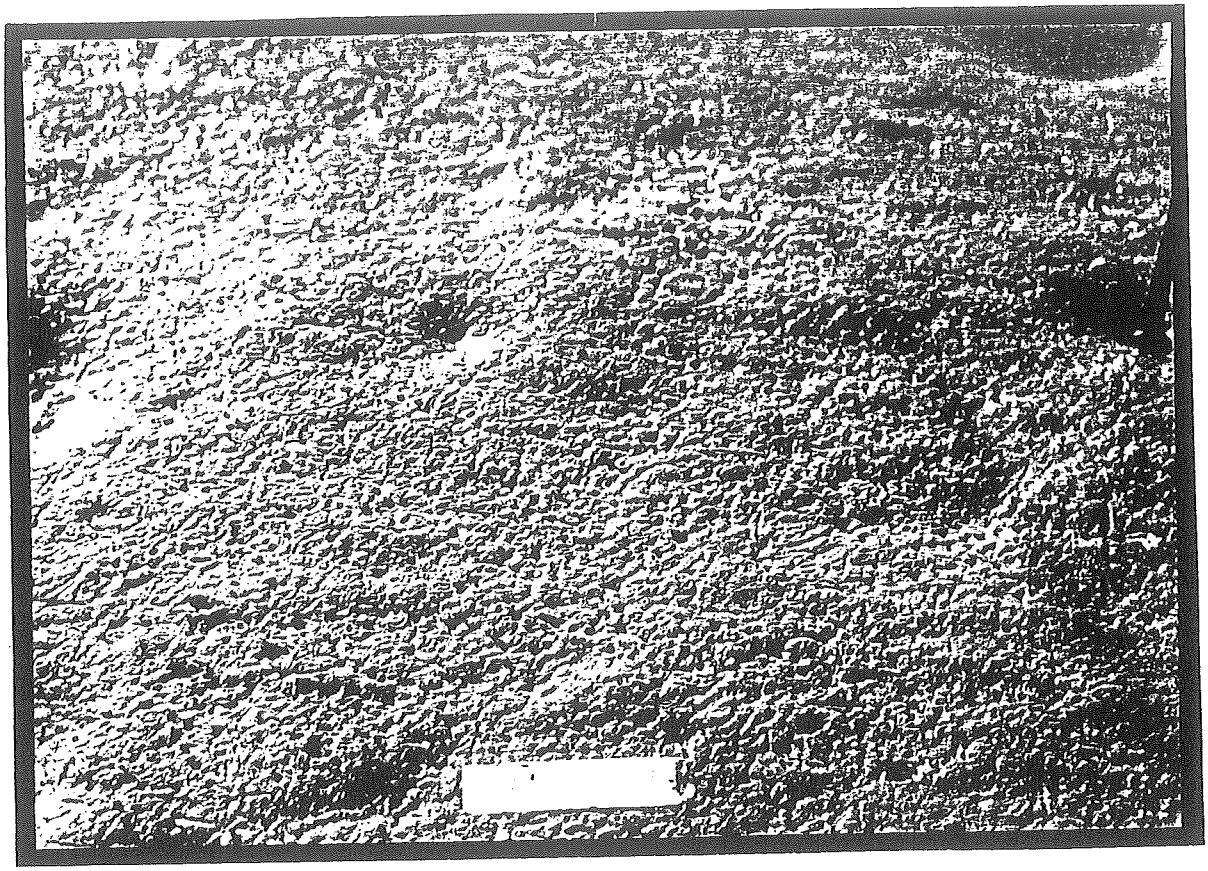

SURFACE FOLLOWING POISONING

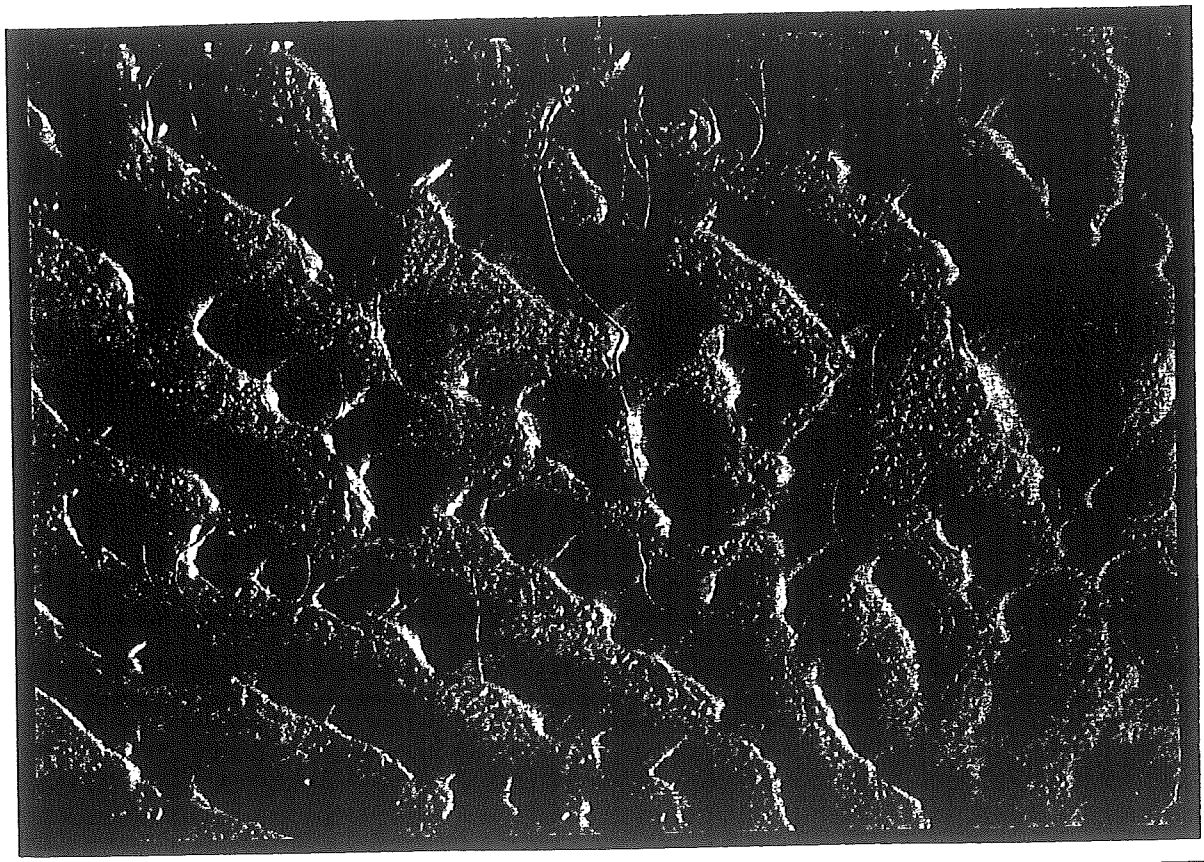

Figure 3.79. Effects of poisoning on sediment surface. A - Typical bioturbated surface. B - Surface 2 days (4 tides) after treatment with 100% formalin.

remaining sample days, the ripples gradually disappeared as the surface became more completely bioturbated. By 30 July (JD 211), *Corophium* burrows were numerous (although few *Corophium* were seen at the surface), the ripples were not visible, and the whole treated area bore the imprint of many shorebird feet, just as in the Control area and the surrounding flat.

Core samples showed that the treatment eliminated both *Corophium* (Fig. 3.80A) and polychaetes (Fig. 3.80B) from the site for the ensuing week. The few animals recovered from samples on days 204 and 206 were probably dead upon collection, but since the samples were fixed prior to screening and sorting, it is not possible to be sure. *Corophium* numbers began to recover by day 211 (12 days after treatment), by which time there was no significant difference in abundance between the Poisoned site and the Control ($t = -2.438$, $p > 0.05$), and by the end of the study numbers of *Corophium* in the treated site were comparable with those in the Control. Polychaete numbers, however, continued to decline in the treated site for the remainder of the experiment. It is not clear whether the continued decline in polychaete abundance in the samples resulted from progressive mortality of deeper-lying worms (i.e., that deeper sediments remained toxic during the study), or whether the worms were killed shortly after treatment, and the decline in numbers relate more to their removal from the sediment as it was recolonised and bioturbated by *Corophium*. It is apparent that there was no effective recolonisation by the polychaetes during this time.

Size-frequency distributions of *Corophium* were examined to ascertain whether recolonisation was effected by specific size groups. Results are shown in Figure 3.81A-F. In general, the bimodal size distribution that prevailed at the beginning of the study persisted in both treated and control plots throughout, although there was a slight preponderance of the larger size classes in the Poisoned plot on JD 204 and 206 (Fig. 3.81B, C). On these two days, evidence of invasion by potential colonists was visible on the site, and it may be that the larger animals persisted longer in what was still apparently an inhospitable environment. It must also be remembered that the very low numbers in these samples mean that size frequency distributions are excessively influenced by the presence of a few individuals in a given size class. During subsequent days there was no significant difference in size frequency distribution between the treated and untreated plots. There seems to be no evidence in these results that recolonisation of disturbed habitat is primarily effected by *Corophium* of a particular size range; however, it might be that the experimental plots were too small relative to the dispersal powers of *Corophium* (which might still be size-related) for such an effect to be seen.

3.11.6 Predator Exclusion Experiment

The Predator Exclosure (Fish Exclosure - FE) and its Control (FEC) were established on day 192, together with other major structures. As shown in Figure 3.75, the screening over the Predator Exclosure resulted in a steady accumulation of sediment inside, reaching 2.5 cm by the end of the experiment. Without the screening, FEC accumulated approximately half of that amount.

Abundances of *Corophium* and polychaetes during the experiment are shown in Figure 3.82A and B; no sample was taken in the Predator Exclosure (FE) on JD 214 in order not to interfere with a DCMU experiment

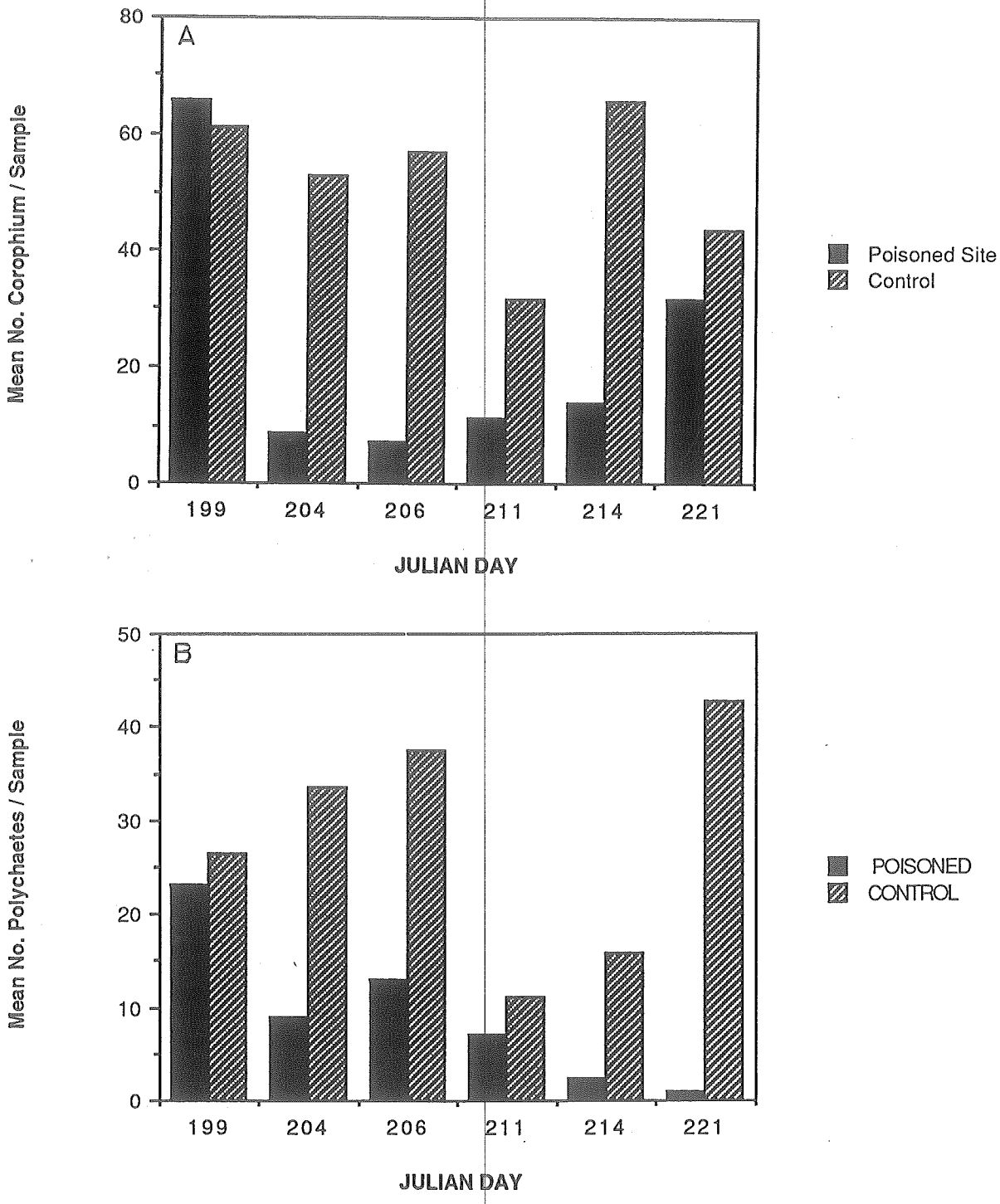

Figure 3.80. Abundance of A *Corophium*, B polychaetes in a plot poisoned with formalin on day 199, and an unpoisoned control plot. Each value is a mean of 3 replicate samples.

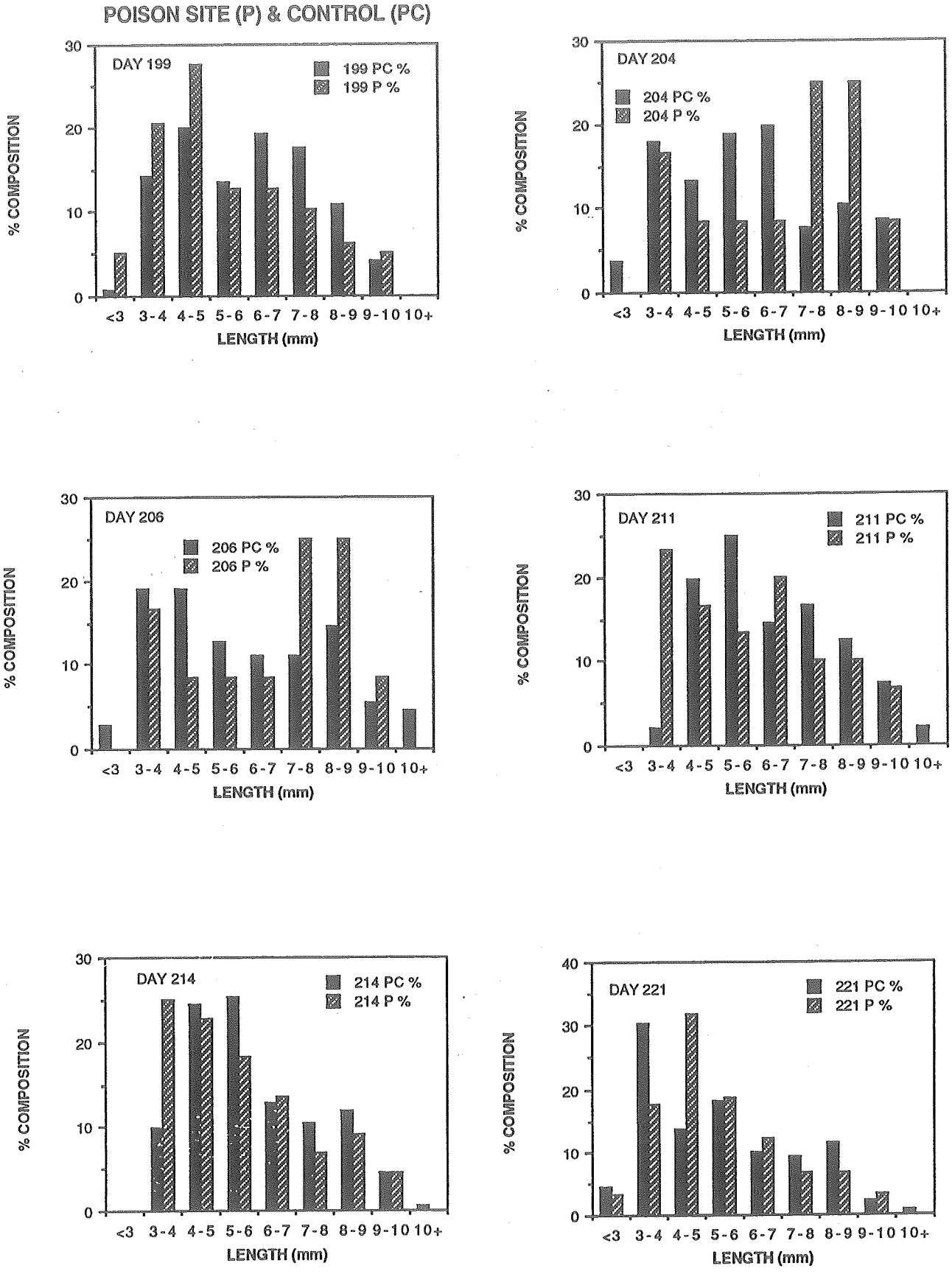

Figure 3.81. Length frequency distributions of *Corophium volutator* in plot poisoned with 100% formalin (P) and a control plot (PC) during LISP experiment.

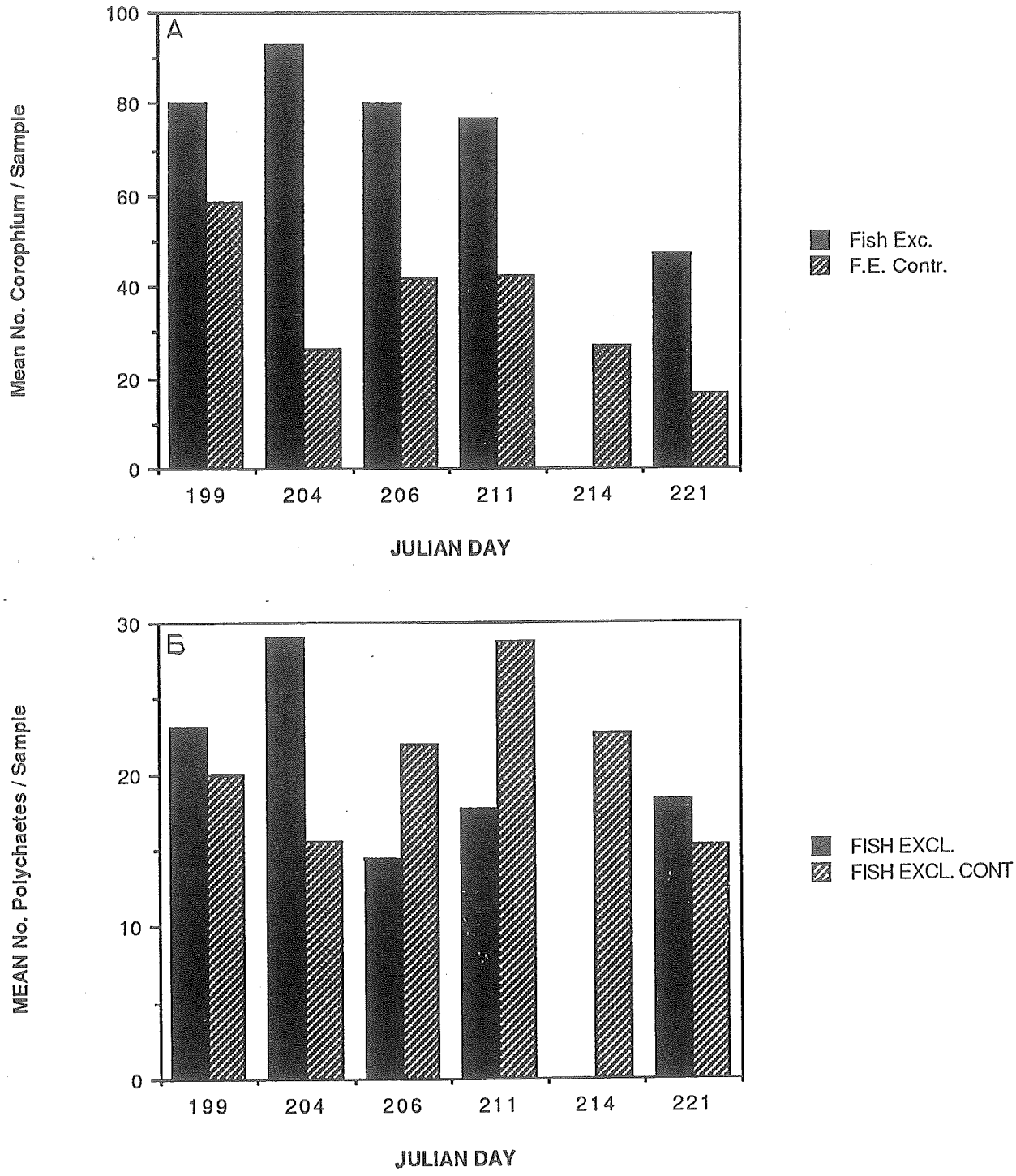

Figure 3.82. Abundance of A *Corophium volutator* and B polychaetes in the predator exclosure (Fish Excl.) and an adjacent control plot (F.E. Contr.). Each value is a mean based on 3 replicate samples.

in that cage being conducted by M. Brylinsky. Results of the exclosure study seem at first sight to show that *Corophium* numbers remained higher in the Exclosure than in the Control, and that polychaete abundance remained approximately the same in the two cages. Overall, *Corophium* were consistently more abundant in the Exclosure (80.3 per sample ± 64.1) than in the FEC (58.7 ± 12.4), although sample variation was so high that paired t-tests conducted on the combined data and separately for each date were all non-significant. It is apparent that the induced sedimentation had little or no detrimental effect on the abundance of *Corophium* (as indicated in SEDEX); the maintenance of relatively high numbers in FE, however, supports the overall assumption that predatory fish and birds are responsible for a steady decline in numbers over the mid-summer period, which is evident when all samples taken from control and other non-experimental areas are combined (Fig. 3.83).

The size-frequency distributions of *Corophium* in the FE and FEC were examined in order to determine whether any effects of the exclosure were size-specific. Results are shown in Figure 3.84A-E. The bimodal pattern of distribution is the same in each cage except that on JD 199 and 204 the lower mode at 4-6 mm was more strongly represented in the FE than the FEC, and the larger individuals were less common. T-tests show that mean size was significantly lower in the FE on these two days ($p < 0.01$), and although mean sizes on subsequent days were not statistically different they were consistently lower in the FE than the FEC. There is little obvious explanation for this effect.

3.11.7 Fish Utilisation of the Tidal Flat

Turbid macrotidal estuaries such as the Southern Bight of Minas Basin are visited by a wide array of fish, some resident, and others migratory (Bleakney and McAllister 1973). The potential impact of these mobile predators on deposited sediments is varied : many of the species prey upon dominant benthic animals such as *Corophium* (Imrie and Daborn 1981; Gilmurray and Daborn 1981; Stone and Daborn 1987), and in so doing leave distinct feeding traces (Cook 1971; Risk and Craig 1976). Other marks arise, particularly from flounder which may bury themselves in the bottom when disturbed (Cook 1971; Stanley 1971). Consequently, extensive utilisation of the tidal flat by bottom-feeding fish may have both direct and indirect effects upon sediment stability. For this reason, a fish trap was erected in a tidal channel northeast of the Barge (cf. Fig. 3.3) to monitor the fish fauna visiting that area of the tidal flat.

The trap consisted of a 1 m x 1.3 m x 1.3 m 'rebar' frame covered with a smelt net having 1 cm mesh. Wings of the same mesh were constructed on either side of the trap, up the sides of the channel, in order to funnel fish through the trap. The seaward side of the frame was built with a panel which could be removed when sampling was not desired, allowing fish to move freely through the trap on both rising and falling tides. During sampling, a collecting bag was attached to the seaward side of the frame prior to the flood tide reaching the trap site, so that fish would be captured as they attempted to leave the flat during the next ebb. Sampling was carried out on nine occasions between 7 July and 4 August; on 22 and 24 July and 3-4 August, both nighttime and daytime ebb tides were sampled in order to provide an indication of any diel periodicity in fish visiting the flat. Subsamples of the four most abundant fish species were taken for analysis of food in the digestive tract.

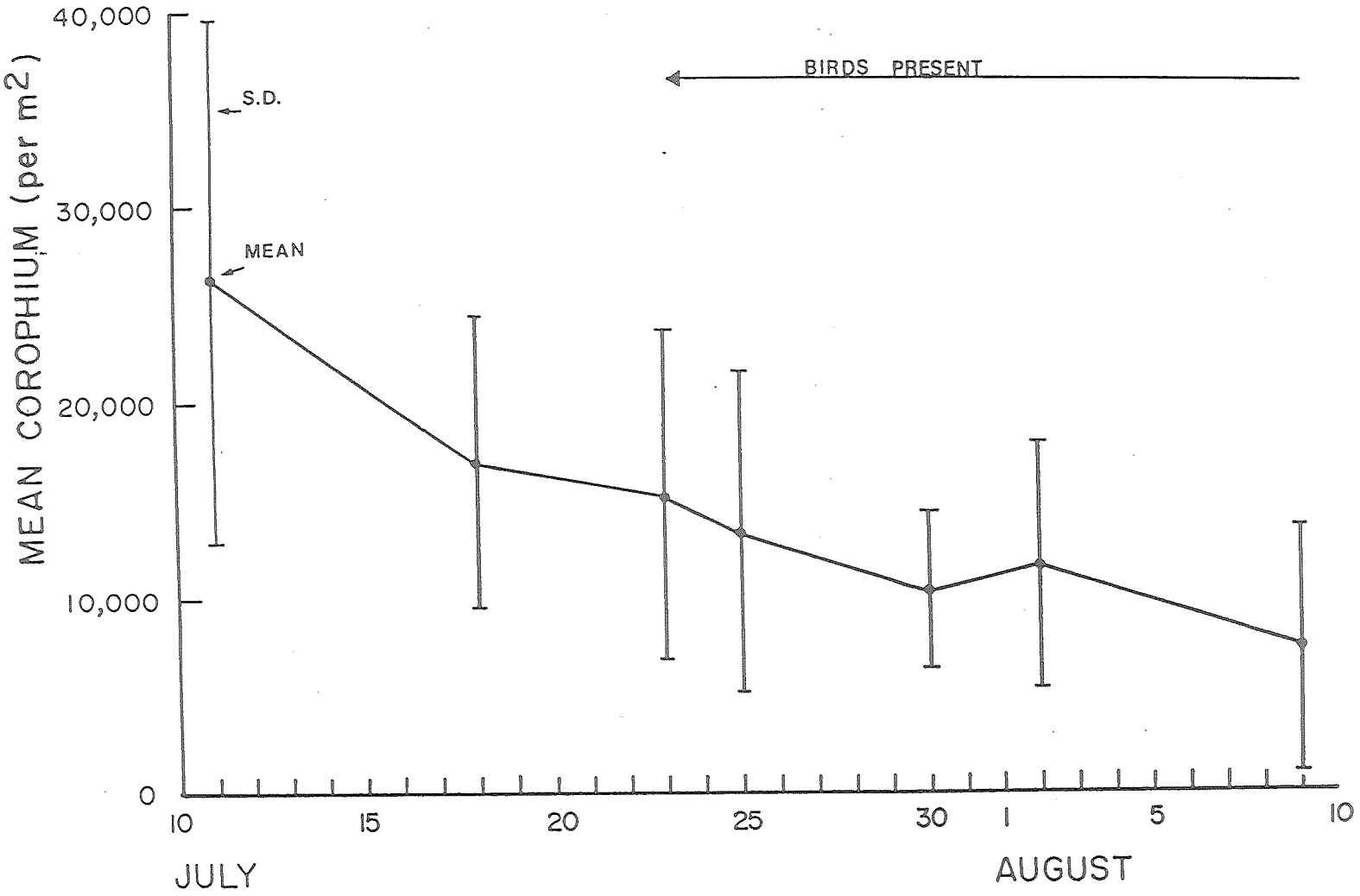

Figure 3.83. Changes in abundance of *Corophium volutator* on Starrs Point flat during the LISP experiment. Mean based on all samples taken from non-experimental areas of the flat. (N>6)

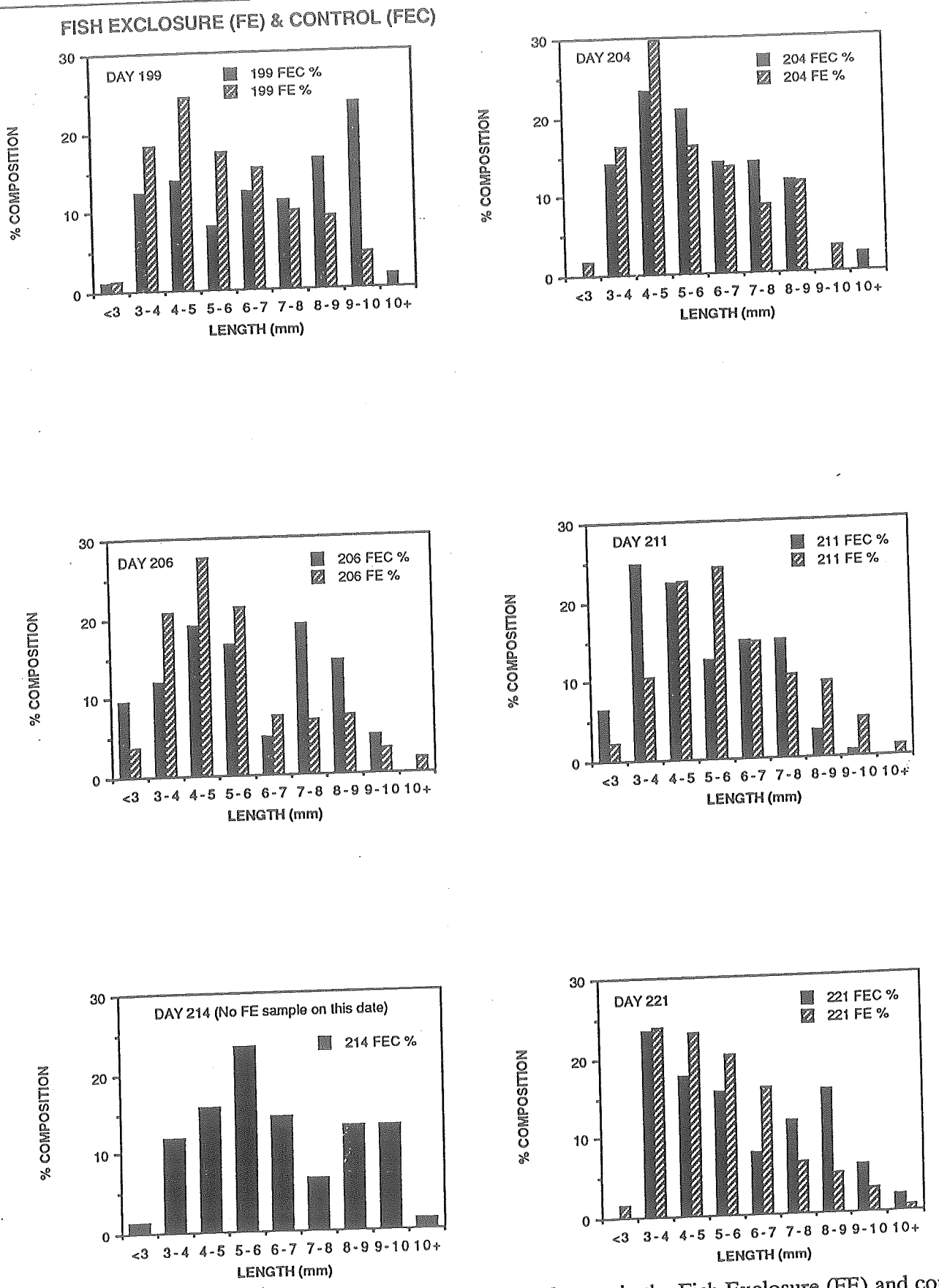

Figure 3.84. Length frequency distributions of *Corophium volutator* in the Fish Exclosure (FE) and control plot (FEC) during LISP experiment.

A list of all species captured or observed in the area is given in Table 3.12; Table 3.13 records the principal species captured on each date.

The most abundant fish visiting the flat were the smooth flounder, tomcod and smelt. Although the results are subject to considerable error because of the large number of different observers used, it is apparent that larger numbers of fish were recorded following a nighttime tide than during the daytime. This may well be related to avoidance of visual predators. When fish removed from the trap, especially adult flounder, were preserved for gut analysis rather than released as was usual, it was apparent that fewer were caught on subsequent sample dates. This suggests that individuals may be rather resident in tidal channels, so that the same fish are caught repeatedly.

Gut analysis showed that all fish collected in the trap appear to be utilising *Corophium* to a considerable extent. Results of gut analyses for four species are shown in Figure 3.85. It is apparent that almost all fish arriving on the flat eat *Corophium*, and thus may be collectively responsible for the decline in *Corophium* abundance during the summer months. This conforms with previous studies which indicate that *Corophium* is the most important invertebrate prey species occupying the intertidal zone of Starrs Point.

3.11.8 Conclusions

These studies collectively provide insight into the relationships on the tidal flat that have significance for the stability of the sediment surface. It is clear that animal activity, particularly the mate-seeking and foraging behaviour of the tubicolous amphipod *Corophium volutator*, and the foraging activities of birds and fish, may increase the roughness of the surface, and thereby increase its susceptibility to erosion. In addition, by controlling the growth of diatoms, *Corophium* probably decreases the enhancement of cohesion related to mucopolysaccharides secreted by the diatoms. The combined effect is to increase sediment erodibility. When the number of *Corophium* at the sediment surface decreases as a result of predation, or a change in *Corophium* behaviour, biogenic enhancement of surficial cohesion increases. This appears to be the evident in the change in sediment friction angle (cf. Table 3.9), the increased cohesion buildup (Fig. 3.6a), and the increases in critical erosion velocity (Fig. 3.62), water content (Fig. 3.62), sediment chlorophyll (Fig. 3.65), and carbohydrate (Fig. 3.66), that occurred towards the end of July. These changes were coincident with the arrival of large numbers of migratory shorebirds, mainly semipalmated sandpipers (*Calidris pusilla*), on or about 23 July. Unfortunately, bird numbers were not monitored during this study, but much research before (e.g., Boates and Smith 1988) and after LISP 89 has shown that with the arrival of shorebirds, the behaviour of the *Corophium* changes, as animals are not as abundant at the surface during the ebb tide as formerly. It thus seems probable that the arrival of these important benthic predators produces an effect that 'cascades' down the food chain to : (a) affect *Corophium* behaviour; (b) decrease grazing pressure on diatoms; (c) increase mucopolysaccharide production; (d) increase surficial cohesion; (e) increase water content; and (f) decrease erodibility (or increase critical erosion velocity).

Table 3.12. Fish Species Visiting the Starrs Point Tidal Flat

(a) Captured :		
Liopsetta putnami	smooth flounder	Adults, juveniles
Pseudopleuronectes americanus	winter flounder	Adult (1 only)
Microgadus tomcod	tomcod	Juveniles
*Alosa pseudoharengus**	alewife	Juveniles
*Alosa aestivalis**	blueback herring	Juveniles
Raja erinacea	little skate	Adults
Osmerus mordax	rainbow smelt	Adults and larvae
Menidia menidia	Atlantic silverside	Larvae
(b) Observed only :		
Squalus acanthias	spiny dogfish	Adults
Acipenser oxyrhynchus	Atlantic sturgeon	Adults

*Juveniles not separately identified, but combined as 'gaspereau'.

Table 3.13. Fish Captured in the Starrs Point Trap

Date	*Liopsetta*	*Microgadus*	*Osmerus*	*Alosa*
July 17	>50	~50	~40	
20	12 A	24	2	~50 J
22 (night)	11 A		1	15 J
22 (day)	6 A			
24 (day)	4 A	10	1	7 J
24 (night)	5 A	9		53 J
Aug. 3	18 A	1	3	~50 J
4 (day)	5 J			
4 (night)	7 A	2		20 J

(A = Adult; J = Juveniles)

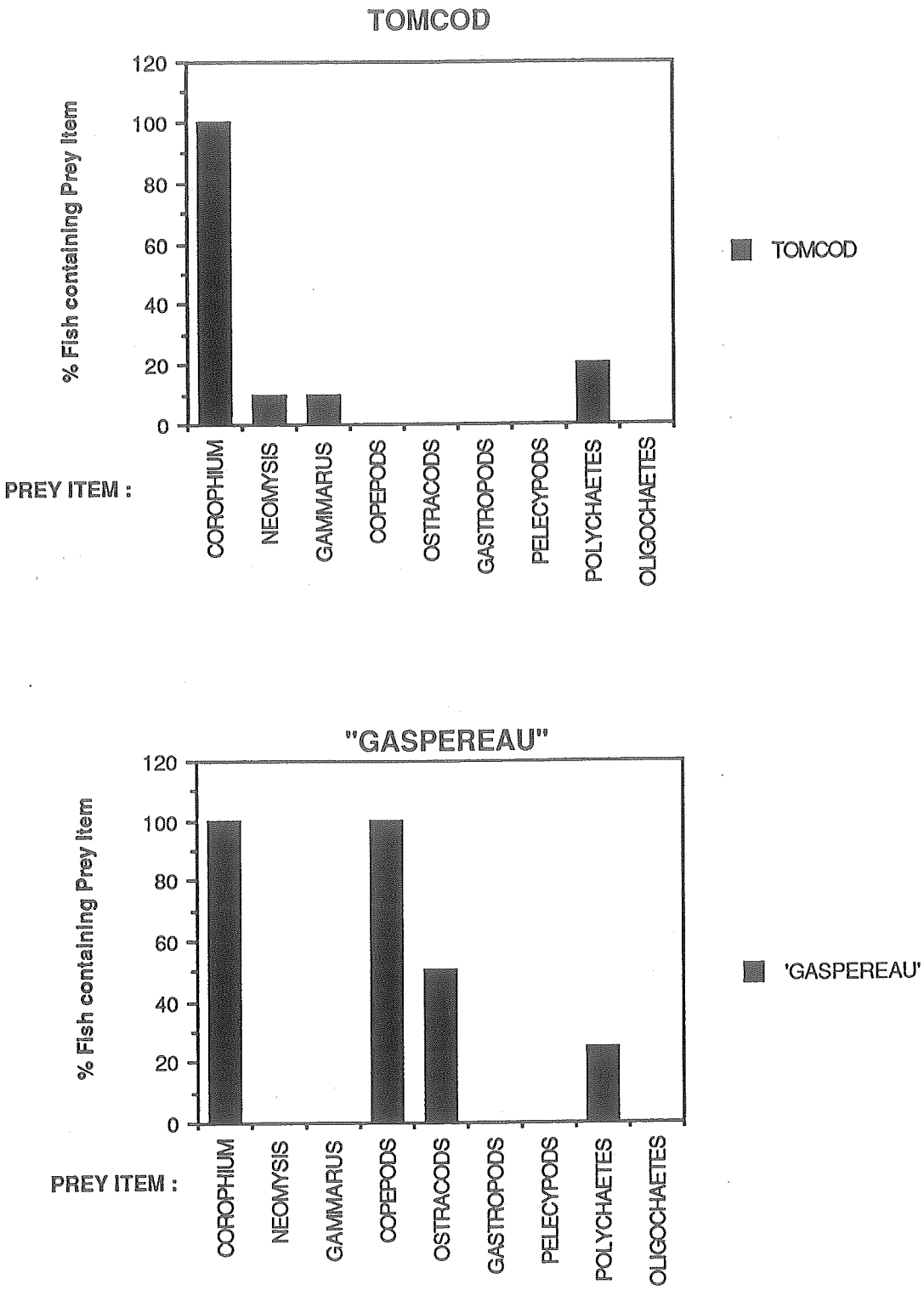

Figure 3.85. Prey utilisation by fish collected from the fish trap during LISP.

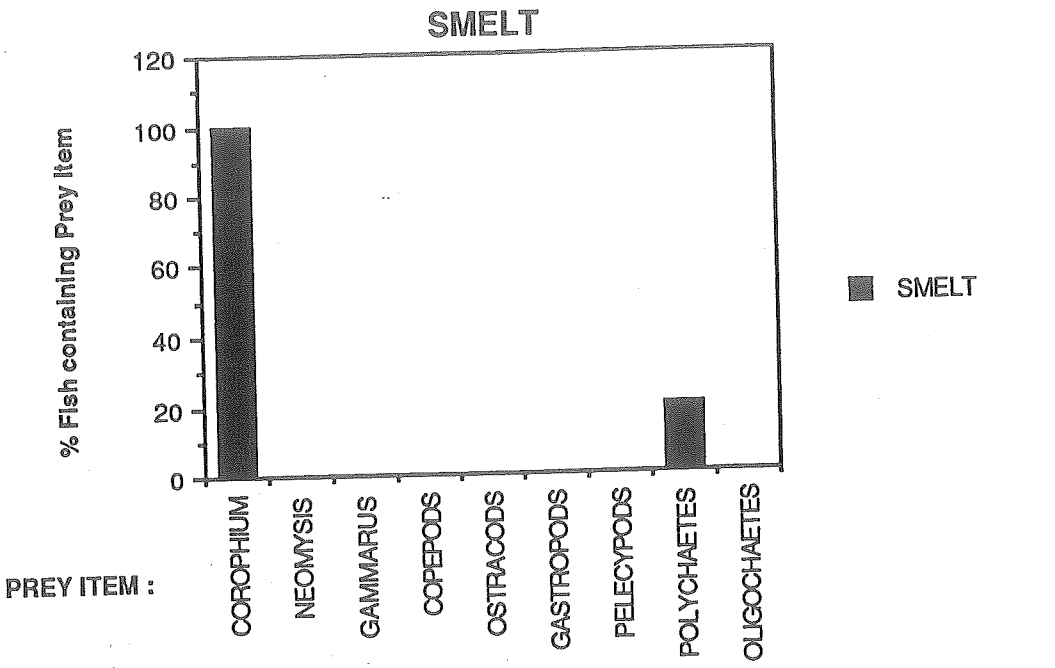

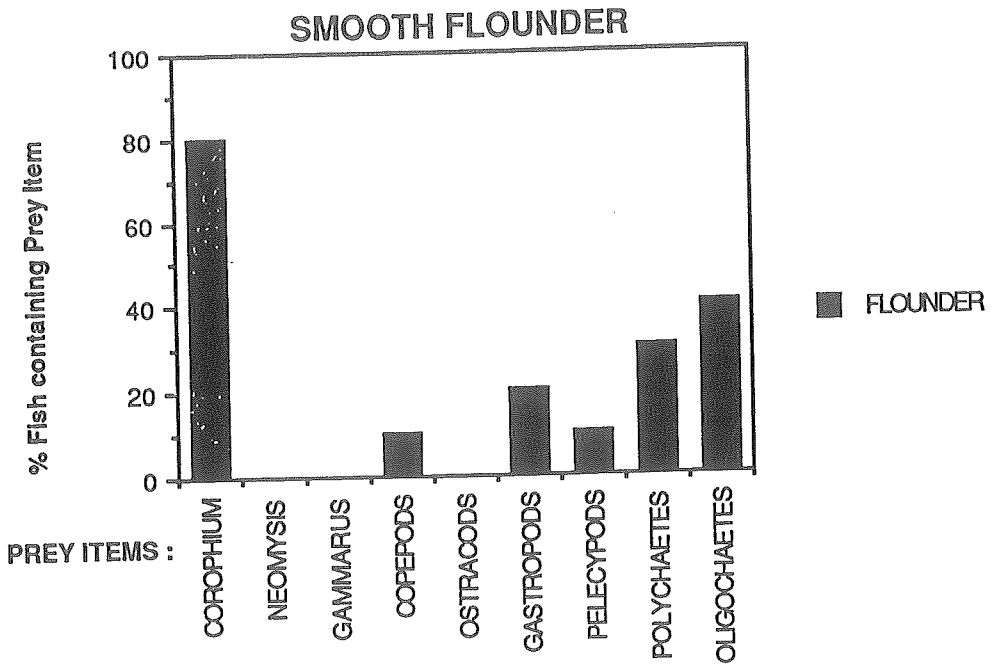

Figure 3.85 Cont.

LITTORAL INVESTIGATION OF SEDIMENT PROPERTIES (LISP)

FINAL REPORT

Part 4. PROJECT OUTPUT

Contract UP A8-001

4. Project Output

Since completion of the field phase, presentations have been made by participants to scientific gatherings in many locations. Several publications are in preparation or have been submitted to refereed journals at the present time. A list of known presentations is given below.

A. Conference Presentations

(a) Estuarine Research Federation Meeting, Baltimore, Md., October 1989

(1) Daborn, G.R., M. Brylinsky and C.L. Amos. Biotic effects on stability of macrotidal sediments.

(2) Daborn, G.R., C.L. Amos, M. Brylinsky, H. Christian, D. DeWolfe, G. Drapeau, B. Long, R.W. Faas, J. Grant, D.M. Paterson, G.E. Perillo, M.C. Piccolo and G. Yeo. LISP 89 - Investigating the dynamic properties of cohesive intertidal sediments (Poster).

(b) American Society of Limnology and Oceanography Annual Meeting, Williamsburg, Va., June 1990

(1) Amos, C.L., J. Grant and G.R. Daborn. Sea Carousel - an *in situ* benthic flume.

(2) Christian, H. and G.R. Daborn. Shear strength testing at the sediment-water interface.

(3) Daborn, G.R., C.L. Amos, M. Brylinsky, H. Christian, G. Drapeau, R.W. Faas, J. Grant, B. Long, D.M. Paterson, M.C. Piccolo, G.E. Perillo and G. Yeo. Sediment dynamics in turbid macrotidal estuaries : the multidisciplinary approach.

(c) International Association of Sedimentology 13th Congress, Nottingham, U.K., August 1990

(1) Faas, R.W. Interaction between adjacent sedimentary environments in a high macrotidal situation, Minas Basin, Bay of Fundy.

(2) Daborn, G.R., C.L. Amos, M. Brylinsky, H. Christian, J. Grant and D.M. Paterson. Influence of biological phenomena on erodibility of fine-grained intertidal sediments in a macrotidal estuary.

(3) Amos, C.L., G.R. Daborn and J. Grant. Results of the measurement of mudflat erosion using an *in situ* benthic flume, Minas Basin, Bay of Fundy.

(4) Christian, H., D. Gillespie and C.L. Amos. Results of a new device to measure the *in situ* shear strength of cohesive sediments, Minas Basin, Bay of Fundy.

(d) 16a Reunion Cientifica de Geofisica y Geodesia, Bahia Blanca, Argentina, Octubre 1990

(1) Piccolo, M.C., G.M.E. Perillo, G.Daborn y C.L. Amos. Variaciones de la temperatura en una planicie de la Bahia de Fundy, Canada.

(e) Conference on Developments in Coastal Engineering, Bristol, U.K., March 1991

(1) Paterson, D.M. and G.R. Daborn. Sediment stabilisation by biological action : significance for coastal engineering.

(2) Daborn, G.R. and D.M. Paterson. LISP-UK : Understanding the behaviour of cohesive sediments (Poster).

(f) Nearshore and Estuarine Cohesive Sediment Transport Workshop, St. Petersburg, Florida, April 1991

(1) Long, B. A new transmission nuclear gauge to monitor mud bottom.

(2) Drapeau, G. Intertidal erosion and sedimentation on a macrotidal flat.

(3) Faas, R.W. Biocyclic controls of mass property variation in surficial sediments; an example from Starrs Point mudflat, Minas Basin, Bay of Fundy.

(g) New England Estuarine Research Society Spring Meeting, Yarmouth, Nova Scotia, May 1991

(1) Daborn, G.R. Biological controls on sediment stability.

B. Other Presentations

During 1990 and 1991, C.L. Amos and G.R. Daborn gave public lectures on LISP and its results at the following institutions :

Bristol University, Cardiff University, Liverpool University, University of Hull, Reading University (Postgraduate Institute of Sedimentology), Southampton University, Polytechnic Southwest, Hydraulics Research Ltd., Wallingford, Dalhousie University, St. Francis Xavier University, Virginia Institute of Marine Science.

LITTORAL INVESTIGATION OF SEDIMENT PROPERTIES (LISP)

FINAL REPORT

Part 5. REFERENCES CITED

Contract UP A8-001

5. References cited

Allen, G.P., J.C. Salomon, P. Bassoulet, Y. DuPenhoat, and C. DeGrandpre. 1980. Effects of tides on mixing and suspended sediment transport in macrotidal estuaries. Sedimentary Geology 26 : 69-90.

Aller, R.C. 1978. Experimental studies of changes produced by deposit feeders on pore water, sediment, and overlying water chemistry. Am. J. Sci. 217 : 1185-1234.

Amos, C.L. 1977. Effects of tidal power structures on sediment transport and loading in the Bay of Fundy - Gulf of Maine system. *In* G.R. Daborn (ed.) Fundy Tidal Power and the Environment. Acadia University Institute Publication No. 28, pp. 233-253.

Amos, C.L. and G.H.E. Joice. 1977. The sediment budget of the Minas Basin, Bay of Fundy, N.S. Bedford Institute of Oceanography Data Series; BI-D-77-3. 411 p.

Amos, C.L. and D.C. Mosher. 1985. Erosion and deposition of fine-grained sediments from the Bay of Fundy. Sedimentology 32 : 815-832.

Amos, C.L., N.A. Van Wagoner, and G.R. Daborn. 1988. The influence of subaerial exposure on the bulk properties of fine-grained, intertidal sediment from Minas Basin, Bay of Fundy. Est. Coast & Shelf Sci. 27 : 1-13.

Anderson, F.E. 1983. The northern muddy intertidal : a seasonally changing source of suspended sediments to estuarine waters—a review. Can. J. Fish. Aquat. Sci. 40 (Suppl. No. 1) : 143-159.

Ariathurai, R. and K. Arulanandan. 1978. Erosion of cohesive soils. Journal of Hydraulics Division, Proceedings of American Society of Civil Engineers 104 : 279-283.

ASTM. 1990. Soil and rock; building stones; geotextiles. Annual Book of ASTM Standards, 4.08, American Society for Testing and Materials, Philadephia, 996 p.

Azmon, E. 1990. Emplacement of clay into sand by infiltration—Discussion. Journal of Sedimentary Petrology 60 : 173-174.

Black, K. 1989. The in situ measurement of sediment erodibility : a review. Unpublished Report submitted to ETSU, Department of Energy, Harwell, U.K. : 31 p.

Black, M.C. 1985. Physical and mechanical properties of estuarine sediments, Minas Basin, Bay of Fundy. Unpublished B.Sc. thesis, Acadia University, Wolfville, N.S.

Bleakney, J.S. and D.E. McAllister. 1973. Fishes stranded during extreme low tides in Minas Basin, Nova Scotia. Can. Field-Nat. 87 : 371-376.

Boates, J.S. 1980. Foraging semiplated sandpipers *Calidris pusilla* L. and their major prey *Corophium volutator* on the Starr's Point mudflat, Minas Basin. M.Sc. thesis, Acadia University, Wolfville, Nova Scotia.

Boates, J.S. and P.C. Smith. 1988. Crawling behaviour of the amphipod *Corophium volutator* and foraging by semipalmated sandpipers, *Calidris pusilla*. Can. J. Zool. 67 : 457-462.

Bowles, J.E. 1970. Engineering properties of soils and their measurement. McGraw-Hill, N.Y. 187 p.

Bray, D.I., D.P. Demerchant, and D.L. Sullivan. 1982. Some hydrotechnical problems related to the construction of a causeway in the estuary of the Petitcodiac River, New Brunswick. Can. J. Civil Eng. 9 : 296-307.

Buchholtz-Ten Brink, M.R., G. Gust, and D. Chavis. 1989. Calibration and performance of a stirred benthic chamber. Deep Sea Research 36 : 1083-1101.

Burt, T.N. 1984. The Carousel : commissioning of a circular flume for sediment transport research. Hydraulics Research Limited Report SR 33.

Burt, T.N. 1985. Field settling velocities of estuary muds. *In* A.J. Mehta (ed.) Estuarine Cohesive Sediment Dynamics. Lecture Notes on Coastal and Estuarine Studies Vol. 14 : 126-150. Springer-Verlag.

Carey, D.A. 1983. Particle resuspension in the benthic boundary layer induced by flow around polychaete tubes. Can. J. Fish. Aquat. Sci. 40 (Suppl. 1) : 301-308.

Christian, H.A. 1989. Geotechnical behaviour of Annapolis Basin intertidal sediments. Geological Survey of Canada Open File Report.

Christian, H.A. and G.R. Daborn. 1990. Shear strength testing at the sediment-water interface. Presented at ASLO 90 - American Society of Limnologists and Oceanographers, College of William and Mary, Williamsburg, Virginia, June 10-14.

Christian, H.A., D. Gillespie, and C.L. Amos. 1990. Results of a new device to measure the *in-situ* shear strength of cohesive sediments, Minas Basin, Bay of Fundy. Thirteenth International Sedimentological Congress in Nottingham, U.K.

Coles, S.M. 1979. Benthic microalgal populations on intertidal sediments and their role as precursors to salt marsh development. *In* R.C. Jefferies and A.J. Davies (eds.) Ecological Processes in Coastal Environments. 1st. Europ. Symp. Brit. Ecol. Soc. Blackwell Scientific Publ., Oxford, pp. 25-42.

Cook, D.O. 1971. Depressions in shallow marine sediment made by benthic fish. J. Sed. Petrol. 41 : 577-578.

Creutzberg, F. and H. Postma. 1979. An experimental approach to the distribution of mud in the southern North Sea. Netherlands Journal of Sea Research 13 (1) : 99-116.

Daborn, G.R. and M.J. Dadswell. 1988. Natural and anthropogenic changes in the Bay of Fundy - Gulf of Maine - Georges Bank System. *In* M.I. El-Sabh and T.S. Murty (eds.) Natural and Man-Made Hazards. D. Reidel Publ., Dordrecht., pp. 547-560.

Daborn, G.R. and C. Pennachetti. 1979a. Physical oceanographic and sedimentological studies in the Southern Bight of Minas Basin. Proc. N.S. Inst. Sci. 29 : 315-333.

Daborn, G.R. and C. Pennachetti. 1979b. Zooplankton studies in the Southern Bight of Minas Basin. Proc. N.S. Inst. Sci. 29 : 465-481.

Davidson, N.C., D. d'A Laffoley, J.P. Doody, L.S. Way, J. Gordon, R. Key, C.M. Drake, M.W. Pienkowski, R. Mitchell, and K.L. Duff. 1991. Nature Conservation and Estuaries in Great Britain. Peterborough, Nature Conservancy Council, 422 p.

Davies, B.E. 1974. Loss-on-ignition as an estimate of soil organic matter. Soil Sci. Soc. Amer. Proc. 38 : 150.

Downing, J.P. 1983. An optical instrument for monitoring suspended particulates in ocean and laboratory. *In* Proceedings of Oceans '83 : 199-202.

Downing, J.P. and R.A. Beach. 1989. Laboratory apparatus for calibrating optical suspended solids sensors. Marine Geology 86 : 243-249.

Dunn, I.S. 1959. Tractive resistance of cohesive channels. Journal of Soil Mechanics and Foundations, Proceedings of American Society Civil Engineers 85 : 1-24.

Dyer, K.R. 1989. Sediment processes in estuaries : future research requirements. Journal Geophysical Research 94 (C10) : 14,327-14,339.

Eckman, J.E., A.R.M. Nowell, and P.A. Jumars. 1981. Sediment destabilization by animal tubes. J. Mar. Res. 39 : 361-374.

Faas, R.W. 1990. A portable rotational viscometer for field and laboratory analysis of cohesive sediment suspensions. J. Coastal Res. (in press).

Faas, R.W. and C.A. Nittrouer. 1976. Postdepositional facies development in the fine-grained sediment of the Wilkinson Basin, Gulf of Maine. Journal of Sedimentary Petrology 46 : 337-344.

Featherstone, R.P. and M.J. Risk. 1977. Effect of tube-building polychaetes on intertidal sediments of the Minas Basin, Bay of Fundy. Journal of Sedimentary Petrology 47 : 446-450.

Fukuda, M.K. and W. Lick. 1980. The entrainment of cohesive sediments in freshwater. Journal of Geophysical Research 85 (C5) : 2813 -2824.

Gilmurray, M.C. and G.R. Daborn. 1981. Feeding pattern of the Atlantic silverside, *Menidia menidia*, in the Southern Bight of Minas Basin. Mar. Biol. Progr. Ser. 6 : 231-235.

Grant, J. 1981. Dynamics of competition among estuarine sand-burrowing amphipods. J. Exp. Mar. Biol. Ecol. 49 : 255-265.

Grant, J., A. Griswold, and G.R. Daborn. 1990. Flume measurements of erosion in bioturbated intertidal mud. *In* Abstract volume of 13th International Sedimentological Congress, Nottingham.

Gratto, G. 1979. The biology of the amphipod *Corophium volutator* (Pallas) in the W. Minas Basin, N.S. M.Sc. thesis, Acadia University, Wolfville, Nova Scotia.

Gray, J.S. 1974. Animal-sediment relationships. Oceanogr. Mar. Biol. Annu. Rev. 12 : 223-261.

Greenberg, D.A. and C.L. Amos. 1983. Suspended sediment transport and depositional modelling in the Bay of Fundy, Nova Scotia—a region of potential tidal power development. Can. J. Fish. Aquat. Sci. 40 (Suppl. 1) : 20-34.

Gust, G. 1976. Observations on turbulent drag reduction in a dilute suspension of clay in seawater. Journal of Fluid Mechanics 75 (1) : 29-47.

Gust, G. 1988. Skin friction probes for field applications. Journal of Geophysical Research 93 : 14,121-14,132.

Hicklin, P.W. and P.C. Smith. 1979. The diets of five species of migrant shorebirds in the Bay of Fundy. Proc. N.S. Inst. Sci. 29 : 483-488.

Hildebrand, L.P., E.B. MacDormand, D.R. Nelson, C.G. Powell, N.A. Rodgers, and J.A. Walker. 1980. Activities of the Job Corps Program : Fundy Tidal Power Development. Unpublished Report submitted to National Research Council Canada, Halifax, Project 16-01-002N, 176 p.

Hill, P.S., A.R.M. Nowell, and P.A. Jumars. 1988. Flume evaluation of the relationship between suspended sediment concentration and excess boundary shear stress. Journal Geophysical Research 93(C10) : 12,499-12,509.

Holland, A.F., R.G. Zingmark, and J.M. Dean. 1974. Quantitative evidence concerning the stabilization of sediments by marine benthic diatoms. Mar. Biol. 27 : 191-196.

Holtz, R.D. and W.D. Kovacs. 1981. An introduction to geotechnical engineering. Prentice-Hall, New Jersey, 733 p.

Hydraulics Research Limited. 1987. Deposition of cohesive sediments in an annular flume. Unpublished Internal Report : 5 p.

Imrie, D.G.I. and G.R. Daborn. 1981. Food of some immature fish of Minas Basin, Bay of Fundy. Proc. Nova Scotian Inst. Sci. 31 : 149-153.

Jensen, A. 1978. Chlorophylls and carotenoids. *In* J.A. Hellebust and J.S. Craigie (eds.) Handbook of Phycological Methods. Cambridge Univ. Press, pp. 59-74.

Kirby, R. and W.A. Parker. 1977. The physical characteristics and environmental significance of fine-sediment suspensions in estuaries. NAS/AAAS Symposium on Estuaries, Geophysics and the Environment. NAS, pp. 110-120.

Kochert, G. 1978. Carbohydrate determination by the phenol-sulphuric acid method. *In* J.A. Hellebust and J.S. Craigie (eds.) Handbook of Phycological Methods. Cambridge Univ. Press, pp. 95-98.

Kranck, K. 1985. Settling behaviour of cohesive sediment. *In* A.J. Mehta (ed.) Estuarine Cohesive Sediment Dynamics. Lecture Notes on Coastal and Estuarine Studies, Vol. 14, Springer-Verlag, N.Y., pp. 151-169.

Kuijper, C.J.M. Cornelisse and J.C. Winterwerp. 1989. Research on erosive properties of cohesive sediments. Journal of Geophysical Research 94 (C10) : 14,341-14,350.

Kusuda, T. and T. Umita. 1982. Erosional process of fine cohesive sediments. Memoirs of Faculty of Engineering, Kyushu University 42 (4) : 317-333.

Ladd, C.C. and R. Foott. 1974. New design procedure for stability of soft clays. Journal of Geotechnical Engineering Division, American Society of Civil Engineers 100 (GT7) : 763-786.

Lambe, W.T. 1951. Soil Testing for Engineers. Wiley, N.Y., 165 p.

Lambe, T.W. and R.V. Whitman. 1969. Soil Mechanics. J. Wiley and Sons, New York, 553 p.

Lambiase, J.J. 1980. Hydraulic control of grain-size distributions in a macrotidal estuary. Sedimentology 27 : 433-446.

Lee, D-Y., W. Lick, and S.W. Kang. 1981. The entrainment and deposition of fine-grained sediments in Lake Erie. Journal of Great Lakes Research 7 (3) : 224-233.

Lick, W. 1982. Entrainment, deposition, and transport of fine-grained sediments in lakes. Hydrobiologia 91 : 31-40.

Luckenbach, M.W. 1986. Sediment stability around animal tubes : the roles of hydrodynamic processes and biotic activity. Limnol. Oceanogr. 31 : 779-787.

Maa, J.P.Y. 1990. The bed stress of an annular flume. Proceedings of Symposium on Estuarine Water Quality Management, Hamburg.

Manzenrieder, H. 1983. Retardation of initial erosion under biological effects in sandy tidal flats. Leichtweiss Inst. Tech., University Braunschweig., pp. 469-479.

Matlock, K.S., D.W. Houseknecht, and K.R. Applin. 1989. Emplacement of clay into sand by infiltration. J. Sed. Pet. 35 : 956-963.

McCall, P.L. and M.J.S. Tevesz (editors). 1982. Animal-Sediment Relations. The Biogenic Alteration of Sediments. Topics in Geobiology Vol. 2, Plenum Press, N.Y., 336 p.

McCurdy, P. 1979. Intertidal invertebrates of Scots Bay and W. Minas Basin, N.S. M.Sc. thesis, Acadia University, Wolfville, Nova Scotia.

Meadows, P.S. 1964a. Experiments on substrate selection by *Corophium volutator* : films and bacteria on sand particles. J. Exp. Biol. 41 : 499-511.

Meadows, P.S. 1964b. Experiments on substrate selection by *Corophium volutator* : depth selection and population density. J. Exp. Biol. 41 : 677-687.

Meadows, P.S. and J. Tait. 1985. Bioturbation, geotechnics and microbiology at the sediment-water interface in deep sea sediments. Proc. 19th Eur. Mar. Biol. Symp., pp. 191-199.

Meadows, P. and J. Tait. 1989. Modification of sediment permeability and shear strength by two burrowing invertebrates. Mar. Biol. 101 : 75-82.

Meadows, P.S. and A. Tufail. 1986. Bioturbation, microbial activity and sediment properties in an estuarine ecosystem. Proc. R. Soc. Edinb. (Sect. B) 90 : 1-14.

Mehta, A.J. and E. Partheniades. 1979. Kaolinite resuspension properties. Journal Hydraulics Division. Proceedings American Society Civil Engineering 105 : 411-416.

Mehta, A.J. and E. Partheniades. 1982. Resuspension of deposited cohesive sediment beds. Eighteenth Conference Coastal Engineering : 1569-1588.

Mehta, A.J., T.M. Parchure, J.G. Dixit, and R. Ariathurai. 1982. Resuspension potential of deposited cohesive sediment beds. *In* V.S. Kennedy (ed.) Estuarine Comparisons. Publ. Academic Press, New York, pp. 591-609.

Neumann, A.C., C.D. Gebelein, and T.P. Scoffin. 1970. The composition, structure and erodibility of subtidal mats, Abaco, Bahamas. J. Sed. Petrol. 40 : 247-297.

Noorany, I. 1984. Phase relations in marine soils. Journal of Geotechnical Engineering, American Society of Civil Engineers 10 (4) : 539-543.

Nowell, A.R.M., P.A. Jumars, and J.E. Eckman. 1981. Effects of biological activity on the entrainment of marine sediments. Marine Geology 42 : 133-153.

Otsubo, K. and K. Muraoka. 1988. Critical shear stress of cohesive bottom sediments. Journal of Hydraulic Engineering 114 : 1241-1256.

Owen, M.W. 1970. A detailed study of the settling velocities of an estuary mud. Hydraulics Research Station, Wallingford, Report No. INT 78.

Owen, M.W. 1977. Erosion of Avonmouth mud. Hydraulics Research Station, Wallingford, Report No. INT 150 : 17 p.

Parrott, D.R., Campanella, R.G., Imber, B. 1987. Seacone - a cone penetrometer for use with the Pisces submersible. IEEE, pp. 1290-1294.

Partheniades, E., R.H. Cross, and A. Ayora. 1968. Further results on the deposition of cohesive sediments. Proceedings Eleventh Conference Coastal Engineering, London, pp. 723-742.

Partheniades, E. and R.E. Paaswell. 1970. Erodibility of channels with cohesive boundary. Journal of Hydraulics Division, Proceedings of American Society of Civil Engineers 96 : 755-771.

Paterson, D.M. 1989. Short-term changes in the erodibility of intertidal cohesive sediments related to the migratory behaviour of epipelic diatoms. Limnol. Oceanogr. 34 (1) : 223-234.

Peirce, T.J., R.T. Jarman, and C.M. de Turville. 1970. An experimental study of silt scouring. Proceedings of Institution of Civil Engineers 45 : 231-243.

Postma, H. 1961. Transport and accumulation of suspended matter in the Dutch Wadden Sea. Neth. J. Sea Res. 1 : 148-190.

Postma, H. 1967. Sediment transport and sedimentation in the estuarine environment. *In* G.M. Lauff (ed.) Estuaries. Publ. American Association for the Advancement of Science, No. 83 : 158-179.

Risk, M.J. and H.D. Craig. 1976. Flatfish feeding traces in the Minas Basin. J. Sed. Petrol. 46 : 411-413.

Rhoades, D.C. and D.J. Stanley. 1966. Biogenic graded bedding. Journal of Sedimentary Petrology 35 : 956-963.

Rhoads, D.C., J.Y. Yingst, and W.J. Ullman. 1978. Seafloor stability in central Long Island Sound : Part 1. Temporal changes in erodibility of fine-grained sediment. *In* M.L. Wiley (ed.) Estuarine Interactions. Publ. Academic Press, New York, pp. 221-244.

Schubel, J.R. and D.J. Hirschberg. 1980. Accumulation of fine-grained sediments in estuaries. *In* River Inputs to Ocean Systems. Proc. SCOR Workshop, Rome, Italy, 26-30 March 1979. UNESCO, pp. 77-83.

Scoffin, T.P. 1968. An underwater flume. Journal of Sedimentary Petrology 38 : 244-246.

Shames, I. 1962. Mechanics of Fluids. Publ. McGraw-Hill Book Company, New York : 555 p.

Sheng, Y.P. and C. Villaret. 1989. Modeling the effect of suspended sediment stratification on bottom exchange processes. Journal of Geophysical Research 94(C10) : 14,429-14,444.

Shepard, F.P. 1954. Nomenclature based on sand-silt-clay ratios. Journal of Sedimentary Petrology 24 : 151-158.

Skempton, A.W. 1970. The Consolidation of Clays by Gravitational Compaction. Quarterly Journal of the Geological Society of London 125 : 373-411.

Stanley, D.J. 1971. Fish-produced markings on the outer continental margin east of the Middle Atlantic States. J. Sed. Petrol. 41 : 159-170.

Sternberg, R.W. 1972. Predicting initial motion and bedload transport of sediment particles in the shallow marine environment. *In* D.J.P. Swift, D.B. Duane and O.H. Pilkey (eds.) Shelf Sediment Transport, Processes and Pattern. Publ. Dowden, Hutchinson and Ross, pp. 61-83.

Stone, H.H. and G.R. Daborn. 1987. Diet of alewives, *Alosa pseudoharengus*, and blueback herring, *Alosa aestivalis*, (Pisces : Clupeidae) in Minas Basin, Nova Scotia, a macrotidal, turbid estuary. Env. Biol. Fish 19 : 55-67.

Strickland, J.D. and T.R. Parsons. 1977. A Practical Handbook of Seawater Analysis. Fisheries Res. Bd.

Canada, Bulletin No. 167, Ottawa, 310 p.

Thorn, M.F.C. and J.G. Parsons. 1980. Erosion of cohesive sediments in estuaries : an engineering guide. *In* Third International Symposium on Dredging Technology. Bordeaux, pp. 349-358.

van Leussen, W. and E. van Velzen. 1989. High concentration suspensions : their origin and importance in Dutch estuaries and coastal waters. J. Coastal Res., Special Issue No. 5, pp. 1-22.

Van Wazer, J.R., J.W. Lyons, K.Y. Kim, and R.E. Colwell. 1963. Viscosity and Flow Measurements : A Laboratory Handbook of Rheology. Interscience Pub., N.Y., 406 p.

Warwick, R.M. and R.J. Uncles. 1980. Distribution of benthic macrofauna associations in the Bristol Channel in relation to tidal stress. Mar. Ecol. Prog. Ser. 3 : 97-103.

Wells, J.T. and J.M. Coleman. 1981. Physical processes and fine-grained sediment dynamics, coast of Surinam, South America. Journal of Sedimentary Petrology 51 : 1053-1068.

West, J.R., D.W. Knight, and K. Shiono. 1986. Turbulence measurements in the Great Ouse estuary. Journal of Hydraulic Engineering 12(3) : 167-180.

Wilkinson, D.L. and I.S.F. Jones. 1988. Developments toward a marine sediment probe. Ocean Sciences Institute, The University of Sydney, Technical Report 10 : 17 p.

Wolanski, E., J. Chappell, P. Ridd, and R. Verbessy. 1988. Fluidization of mud in estuaries. Journal of Geophysical Research 93 : 2351-2361.

Yingst, J.Y. and D.C. Rhoads. 1978. Seafloor stability in central Long Island Sound : Part II. Biological Interactions and their potential importance for seafloor erodibility. *In* M.L. Wiley (ed.) Estuarine Interactions. Publ. Academic Press, New York, pp. 245-260.

Young, R.A. 1977. Seaflume : a device for *in-situ* studies of threshold erosion velocity and erosional behaviour of undisturbed marine muds. Marine Geology 23 : M11-M18.

Zeman, A.J. 1983. Erosion of cohesive sediments; bibliography and annotated abstracts. Internal Report 354, Inland Waters Directorate, Burlington, 93 p.